RADIATION EFFECTS ON EMERGING ELECTRONIC MATERIALS AND DEVICES

FINAL PERFORMANCE REPORT PREPARED FOR:

Kitt Reinhardt
AFOSR/NE
875 N. Randolph Street
Suite 325, Room 3112
Arlington, VA 22203

Vanderbilt University MURI Program

Electrical Engineering and Computer Science Department

Box 1608, Station B

Nashville, TN 37235

Contract #FA9550-05-1-0306

Report Documentation Page

Form Approved
OMB No. 0704-0188

1. REPORT DATE	2. REPORT TYPE	3. DATES COVERED
17 JAN 2010		**00-09-2005 to 00-01-2011**

4. TITLE AND SUBTITLE	5a. CONTRACT NUMBER
Radiation Effects On Emerging Electronic Materials And Devices	5b. GRANT NUMBER
	5c. PROGRAM ELEMENT NUMBER
6. AUTHOR(S)	5d. PROJECT NUMBER
	5e. TASK NUMBER
	5f. WORK UNIT NUMBER
7. PERFORMING ORGANIZATION NAME(S) AND ADDRESS(ES) **Institute for Space and Defense Electronics at Vanderbilt University,1025 16th Avenue South, Suite 200,Nashville,TN, 37212**	8. PERFORMING ORGANIZATION REPORT NUMBER
9. SPONSORING/MONITORING AGENCY NAME(S) AND ADDRESS(ES)	10. SPONSOR/MONITOR'S ACRONYM(S)
	11. SPONSOR/MONITOR'S REPORT NUMBER(S)

12. DISTRIBUTION/AVAILABILITY STATEMENT
Approved for public release; distribution unlimited

13. SUPPLEMENTARY NOTES

14. ABSTRACT

15. SUBJECT TERMS

16. SECURITY CLASSIFICATION OF:			17. LIMITATION OF ABSTRACT	18. NUMBER OF PAGES	19a. NAME OF RESPONSIBLE PERSON
a. REPORT **unclassified**	b. ABSTRACT **unclassified**	c. THIS PAGE **unclassified**	**Same as Report (SAR)**	**145**	

REPORT DOCUMENTATION PAGE

Form Approved
OMB No. 0704-0188

PLEASE DO NOT RETURN YOUR FORM TO THE ABOVE ORGANIZATION.

1. REPORT DATE *(DD-MM-YYYY)*	2. REPORT TYPE	3. DATES COVERED *(From - To)*
01/17/10	Final	9/2005 - 01/2011

4. TITLE AND SUBTITLE
Radiation Effects on Emerging Electronic Materials and Devices

5a. CONTRACT NUMBER
FA9550-05-1-0306

5b. GRANT NUMBER

5c. PROGRAM ELEMENT NUMBER

6. AUTHOR(S)
Schrimpf, Ron; Fleetwood, Dan; Pantelides, Sokrates; Feldman, Len; Law, Mark; Cressler, John; Garfunkle, Eric; Lucovsky, Gerald; Barnaby, Hugh

5d. PROJECT NUMBER

5e. TASK NUMBER

5f. WORK UNIT NUMBER

7. PERFORMING ORGANIZATION NAME(S) AND ADDRESS(ES)
Institute for Space and Defense Electronics at Vanderbilt University
1025 16th Avenue South, Suite 200
Nashville, TN 37212

8. PERFORMING ORGANIZATION REPORT NUMBER

9. SPONSORING/MONITORING AGENCY NAME(S) AND ADDRESS(ES)
USAF, AFRL
AF Office of Scientific Research
875 N. Randolph St., Room 3112
Arlington, VA 220203

10. SPONSOR/MONITOR'S ACRONYM(S)
AFOSR

11. SPONSOR/MONITOR'S REPORT NUMBER(S)
AFRL-OSR-VA-TR-2012-0116

12. DISTRIBUTION/AVAILABILITY STATEMENT
Unlimited

13. SUPPLEMENTARY NOTES

14. ABSTRACT

This report documents work conducted as part of a five-year Multi-disciplinary University Research Initiative (MURI) in the area of Semiconductor Radiation Physics. The objectives of this program are to examine and understand the underlying physical phenomena that control the radiation response of semiconductor technologies incorporating emerging materials and devices. The radiation response and electrical properties of technologies that exhibit exception promise for application in DoD systems are investigated experimentally and through application of advanced theory and simulation. The overall purpose is to develop knowledge and tools that will guide development of future radiation-hardened electronics. This MURI program includes researchers from Vanderbilt University, The University of Florida, Georgia Institute of Technology, North Carolina State University, Rutgers University and Arizona State University and strong collaboration with leading industrial and government labs.

15. SUBJECT TERMS
Radiation Effects, SiSio2 Interface Gate Dielectrics, MOS Devices, SiGe Devices, Single Event Upset, MOSFETs, SEU Simulations, Multi-Bit Upset, Deep Trench Isolation Devices, Ions Chanelling

16. SECURITY CLASSIFICATION OF:			17. LIMITATION OF ABSTRACT	18. NUMBER OF PAGES	19a. NAME OF RESPONSIBLE PERSON
a. REPORT	b. ABSTRACT	c. THIS PAGE			Ron Schrimpf
U	U	U	UU	145	19b. TELEPHONE NUMBER *(Include area code)* 615.343.0507

Reset

CONTENTS

CONTENTS (CONTINUED)

CONTENTS (CONCLUDED)

FIGURES

FIGURES (CONTINUED)

FIGURES (CONTINUED)

FIGURES (CONTINUED)

FIGURES (CONTINUED)

FIGURES (CONCLUDED)

I.0 OBJECTIVES

This final report documents work conducted as part of a five-year Multi-disciplinary University Research Initiative (MURI) in the area of Radiation Effects on Emerging Electronic Materials and Devices. The objectives of this program are to examine and understand the underlying physical phenomena that control the radiation response of semiconductor technologies incorporating emerging materials and devices. The radiation response and electrical properties of technologies that exhibit exceptional promise for application in DoD systems are investigated experimentally and through application of advanced theory and simulation. The overall purpose is to develop knowledge and tools that will guide development of future radiation-hardened electronics. This MURI program includes researchers from Vanderbilt University, the University of Florida, Georgia Institute of Technology, North Carolina State University, Rutgers University, and Arizona State University and strong collaboration with leading industrial and government labs.

The combined effects of advances in microelectronic materials and device structures have resulted in more changes to underlying integrated-circuit technologies over the past decade than in the previous forty years. As integrated circuits become smaller and more complex, it is increasingly difficult to predict their responses to radiation and to guarantee reliable operation. These problems are compounded by the incorporation of new materials and device structures. Before the 1990s, only seven elements were in common use in integrated circuits; currently more than half the elements in the periodic table are in use or under evaluation. Simultaneously, device dimensions have reached approximately 1 nm vertically and several 10s of nm horizontally. The interaction of radiation with these new materials in such small volumes can cause unexpected and challenging reliability problems. For some advanced technologies, the error rates observed in satellite systems have been orders of magnitude greater than those predicted by conventional ground-based testing and simulation methods. Understanding and mitigating these radiation-induced errors is the key reliability challenge associated with deploying future generations of electronics in space and defense systems. Energy absorption, carrier generation, carrier transport, charge trapping and defect formation and dynamics depend on the specific materials used in the ICs. Sensitivity to the electrostatic effects of radiation-induced trapped charge, lifetime degradation, and device-edge and inter-device leakage depend on the detailed device geometries and doping profiles. Moreover, high-speed circuits exhibit increased vulnerabilities to single-event effects, including multiple-bit upsets that result from aggressive scaling, and large enhancements relative to ion-strike angle that are much greater than for earlier generations of technology. While it was possible to study total dose and single event effects separately in larger devices, the boundary is now increasingly less clear as a single event may induce charging or damage in the entire device.

The research conducted as part of this program combines experiments on emerging materials and devices with atomic-scale materials theory and a high performance computing-based radiation-effects simulation approach to develop guidelines for design and application of advanced electronic technologies in radiation environments. The emphasis is on technologies that show the most promise for defense and space systems. Experimental samples were fabricated in the labs of MURI team members and acquired through collaborations with industrial and government laboratories. The technologies examined include alternative gate dielectrics, strained-layer transistors, silicon-on-insulator (SOI) devices, FinFETs, SiGe devices, and ultra-small CMOS transistors. Samples were irradiated using particle and photon sources and the results were interpreted using an approach that combines first-principles quantum mechanical analysis of defects with engineering-level modeling.

A new simulation approach, based on determining the device-level response to an ensemble of realistic particle-generated track structures, was used to analyze single-event effects in ultra-small devices. This approach, which employs a Monte Carlo tool developed at Vanderbilt, allows the most accurate analysis to date of single-event upsets and transients, as well as emerging issues like localized displacement damage and microdose effects. The simulation tool, Monte Carlo Radiative Energy Deposition (MRED), includes the GEANT4 libraries developed by the high energy physics community as well as other models for the interaction of radiation with matter. The approach is complemented by atomic-scale calculations of radiation-induced atomic displacements, defect generation, and subsequent charging.

2.0 STATUS OF EFFORT

The program ended in August of 2010, following a three-month no-cost extension. Some of the major accomplishments of this program include:

- The groups at North Carolina State, Rutgers, and Vanderbilt collaborated to develop the most extensive understanding to date of the radiation response of alternative gate dielectrics. This is a very significant issue for application of future CMOS technology generations in DoD systems. These new gate dielectrics, particularly those based on hafnium, were introduced into production in the 45-nm CMOS technology node. The higher dielectric constant of hafnium-based films compared to silicon dioxide allows a greater physical thickness for the film while still providing sufficiently high capacitance per unit area. This greater thickness, however, can increase the sensitivity to total ionizing dose. Among the most important findings is that HfSiON films have superior total-ionizing-dose radiation response compared to other Hf-based alternative dielectrics. In addition, the combined effects of radiation and electrical stress were found to be worse than a linear combination of the individual effects in some films.
- North Carolina State produced HfO_2 films on Ge substrates that have interfacial properties equivalent to those of thermal oxide on Si. The key step is the formation of the interfacial layer. This material system is important because of the potential to build devices with better drive current, particularly for p-channel transistors, but the carrier-transport properties have been limited by poor interfacial quality. NCSU provided devices to Vanderbilt for radiation characterization. Vanderbilt conducted detailed radiation studies of HfO_2 on Ge devices and found that the total-dose radiation response is promising.
- Vanderbilt performed systematic studies of defect stability, hydrogen transport, and interfacial reactions in irradiated SiO_2 on Si using density functional theory. DFT is the state-of-the-art method for analyzing defects in solids. The resulting understanding of the properties of hydrogen in SiO_2/Si is the most thorough examination of the fundamental processes responsible for radiation-induced interface traps performed to date.
- Vanderbilt developed a physical model of bias-temperature instability (BTI) in Si devices and showed that the processes responsible for BTI and radiation-induced degradation have a common origin. In particular, it was found that hydrogen originating in the Si substrate plays a key role in both negative bias temperature instability and enhanced low-dose-rate sensitivity.
- The University of Florida and Vanderbilt collaborated to perform the first controlled measurements of radiation response in strained-Si technologies. Strained Si is the key

3.0 ACCOMPLISHMENTS/FINDINGS

3.1 TID Effects on 1-T DRAMs:

We have characterized the total ionizing dose response of two SOI FinFET technologies operated in 1T-DRAM mode, one with poly-crystalline Si gates and a SiO_2 gate dielectric, and the other with metal gates and a high-K gate dielectric. These devices were programmed using both back-gate pulse and gate induced drain leakage (GIDL) programming methods. 1T-DRAM cells programmed with back-gate pulses are quite sensitive to total ionizing dose radiation, with the memory sensing margin and retention time decreasing significantly with increasing dose. In contrast, the sensing margin and retention time show high tolerance to total ionizing dose (TID) irradiation when the 1T-DRAM cells are programmed via gate induced drain leakage (GIDL); see Fig. 1. The sensing margin increases significantly with decreasing gate length for 1T-DRAM cells programmed via GIDL. We conclude that capacitor-less 1T-DRAMs programmed via GIDL are strong candidates for embedded memory applications for ultimately scaled CMOS devices in high-TID applications. [E. X. Zhang, D. M. Fleetwood, F. El Mamouni, R. D. Schrimpf, M. L. Alles, W. Xiong, K. Akarvardar, and S. Cristoloveanu, "Total ionizing dose effects on FinFET-based capacitor-less 1T-DRAMs," accepted for publication in *IEEE Trans. Nucl. Sci.*, 57, no. 6, Dec. 2010.]

3.2 Low Frequency Noise, Moisture Effects, and Aging

We have found that the room temperature 1/f noise gate-voltage and frequency dependences of pMOS transistors are affected significantly by moisture exposure and total dose irradiation. The voltage noise power spectral density $S_{Vd} \sim (V_g - V_t)^{-\beta}$, where V_t is the threshold voltage, V_g is the gate voltage, and β is a measure of the gate-voltage dependence. For pMOS devices (Fig. 2), pre-irradiation, β ranges from 0.4 to 0.9, and the frequency exponent, $\alpha = -\partial \ln S_{Vd}/\partial \ln f$, is greater than unity. Post-irradiation, the gate-voltage and frequency dependences change significantly, with $\beta >> 1$, and α much closer to unity. For nMOS devices (Fig. 3), pre-irradiation, $\beta \geq 1.6$ and $\alpha \approx 1$, with little change after irradiation. We attribute these observed changes in pMOS noise to changes in the trap density and energy distribution, $D_t(E_f)$, of these devices. Before irradiation, $D_t(E_f)$ increases

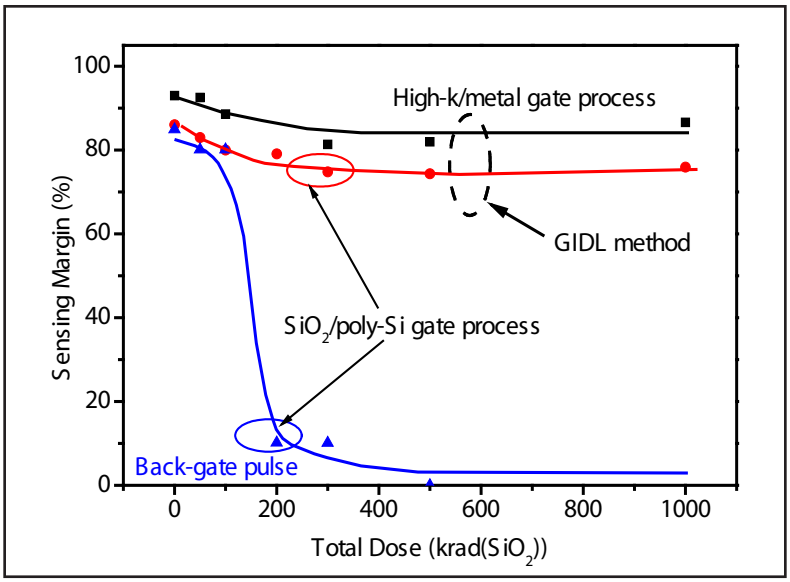

Fig. 1. Sensing margin as a function of total ionizing dose for nMOS 1T-DRAM cells programmed by back-gate pulse and GIDL methods.

toward the valence band edge, but after irradiation, the distribution typically is more uniform. Moreover, for some moisture-exposed devices, $S_{Vd}\mu \sim (V_g - V_t)^{-3}$ after irradiation, indicating a $D_t(E_f)$ that increases toward midgap. We conclude that irradiation and/or moisture exposure can greatly affect the defect energy distributions for these devices, and that the observed nMOS and pMOS noise can be described by a simple trapping model with an energy-dependent trap distribution. [S. A. Francis, A. Dasgupta, and D. M. Fleetwood, "Effects of total dose irradiation on the gate-voltage dependence of the 1/f noise of nMOS and pMOS transistors," *IEEE Trans. Electron Dev.* 57, 503-510 (2010).]

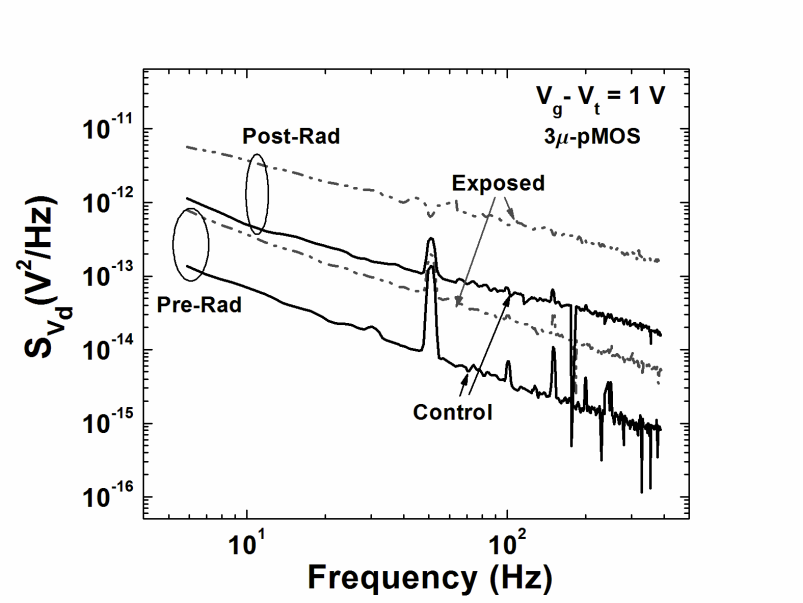

Fig. 2. SVd as a function of frequency for 3 μm x 16 μm pMOS transistors from control and moisture-exposed parts, before and after 500 krad(SiO2) total dose irradiation.

3.3 Defects and Hydrogen

We have performed an extensive investigation of the energetics of the interactions between molecular hydrogen and common defects in SiO_2 that are typically associated with O deficiency. We find that H_2 does not easily crack at neutral vacancies, but it will crack efficiently at O vacancy sites that have captured a hole and relaxed into the puckered configuration of an E_γ' defect (Fig. 4), releasing a proton into the oxide. This leads to a reduction in oxide-trap charge and an increase in interface-trap charge with time. Isolated Si dangling bonds also can play a role in cracking H_2 depending on their concentration. These results provide significant insight into the underlying causes of latent interface trap buildup in MOS devices and enhanced low-dose-rate sensitivity in linear bipolar devices. (Fig. 5.) These are longstanding problems in the radiation effects community. [B. R. Tuttle, D. R. Hughart, R. D. Schrimpf, D. M. Fleetwood, and S. T. Pantelides, "Defect interactions of H_2 in SiO_2: Implications for ELDRS and latent interface trap buildup," accepted for publication in *IEEE Trans. Nucl. Sci.*, 57, no. 6, Dec. 2010.]

We have also found that enhanced low-dose-rate sensitivity (ELDRS) in lateral and substrate pnp bipolar devices can occur because of the much lower probability for electron capture by protons in SiO_2, as compared to mobile or trapped holes. New experimental results and a critical evaluation of previous work demonstrate that, at high dose rates and/or in oxides with low concentrations of

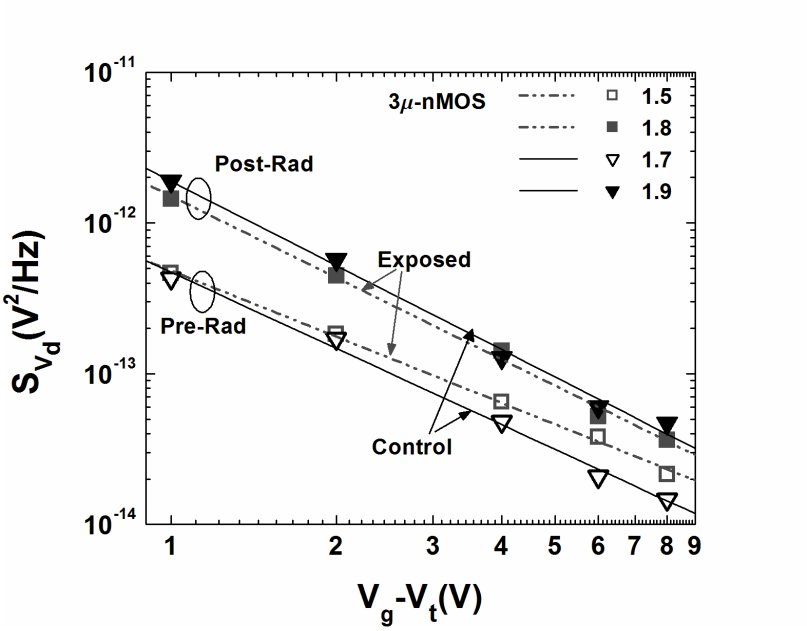

Fig. 3. SVd at ~10 Hz as a function of Vg–Vt for 3 µm x 16 µm nMOS transistors from the control and moisture-exposed parts, before and after 500 krad(SiO2) total dose irradiation.

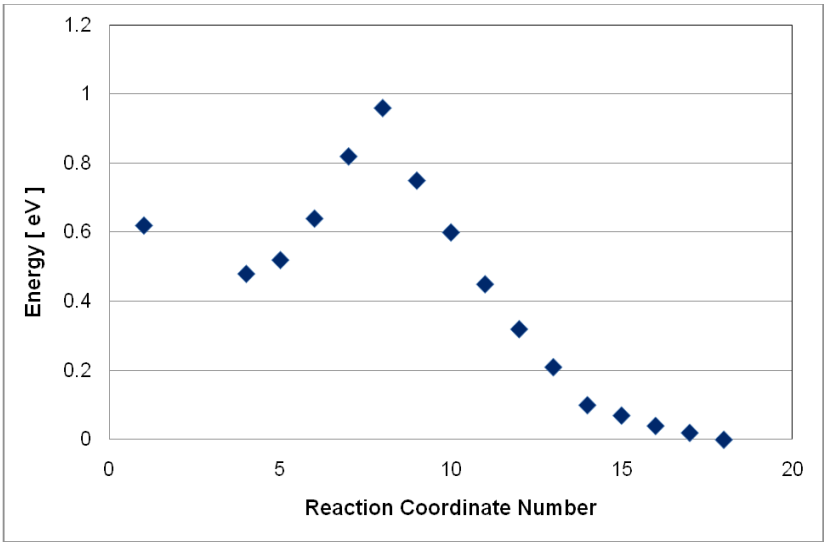

Fig. 4. The reaction energy for H_2 dissociating at a positively charged, puckered vacancy.

hydrogen, electrons can more easily neutralize slowly diffusing or metastably trapped holes via annihilation (recombination) or compensation (offsetting trapping) before the holes can release H^+. In contrast, at low dose rates and/or in oxides with higher concentrations of hydrogen, which can react with and modify the structure of O-vacancy-related defects, it is more likely that holes can release H^+ during transport. This is because the cross section for electron capture by H^+ is several orders of magnitude smaller than the electron capture cross section for a slowly moving or metastably trapped hole (Fig. 6). This enhanced proton release at low dose rates or in oxides with high hydrogen concentrations can lead to increased interface trap formation, which is the most common source of enhanced gain degradation in lateral and substrate pnp bipolar transistors. This provides significant insight into the longstanding problem of ELDRS in linear bipolar transistors.

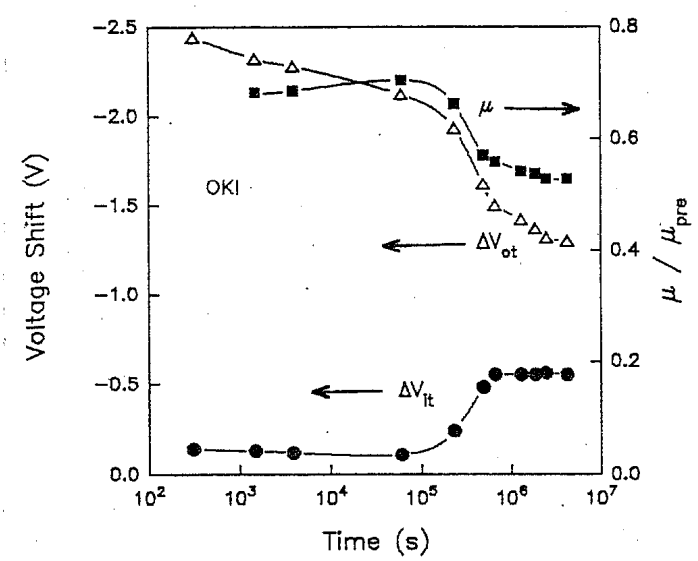

Fig. 5. Threshold voltage shifts due to oxide- and interface-trap charge ΔVot and ΔVit, as well as the ratio of post-irradiation to pre-irradiation mobility μ/μpre, for pMOS transistors from Oki Semiconductor, irradiated to 75 krad(SiO2) at a dose rate of ~ 240 rad(SiO2)/s and annealed at 100 ºC. The irradiation and annealing bias was +6 V. ΔVot and ΔVit were estimated via the midgap charge separation technique. (After J. R. Schwank, et al., IEEE Trans. Nucl. Sci., vol. 39, no. 6, pp. 1953-1963, Dec. 1992.)

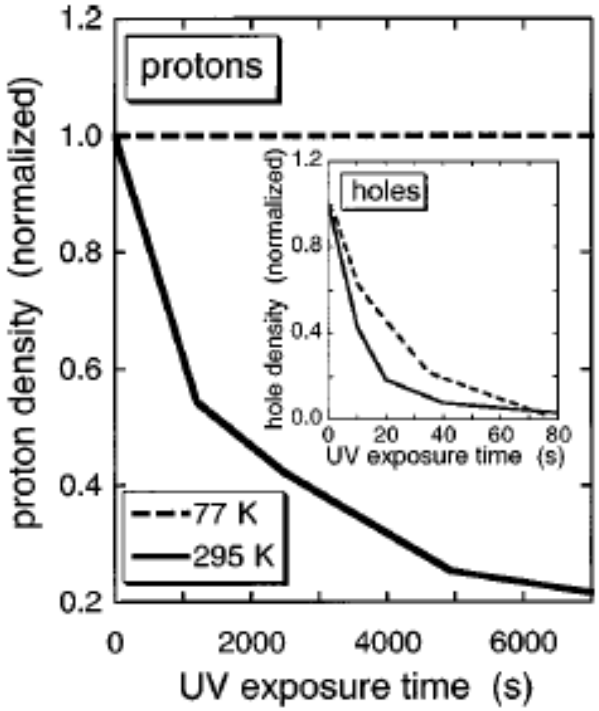

Fig. 6. Relative charge neutralization rates for trapped holes and protons in ~ 1 μm oxides grown on zone-melt recrystallized SiO_2 during 5 eV ultraviolet illumination for the same exposure conditions at 295 K and 77 K. This energy is high enough to inject electrons over the 3.1 eV Si-to-SiO_2 barrier, but too low to create electron-hole pairs in SiO_2. (After K. Vanheusden, et al. *Appl. Phys. Lett.*, 72, no. 1, pp. 28-30, 1998.)

[D. M. Fleetwood, R. D. Schrimpf, S. T. Pantelides, R. L. Pease, and G. W. Dunham, "Electron capture, hydrogen release, and enhanced gain degradation in linear bipolar devices," *IEEE Trans. Nucl. Sci.* 55, 2986-2991 (2008).]

3.4 Defects in High-K Gate Oxides

We have characterized radiation induced charge trapping in ultrathin HfO_2-based n-channel MOSFETs as a function of dielectric thickness and irradiation bias following exposure to 10 keV X-rays and/or constant voltage stress. Positive and negative oxide-trap charges are observed, depending on irradiation and bias stress conditions. No significant interface-trap buildup is found in these devices under these irradiation and stress conditions. Enhanced oxide-charge trapping occurs in some cases for simultaneous application of constant voltage stress and irradiation, relative to either type of stress applied separately (Fig. 7). Room temperature annealing at positive bias after irradiation of transistors with thicker gate dielectric films leads to positive oxide-trapped charge annihilation and/or neutralization in these devices, and net electron trapping. The oxide thickness dependence of the radiation response confirms the extreme radiation tolerance of thin HfO_2 dielectric layers of relevance to device applications, and suggests that hole traps in the thicker layers are located in the bulk of the dielectric. A revised methodology is developed to estimate the net effective charge trapping efficiency, f_{ot}, for high-κ dielectric films. As a result, estimates of f_{ot} for Hf silicate in previous work by Felix et al. (2002) are reduced by up to 18 %. [S. K. Dixit, X. J. Zhou, R. D. Schrimpf, D. M. Fleetwood, S. T. Pantelides, R. Choi, G. Bersuker, and L. C. Feldman, "Radiation induced charge trapping in ultrathin HfO_2-based MOSFETs," *IEEE Trans. Nucl. Sci.* 54, 1883-1890 (2007).]

Charge trapping characteristics were investigated for MOS capacitors with 6.8 nm HfO_2 layers and 1.0 nm interfacial silicon oxynitrides; the effective oxide thickness of the high-κ gate dielectric layers is 2.1 nm. These devices were irradiated with 10-keV X-rays or subjected to constant voltage stress, and then annealed for ten minute intervals of alternating positive and negative gate bias at temperatures between 25 and 150 ºC. The resulting oxide-trap (Fig. 8) and interface-trap charge (Fig. 9) densities exhibit reversible buildup and annealing that depend strongly on bias and temperature. Additional defect-density growth with time was observed as a result of charge injection into the gate stack during the annealing process (Fig. 10). This defect-density growth increases with increasing annealing time and temperature. After irradiation, the most of the reversibility in the charge trapping is due to metastable electron traps in the near-interfacial dielectric layers. After constant voltage stress, the motion, reactions, and trapping of protons at or near the Si/oxynitride interface are more important to the observed device response than are metastable electron traps. This is a result of reduced electron-hole pair creation during low-energy constant-voltage stress, as compared to high-energy X-ray irradiation. These results illustrate the importance of both electron traps and protons to the ionizing radiation response and long-term reliability of MOS devices with high-κ gate dielectrics. [X. J. Zhou, D. M. Fleetwood, L. Tsetseris, R. D. Schrimpf, and S. T. Pantelides, "Effects of switched-bias annealing on charge trapping in HfO_2 gate dielectrics," *IEEE Trans. Nucl. Sci.* 53, 3636-3643 (2006).]

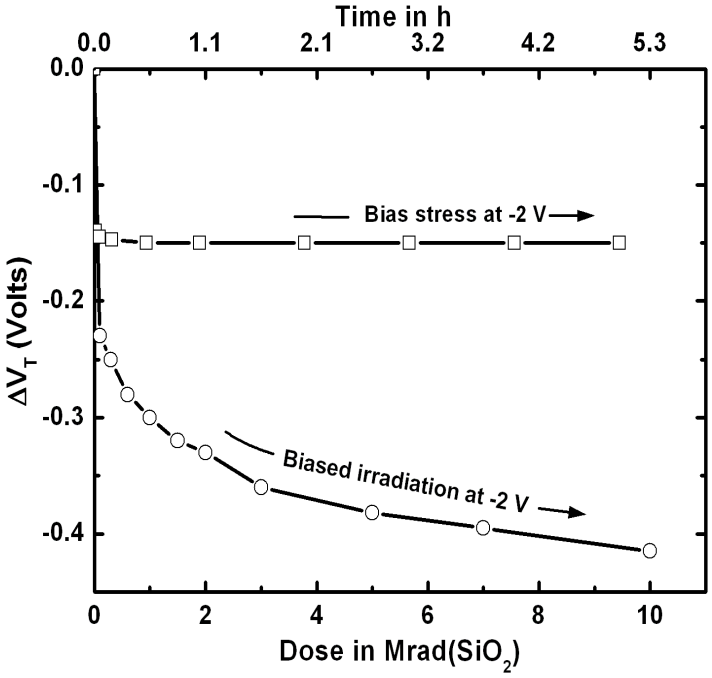

Fig. 7. Threshold voltage shifts (ΔVT) due to constant voltage stress, CVS (-2 V), and CVS (-2 V) + irradiation. The bottom x-axis shows the dose in Mrad(SiO2). The top x-axis shows the time during CVS.

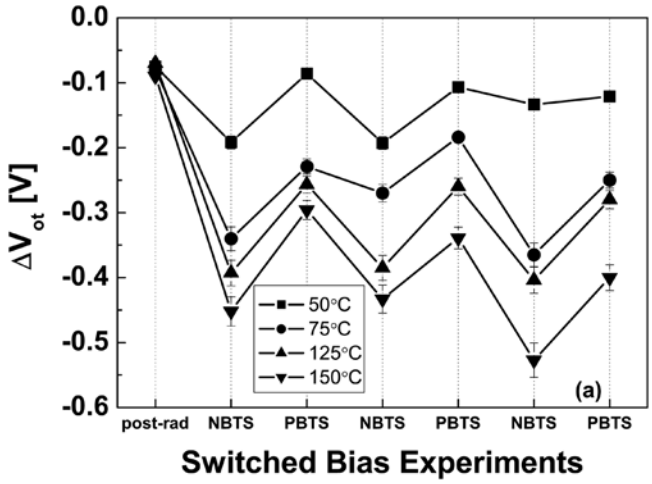

Fig. 8. ΔV_{ot} (a) for Al/HfO_2+SiO_xN_y/Si pMOS capacitors irradiated to 1.0 Mrad(SiO_2) with 10-keV X-rays, followed by a series of switched bias anneals at 50 to 150 °C. The gate bias for irradiation is 0.3 V. The switched bias anneals are ± 0.3 V (PBTS, NBTS), and the stress time was 600 s each.

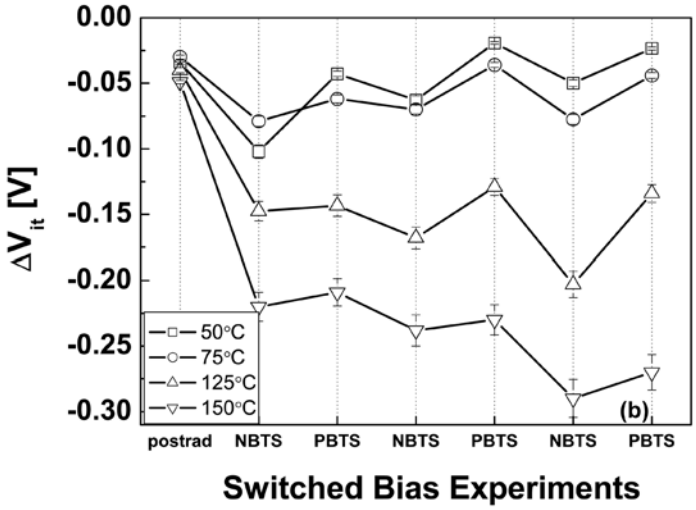

Fig. 9. ΔV_{it} for Al/HfO_2+SiO_xN_y/Si pMOS capacitors irradiated to 1.0 Mrad(SiO_2) with 10-keV X-rays, followed by a series of switched bias anneals at 50 to 150 °C. The gate bias for irradiation is 0.3 V. The switched bias anneals are ± 0.3 V (PBTS, NBTS), and the stress time was 600 s each.

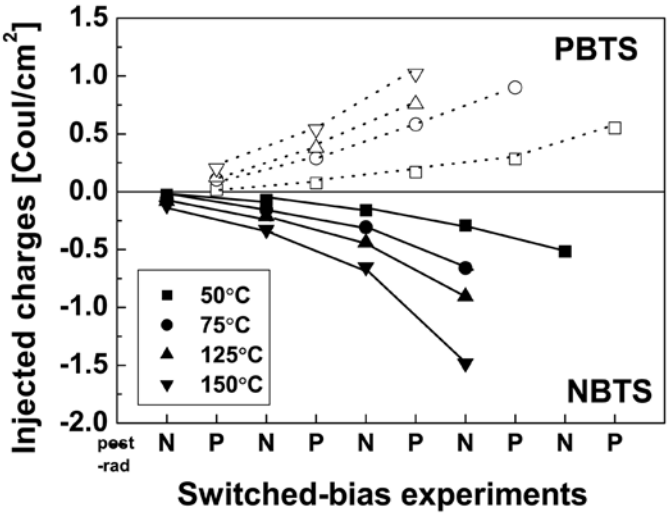

Fig. 10. Cumulative injected charge densities for switched-bias annealing at elevated temperatures after irradiation. The capacitor area A = 5.6 ´ 10-4 cm2. The experimental conditions are the same as Fig. 1. Cumulative charge densities during PBTS are shown in the upper part of the figure, and cumulative charge densities during NBTS are shown in the lower half. These densities do not include the portions of the anneal when the device was in the opposite bias state, so the total charge is obtained by adding the charge densities in the upper and lower halves of the figure.

3.5 A Comprehensive Understanding of the Efficacy of N-Ring SEE Hardening Methodologies in SiGe HBTs

Georgia Tech's contributions to this five year MURI on radiation effects centered on the radiation response and damage mechanisms in device and circuits built from silicon-based heterostructures, including primarily silicon-germanium (SiGe) heterojunction bipolar transistors (HBTs), SiGe modulation doped FETs (MODFETs), and strained-silicon CMOS.

We investigate the efficacy of mitigating radiation-based single event effects (SEE) within circuits incorporating SiGe heterojunction bipolar transistors (HBTs) built with an N-Ring, a transistor-level layout-based radiation hardened by design (RHBD) technique. Previous work of single-device ion-beam induced charge collection (IBICC) studies has demonstrated significant reductions in peak collector-collected charge and sensitive area for charge collection; however, few circuit studies using this technique have been performed. Transient studies performed with Sandia National Laboratory's (SNL) 36 MeV ^{16}O microbeam on voltage references built with SiGe N-ring SiGe HBTs have shown mixed results, with reductions in the number of large voltage disruptions in addition to new sensitive areas of low-level output voltage disturbances. Similar discrepancies between device-level IBICC results and circuit measurements are found for the case of digital shift registers implemented with N-ring SiGe HBTs radiated in a broadbeam environment at Texas A&M's Cyclotron Institute. The over-all error cross-section of the N-ring-based register is found to be larger than the standard SiGe register, which is clearly counter-intuitive. We have worked to resolve the discrepancy between the measured circuit results and the device-level IBICC measurements, by re-measuring single-device N-ring SiGe HBTs using a time-resolved ion beam induced charge (TRIBIC) set-up that allows direct capture of nodal transients. Coupling these measurements with full 3-D TCAD simulations provides complete insight into the origin of transient currents in an N-ring SiGe HBT. The detailed structure of these transients and their bias dependencies are discussed, together with the ramifications for the design of space-borne analog and digital circuits using SiGe HBTs.

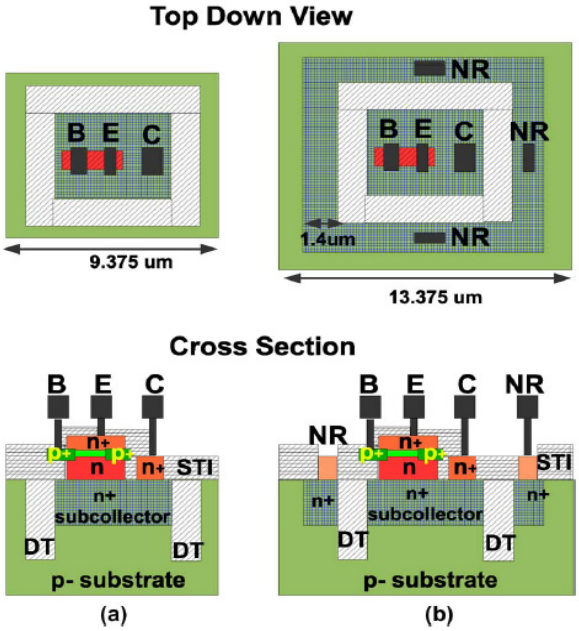

Fig. 11. RHBD approach using n-rings for SiGe HBTs.

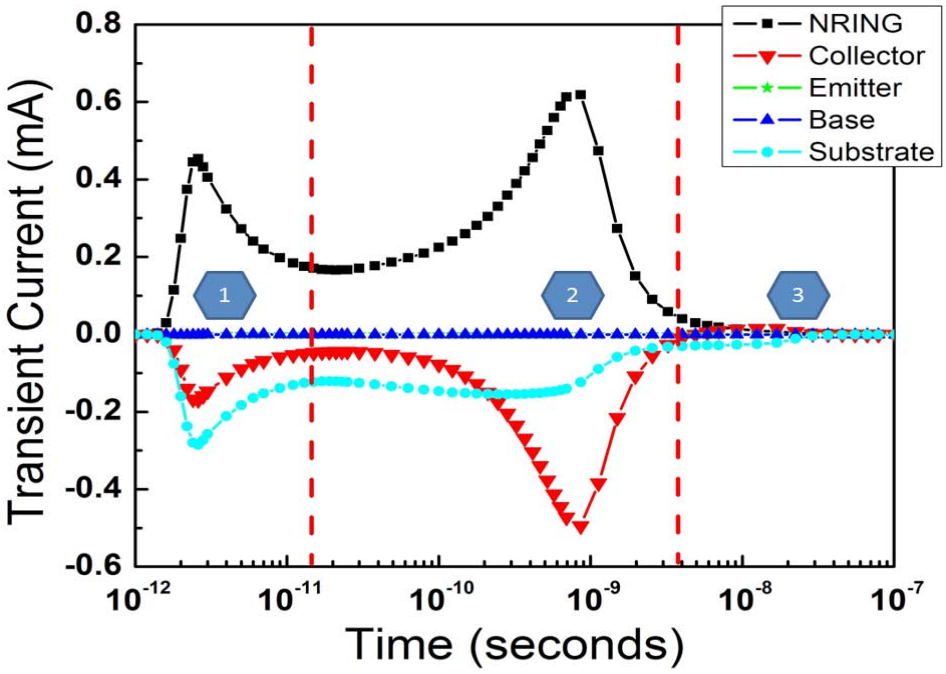

Fig 12. Simulated transient waveforms for an ion strike through the N-ring of an N-ring SiGe HBT biased with 3 V on the N-ring and collector and all other terminals ground.

3.6. Single Event Transient Hardness of a New Complementary (npn + pnp) SiGe HBT Technology on Thick-film SOI

We report heavy-ion microbeam and total dose data for a new complementary (npn + pnp) SiGe on thick-film SOI technology. Measured transient waveforms from heavy-ion strikes indicate a significantly shortened transient upset current, while maintaining the total dose robustness associated with SiGe devices. Heavy-ion broad-beam data confirms a reduced single event upset (SEU) cross-section in a high-speed shift register circuit.

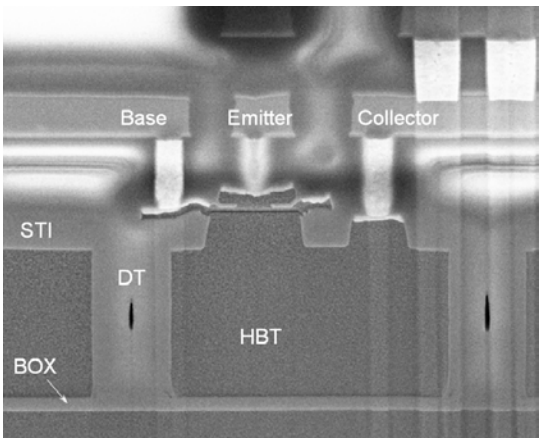

Fig. 13. SEM cross-section of a SiGe HBT on thick film SOI.

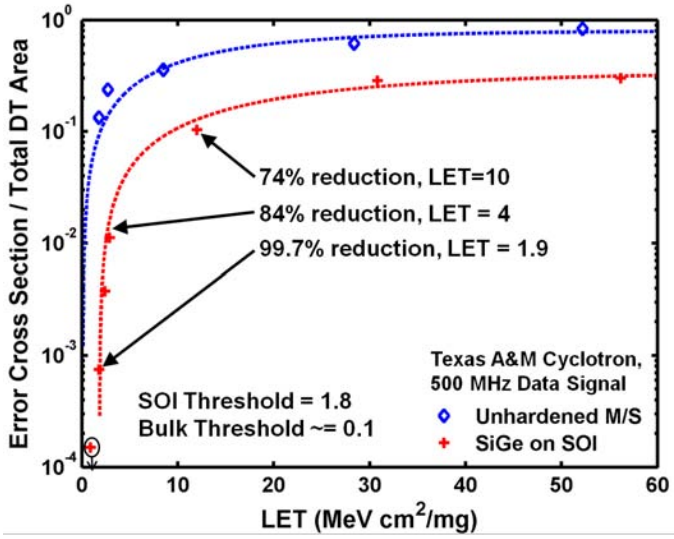

Fig. 14. Measured improvement in SEU cross-section and LET for SiGe on SOI.

3.7 Single Event Transient Response of SiGe Voltage References and Its Impact on the Performance of Analog and Mixed-Signal Circuits

We investigated the single-event transient (SET) response of bandgap voltage references (BGRs) implemented in SiGe BiCMOS technology through heavy ion microbeam experiments. The SiGe BGR circuit was used to provide the input reference voltage to a voltage regulator. SiGe HBTs in the BGR circuit were struck with 36 MeV oxygen ions and the subsequent transient responses were captured at the output of the regulator. Sensitive devices responsible for generating transients with large peak magnitudes were identified. To determine the effectiveness of a transistor-layout-based radiation hardened by design (RHBD) technique with respect to immunity to SETs at the circuit level, the BGR circuit implemented with HBTs surrounded by an alternate reverse-biased pn junction (n-ring RHBD), were also bombarded with oxygen ions and subsequent SETs captured. Experimental results indicated that the number of events with large peak magnitude have been reduced in the RHBD version; however, with the inclusion of the n-ring RHDB, new locations for the occurrence of transients (albeit with smaller peak magnitude) were created. Transients at the transistor level were also independently captured. It was demonstrated that while the transients are short at the transistor level (ns duration), relatively long transients are obtained at the circuit level (100's of ns). In addition, the impact of the SET response of the BGR on the performance of an ultra-high speed 3-bit SiGe analog-to-digital converter (ADC) was investigated through simulation. It was shown that ion-induced transients in the reference voltage could eventually lead to data corruption at the output of the ADC.

3.8 Re-examining TID Hardness Assurance Test Protocols for SiGe HBTs

We investigated the applicability of current TID test protocols in the context of advanced transistor technologies such as SiGe HBTs. In SiGe HBTs, an unexpected shift in collector current was observed during total dose irradiation. Using both device and circuit measurements, we investigated

this phenomenon and assessed its potential importance in hardness assurance of SiGe components. TCAD simulations were performed to explain the observed current shifts.

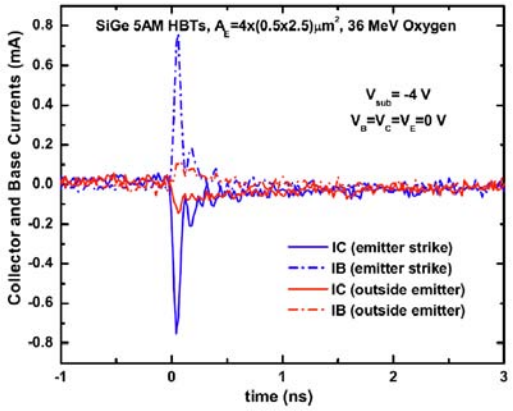

Fig. 15. Collector and base transient currents for strikes over and outside the emitter area for standard HBTs.

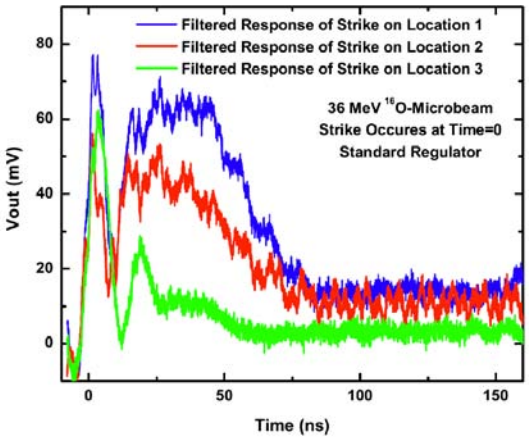

Fig. 16. Single-event transient response of the regulator for three different strike locations.

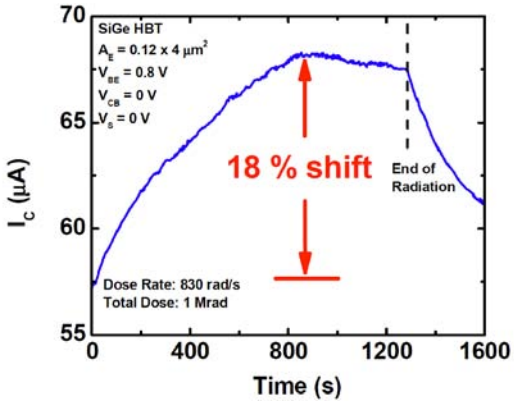

Fig. 17. Collector and base currents of a SiGe HBT under irradiation of 1 Mrad. Radiation stopped at 1,275 s, but biasing continued until a total of 1,600 s was reached.

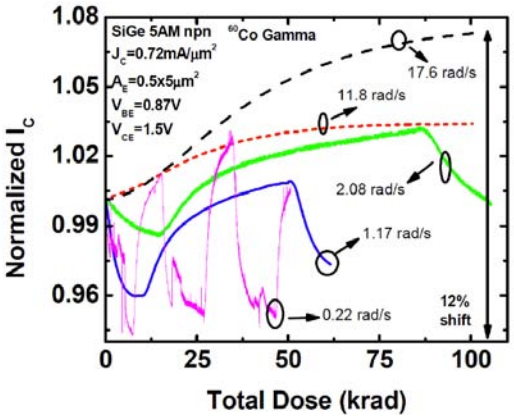

Fig. 18. Normalized collector current during gamma TID testing. Each device was forward-biased at the same VBE and VCE, and the dose rates were 17.6, 11.8, 2.08, 1.17, and 0.22 rad(Si)/s.

3.9 A Novel Device Architecture for SEU Mitigation: The Inverse-Mode Cascode SiGe HBT

We investigated, for the first time, the potential for SEE mitigation of a newly-developed device architecture in a 3rd generation high-speed SiGe platform. This new device architecture is termed the "inverse-mode cascode SiGe HBT" and is composed of two standard devices sharing a buried subcollector and operated in a cascode configuration. Verification of the TID immunity was demonstrated using 10 keV x-rays, while an investigation of the SEE susceptibility was performed using a 36 MeV ^{16}O ion. IBICC results show strong sensitivities to device bias with only marginal improvement when compared to a standard device; however, by providing a conductive path from the buried subcollector (C-Tap) to a voltage potential, almost all "collected" charge is induced on the C-Tap terminal instead of the collector terminal. These results were confirmed using full 3D TCAD simulations which also provides insight into the physics of this new RHBD device architecture. The implications of biasing the C-Tap terminal in a circuit context are also addressed.

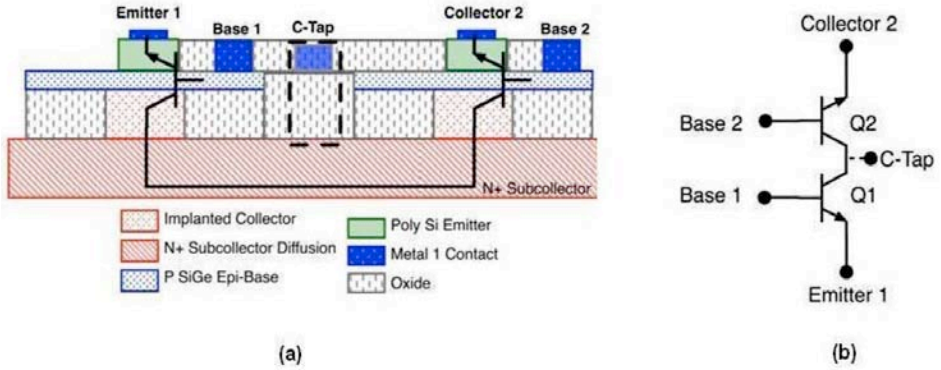

Fig. 19. (a) Cross-section of a representative inverse-mode cascode SiGe HBT device showing active layers as well as the modification needed to form the second variant ofthe device with C-Tap in addition to the (b) schematic of the inverse-mode cascode SiGe.

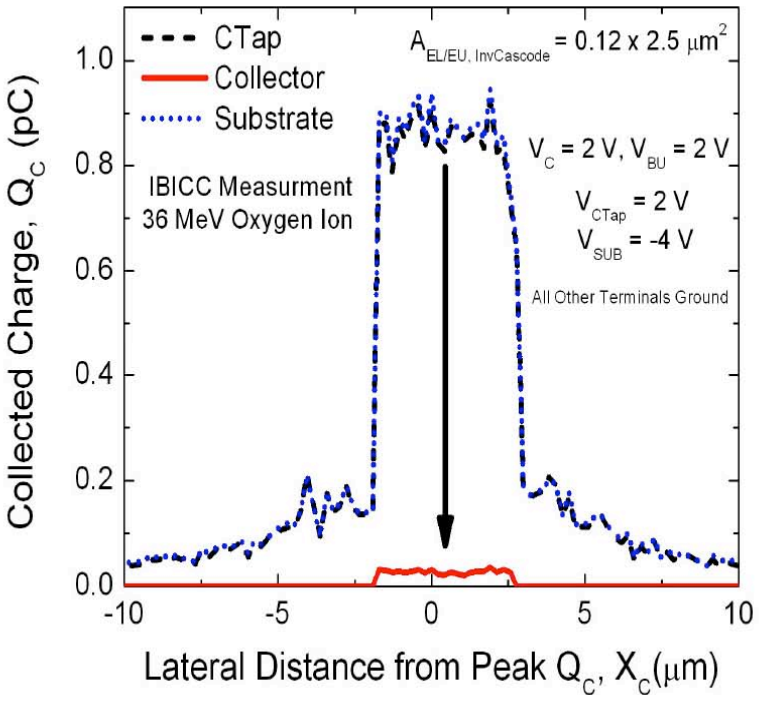

Fig. 20. Measured 2-D cut of the electrical collector-collected charge data for the inverse cascode with C-Tap showing nearly complete mitigation of charge collection on the electrical collector terminal.

3.10 Novel Total Dose and Heavy-Ion Charge Collection Phenomena in a New SiGe HBT on Thin-Film SOI Technology

We investigated the impact of 63 MeV proton radiation (up to a total dose of 2 Mrad(SiO_2)) on the AC and DC performance of a new high-performance SiGe HBT-on-SOI technology from STMicroelectronics. For the first time, we compare the radiation response of this SiGe HBT-on-SOI with that of a bulk SiGe HBT fabricated with an identical emitter-base structure. That is, the only differences between the devices are the substrate (bulk vs. SOI) and the collector doping. More importantly, the devices under study feature an innovative CBEBC layout (with off-plane base contacts), which significantly improves the AC performance. This work analyzes for the first time the impact of the novel C^BE_BC layout on both Total Ionizing Dose (TID) and SEU response. Experimental data and calibrated 3D TCAD simulations demonstrate that, in the inverse mode,

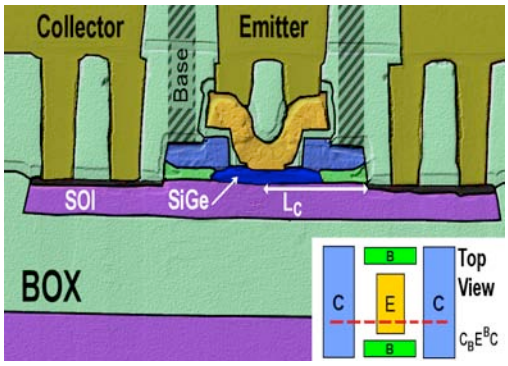

Fig. 21. Cross-sectional TEM micrograph of the SiGe HBT-on-SOI with C_BE^BC layout.

the current flow along the large oxide surface between the collector and the base can be altered by substrate bias, reducing the radiation-induced leakage. In addition, calibrated 3D TCAD simulations of heavy ion strikes in the center of the emitter indicate that the CBEBC layout is characterized by novel charge collection phenomena. Finally, for the first time, the thermal resistances (R_{TH}) of the bulk and SOI SiGe HBTs have been compared before and after irradiation over the temperature range of 300 K to 390 K, demonstrating that radiation exposure increases R_{TH} in SOI devices.

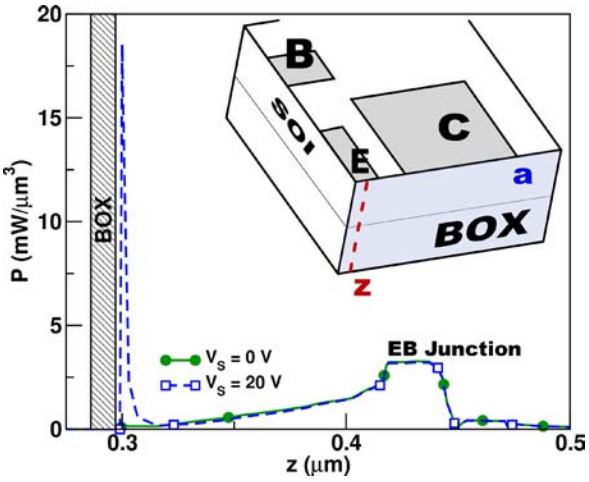

Fig. 22. 1D plots of power density in a SiGe HBT on SOI for $V_S = 0$ V and $V_S = 20$ V, along the line z indicated in the inset.

3.11 On the Radiation Tolerance of SiGe HBT and CMOS-based Phase Shifters for Space-based, Phased-Array Antenna Systems

We report the first irradiation results on high-frequency SiGe HBT and CMOS phase shifters for space- based, phased-array antennas used in radar or wireless communications systems. Both phase shifter circuits remain functional with acceptable dc and RF performance up to multi-Mrad proton exposure, and are thus suitable for many orbital applications. In addition, simulation results probing the limits of phase shifter performance in a radiation environment are presented. The CMOS phase shifter simulations show a large immunity to changes caused by increased leakage currents, while the SiGe HBT phase shifter exhibits only marginal performance degradation caused by shifts in the bias currents due to leakage in the bias networks.

3.12 Dose Rate Effects in SiGe HBTs

As an ongoing study of radiation dose rate effects in advanced SiGe HBTs, we have refined our previous results with better statistics with a large amount of data from gamma, proton, and x-ray radiation sources, with dose rates ranging from 0.1 rad(Si)/sec to 1 krad(Si)/sec. Shown below are excess base current density characteristics from 3 different radiation sources extracted from forward and inverse mode operation, respectively.

From the collapsed data, we found that the DC characteristics showed noticeable (and unexpected) dependencies on both dose rates and radiation source type. Moreover, the emitter-base (E-B) spacer

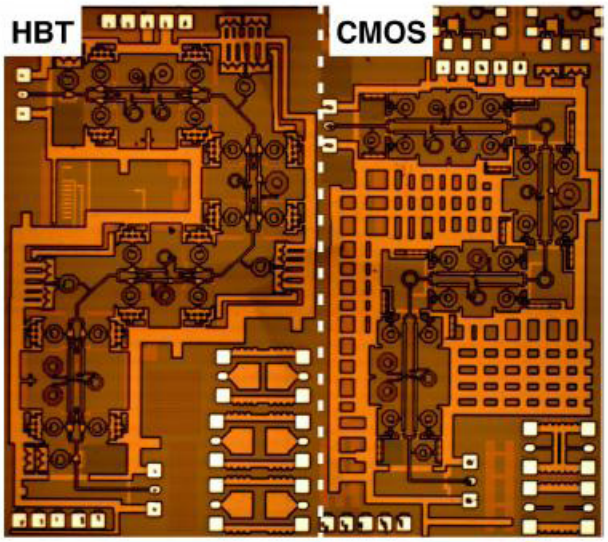

Fig. 23. Micrograph of the SiGe HBT (left) and CMOS (right) phase shifters.

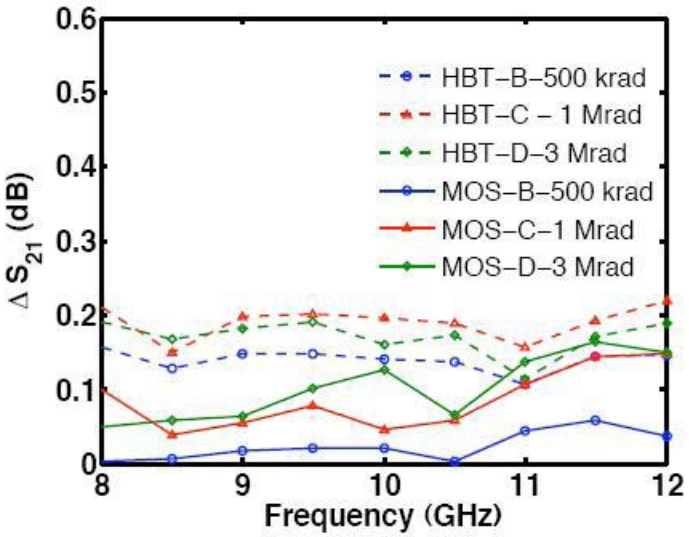

Fig. 24. Change in insertion loss between pre- and post-irradiation of 500 krad, 1 Mrad, and 3 Mrad for both MOS and HBT phase shifters.

and shallow trench isolation regions seem to react differently and do not provide a good correlation with macroscopic dose and/or dose rate from different sources. Therefore, as suggested in our previous report, microdosimetry effects in SiGe HBTs are being examined, with the possibility of non-equilibrium conditions in the secondary electrons resulting from interactions with created photon field. We have found that the x-ray dose-rate trends are qualitatively consistent with the observed inverse-mode ΔI_B; that is, increasing the x-ray dose rate yields a considerably larger inverse-mode noise power spectral density. We attribute the dose enhancement effects observed from x-ray irradiated devices to photon interaction with Cu/W metallization and these results show a good qualitative agreement with GEANT4 –MRED simulations on SRAMs (conducted by Vanderbilt). It should be noted that the E-B spacer is a complicated oxide nitride composite stack, whereas the STI is a CVD oxide deposited in an RIE etched trench – ie, fundamentally different in composition and hence potential radiation response. These types of films can trap both

electrons and holes, depending on the processing conditions, the radiation dose and source, and the radiation bias condition. We conclude that fundamental differences exist in a manner by which the local recombination rates in the E-B and STI interface regions demonstrate a differing response to the radiation type and dose rate. For instance, charge trapping in the STI may effectively "push" the spatial recombination rate peak away from the STI region and into the bulk Si of the CB junction, where x-rays do not change recombination rates, but protons (and gamma rays) may. In this scenario, the x-ray response of the device would "appear" to be decreased with respect to the proton/gamma response. We are continuing to probe these mechanisms via calibrated TCAD simulations.

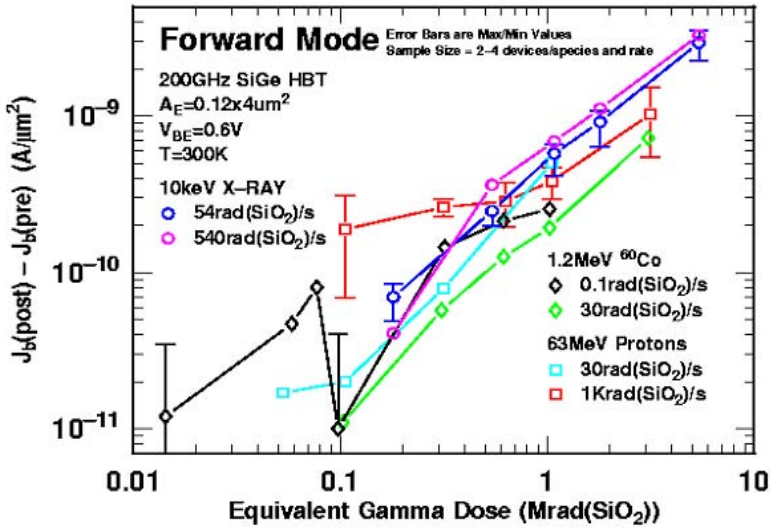

Fig. 25. Forward mode ΔJ_B for proton, gamma, and X-ray as a function of equivalent gamma dose.

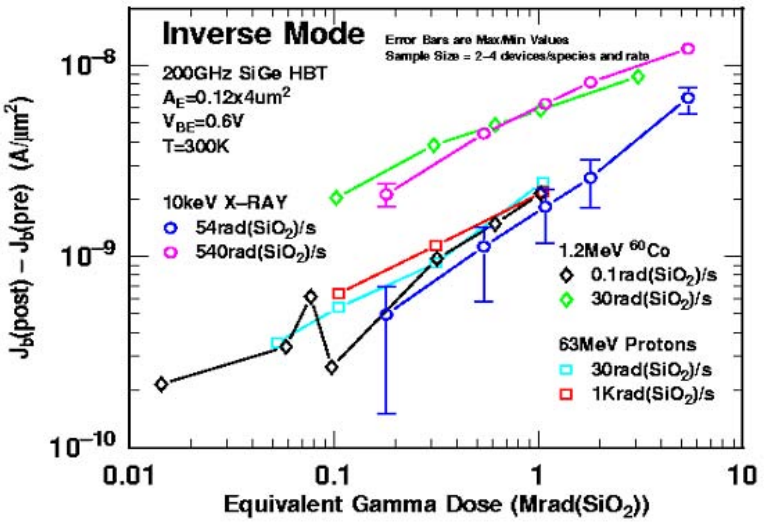

Fig. 26. Inverse mode ΔJ_B for proton, gamma, and X-ray as a function of equivalent gamma dose.

3.13 Investigations of Cryogenic Radiation Effects in SiGe HBTs

Cryogenically-operated devices simultaneously exposed to irradiation is a newly emerging topic special interest to NASA's Lunar and Martian robotics and human exploration missions as well as DoD for orbital space systems. To investigate total dose effects in SiGe HBTs at cryogenic temperatures, we have irradiated SiGe HBTs from both IBM 1st generation (5AM) and 3rd generation (8HP) technologies at 77K with 63 MeV protons, and measured the DC characteristics at both 77K and room temperature. Shown below are the forward Gummel characteristics from both 8HP and 5 AM HBTs, respectively, irradiated at 300K and 77K.

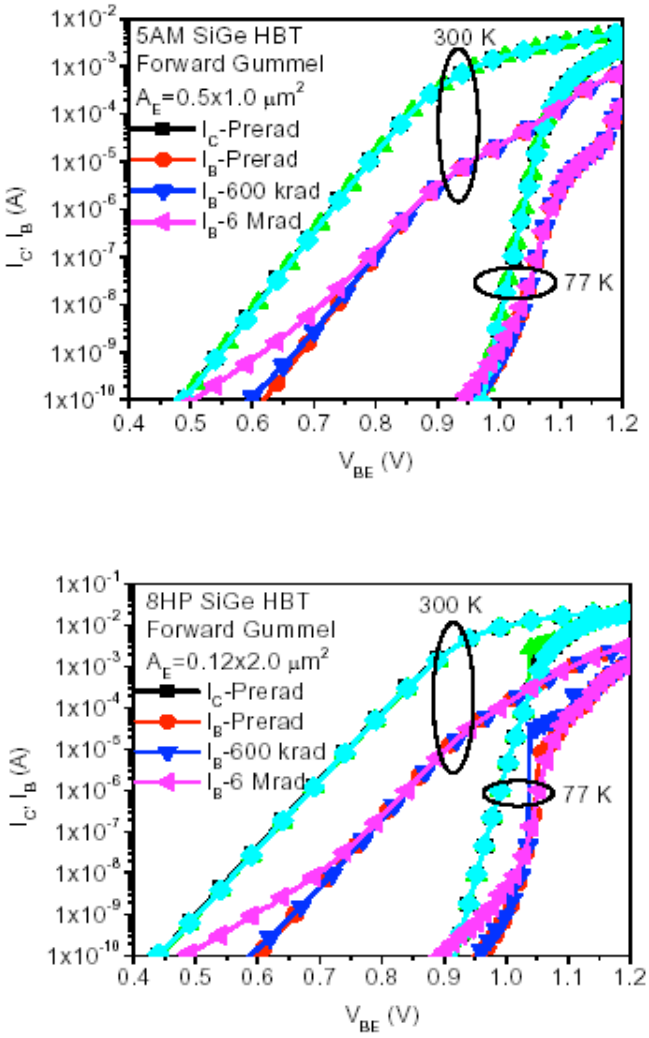

Fig. 27. Forward Gummel characteristics of 5AM and 8HP SiGe HBTs, respectively, from proton radiation performed at room temperature and 77K.

3.14 Advanced Simulation Tools for Radiation Effects

The Florida Object Oriented Device Simulator (FLOODS) is a general purpose device simulation tool built that is capable of 1, 2, and 3 dimensional simulation. In the past it has been used to simulate SiGe RF bipolar devices, noise in advanced CMOS structures, GaN chemical sensors, and infrared detectors. It can handle a wide variety of device types because the governing physics is not hard-coded. The user can define scripts in a simple language, alagator, that describes the governing equations for the system. This makes it relatively straightforward to handle different physical situations out of the mainstream of CMOS logic devices.

We have been enhancing FLOODS to handle SEU simulations. This has included activity in both the numerical and physical approximations. The numerical approximation work has centered around trying to create simpler three-dimensional adaptation during simulation. SEU problems deposit a large charge that requires fine grid spacing and then diffuses away, which reduces the grid requirement. In addition, automatic simulation of thousands of events requires the grid to adapt to the charge distribution automatically. On the physical modeling side, we have focused on mobility updates and work on hydrogen modeling.

3.15 Numerical Enhancements

The major immediate issue was enabling transient simulation. FLOODS had been developed primarily for DC and AC small-signal simulation, both of which are inappropriate for SEU simulation needs. FLOODS was enhanced to include transient simulation using the TRBDF2 method. TRBDF2 has been used in device and process simulators for over twenty years. The method is A-stable and includes techniques to automatically adapt the time step size based on local truncation error. Algorithms already existed inside alagator to do TRBDF2, but these needed to be connected to the device command and contact specifications.

We also explored parallel processing, although the results did not appear to be promising. We completed a port to an IBM cluster under the AIX operating system. One of the linear algebra packages in FLOODS does have parallel compute capability and we enabled that and create a threaded version of FLOODS. The alagator scripting language is coded to take full advantage of modern pipelined processors. Operators are applied to vectors of results from multiple elements at once. Precomputation and storage of results is already enabled to prevent redundant calculations. For small-scale parallelism, we can subdivide the problem physically. One processor can assemble Poisson's equation, another can assemble electron continuity, and so on. Depending on the modeling complexity, this efficient for up eight processors. Breaking the assembly this way is attractive because there are very few memory overlap issues. The code is already structured in some ways to take advantage of this type of parallelism. However, our work here was only able to provide a factor of 2 improvement on a four processor system.

The set of coupled, time-dependent partial differential equations that govern semiconductor device behavior are usually expressed as Poisson's equation and drift-diffusion continuity equations for electrons and holes. These expressions are normally evaluated in a numerical device simulator using Scharfetter-Gummel (SG). The SG approach is very stable, but it has the limitation the current is not defined continuously. For most simulations, this is not an issue as a grid can be constructed that has edges aligned with the current flow. This is not possible in the case SEU, because particle current can be generated anywhere in the device from a radiation strike. A change of variables can

allow the particle currents to be expressed in terms of the quasi-fermi levels and then this can be discretized directly. This approach allows the current to be defined continuously over space.

Our work on this problem shows that the quasi-fermi level approach works well and often offers a computational advantage over the SG approach. For some cases, a 30% improvement in performance could be noted for the quasi-fermi level approach and only rarely did this ever exceed the SG computation time. Solution accuracy was equivalent for equivalent grid spacings in the simulation.

We have also developed a nested grid scheme that is specific to SEU simulation. After a radiation strike, we know that the peak carrier concentration exists at that time. From there on time, the carrier concentrations only reduce. As the carrier concentration reduces, we can also reduce to a coarser grid. Figure 28 shows our scheme, which requires successive grid refinement along the particle strike at time zero. Multiple passes at grid refinement are used and each pass is stored for future reference. As the carrier concentration spreads and the peak reduces, each prior refinement is used in turn. So the grid eventually coarsens back to the original structure. Figure 29 shows what the grid looks like after three levels of refinement.

Figure 30 shows the computation result of this process. The vertical scale represents error as measured by the change in the total collected charge. The horizontal scale represents the simulation CPU time normalized to the fastest simulations. As expected, the blue line for the uniform grid shows that error increases and CPU time decreases as the grid is reduced. Uniform grids are rarely used, so the green line represents our best attempt at generating a custom grid. The red line represents results from the adaptive grid scheme. The same level of collected charge accuracy can be obtained with an order of magnitude less CPU time.

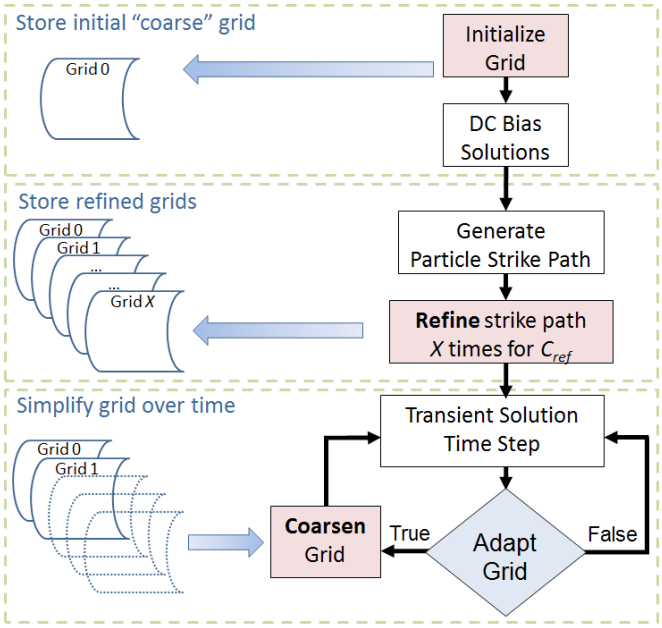

Fig. 28. Proposed grid refinement algorithm.

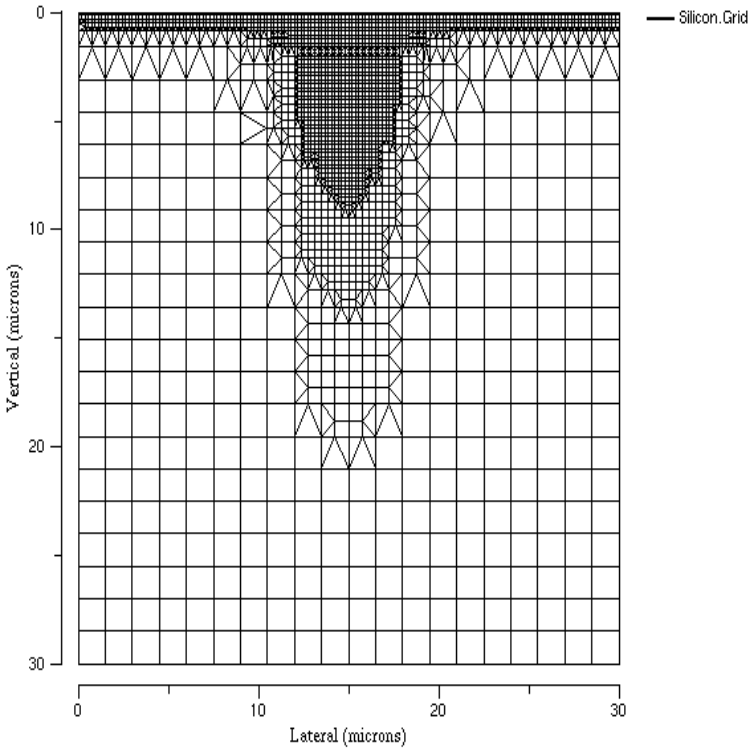

Fig. 29. Adaptive grid at peak refinement level (X=3) for the N+/P diode simulations.

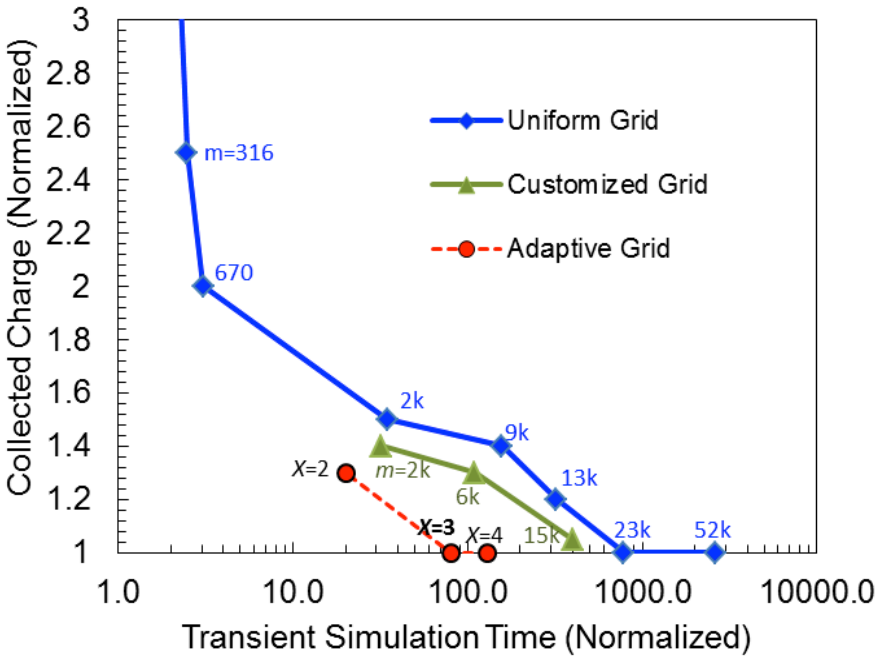

Fig. 30. nMOSFET SEU results. The number of *m* grid points is given next to each data point. The results were normalized and a value of 1.0 on both scales represents the optimal result.

3.16 Physical Model Enhancements:

Most of our work on the physical side focused on improvements in mobility modeling for SEU simulation. There have been three main areas – improved handling of piezoresistance changes, carrier-carrier scattering, and a unified approach for mobility.

Advanced devices have built-in mechanical strain to enhance channel mobility. This is easy to model for a MOSFET, because the primary current path is fixed along the silicon / oxide interface. The strain can be computed here and a mobility enhancement computed for the channel based on the strain. This approach will not work for SEU, because current flow can be in arbitrary directions. In addition, the strain changes over the device structure significantly so current flow generated well below the surface by the strike cannot use the channel strain to estimate mobility.

We have implemented the entire piezoresistance matrix and related the changes in mobility to both the local strain and current flow direction. This couples more easily with the quasi-fermi level approach with finite elements, because the basis function for computing current and mechanical strain are identical and easy to map on to each other. In the general case, we use the gradient of the quasi-fermi level to get the local current direction. This is then mapped to appropriate crystallographic directions and transformed geometrically to a piezoresistance change which is implemented as a change in the carrier effective mass.

Figure 31 shows a comparison between experiment and simulated collected charge as a function of applied strain to the device In this experiment, p-n diodes were used as the collector and charge was generated from a laser strike. The wafers were bent externally using a calibrated four-point bending jig. Therefore the strain was able to be varied independent of changes in the device structure. Collected charge varies with the applied strain nearly linearly. Simulation of the strain influence on mobility correlated well with the observed experimental results.

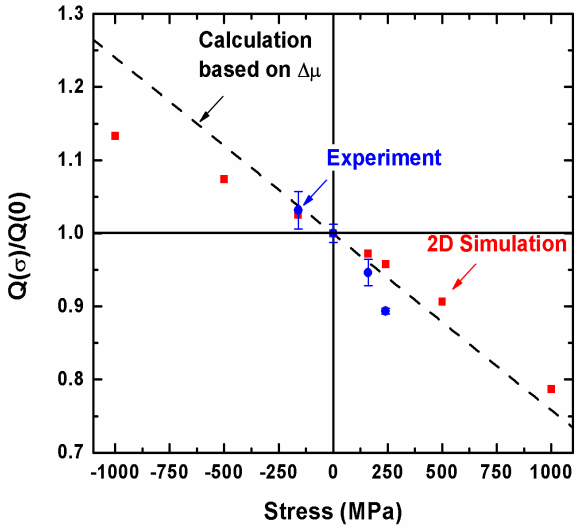

Fig. 31. Collected Charge from experiment and simulation as function of externally applied strain.

One advantage of simulation is that it can predict effects beyond those that can be reached experimentally. Figure 32 shows the simulated current spikes at a wide range of strains, beyond what can be reached with the four point bending jig without breaking the samples. The change between 1 GPa of compressive stress to 1 GPa of tensile stress results in about a 70% change in the peak current value. 1GPa is typical of stress being used in advanced strain engineered device structures.

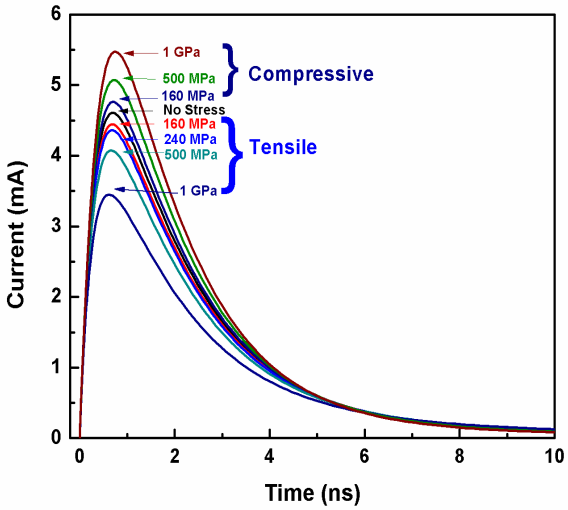

Fig. 32. Simulated laser-induced current transients as a function of <110> uniaxial mechanical stress.

On the physical side, we have implemented Klaassen's mobility model that includes terms for minority carrier scattering. These are important and can be controlling for SEU event simulations. During our work, we discovered that the Klaassen's mobility model does not account for carrier-carrier scattering at high carrier concentrations accurately. This is, of course, the exact condition that a SEU simulation faces.

We added a carrier-carrier scattering term to the Klaassen model for simulation of SEU. Figure 33 shows the effect of carrier-carrier scattering and compares models to experimental. As previously discussed, the Klaassen / Philips model highly overestimates mobility at electron-hole levels over 10^{17} cm^{-3}. In contrast, the Dorkel-Leturcq model uses a similar approach to carrier-carrier scattering as the proposed model. The Dorkel-Leturcq model fits well for lower carrier concentrations but at higher level begins to under predict mobility. Another issue is that at high-injection levels of more than 5×10^{19} cm^{-3}, the Dorkel-Leturcq model predicts a negative mobility. Our new model fits this region quite well.

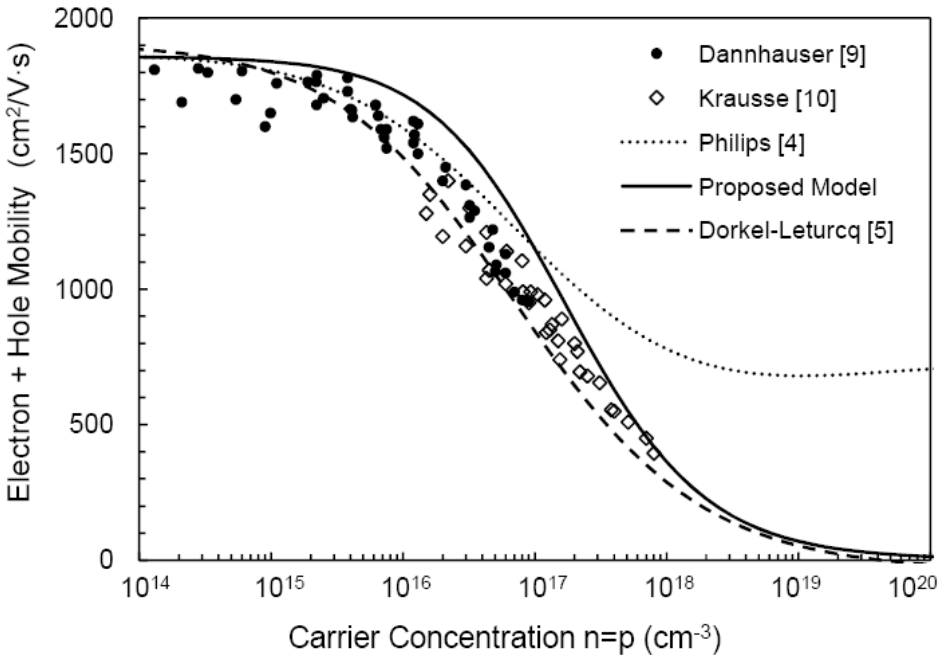

Fig. 33. Sum of electron and hole mobility as a function of carrier concentration at 300 K versus experimental data. Symbols represent experimental data.

This model, however, does not handle bipolar high injection conditions accurately. It should only be used for SEU cases. Recently, we have developed a new, unified mobility approach to address this short-coming. This paper is in preparation and should appear shortly.

3.17 Advanced Dielectrics

X-ray absorption and photoemission spectroscopy, XAS and XPES, measurements performed at SSRL have been used to obtain the conduction band edge and O-vacancy defect states for the second and third row TM oxides, (i) ZrO_2 and Y_2O_3 and (ii) HfO_2, respectively. For the first time many-electron charge-transfer multiplet (CTM) theory has been extended to interpretation of O K edge spectra. A related multiplet approach, based on Tanabe-Sugano energy level diagrams, has also been applied, again for the first time, to a d^2 model for O-atom vacancy defect features in the O K pre-edge regime.

O K spectral assignments have generally been based on density of state comparisons that neglect final state effects due to O atom 1s state core holes. Similarly, theoretical studies for O-vacancy defects in HfO_2 and ZrO_2, also based on density functional theory (DFT) have not taken proper account of the strongly correlated nature of TM-atom d-states. Resulting defect state energies are inherently flawed with serious errors in interpreting defect state energies in spectroscopic ellipsometry (SE). A self-consistent interpretation, based on the new approaches for O K edge and defect states demonstrates how these two studies can be combined to correctly assign SE defect state energy relative to conduction band edges. CTM theory is applied to $M_{2,3}$ and O K edge XAS for nano-grain thin film ZrO_2, and the O K edge XAS of HfO_2. Tanabe-Sugano diagrams have been used to assign spectral features in O K edge spectra to O vacancy defects using the d^2 occupancy model.

There has been considerable interest in Ge substrate channel regions for applications in scaled complementary MOS (CMOS) devices, particularly for p-MOSFETs. Many studies have attempted to use Ge native dielectrics such as GeO_2, GeON and Ge_3N_4 as interfacial transition regions (IRTs) between a Ge substrate and a high-K dielectric. In general, p- channel metal oxide semiconductor field effect transistors (p-MOSFETs) fabricated on Ge with Ge-based ITRs and high-K dielectrics such as HfO_2 and ZrO_2 have yielded acceptable levels of performance for integration into scaled CMOS with interfacial trap densities in the mid 10^{11} cm^{-2} range.

In contrast, our previously reported study of n-MOS capacitors (n-MOSCAPS) with a n-Ge/GeO_2/SiO_2 gate stack structure displayed interfacial charge densities > mid 10^{12} cm^{-2}. More recently, n-MOSFETs with Ge_3N_4 and GeON ITRs, and high-K dielectrics have been essentially *written off technology roadmaps* because of high defect densities, >5x10^{12} cm^{-2} at the Ge/gate dielectric interface. None of these studies has identified the source of trapping, e.g., a dangling bond or other intrinsic bonding defect.

This work focused on an alternative approach based on spectroscopic evaluation of Ge surface preparation and remote plasma enhanced chemical vapor deposition (RPECVD) of GeO_2. This process is qualitatively similar to previous studies by our group which first identified a pathway to producing device quality deposited SiO_2. This approach is based on a processing protocol that ensures separate and independent control of interface and bulk properties. The GeO_2 films prepared in this way represent a break-through in technology that will have a significant impact on radiation hard devices. Continuing support for this research by DTRA and the NSF will complete the evaluation process, with test devices and radiation stress studies.

3.18 XAS studies of Gate Dielectrics

A. Background and Research Issues

Soft X-ray (or vacuum ultra violet, VUV) absorption and photoemission spectroscopies (XAS and XPES) have been used to study conduction band edge, and O-vacancy defect states in ZrO_2 and HfO_2. XAS studies were performed at the Stanford Synchrotron Research Lightsource (SSRL). Hund's rules apply for strongly correlated d-state occupancy in O-vacancy defects so that Tanabe-Sugano diagrams for d to d' transitions can be used to describe the excited states of these defects. This includes negative ion states that act as electron traps. Density functional theory (DFT) studies of O-vacancy defects in HfO_2 and ZrO_2 have previously been applied to the electronic states of these defects. These calculations assumed that two electrons associated with the vacancy are distributed on the transition metal, Hf and Zr, d-states bordering the vacancy in a way that was not consistent with Hund's rule occupancy, yielding doubly occupied ground and negative ion states. This has lead to quantitative errors in interpreting defect state energies in spectroscopic ellipsometry (SE) studies, and in applying results to electrical measurements, as well. Tanabe-Sugano energy level diagrams in this report in Fig 34 are applied to an *equivalent d^2 state* model for O-vacancy defects in the O K pre-edge regime providing a correct assignment for SE features and their relationship to electronically active traps.

B. Conduction Band Edge States

O-vacancy defect states are introduced into the forbidden energy gap, and as such their energies relative to conduction and valence band edges are important for identifying the energies of electronically active hole and electron traps relative to these band edges. Doubly occupied defect

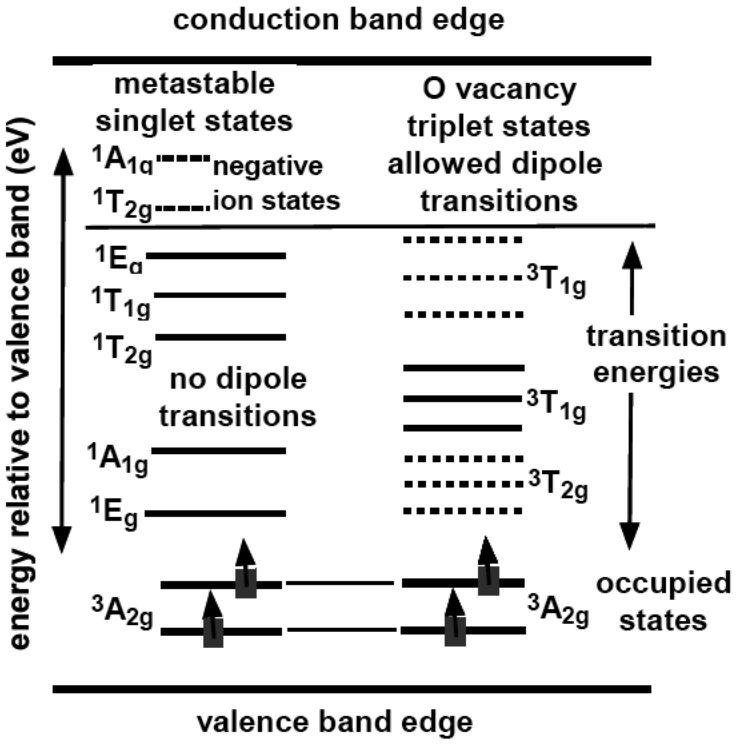

Fig. 34. Energy level diagram for O-vacancy defects, constructed from Tanabe-Sugano diagram for a d^2 occupancy.

states have previously been identified at the valence band edge for TiO_2, ZrO_2 and HfO_2 using XPES spectroscopy. The excited states of these defects have been detected by second derivative analysis of pre-edge of O K edge XAS spectra, but have not as yet been addressed quantitatively using a many-electron theory approach.

Charge transfer multiplet (CTM) approach is applied for first time applied to O K edge spectra for nano-grain thin film ZrO_2 and HfO_2, the most important aspect of this illustrated in Fig. 35 for ZrO_2. This approach takes into account a localization of the O K edge core hole, and a coherent process in which this is filed from O-atom 2p π states in the valence band. For ZrO_2, this coherent excitation process yields a final O $2p^5 4d^1$ state that has the same symmetry as the $M_{2,3}$ final states. Consider first $M_{2,3}$ feature spin-orbit splitting. For the Zr $M_{2,3}$ spectrum this is the Zr 3p spin orbit splitting of ~13 eV. For the O K edge states, the corresponding spitting of ~10 eV is between O 2p σ-bonding and π-bonding/non-bonding valence band states as indicated in Fig. 33. For purposes of this section of the report that focuses on O-atom vacancies, this approach to conduction band edge states provides a way to correlate the energies of excited O-atom vacancy and negative ion states with the band edge Zr 4d and Hf 5d E_g states, and as such with effective band edge energy for alignment of states $Zr(Hf)O_2$-Si interfaces. This aspect of CTMs for O K edge features and its relationship to SE and electrical measurements will be addressed in more detail elsewhere.

C. Spectroscopic Studies of O-vacancy States

Figure 36 includes O K edge - pre-edge spectra for 5 nm thick films of HfO_2, and cubic Hafnia with Y atoms substituted on~ 15% of the Hf sites. The +3 charge of each Y atom is compensated by an O-atom vacancy that is part of the host crystal electronic structure and does not contribute localized

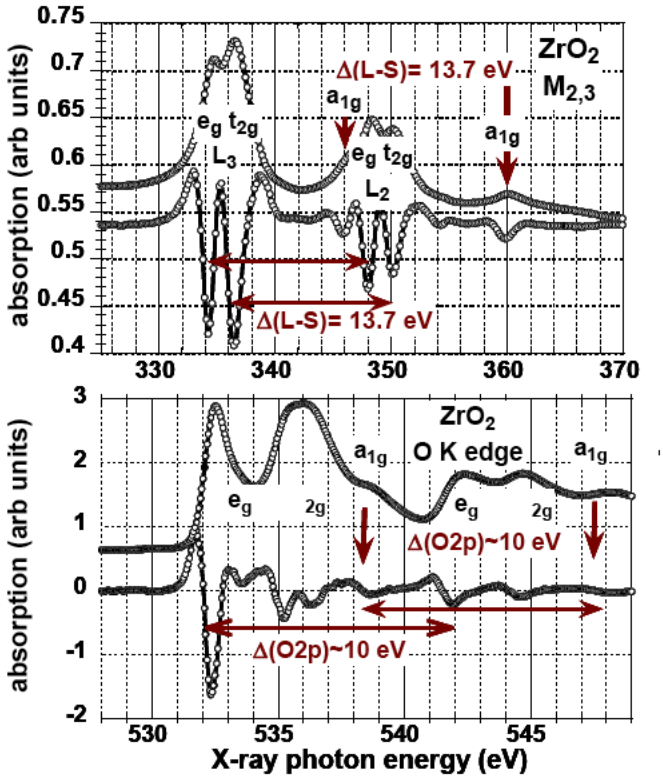

Fig. 35. M and O K traces and 2nd derivative for nano-grain ZrO_2. Symmetries, and spin-orbit and O 2p splittings are shown.

defect states with d-d' transitions, including negative ion states. The ground state symmetry for the d^2 configuration in 8-fold cubic symmetry is the same as the d^8 symmetry for 6-fold octahedral symmetry. This ground state is an "s-like" or one-dimensional triplet state, $^3A_{1g}$. Based on the appropriate Tanabe-Sugano diagram energy levels in Fig. 34, the allowed optical transitions are to "p-like", $^3T_{1g}$ and $^3T_{2g}$ states as indicated in the diagram. The negative ion states are $^1A_{1g}$ and $^1T_{1g}$, and these can be occupied by electron injection from the conduction band and contribute to trap-assisted tunneling (TAT) observed in both HfO_2 and ZrO_2 films that are thicker than 3-5 to 4 nm [1]. TAT is suppressed in films thinner than ~ 2 nm.

The unit cell, and extended unit-cell symmetry in the tetragonal HfO_2 is higher than that in the compositionally averaged alloy structure of cubic Hafnia, and this is reflected in the differences in symmetry of the respective $^3T_{1g}(P)$ structures in Fig. 36. The three features in each symmetry designated d-d' transition is a manifestation of the 3-fold degeneracy.

The symmetry of the same three features in monoclinic HfO_2 with a seven-fold coordinated Hf is significantly reduced. There is an increase in the number of features for d-d' transitions to 14 from 9 in tetragonal HfO_2. This is due to singlet-triplet mixing, and is present for negative ion states as well

D. Summary of Significant Results

(a) The conduction band states observed in O K edge X-ray spectroscopy have the same relative energies as those observed in SE, and cannot be interpreted as a joint density of states as originally proposed.

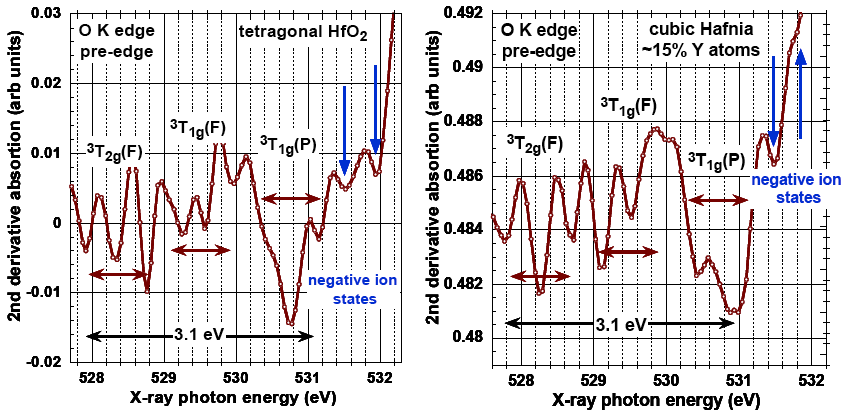

Fig. 36. O K pre-edge spectra for d-d' dipole allowed transitions and dipole forbidden negative ion states: (right) in tetragonal HfO_2, and (left) cubic hafnia.

(b) The Zr $M_{2,3}$ spectrum, and O K edge spectrum of both ZrO_2, as well as the $L_{2,3}$ spectrum and O K edge of TiO_2 must be analyzed in terms CTM theory, contrary to the previous model proposed.

(c) In this report O-vacancy defects are described by a theory that takes proper account of Hund's rule occupancy, and therefore DFT theories used previously are not valid. The energy levels of the d- d□ transitions from the d_2 ground state, and negative ion states as well are obtained by application of Tanabe-Sugano energy level diagrams.

(d) Differences in the band edge symmetry between non-crystalline SiO_2 and HfO_2 account for absence of trap-assisted tunneling.

(e) Gd_2O_3 and Lu_2O_3 display similar pre-edge O-vacancy defects in their O K edge spectra. The as-deposited Lu_2O_3 spectra is included in Fig. 37

3.19 Conduction Band Edge Excitonic States and Electron Trapping in Dielectrics

A. Introduction

The performance and reliability of a gate dielectric, (i) non-crystalline SiO_2, Si_3N_4, a Si Oxynitride alloy, or (ii) a high-$\varkappa$ transition metal oxide are determined by band edge intrinsic bonding states, intrinsic bonding defects and macroscopic strain. This final report identifies significant differences between band edge excitonic states in (i) SiO_2, and (ii) Si_3N_4, and Si oxynitride alloys, $(Si_3N_4,X(SiO_2)1\text{-}X$. These provide an explanation for differences in trapping and trap-assisted (TAT). Differences between symmetries of band edge states in SiO_2 and transition metal oxides also explain differences in TAT injection from negatively biased n-type Si substrates.

A connection between (i) strain-reducing medium range order (MRO), and (ii) nano-scale separation into hard-soft mixtures in non-crystalline SiO_2 is explained by many-electron theory applied to Si-atom "d-like states". These states participate in and O pπ to Si dπ back-donation of electrons, yielding shortened Si-O bond-lengths and MRO atom-pair correlations. These bonding interactions specifically identify a coherence length of ~1 nm associated with hard 6-member rings/ring segments encapsulated by compliant or 5- and 7-member rings/ring segments into a nano-grain hard-soft nano-structure, reducing macroscopic strain and giving SiO_2 unique reliability properties.

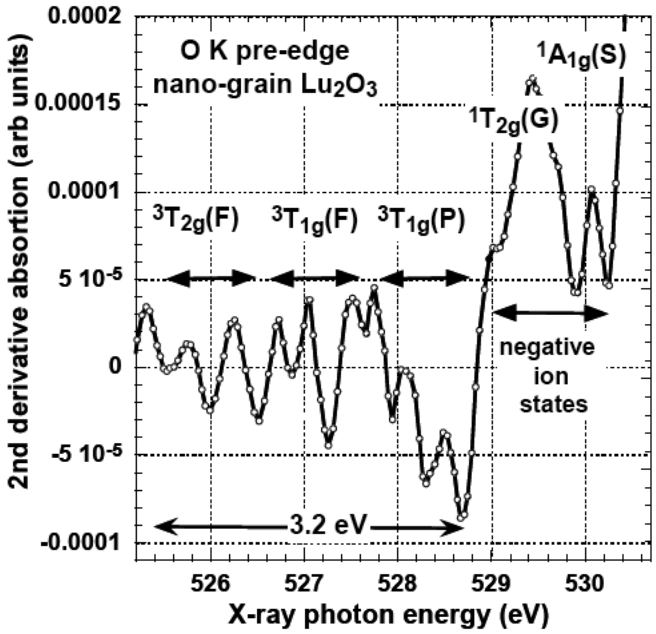

Fig. 37. O-vancancy states in the pre-edge spectra of nano-grain Lu_2O_3.

B. Experimental Procedures

Five nm thick films of SiO_2, Si_3N_4, and Si oxynitride alloys were remote plasma deposited on nitrided superficially oxidized Si(001). These films were annealed in Ar at a temperature of ~950°C. Si $L_{2,3}$, and O and N K edge spectra were obtained by X-ray absorption spectroscopy (XAS) at the Stanford Synchrotron Research Lightsource (SSRL).

C. Experimental Results

Figure 38 compares the Si $L_{2,3}$ spectra of non-crystalline SiO_2 and crystalline Si. The band edge states in these two materials that comprise the Si-SiO_2 interface are "s-like" non-degenerate 2A1g states. Figure 39 is the 2nd derivative spectrum of the band edge states in non-crystalline, thin film plasma deposited SiO_2 that has been annealed at ~950°C. There is a one-to-one correspondence between the energy differences in eV units of band edge states as determined by visible and vacuum UV spectroscopies, and in the O K edge spectra. An X-ray energy of 529.25±0.1 eV corresponds to an energy of 8.9 eV for the band-gap of non-crystalline SiO2. In order of decreasing X-ray energy, and as marked in Fig. 39, the features in the O pre-edge derivative spectra correspond to: i) the band-gap, Eg, ii) two bound excitons, E_2 and E_1, iii) negative ion states between 529.1 and 527.4 eV, and iv) four intra-d state transitions for the O-atom vacancy defect represented by a high-spin d^2 state. The symmetries of these states are identified using the Tanabe-Sugano diagrams. The combination of the localized $^2A_{1g}$ excitonic states at the SiO_2 band edge, and the $^1A_{1g}$ and $^1T_{2g}$ symmetries of unoccupied negative ion states of O-vacancy defects does not support dipole allowed fast radiative decay into negative ion states. This explains why TAT processes have not been reported for negatively biased n-type Si in Si-SiO_2 gate stack structures. In contrast, the symmetries of band edge ZrO_2 and HfO_2 states allows tunneling injection to the negative ion states of O-vacancy defects. This explains the TAT processes initiated by electron injection from n-type Si substrates that have been reported for ZrO_2 and HfO_2 MOS structures.

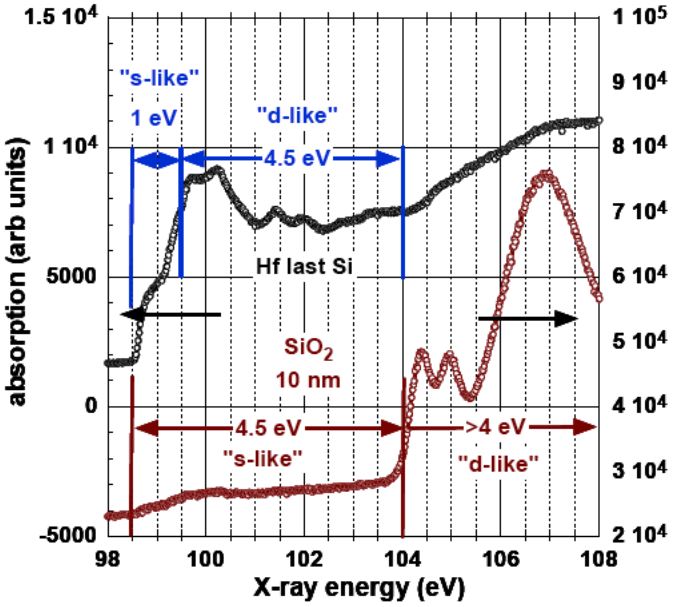

Fig. 38. $L_{2,3}$ spectra for c-Si and nc-SiO_2.

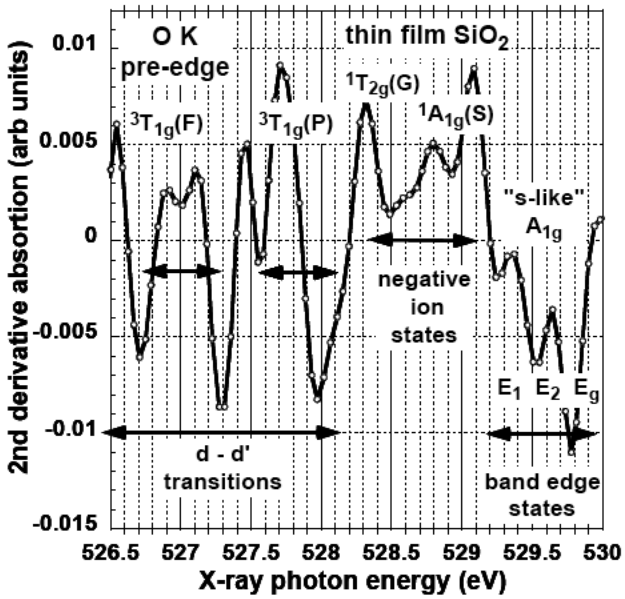

Fig. 39. Pre-edge O K spectra for nc thin film SiO_2.

Figures 40 and 41 indicate respectively, (i) O K band edge, and pre-band edge states of non-crystalline Si_3N_4,, and expanded scale plots of the negative ion states of (ii) Si_3N_4,and (ii) a $(Si_3N_4,0.5(SiO_2)0.5$ Si oxy-nitride alloy that has been used as alternative gate dielectric in the first eight to ten years of the 21st century. There is a significant qualitative difference between Fig.39 for SiO_2 and Fig. 40 for Si_3N_4, that is related to the difference in the number of p electrons in the ground states of O- and N-atoms, four for O, and five for N. This correlates with the singly occupied 2pπ state that gives rise to sharp spectral feature at 400 eV in Si_3N_4,, and Si oxynitride alloys including compositions both SiO_2-rich and Si_3N_4,-rich as well. It is significant to note that the final state for the N-atom "pπ

to pπ*" transition is at an energy that is between the band edge excitonic states of Si_3N_4, and Si oxynitride alloys, and the negative ion states associated with N-vacancy defects in these dielectrics.

This difference in the ordering of electronic states manifests itself in Si_3N_4 dielectric thin films by promoting TAT and/or Poole-Frenkel transport. The final state symmetry of the N-atom pπ to pπ*

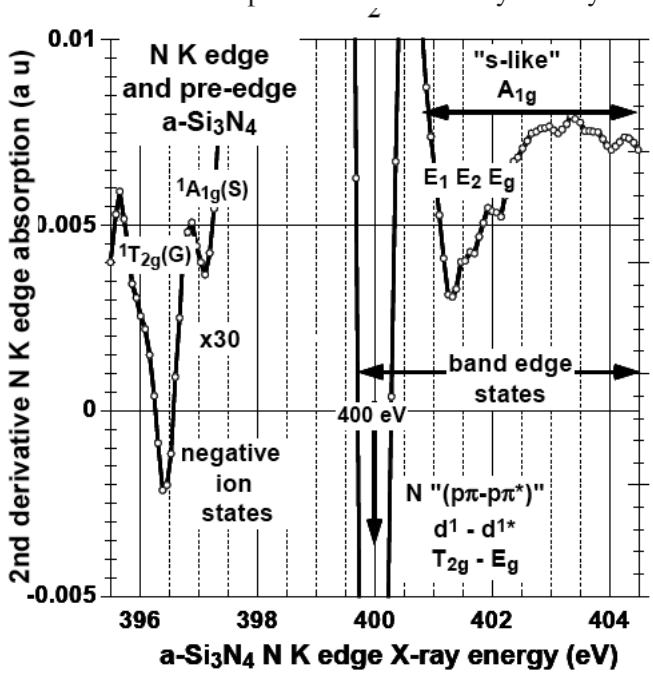

Fig. 40. N K edge and pre-edge spectra - Si_3N_4.

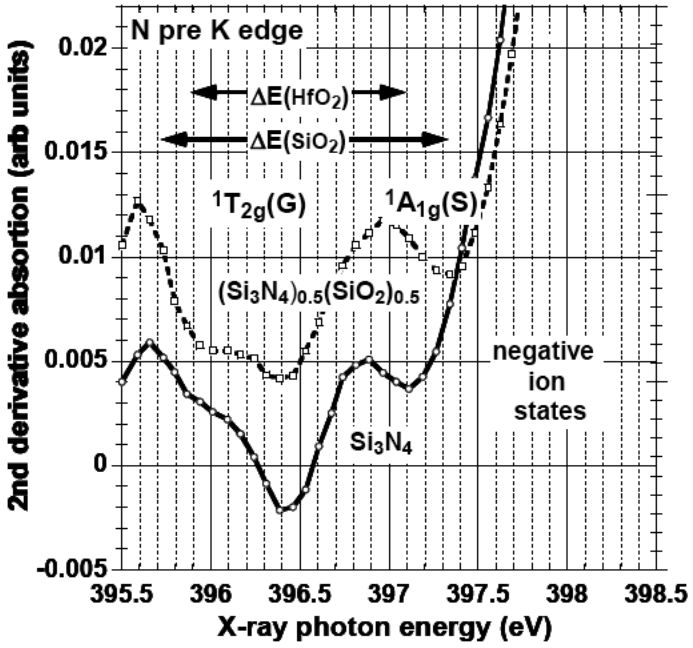

Fig. 41. Expaded x-axis for N K pre-edge spectra for Si_3N_4 and Si oxynitride alloys.

transition provides a transport channel between the "s-like" symmetry of the band edge states, and the even symmetry of the negative ion states. In addition, it is likely that this state plays a role in the Negative Bias Temperature Instability, NBTI, that is much stronger in N-containing dielectrics than SiO_2.

Finally, Fig. 42 presents the O K pre-edge spectra of $(SiO_2)_{0.3}(HfO_2)_{0.3}(Si_3N_4,)_{0.4}$, or HfSiON334. The three relative sharp features between 530.2 and 531.5 eV and associated with band edge states of SiON alloys as indicated in Figs. 39 and 40. The lower eV features in this figure, are associated with O-vacancies with Hf neighbors, as represented by a d2 state. The symmetry designations, and spectral width of these states are very nearly the same as the defect states for O-vacancies in HfO_2 as displayed in Fig. 37. The SiON band edge states overlap the negative ion states of the O-vacancy defects. They are on different atoms, and the density of the HfO_2 negative ion states is at least three orders of magnitude smaller than the SiON states. This assignment is supported by the results in Fig. 43 which indicate that the conduction band edge states in the HfSiON334 alloy are those displayed in Fig. 42 and designated there as Si band-edge "s-like", one dimensional A_{1g} states. This overlap explains why this current-voltage studies of gate stacks with this alloy do display TAT, and why the response to X-ray stress is essentially the same as that of SiO_2, in particular there is no build up of negative space charge since the negative ion states are not accessible due to overlap in energy that has been used to explain the spectral data in Fig. 42.

D. Summary of Significant Results

The different symmetries of $^2A_{1g}$ excitonic states at the SiO_2 band edge, and O-vacancy $^2A_{1g}$ and $_1T_{2g}$ unoccupied negative ion states effectively prevents injection into these negative ion states suppressing trap-assisted tunneling (TAT). The combination of symmetries of ZrO_2 and HfO_2 band edge states allows TAT for electron injection from n-type Si substrates. The differences in O and N-atom p-states (4 compared with 3) results in a N-atom pπ to pπ* transition sandwiched between the "s-like" symmetry of band edge states, and the even symmetry of N-vacancy negative ion

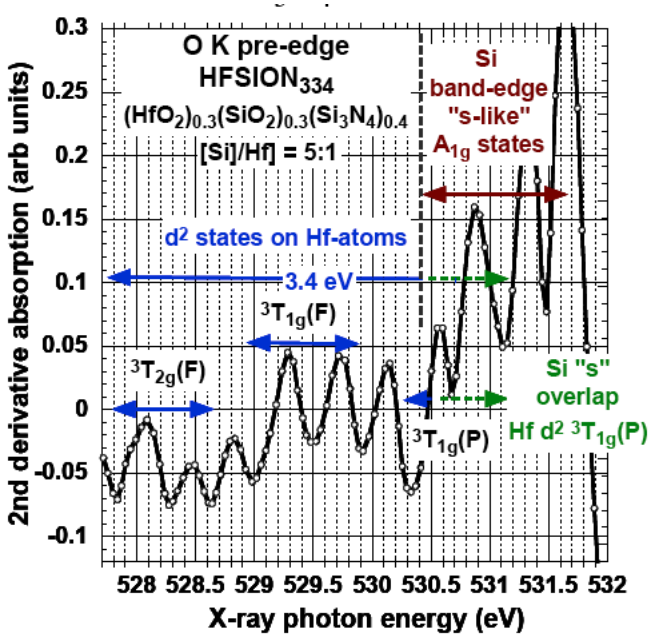

Fig. 42. O K pre-edge spectra - $SiOn_{334}$.

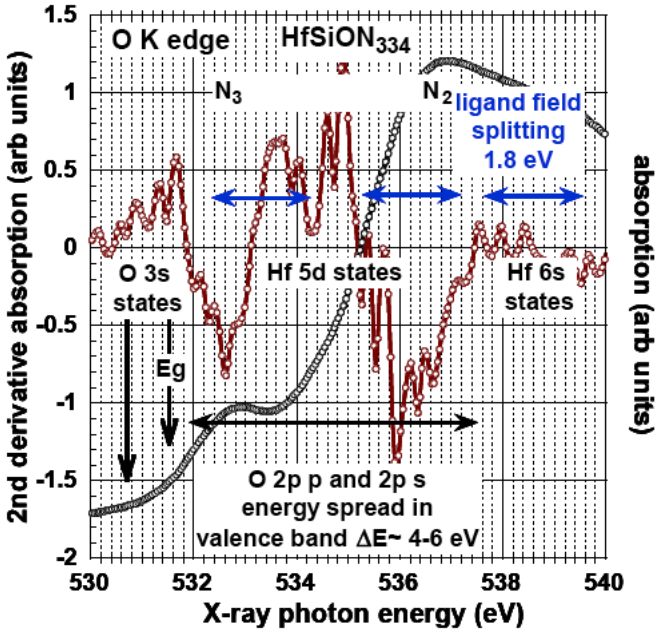

Fig. 43. O K edge and pre-edge $SiOn_{334}$.

states. This provides a "pathway" for TAT processes, well known in Si_3N_4, and extending to Si oxynitride alloys, e.g., HfSiON334, as well.

3.20 Low Defect Density Remote PECVD GeO_2

A. Introduction

Contrary to the conventional wisdom, there are not a larger number of different defect states within the band-gap of SiO_2. Instead the energies of absorption and luminescent transitions have been assigned to transition energies of a d^2 high spin state localized on one the two Si atoms associated with the formation of an O-atom vacancy. When one of these electrons is removed by exposure to UV radiation, γ-rays, x-rays, and/or high-energy electrons, the singly occupied state is the well-known E' center. The O-atoms generated in the defect activation process, $_{3/2}$O-Si-O-Si-$O_{3/2}$ = $_{3/2}$O-Si[0e]+ + -[2e]Si-$O_{3/2}$ + O^0, contribute to hole-related states, O_0 + $_{3/2O}$-Si-O-Si-$O_{3/2}$ = $_{3/2}$O-Si-(O-[1h]-O)^0 + ^{0}[1e]Si-$O_{3/2}$, identified by electron spin resonance (ESR).

A similar decomposition reaction to the one quoted for SiO_2, occurs for GeO_2 in the quartz (4-fold Ge and 2-fold O) bonding arrangement, that present in non-crystalline bulk GeO_2 glass. Based on bond-enthalpies, the barrier for the GeO_2 decomposition reaction is reduced, and hence the defect density of bulk glasses is higher, and the surface reaction rate for oxidation of bulk Ge is higher. I have performed experiments on this glass in 1976, and it did indeed have a yellow color in transmission. All studies have to date have yield a band-gap of ~5.5 eV, consistent with this yellow color. The same band gap has been reported for GeO_2 formed by oxidation of bulk Ge. The issue is how to produce GeO_2 with a lower defect density than that of the bulk glass, and thermally-oxidized Ge surface. The answer is simple and straight-forward: our group uses a non-equilibrium low temperature plasma-assisted process, and then determine how the defects created by the decomposition reaction change with post-deposition annealing temperature in inert ambients. This is exactly what we have done, and it works very well!! It must be pointed out that the rutile 6-fold coordinated Ge form of non-crystalline (and crystalline as well) GeO_2 is highly soluble in water

(hygroscopic), while the quartz 4-fold coordinated form is not. This is important for technological applications, and is validated by our experience with measurements made on films of the quartz-like non-crystalline form at two SSRL runs spaced by more than 4 weeks.

3.21 Summary of Preliminary Results for Plasma Deposited GeO_2 Thin Films

A. Introduction

Most of the results below come from XAS measurements made at SSRL. These are combined with depth resolved CLS by the Brillson group at The Ohio State University. Finally, by a model for the Ge-GeO_2 interface is proposed based on our measurements in combination with comparison between spectroscopic ellipsometry measurements of Aspnes and co-workers on crystalline Si and Ge, and theoretical/experimental values of band offset energies between Si and SiO_2, and Ge-GeO_2 interfacial regions.

B. RPECVD Growth of GeO2 Thin Films

The thin films of GeO_2 were deposited by remote plasma enhanced chemical vapor deposition onto (i) remote plasma nitrided (RPAN) surfaces of crystalline Si and Ge to prevent oxidation during film growth, and (ii) wet-chemical cleaned Ge surfaces, using a process that gives minimal GeO_2 native oxide growth. Films were subsequently annealed (1 minute RTA's) in Ar at temperatures of 400°C, 600°C and 700°C.

C. Summary of XAS and DRCLS Results

(i) empty conduction band states (nitrided Si substrates) - Fig. 44 - (a) separation in "s-like" and "d-like" states a higher energies; (b) similar ΔE with respect to band gaps of 9.5 eV for GeO_2 and 8.9 eV for SiO_2; (c) 2nd derivative spectra (not shown) indicate two bound excitons - spacing ~ 0.2 eV; (d) "d-like" sharper in GeO_2.

(ii) empty conduction band states (cleaned Ge substrates) - Fig. 45 - (a) as deposited GeO_2 films, and films annealed at 700°C in Ar display spectra qualitatively different than those in Fig. 44 with features that are broader, and less well defined, whereas (b) films annealed at 400°C and 600°C display sharper features similar to those in Fig. 44; these spectra are higher energy because the 2p states of the Si conduction band are at lower energy than the 3p states of Ge because of repulsion effects associated with the occupied Ge 3d shallow core states.

(iii) Figs. 46 and 47 compare respectively (a) the spectral dependence of the DRCLS spectrum, and (b) the integrated response. The spectral dependence and relative integrated response are different for the lease defect processing -- deposition on clean Ge followed by annealing at 400 C and 600C. The spectral response is peaked at lower eV significantly higher emission in the three more defective samples, and the integrated response is a factor of 10 or higher in the defective samples as well.

D. Band Off-sets at "Ideal"(No Interfacial Transition Regions)" Ge-GeO_2 and Si-GeO2 Interfaces

Based on the valence and offset energies for Si-SiO_2, and Ge-GeO_2, conduction and valence band energies relative to Si and Ge have be estimated. The conduction band energy is about 1.5 eV higher for Ge-GeO_2, and the valence band energy is about 1 eV smaller. This is indicated in Fig. 48.

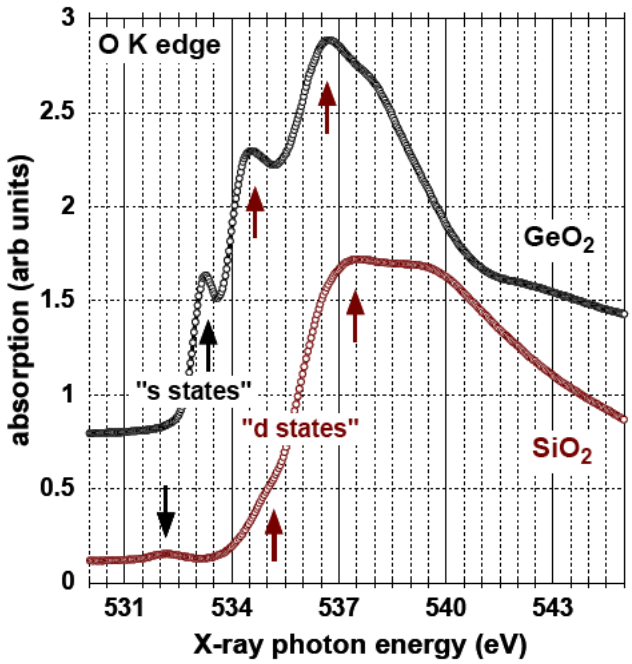

Fig. 44. O K edge spectra: SiO_2 and GeO_2.

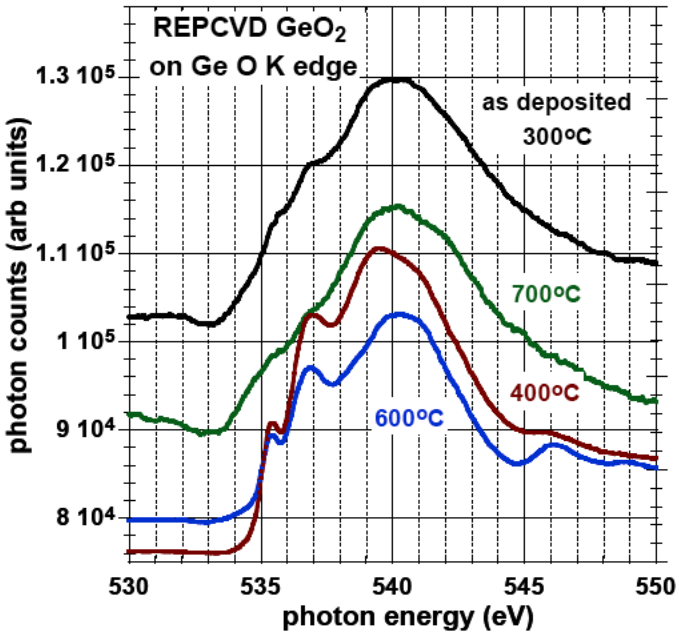

Fig. 45. O K edge spectra: GeO_2 on Ge.

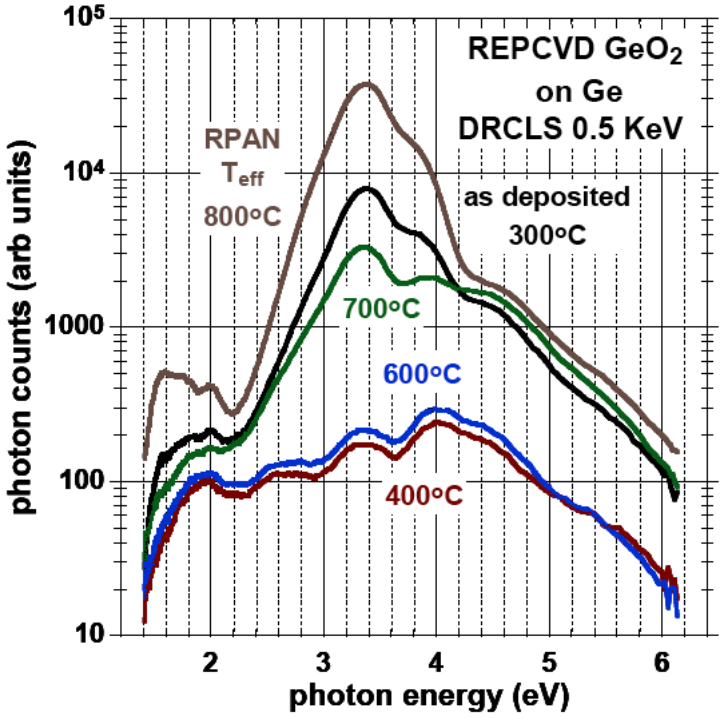

Fig. 46. DRCLS spectra of GeO2 films on Ge substrates.

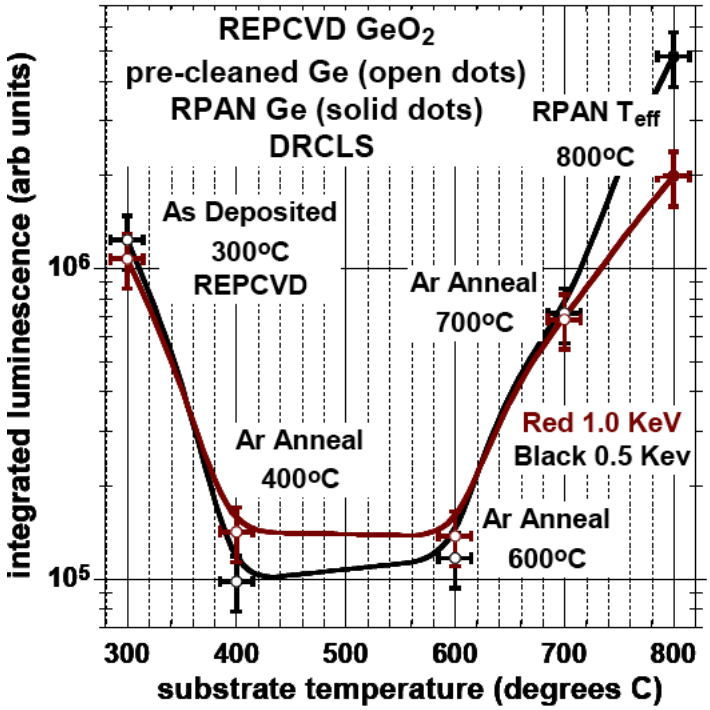

Fig. 47. Integrated DRCLS spectra of GeO_2 films on Ge substrate.

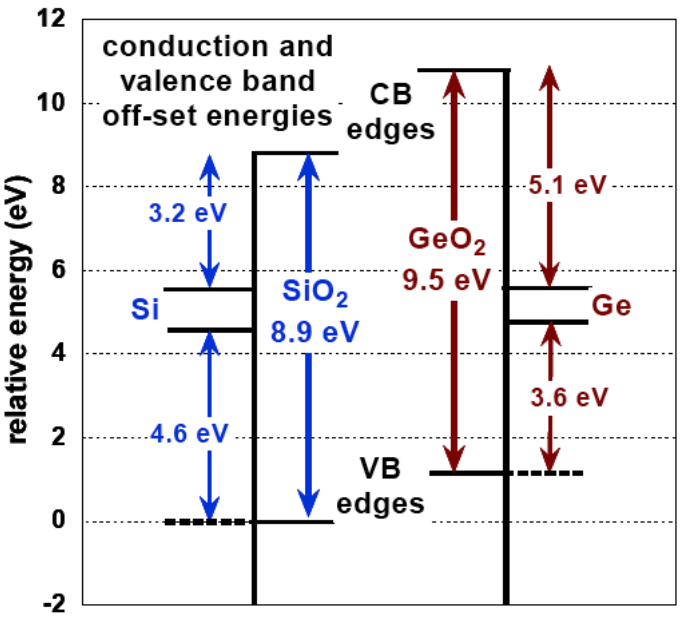

Fig. 48. c-Si and c-Ge band edge alighments with SiO_2 and GeO_2, respectively.

3.22 Total Ionizing Dose and Single Event Effects in Strained Si Technologies

Uniaxial strained-silicon (Si) and high-k gate dielectrics are key technologies used to enhance transistor performance for sub 100-nm logic technology nodes. Uniaxial mechanical stress improves device characteristics such as mobility and gate tunneling current, with minimal stress-induced threshold-voltage shifts. Strained-silicon technology increases drive current using additional process features such as tensile SiN capping layers to create tensile stress in nMOSFETs and compressive SiN capping layers and SiGe source/drain regions to create compressive stress in pMOSFETs. Channel stresses of up to 1.5 GPa can be produced using these stressors. These strained-Si processes also induce additional stress (≤ 1 GPa) such as uniaxial or biaxial stress in the source/drain region. The combined effects of the stressors cause changes in carrier mobility in the source/drain and bulk (substrate) regions, as well as in the channel.

Radiation-hardened devices technology for space and military electronics market has strongly influenced by MOS devices technology for commercial electronics market. Since the cost of making radiation hardened devices becomes more expensive, people who are working for electronics in the radiation environment make their effort to reduce the cost using commercial technology. However, no systematic study how strained Si technology responds to radiation environment has been done yet. This work investigates the effect of strained mechanical stress on total ionizing dose effects on strained nMOSFETs and laser induced current transients in strained Si diodes experimentally and theoretically.

A. Total Ionizing Dose Effects on Strained HfO_2-based nMOSFETs

High-k gate dielectrics have been implemented to reduce transistor gate leakage current in the 45 nm CMOS technology node. Hafnium-based dielectrics with a relative dielectric constant of ~15 to 26 have emerged as the materials of choice for high-k gate dielectrics. Although radiation damage of HfO_2-based MOS devices has been studied in recent years, the effects of uniaxial mechanical

stress on the ionizing radiation response of HfO_2-based MOS devices have not been reported. Hole trapping is observed to be dominant in HfO_2 [17, 18] dielectric layers, similar to SiO_2. The effects of mechanical stress on the ionizing radiation response of SiO_2-based MOS devices have been reported, but the mechanical stress (≤ 4 MPa) produced in these studies by changing the gate electrode thickness is much smaller than that used in strained-Si technology (~ 1 GPa).

In high-k transistors, remote Coulomb scattering (RCS) is one of the main factors limiting the mobility. In commercial devices, most of the RCS effect comes from fixed charges generated by the fabrication process. Similarly, radiation-induced charges may increase RCS. Owing to the ubiquitous use of high-k based strained-Si technology in the future, it is important to address the radiation response of these devices as a function of stress. In this work, we investigate the effects of uniaxial stress on the radiation-induced threshold voltage shifts and mobility degradation in HfO_2-based nMOSFETs using controlled external mechanical stress.

Experimental Details

Radiation-induced threshold voltage shifts and mobility degradation in mechanically stressed HfO2-based nMOSFETs are extracted from drain current-gate voltage (ID-VGS) characteristics. The samples used in this study are TiN/HfO2 gate stack nMOSFETs on Si (001) wafers with <110> channel direction. The high-k gate dielectric is 7.5 nm in physical thickness. The thickness of the SiOx interlayer is 1 nm. The effective oxide thickness (EOT) of these transistors is 2.3 nm. The aspect ratio (W/L) of the transistors used in this investigation is 10 μm/3 μm. Strain in the devices is produced by applying uniaxial mechanical stress using a four point bending jig, as shown in Fig. 49. The devices are irradiated in an ARACOR 10-keV X-ray irradiation system under different values of stress (100 MPa and 200 MPa tensile, no stress, and 200 MPa compressive), at –2 V gate bias, with the source, drain, and body grounded.

Table 1. Total ionizing dose (in SiO_2) experimental matrix.

Mechanical Stress / Radiation Dose	Compressive 200MPa	0MPa	Tensile 100MPa	Tensile 200MPa
Pre-rad (0 Mrad)	X	X	X	X
0.5 Mrad	X	X	X	X
1 Mrad	X	X	X	X
5 Mrad	X	X	X	X

Although the maximum applied stress (~200 MPa) in this investigation is about 20% of that produced by process-induced stressors (~ 1GPa), the experiments provide insight into the effects of stress on radiation-induced threshold voltage shifts; this approach is analogous to previous work describing the effects of stress on unirradiated MOS threshold voltages. Samples are irradiated to a cumulative dose of 5 Mrad(SiO_2) at a dose rate of 31.5 krad(SiO_2)/min; the experimental matrix is shown in Table 1. Post irradiation I_D-V_{GS} curves are measured using an Agilent 4156 semiconductor parameter analyzer. Threshold voltage shifts (ΔV_T) are monitored as a function of radiation dose for different applied uniaxial mechanical stresses. Threshold voltages are extracted using a constant-

current (CC) method. Pre- and post-irradiation subthreshold behavior is also studied. –2 V gate bias stress experiments without irradiation are performed to separate the contributions of bias-induced charge trapping/creation in these gate dielectrics from the radiation-induced shifts. Electron mobility, $\mu = I_D L_g / W C_{ox} (V_{GS} - V_T) V_{DS,}$ is extracted as a function of gate over-drive voltage ($V_{GS} - V_T$) at low drain voltage ($V_{DS} = 0.1$ V), where L_g is the channel length, W is the channel width, C_{ox} is the gate oxide capacitance per unit area, and V_T is the threshold voltage.

Threshold voltage instability is one of the main issues in high-k devices. In this work, threshold voltage shifts are measured after being stabilized by sweeping the I_D-V_{GS} curves before and after irradiation. For the samples used in this investigation, the threshold voltage shift stabilizes generally after the second I_D-V_{GS} curve after irradiation or bias stress. The stabilization occurs because charges in shallow hole trap sites in the SiO_x or HfO_2 may detrap, or holes in deeper trap

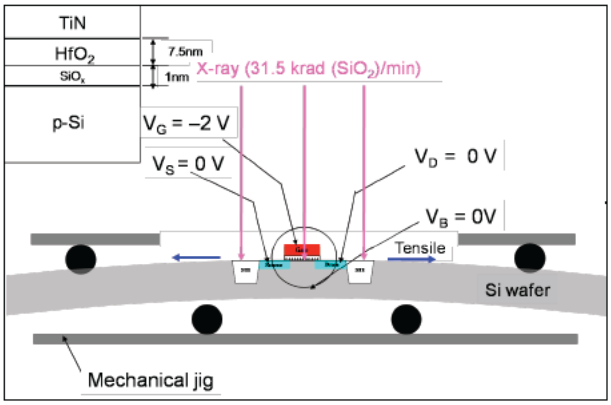

Fig. 49. Experiment setup for measuring total ionizing dose (TID) effects on a mechanically strained nMOSFET, and cross section of gate stack of

sites near the interface may recombine with injected electrons during the first I_D-V_{GS} sweep under a given irradiation or bias condition. The effect of hot carrier injection on the threshold voltage shift during multiple *I-V* sweeps is expected to be negligible since V_{DS} is very low (~100 mV) and there is no abrupt increase in gate leakage. Previous work by Dixit et al. focused on the threshold voltage shift of the first *I-V* curve, which includes the effects of transient shifts. This work focuses instead on the changes in radiation-induced charge trapping under uniaxial mechanical stress after the threshold voltage stabilizes.

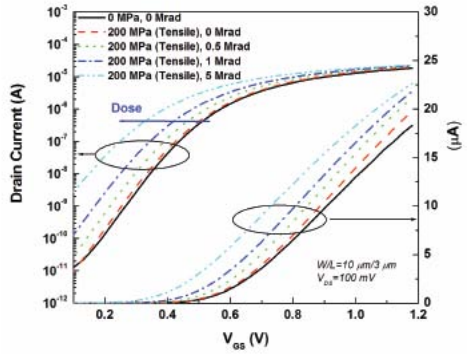

Fig. 50. Semilog and linear plots of the ID-VGS characteristics as a function of the accumulated x-ray dose (in SiO2) under tensile stress of 200 MPa.

Results and Discussion

Hole trapping in the gate oxide is the dominant radiation-induced charge for these devices under the irradiation conditions, as seen by the decrease in the threshold voltage as shown in Fig. 50. This agrees with previous results on HfO_2-based nMOSFETs. Threshold voltage shifts (ΔV_T) can be caused by interface trapped charge (ΔV_{it}) and oxide trapped charges (ΔV_{ot}). Since there is no significant change observed in the subthreshold slope in Figure 50, the threshold voltage shifts are caused mainly by an increase in ΔV_{ot}. Transistors irradiated under other stress conditions (compressive (200 MPa), no stress, and tensile (100 MPa)) are also dominated by positive charge trapping.

Radiation Induced Threshold Voltage Shifts Under Mechanical Stress

The effects of applied mechanical stress on charge trapping are characterized by monitoring threshold voltage shifts at each radiation dose. The tensile stress effect is shown in Fig. 51. Increasing tensile stress results in less threshold voltage shift at each dose level than that measured for devices irradiated with no stress applied. Smaller threshold-voltage shifts are observed after applying only bias for a total time of 2.5 h, which is equivalent to the time required for 5 Mrad(SiO_2) irradiation. Tensile stress also reduces the threshold voltage shift resulting only from the bias. The data points

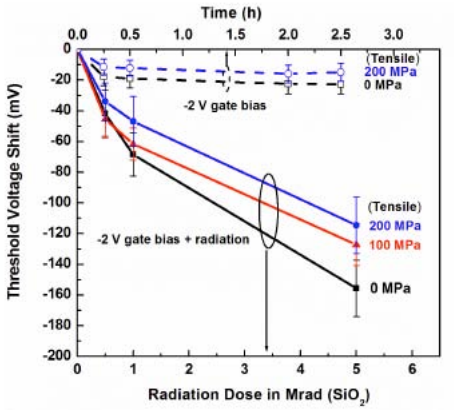

Fig. 51. Threshold voltage shifts (ΔVT) due to –2 V gate bias + radiation and –2 V gate bias without radiation under no stress, tensile stress of 100 MPa, and 200 MPa

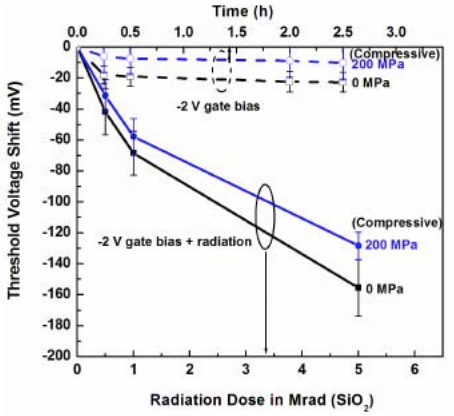

Fig. 52. Threshold voltage shifts (ΔVT) due to –2 V gate bias + radiation and –2 V gate bias without radiation under no stress, compressive stress of 200 MPa conditions.

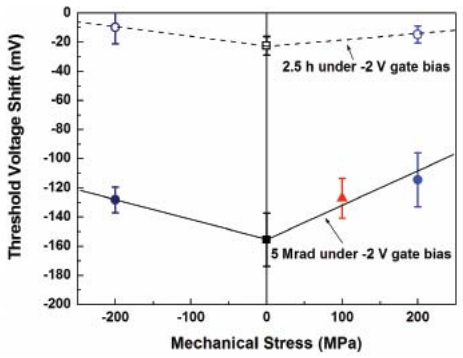

Fig. 53. Threshold voltage shifts (ΔVT) vs. mechanical stress after 5Mrad (SiO2) and 2.5 h under -2 V gate bias (positive (+): tensile, negative (-): compressive)

are the average threshold voltage shifts at each radiation dose or bias time. The error bars in the data points represent the standard deviation in the data at each dose and stress level. Fig. 52 shows a similar trend for the threshold voltage shifts under 200 MPa of compressive stress.

In contrast to the reported stress dependence of the SiO_2 nMOSFET threshold voltage shift under irradiation, both applied tensile and compressive uniaxial stress reduce the threshold voltage shifts in devices with HfO_2 and SiO_x dielectrics in Fig. 53 that are either irradiated under bias, or subjected only to bias stress without irradiation, for comparison. A possible explanation of these results is that compressive and tensile uniaxial mechanical stress both lower the hole trap energy level in HfO_2 and/or SiO_x, reducing hole trapped charges. In recent work, trap-assisted gate tunneling current in high-k MOS capacitors increased under both compressive and tensile stress, suggesting that the hole trap energy distribution may be shifted to lower average values by uniaxial mechanical stress. In addition, an increase in trap assisted tunneling in thin (2.5 nm) SiO_2 results from reduced

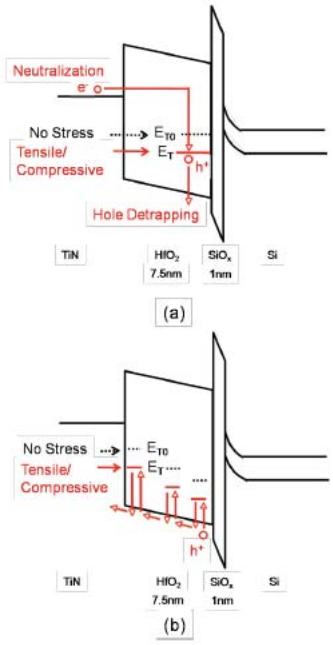

Fig. 54. (a) Charge detrapping/ neutralization model; (b) multiple trapping-detrapping hole transport model.

trap activation energy due to both compressive and tensile stress. Uniaxial mechanical stress may change the trap energy levels by changing bond lengths and angles in HfO_2 and SiO_x. This is consistent with previous works on the oxygen vacancy defect that show that the trap microstructure and energy levels can be changed by stretching the Si-Si bonds and/or changing the bond angles.

We consider two possible reasons why lowering hole trap energy levels may reduce charge trapping in HfO_2 and/or SiO_x. First, uniaxial mechanical stress may enhance the detrapping of holes in shallow trap sites or the neutralization in deep trap sites by electron injection, as illustrated in Fig. 54(a). This reduction in hole trap energy increases the probability that these defects can emit a trapped hole or capture an electron to compensate a nearby trapped hole. Trapped holes in deep trap sites can be neutralized by capturing electrons.

Second, the effective hole mobility in the gate dielectrics along the <001> direction under uniaxial mechanical stress may be increased by reducing the average trap energy level. Hole transport in thin (~10 nm) high-k oxides can be described by a multiple trapping model. This motion is illustrated schematically in Fig.54(b). Reduced trap energy levels also can increase the effective hole mobility, which is proportional to $\exp(-E_a/kT)$ [38], where E_a is the hole trap activation energy, k is the

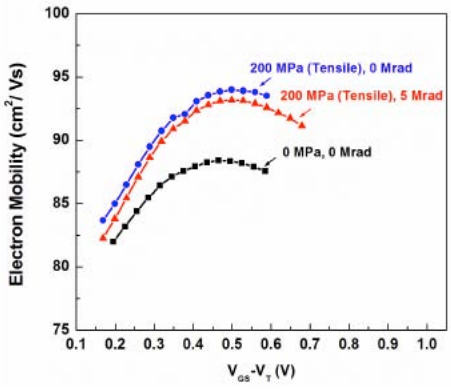

Fig. 55. Electron mobility vs. gate over-drive voltage (VGS-VT) for the cases of no stress, tensile stress of 200 MPa, and 5 Mrad(SiO2) under tensile stress of 200 MPa.

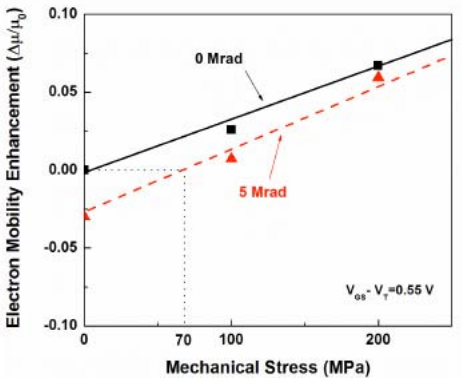

Fig. 56. Electron mobility enhancement vs. mechanical stress before and after 5 Mrad(SiO2) irradiation.

Boltzman constant, and T is temperature. Hence, strain-induced lowering of hole trap energy levels may reduce charge trapping in HfO_2 and SiO_x.

Radiation Induced Mobillity Degradation under Mechanical Stress

Electron mobility is shown as a function of gate over-drive voltage ($V_{GS}-V_T$) in Fig. 55. 200 MPa of tensile stress enhances the electron mobility at all gate biases. Electron mobility degradation for devices irradiated to 5 Mrad(SiO_2) under 200 MPa of tensile stress is ~ 1% at $V_{GS}-V_T = 0.55$ V, compared to the pre-irradiation 200 MPa case, but the electron mobility is still higher than the unstressed case. Fig. 56 shows the electron mobility enhancement as a function of stress before and after 5 Mrad(SiO_2) irradiation. The mobility enhancement compared to unstressed devices is positive after a total dose of 5 Mrad(SiO_2) at all tensile stress levels above 70 MPa, indicating that the benefit of strained Si is not lost after irradiation.

B. Laser- induced Current Transients in Strained Si Diodes

Single event transients (SETs) and single event upsets (SEUs) are related to collection of radiation-generated charge at sensitive circuit nodes. Although strained-Si technology is widely adopted, the effects of mechanical stress on current transients generated by laser or ion strikes at the source/drain regions have not been reported. It is important to understand how mechanical stress affects these transient pulses since the transport of the radiation-generated carriers in the substrate is affected by stress. Laser-induced current transients on a uniaxially stressed Si N+/P junction diode are reported in this paper. An N+/P diode is a good representation of the source/drain junctions that are responsible for charge collection in n-channel MOSFETs. P-channel MOSFETs are also important for considering SETs and SEUs. However, stress-induced electron mobility enhancement is easier to understand than that of holes, so N+/P diodes are used in this work.

The shapes of current transients and the amount of collected charges are measured as a function of stress, because both of them are crucial in predicting SETs and SEUs in circuits. Controlled external mechanical stress is applied via a four-point bending jig while the samples are irradiated using a picosecond pulsed laser. The characterization system is based on the direct measurement of the current transients. The FLOODS simulation tool is used to explain the mechanisms responsible for the differences in charge collection between stressed and unstressed devices. Additionally, the simulations provide insight into the effects of high mechanical stress (~1 GPa) on laser-induced current transients, above the maximum stress that could be applied using the four-point bending jig (240 MPa on these samples).

Experimental Details

The laser-induced current transients in mechanically-stressed Si N+/P diodes are captured using a high-speed measurement system with an integrated four-point bending jig, as shown in Fig. 9. The samples used in this study are N+/P diodes fabricated on (001) Si wafers using a standard 130-nm CMOS technology. The active area of the diodes is 50 μm × 100 μm. Nickel silicide (NiSi), silicon oxide (SiO_x), and copper (Cu) patterns are present on top of the diodes as shown in Fig. 10 using transmission electron microscopy (TEM) and energy-dispersive X-ray spectroscopy (EDS). The thickness of the NiSi, SiO_x, and Cu patterns is ~20 nm, 720 nm, and 280 nm, respectively. The doping densities of the n^+, p-well, and p-substrate are ~10^{20}, ~10^{18}, and ~10^{16} cm^{-3}, respectively. The shallow trench isolation (STI) in these devices is an additional source of mechanical stress. However, STI-induced stress in the center of the large diodes is negligible. Uniaxial mechanical stress along the <110> direction is applied using a four-point bending jig.

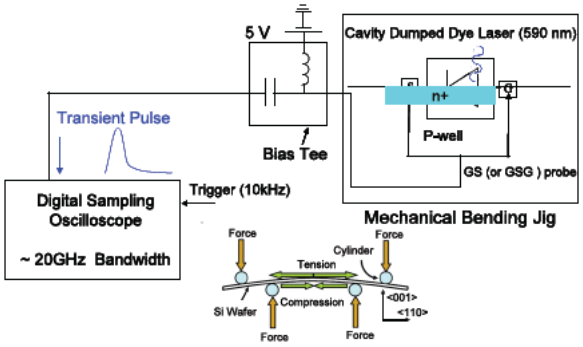

Fig. 57. Laser-induced current transient measurement system using a four- point bending jig.

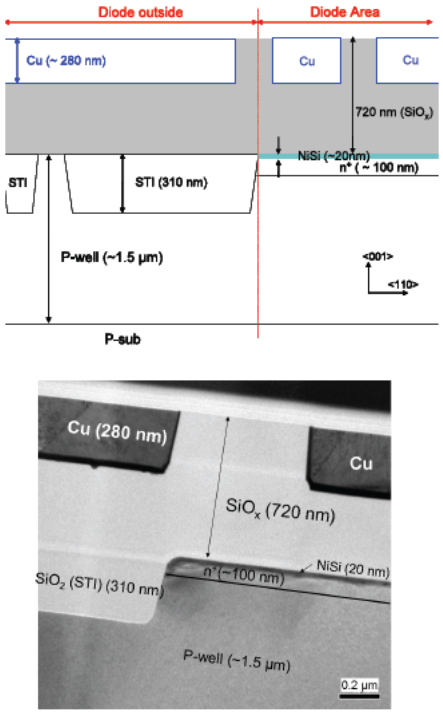

Fig. 58. Schematic of N+/P diode structure through TEM and EDS analysis (not to scale) and TEM image.

A cavity-dumped dye laser with a wavelength of 590 nm, a pulse energy of 218 pJ, and a pulse width of 1 ps is used to inject electron-hole pairs in the diode. The laser direction is normally incident to the diode surface and has a spot size of 12 μm in diameter. The peak carrier concentration produced by the laser is ~1.6 × 10^{19} cm^{-3}. The pulse laser energy reaching the diode active area is smaller than the value measured at the surface of the structure due to the optical properties of the layers on top of the diode. The transient measurement system uses a Tektronix TDS8200 digital sampling oscilloscope with 80E03 sampling module (20 GHz bandwidth) and is connected to the device using a bias tee (10 kHz to 40 GHz) and a ground-signal-ground (GSG) probe tip (DC to 40 GHz).

Current transients on the N+/P diode are measured under different values of stress (160 MPa and 240 MPa tensile, no stress, and 160 MPa compressive) with a 5 V reverse bias. Although the maximum applied stress (~240 MPa) in this investigation is about 16% of that produced by process-induced stressors (~ 1.5 GPa), the experiments still show the dominant mechanisms in the effects

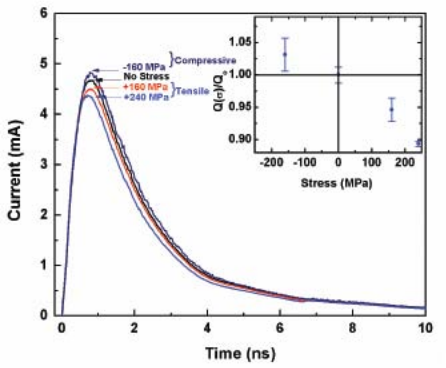

Fig. 59. Laser-induced current transients and the ratio of collected charge measured as a function of <110> uniaxial mechanical stress.

of stress on SETs; this approach is analogous to previous works describing the effects of stress on unirradiated MOS devices.

Experimental Results

The effect of the applied mechanical stress on maximum current and charge collection is characterized by monitoring laser-induced current transients at each uniaxial stress value. Increasing tensile stress results in lower maximum currents (I_{max}) and collected charges (Q) than those measured under no stress, as shown in Fig. 59 for times up to 10 ns after the laser pulse strikes the device. Each transient curve is measured using an averaging technique (100 points) in the sampling oscilloscope. Q is obtained by integrating the measured transient as a function of time. The data points are the average Q at each level. The error bars in the data points represent the standard deviation in the data at that stress level. Opposite to tensile stress, compressive stress increases I_{max} and Q. A decrease/increase in I_{max} and Q under tensile/compressive stress can be explained by a 1-D transient analytical solution.

Current transients ($I(t)$) are proportional to $N\mu_{n\square}$ in the solution, where N is the number of laser-generated electron-hole pairs and $\mu_{n\square}$ is electron mobility along the <001> direction. $\mu_{n\square}$ is the dominant contribution for electron mobility, because electrons are mainly moving in the <001> direction due to applied field along the <001> direction for the large diodes used in the experiment. N as a function of depth in Si is defined as

$$N(z) = \frac{\alpha(\sigma)}{\hbar\omega}\exp(-\alpha(\sigma)z)\int_{-\infty}^{\infty} I_0(z,t)dt \qquad (1)$$

where α is the absorption coefficient of Si, $\hbar\omega$ is the photon energy (2.1 eV), z is depth in the Si, I_0 is the intensity of the laser beam, and t is the time. α depends on the band gap, where a normalized stress dependent α is defined as

$$\frac{\Delta\alpha(\sigma)}{\alpha} = \frac{\Delta E_g(\sigma)}{\hbar\omega - E_g} << 1, \quad \hbar\omega > E_g \qquad (2)$$

where σ is the mechanical stress, and E_g is the Si band gap (1.12 eV). Based on (1) and (2), a change in N as a function of uniaxial tensile stress and the depth into Si is plotted in Fig. 12. Since stress-induced bandgap narrowing in Si is minimal (~0.01 eV at 240 MPa of both compressive and tensile stress), an increase in α of Si for this range of mechanical stress is negligible. As a result, there is

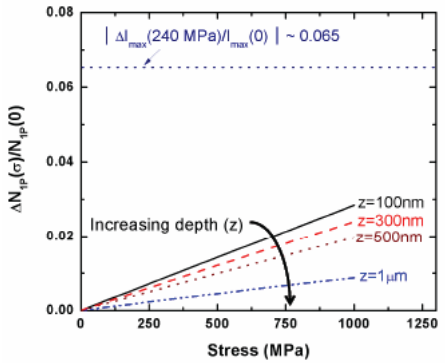

Fig. 60. The number of laser-generated electron-hole pairs as a function of depth (z) and <110> uniaxial

no significant increase calculated in N at each depth under mechanical stress, less than 1% at 240 MPa of tensile stress, as shown in Fig. 60.

Since the change in N due to stress is minimal, a ~6.5% decrease in I_{max} at 240 MPa of tensile stress is caused mainly by a decrease in electron mobility along the <001> direction. Likewise, for compressive stress, an increase in I_{max} results from an increase in electron mobility along the <001> direction, because strain-induced band gap narrowing is very small (~0.01 eV at 240 MPa). This suggests that a decrease/increase in electron mobility along the <001> direction under tensile/compressive stress ($\Delta\mu_{n\square}$) results in a decrease/increase in I_{max}. The experimental results and qualitative analysis both can be explained by previous results on piezoresistance (π) coefficients in Si.

$$\pi = -\frac{\mu(\sigma) - \mu(0)}{\sigma\mu(0)} = -\frac{\Delta\mu}{\sigma\mu(0)} \qquad (3)$$

The π coefficient represents changes of mobility resulting from applied stress,

where $\mu(\sigma)$ and $\mu(0)$ are the mobility with and without stress, respectively, and $\Delta\mu$ is the change in the mobility. Changes (increase or decrease) of the electron mobility result from changes of the average electron effective mass (m^*), due to repopulation of electrons under mechanical stress. For example, Fig. 61 shows that tensile stress splits the conduction bands into Δ_2 and Δ_4. Electrons repopulate from the Δ_4 valley into the Δ_2 valley. Average effective mass along the <110> direction (m_{ll}) decreases under tensile stress in the same direction, but average effective mass along the <001> direction ($m_{\square}$) increases under tensile stress in the <110> direction. Thus, <110> tensile stress decreases the electron mobility along the <001> direction ($\mu_{n\square}$), because μ is inversely proportional to m^*. The opposite dependence is expected with compressive stress. The concept of the π coefficient is implemented in current-transient simulations for diodes under mechanical stress in the next section. Q is also proportional to the funneling length, $L = (1+\mu_{n\square}/\mu_{p\square})W$, where $\mu_{p\square}$ is the hole mobility along the <001> direction, and W is the depletion width . A change in hole mobility along the <001> direction ($\Delta\mu_{p\square}$) under uniaxial mechanical stress is negligible (~ 0.3% at 250 MPa). Therefore, the change of the collected charge (ΔQ) as a function of the applied mechanical stress is also dominated by the change in electron mobility ($\Delta\mu_{n\square}$). By applying the same concepts for analyzing $I(t)$ and L as in the N+/P diodes above, it is possible to predict how current transients in P+/N diodes would change under mechanical stress. Since $I(t)$ is proportional to $N\mu_{p\square}$ and $\Delta\mu_{p\square}$ (~ 1% at 1 GPa) is not significant, the change in I_{max} is not expected to be significant under stress. Q is likely to increase with tensile and decrease with compressive stress, because L is equal to

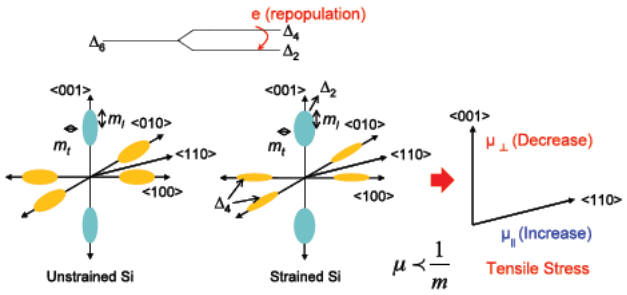

Fig. 61. Uniaxial tensile stress effect on electron mobility.

$(1+\mu_{p□}/\mu_{n□})W$ and affected by $\Delta\mu_{n□}$. However, further experimental data are required to verify the analytical analysis of current transients in P+/N diodes under mechanical stress.

TABLE 2.

Values of piezoresistance (π) coefficients (10^{-5} MPa $^{-1}$) used in FLOODS[57]

	π_{11}	π_{12}	π_{44}
Electron	-102.2	53.4	-13.6
Hole	6.6	-1.1	138.1

TCAD Simulation and Results

Based on the previous experimental analysis, FLOODS simulations are performed to understand the mechanisms of carrier transport under uniaxial stress and to predict how high stress (~1GPa) affects the current transients in diodes. The Masetti and Brooks-Herring mobility models are used to account for carrier transport in a high injection case. Shockley-Read-Hall and Auger band-to-band recombination models are also considered. The number and distribution of electron-hole pairs generated by the laser pulse is calculated by a single-photon absorption (SPA) equation.

Before analyzing the effects of stress on current transients, baseline simulations under no stress are performed. These results are matched to the measured current transient under no stress. It is very important to understand the physics that dominates current transients in an unstressed case in order to predict the results under a stressed case. A 2-dimensional simulation structure, shown in Fig. 62, is built based on analysis of the structure and material of the N+/P diodes, as shown in Fig. 58. The width and depth of the diodes are 100 μm and 10 μm, respectively. The SiO_x, Cu dummy patterns, and NiSi are not implemented in the simplified FLOODS simulations. However, the omitted layers can reduce laser energy due to the reflection, absorption, and transmission properties of each

$$\begin{bmatrix} \pi_{11} & \pi_{12} & \pi_{12} & 0 & 0 & 0 \\ \pi_{12} & \pi_{11} & \pi_{12} & 0 & 0 & 0 \\ \pi_{12} & \pi_{12} & \pi_{11} & 0 & 0 & 0 \\ 0 & 0 & 0 & \pi_{44} & 0 & 0 \\ 0 & 0 & 0 & 0 & \pi_{44} & 0 \\ 0 & 0 & 0 & 0 & 0 & \pi_{44} \end{bmatrix} \begin{bmatrix} \sigma_{xx} \\ \sigma_{yy} \\ \sigma_{zz} \\ \sigma_{yz} \\ \sigma_{zx} \\ \sigma_{xy} \end{bmatrix} = \begin{bmatrix} \Delta\rho_{xx}/\rho_{xx} \\ \Delta\rho_{yy}/\rho_{yy} \\ \Delta\rho_{zz}/\rho_{zz} \\ \Delta\rho_{yz}/\rho_{yz} \\ \Delta\rho_{zx}/\rho_{zx} \\ \Delta\rho_{xy}/\rho_{xy} \end{bmatrix} = \begin{bmatrix} -\Delta\mu_{xx}/\mu_{xx} \\ -\Delta\mu_{yy}/\mu_{yy} \\ -\Delta\mu_{zz}/\mu_{zz} \\ -\Delta\mu_{yz}/\mu_{yz} \\ -\Delta\mu_{zx}/\mu_{zx} \\ -\Delta\mu_{xy}/\mu_{xy} \end{bmatrix} \quad (4)$$

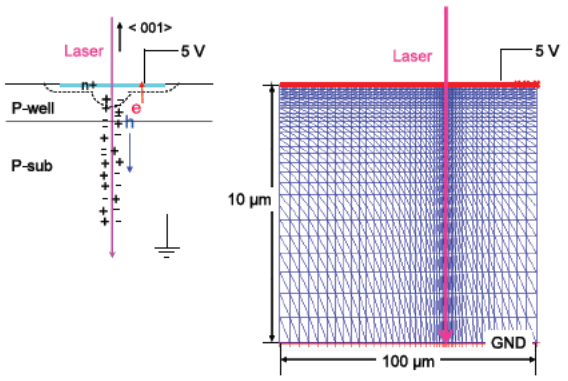

Fig. 62. Schematic of laser-induced current transients and 2-dimensional simulation structure of an n+p diode.

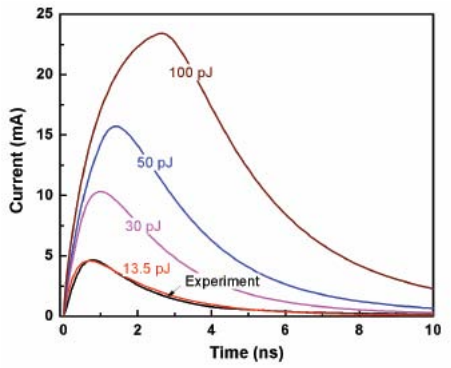

Fig. 63. Simulated energy dependence of laser-induced current transients.

material. Fig. 63 shows that a decrease in laser pulse energy results in a decrease in the peak current and charge collection. The simulated result for the case of pulse energy of 13.5 pJ agrees with the experiment result, as shown in Fig. 63. However, the pulse energy (13.5 pJ) is much different from the measured pulse energy (218 pJ). The discrepancy can be explained by the absorption, reflection, and transmission properties of each layer over the active region of the diode. Since 43% of the spot area of incident laser is occupied by Cu dummy patterns which block the laser, only 57% of

$$\begin{bmatrix} \frac{\mu_{xx}-\Delta\mu_{xx}}{\mu_{xx}} & \frac{-\Delta\mu_{xy}}{\mu_{xy}} & \frac{-\Delta\mu_{xz}}{\mu_{xz}} \\ \frac{-\Delta\mu_{xy}}{\mu_{xy}} & \frac{\mu_{yy}-\Delta\mu_{yy}}{\mu_{yy}} & \frac{-\Delta\mu_{yz}}{\mu_{yz}} \\ \frac{-\Delta\mu_{xz}}{\mu_{xz}} & \frac{-\Delta\mu_{yz}}{\mu_{yz}} & \frac{\mu_{zz}-\Delta\mu_{zz}}{\mu_{zz}} \end{bmatrix} \begin{bmatrix} J_x(0) \\ J_y(0) \\ J_z(0) \end{bmatrix} = \begin{bmatrix} J_x(\sigma) \\ J_y(\sigma) \\ J_z(\sigma) \end{bmatrix} \quad (5)$$

incident laser energy is transmitted. Next, only 78% of the energy is transmitted through the 720 nm SiO_x, due to reflection losses at the interfaces. Lastly, 16% of the energy is transmitted through NiSi. Therefore, the calculated pulse laser energy reaching the diode active area is ~15.5 pJ, ~7.1% (= 0.57 x 0.78 x 0.16) of the incident energy. If the thickness of each layer varies by ~10% and the composition of the $NiSi_x$ also varies, the calculated laser energies range from 12.5 to 22 pJ. The collected charge in the simulation (12.8 pC) agrees well with the average collected charge in the experiment (12.3 pC). As a result, the amount of energy used in the simulations to produce

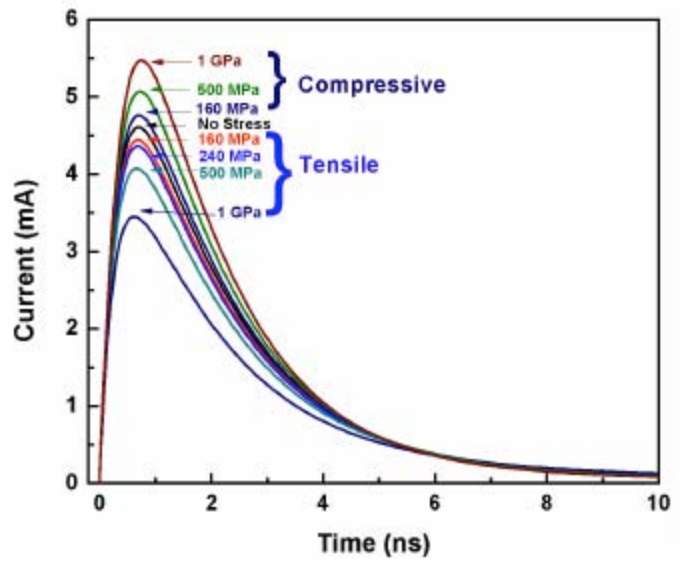

Fig. 64. Simulated laser-induced current transients as a function of <110> uniaxial mechanical stress.

agreement with the experiments, 13.5 pJ, is reasonable. A piezoresistive mobility model based on Smith's π-coefficients is used to consider mobility enhancement under mechanical stress, as shown in Table 2. The 6 x 6 piezoresistive model is defined as

where π_{ij}, σ_{ij}, ϱ_{ij}, and μ_{ij} are components of the piezoresistance coefficient, mechanical stress, resistivity, and carrier mobility, respectively, and $\Delta\varrho_{ij}/\varrho_{ij}$ and $\Delta\mu_{ij}/\mu_{ij}$ are fractional changes in resistivity and mobility.

The doping dependence of the π-coefficients is considered. From (4), currents are calculated as a function of mechanical stress. Current densities are expressed as

where $J_i(0)$ and $J_i(\sigma)$ are current density components with and without stress based on a Cartesian coordinate system, respectively. The simulated current transients in Fig. 64 show the same trend as the experimental data in Fig. 59. I_{max} and Q in the simulations also agree with the experiments, as shown in Figs. 65 and 66. The data points in the experiments are the average I_{max} and Q at each stress level. The error bars in the data points represent the standard deviation in the data at each stress level. The simulation results predict that I_{max} and Q under 1 GPa of tensile stress will decrease by ~23% and ~21%, respectively. Analogous to tensile stress, 1 GPa of compressive stress increases I_{max} and Q by 17% and 13%, respectively. These experiment and simulation results for strained N+/P diodes show that uniaxial stress changes the shape of current transients and collected charges.

To apply the strain engineering concepts for mitigating SETs and SEUs in deep submicron devices, we need to understand the differences between these large diodes and deep submicron devices. Due to the scaling of devices, the size of source/drain junctions is smaller than that of a radiation-generated e-h pair cloud. While out-of-plane transport of those carriers dominates current transients in these large diodes, both out-of-plane and in-plane transport of radiation-generated carriers under mechanical stress should be considered for scaled devices. Mechanical stress can either enhance or degrade mobility, depending on the orientation. For example, <110> uniaxial tensile stress

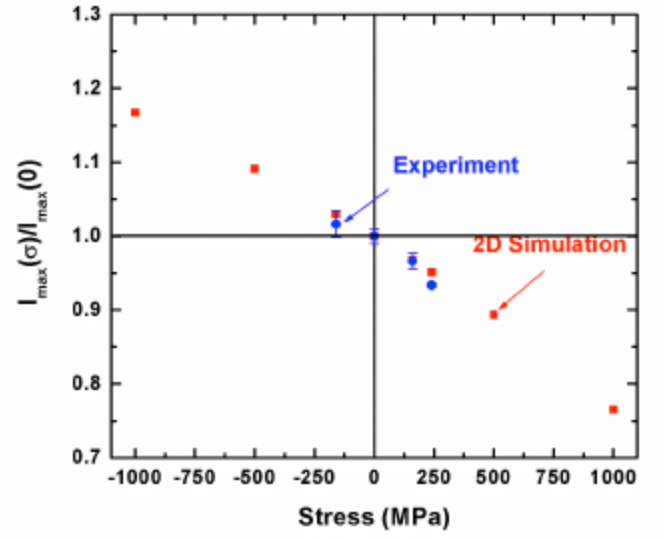

Fig. 65. Peak current (Imax) as a function of mechanical stress. (positive (+) : tensile, negative (-): compressive)

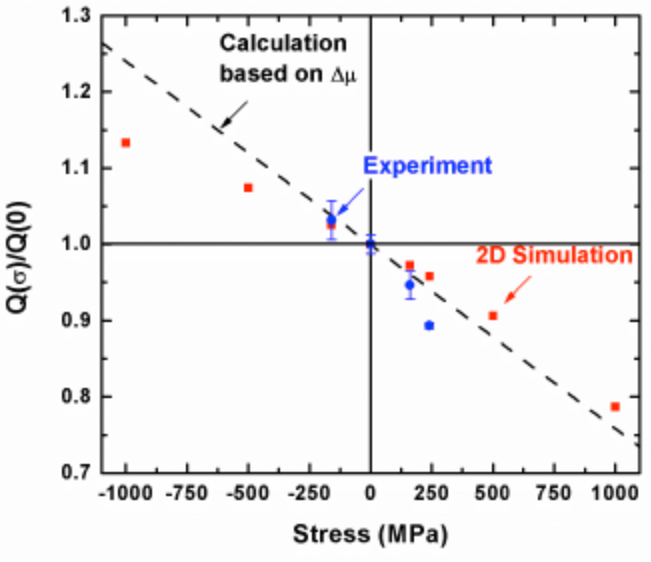

Fig. 66. Collected charges (Q) until 10 ns. (positive (+) : tensile, negative (-): compressive)

increases electron mobility along the <110> direction, but decreases it in the <001> direction. For commercial off-the-shelf (COTs) chips, strained-Si technology is implemented to increase carrier mobility along the channel (in-plane) direction. It is necessary to evaluate whether strained-Si have beneficial or detrimental trade-offs between chip performance and radiation effects.

C. Summary and Conclusion

Positive charge trapping is the dominant radiation-induced degradation mechanism in both unstressed and mechanically stressed HfO_2-based nMOSFETs. Uniaxial tensile and compressive stresses in nMOSFETs decrease the amount of net positive charge trapping and reduce the threshold voltage shift. This is attributed to enhanced detrapping of holes or compensating electron trapping

in HfO_2 or SiO_x, and/or increasing effective hole mobility in the gate dielectric. Electron mobility enhancement produced by the stress is retained in the irradiated devices. Uniaxial strain engineering has the potential to maintain drive current (mobility) enhancement significantly in advanced HfO_2-based MOSFETs, even after irradiation to the relatively high total doses (5 Mrad(SiO_2)) reported here.

Uniaxial tensile stresses in Si N+/P diodes decrease the maximum peak currents and collected charges for laser-induced current transients. Quantitative analysis and FLOODS simulation results suggest that this can be attributed to the degradation of electron mobility along the <001> direction. Unlike uniaxial tensile stress, uniaxial compressive stress shows the opposite trend. Therefore, uniaxial strain engineering has the potential to control the shape of single event transients and the amount of charges collected in devices. Furthermore, these results suggest that strained-Si technology has a significant impact on SETs and SEUs at the circuit level.

Acknowledgements

This work was supported by the Air Force Office of Scientific Research (AFOSR) through the MURI program. The author thanks Gennadi Bersuker in SEMATECH and E. Simoen in IMEC Leuven for providing valuable samples used in the research

3.23 Analysis and Modeling of Total-Ionizing-Dose (TID) Effects

This report summarizes technical results and key findings from Arizona State University for the Vanderbilt University AFOSR MURI program on radiation effects. Over the past five years. ASU efforts have focused on the analysis and modeling of total-ionizing-dose (TID) effects in semiconductor materials and devices. The specific topics summarized in this final report pertain to ASU's research on:

- basic mechanisms of defect buildup in isolation oxides
- total ionizing dose effects characterization and modeling in advanced CMOS transistors

The ASU effort was directed by Dr. Hugh Barnaby. Several graduate students were supported during the program including three Ph.D. students: Xiao-Jie Chen, Michael Mclain, and Ivan Sanchez Esqueda. Both Mclain and Chen completed their doctorates during the program.

The results of the modeling and experimental work performed by the ASU team have lead to significant improvements in the basic models that describe ionizing radiation-induced defect buildup semiconductor oxides. Modeling refinements have helped identify key mechanisms related to dose rate sensitivity, in-package hydrogen contamination, response saturation, and defect annealing. Physical models, primarily expressed as systems of differential equations, were implemented in numerical simulators and the results compared to experimental data for validation. The rigorous model validation and parameterization performed during the course of the program was the first of its kind for advanced CMOS technologies (below the 100 nm node). In addition to the physical model development, techniques for device level analytical modeling of TID effects, from defect generation to radiation-enabled compact modeling were developed at ASU for the MURI. The techniques were integrated into a predicative technology modeling (PTM) package for radiation effects that generates validated compact models for radiation damage from user specified input conditions (e.g., environments and system states). The general flow of the PTM for radiation methodology is summarized in Fig. 67. This effort produced for the first time surface-potential-based models for ionizing radiation effects in both bulk and SOI CMOS.

A. Basic Mechanisms for Defect Buildup

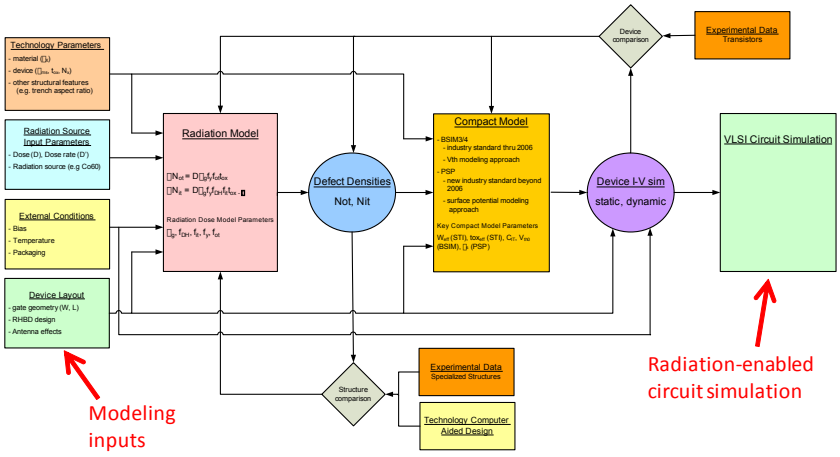

Fig. 67. Flow diagram describing approach to predictive technology modeling for radiation effects.

Model Overview

In this task, models describing the processes involved in radiation-induced defect generation were adapted and in some case extended to address effects in emerging technologies. These processes include those which lead to the buildup of trapped oxide charge (N_{ot}) in isolation oxides and traps at the interface between dielectric and semiconductor materials. The processes for N_{ot} generation, illustrated in Fig. 68, include electron-hole pair generation, geminate recombination, charge transport, and trapping. The key differential equations used to model these processes are

and

.

$$\frac{\partial f_p}{\partial x} = \dot{D} k_g f_y - \frac{\partial p}{\partial t} \tag{1}$$

Eq. 1 captures the relationship between ionizing dose rate ($\dot{D}$) and hole flux transport (f_p) and Eq.

$$\frac{\partial N_{ot}}{\partial t} = \left(N_T - N_{ot}(t)\right)\sigma f_p - \frac{N_{ot}(t)}{\tau}. \tag{2}$$

2 models the buildup and annealing of trapped oxide charge as a function of carrier reactions with

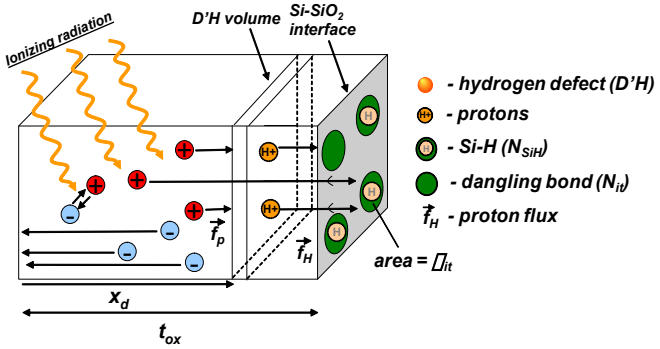

Fig. 68. Processes for oxide trapped charge buildup.

fixed defect sites.

The interface trap (N_{it}) model, illustrated in Fig. 69, shares similar processes with the charge trapping model, e.g.; carrier generation, geminate recombination, and flux-based carrier transport. The N_{it} model is differentiated by its dependence on hydrogen content in the oxide (or other dielectric) during radiation exposure. This was demonstrated experimentally in this program. For interface traps, key model equations include

and

$$\frac{\partial f_H}{\partial x} = N_{DH}\sigma_{DH} f_p - \frac{\partial H^+}{\partial t} \tag{3}$$

Eq. 3 captures the relationship between hole and hydrogenated defect reactions and proton flux

$$\frac{\partial N_{it}}{\partial t} = \left(N_{SiH} - N_{it}(t)\right)\sigma_{it} f_H - \frac{N_{it}(t)}{\tau_{it}}. \quad (4)$$

transport (f_H) and Eq. 4 models the buildup and annealing of interface traps as a function of proton reactions with passivated bonds.

Hydrogen and Dose Rate Effects

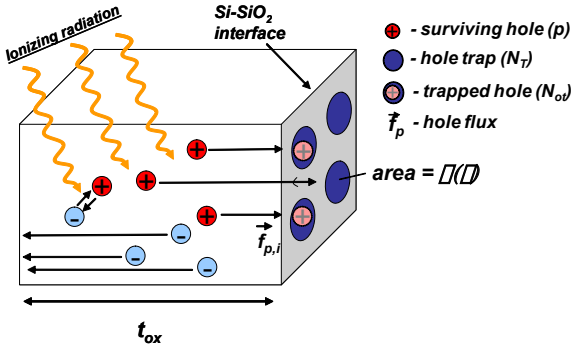

Fig. 69. Processes for interface trap buildup.

Experiments, conducted by ASU, revealed that exposure of a device oxide to molecular hydrogen prior to irradiation can have a very significant impact on the build-up of interface traps. This effect is shown in Fig. 70. In this plot the density of interface traps after a fixed radiation dose (specifically 30 krad(Si)) is shown to increase as the H_2 content in the gas surrounding the sample is increased. These results were reported by Jie Chen after he performed combined irradiations and hydrogen soaks on annular transistors fabricated in a commercial bipolar process [1]. Chen also developed a model for the observed effect based on the diffusion of H_2 from the gas ambient into the device oxide. Reactions between radiation-induced carriers in the oxide and hydrogen species were used to derive the closed form expression

which relates molecular hydrogen concentration to the post-irradiation interface trap density.

$$\Delta N_{it} \approx \kappa \left(N_{D_oH} + \frac{k_1 (N_{H_2})^{\frac{1}{2}}}{1 + k_2 (N_{H_2})^{\frac{1}{2}}} \right), \quad (5)$$

Parameters for the expressions (□, k_1, and k_2) were shown to be related to defect density in the oxide, reaction cross-sections for holes, protons, and interfacial defect sites, oxide thickness, total dose, hydrogen diffusivity, and carrier yield. Fig. 70 shows how the model, with appropriately chosen parameters, can give an excellent fit to the experimental data.

Chen and Barnaby followed up on this work by adding another important variable, irradiation dose rate, into the input matrix. The results and models describing the impact of hydrogen on dose rate response in oxides were first reported in this MURI program. Fig 71 plots N_{it} buildup vs. dose rate for devices exposed to different levels of H_2 (100%, 1% and < 0.01%) prior to and during radiation exposure. For these experiments the total dose level was fixed at 30 krad (Si). As the figure shows, increased levels of hydrogen raise the high and low dose rate saturation levels

and shift the transition dose rate to higher levels. Chen reproduced these effects by modeling hole reactions with hydrogenated defects (adapted from Mclean and others) and annihilating reactions between electrons and holes. Eqs. 6 and 7 are the key reactions in Chen's adapted model:

In (6), DH is a hydrogenated defect in the oxide. In (7) Chen adds electron and hole recombination.

$$DH + p \rightarrow D + H+, \quad (6)$$

$$p + n \rightarrow X. \quad (7)$$

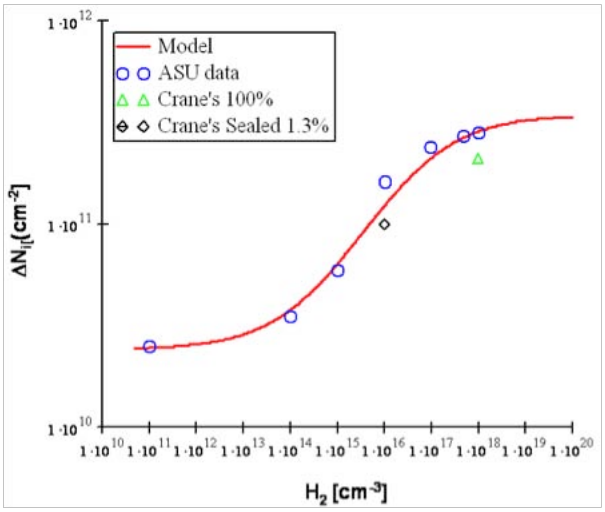

Fig. 70. Fit of model described by (5) to data obtained from experiments.

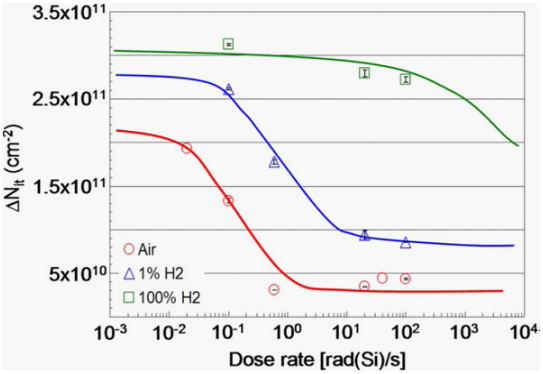

Fig. 71. Measured N_{it} as a function of dose rate for different hydrogen concentrations in thermal oxides

Fig. 72 shows the simulated model results.

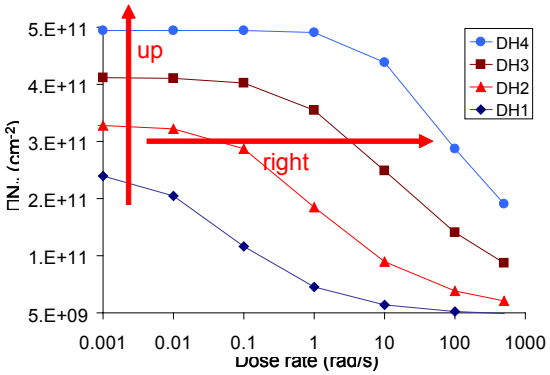

Fig. 72. Simulation of N_{it} formation as a function of dose rate for different hydrogen concentrations.

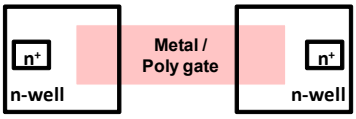

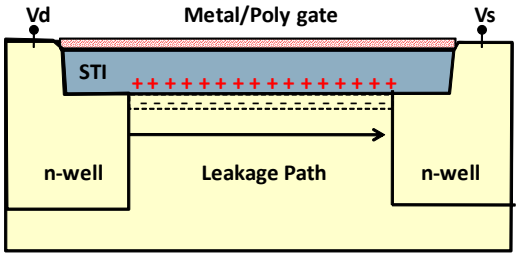

Fig. 73. Layout and cross-sectional view of the NW FOXFET.

Models for TID Defect Buildup in CMOS Isolation Oxides

In this effort, CMOS field oxide test structures, FOXFETS and FOXCAPs, were designed and fabricated in order to provide data for model validation. While several design variants were developed for the program, the most effective characterization tool was an n-well (NW) FOXFET devices fabricated in a 90 nm commercial bulk CMOS low-standby power (LSP) technology. Fig. 73 provides illustrations of the layout and cross-sectional view of the standard NW FOXFET used for the testing. CMOS test structures were irradiated in several ^{60}Co irradiation sources (ASU, BAE systems, and NRL) so that the responses to different dose rates could be determine. Fig. 74 plots oxide trapped charge extracted from the FOXFET data as a function of irradiation and anneal time. These data indicate similar trends in the total dose responses and anneal rates (i.e. no strong dose rate dependence observed).

Data sets, such as the one in Fig. 74, was used to build and verify an analytical model for the various processes involved in trapped charge formation and annealing in isolation oxides. The key equation, expressed formally in [7], is

$$\Delta not = D\Delta tgont\sigma pfy,pxp - not\sigma nfy,nxn - m\cdot\Delta tln(10)\cdot t\,, \qquad (8)$$

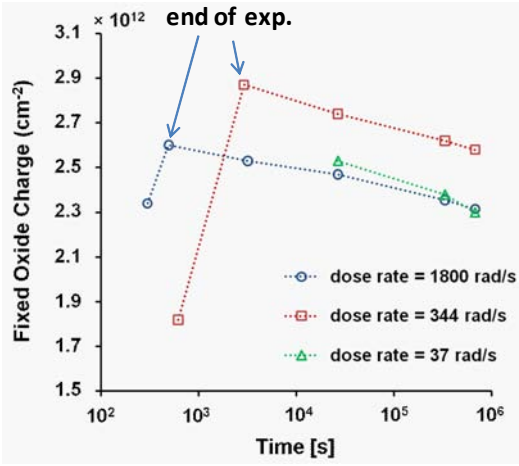

Fig. 74. N_{ot} vs time extracted during and after 60Co exposures at different dose rates.

which describes the dependence of trapped charge buildup and removal in oxides on the flux and trapping of carriers in the oxide (i.e., both holes and electrons) and a time dependent annealing function. As illustrated in Fig. 75, the analytical model (solid line labeled 'ANYL') accurately reproduces the amount of trapped charge buildup as a function of radiation exposure time for dose rates of 1800 rad/s, 344 rad/s, and 20 rad/s. The experimental data in the figures are represented by the symbols and labeled 'EXP'.

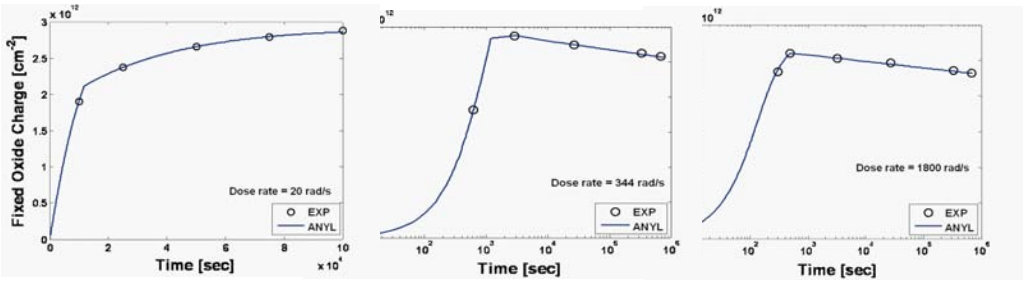

Fig. 75. Not vs. time data and analytical model fits for three different dose rates.

B. TID Effects Characterization and Modeling in Advanced CMOS Transistors

Overview

In the MURI program, ASU utilized the PSP compact modeling framework to build analytical models for TID effects in CMOS transistors. Radiation-enabled compact models were constructed with highly accurate surface-potential based formulations. Model development was performed on both bulk and SOI CMOS technologies. Extensive experiments and TCAD simulations were conducted to validate the models.

Bulk CMOS

Ionizing-radiation effects in bulk CMOS devices were incorporated into the industry standard surface-potential based compact model (PSP). The inclusion of total ionizing dose (TID) effects into PSP was accomplished by renormalization of the surface potential equation (SPE) in order to make the PSP formulation applicable to irradiated devices. Model verification was performed via comparison to experimental data obtained from the NW FOXFET devices fabricated in a 90

nm low-standby power commercial bulk CMOS technology. The model accurately describes contributions to off-state currents from inter-device leakage and demonstrates its capabilities for simulating radiation-induced degradation in advanced CMOS integrated circuits (ICs). Eqs. 9-11 represent the key functions for the model.

$$(V_g - V_{FB} - \xi\psi_s)^2 = \gamma^2\phi_t H(\beta\psi_s), \tag{9}$$

$$V_{FB} = \Phi_{MS} - \frac{q}{C_{ox}}\left(N_{ot} + D_{it}\phi_b\right), \text{ and} \tag{10}$$

$$I_{ds} = \frac{W}{L}\mu_{eff} C_{ox}\left(q_{im} + \alpha_m\phi_t\right)\Delta\psi\,. \tag{11}$$

Eq. 9 is the implicit surface potential equation (SPE). Eq. 10 is the flatband equation, which captures the impact of the radiation-induced defects. Eq. 11 is the drain current equation using the symmetric linearization method. ASU reported the results in [8]. Through renormalization of the SPE, ASU researchers were able to build compact models that produced extremely accurate fits to the transistor (FOXFET) data, both prior to and after high levels of radiation exposure. As an example, Fig. 76 shows the alignment between the Id vs. Vgs data (symbols) and model (solid line).

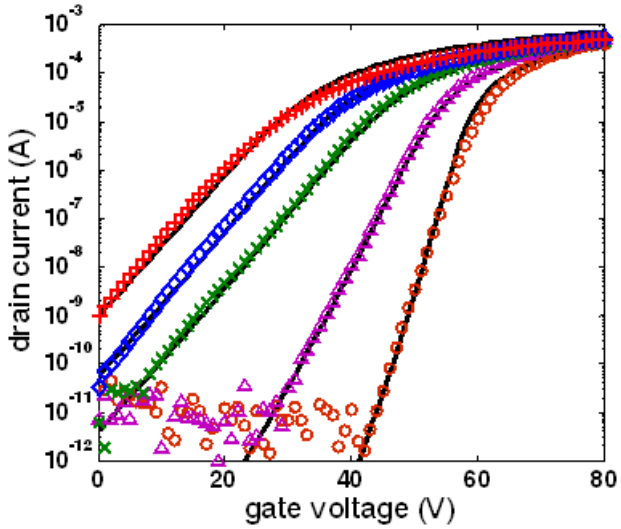

Fig. 76. I_d-V_{gs} characteristics obtained analytically (solid lines) and experimental data (symbols) at the different levels of TID (V_d = 0.1 V, V_s = V_b = 0 V).

Silicon-on-Insulator CMOS

ASU's research effort on SOI devices for the MURI program focused on modeling radiation effects on single and multiple gate devices. For the conventional single gate transistor (shown in Fig. 77), ASU developed a model for the GIDL enhancement of back channel leakage which was reported previously.

In the model, holes injected into the floating body from a band-to-band tunneling current ($J_{p,BBT}$) charge the body of an n-channel SOI FET to a potential V_B. This effect is expressed mathematically as,

$$V_B = \phi_t \ln\left(1 + \frac{J_{p,BBT} \cdot W_N \cdot N_D}{q \cdot D_p \cdot n_i^2}\right) \quad (12)$$

Radiation damage to the thick buried oxide introduces a defect potential which is proportional to the sum of oxide trapped and interface trap defects. This defect potential is expressed mathematically as,

$$\phi_{nt} = \frac{q}{C_{oxf}}\left[N_{ot} - D_{it}\left(\psi_b - \phi_f\right)\right] \quad (13)$$

The combined effect of damage to the buried oxide and body charging from GIDL significantly reduced the back-gate threshold voltage and enhanced leakage current in floating body SOI devices. ASU successfully modeled this effect with calibrated Eqs. 12, 13, and

$$\left(V_{GF} - \Phi_{MS}^{f} - \psi_s - V_B\right) - \left(\frac{t_{ox}}{t_{box}}\right)^2 \left(V_{GB} - \Phi_{MS}^{b} + \phi_{nt} - \psi_b - V_B\right) = \gamma^2 \left(\phi_t\right)\left[H_{front}\left(\psi_s\right) - H_{back}\left(\psi_b\right)\right] \quad (14)$$

Eq. 14 is the modified double gate SPE used for SOI transistors.

In addition to the conventional single gate SOI modeling effort, ASU also performed an extensive examination of radiation effects on multiple gate transistors. This study revealed a strong geometric dependence of TID sensitivity in SOI multiple gate FETs, specifically FinFETs structures. This dependence was related to the FinFET width. Shown in Fig. 79 are 2D TCAD contour plots of two FinFETs used in the analysi. The devices are identical except in the width of the silicon film (t_{Si}) which defines the fin. For the structures shown in Fig. 79, one fin width is 10 nm and the other is 50 nm. The figure illustrates the potential contour in the silicon body as a result of charge buildup in the buried oxide. As the numerical results show, the wider devices is more responsive to the defects, thus more sensitive to radiation damage. Sanchez Esqueda et al. derived an analytical model for this effect which they reported. Fig. 80 shows how the model compares to the results of radiation experiments on a sub 100 nm FinFET technology. In this figure, model predictions of increased off-state leakage current vs. dose is compared to experimental data on devices with 80 nm and 40 nm fin widths. The data was obtained in collaboration with researchers at Vanderbilt Univerisity.

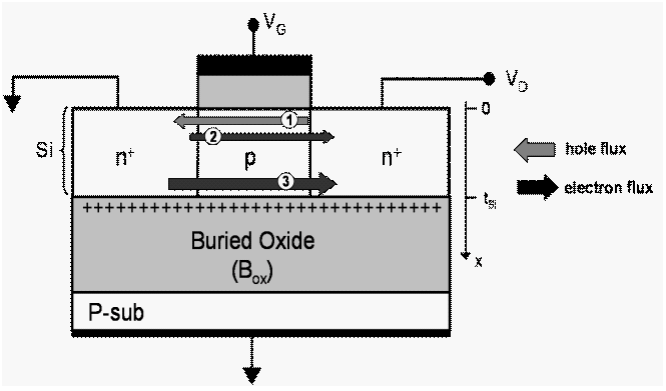

Fig. 77. Cross-section illustrating three current processes related to the radiation response on I-V characteristics of FD-SOI transistor

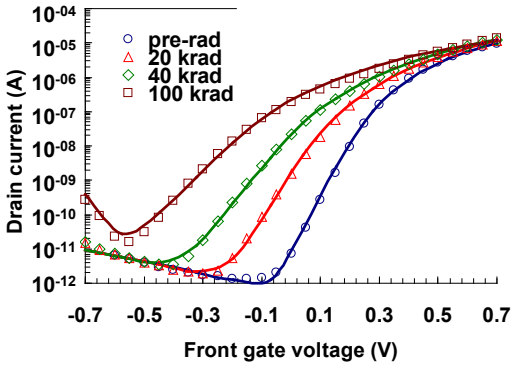

Fig. 78. Plot of ID vs. VGF characteristics obtained experimentally (symbols) as well as the simulated curves (solid lines) with VD = 1.4 V.

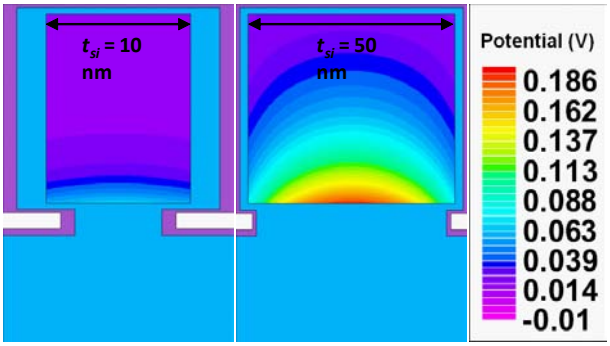

Fig. 79. Numerical simulation results showing greater impact of Not buildup in wider FinFET designs.

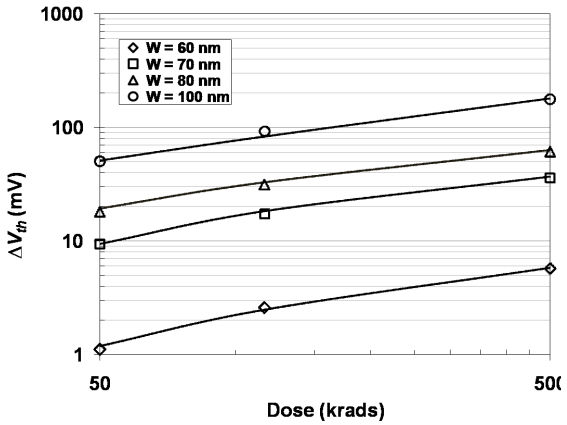

Fig. 80. Theshold voltage shift vs. dose for different fin widths (solid line is the model and symbols are experimental data)

3.24 Theory of Phenomena Induced by Energetic Ion Beams

A. Stopping Power of Channeled Ions in Si

When an ion beam hits a crystal, the primary event is energy transfer from the ions to the solid. The energy transfer may induce atomic displacements. In the simplest case, an ion beam can be "channeled" through the low-electron-density interstitial regions of Si. The energy loss to

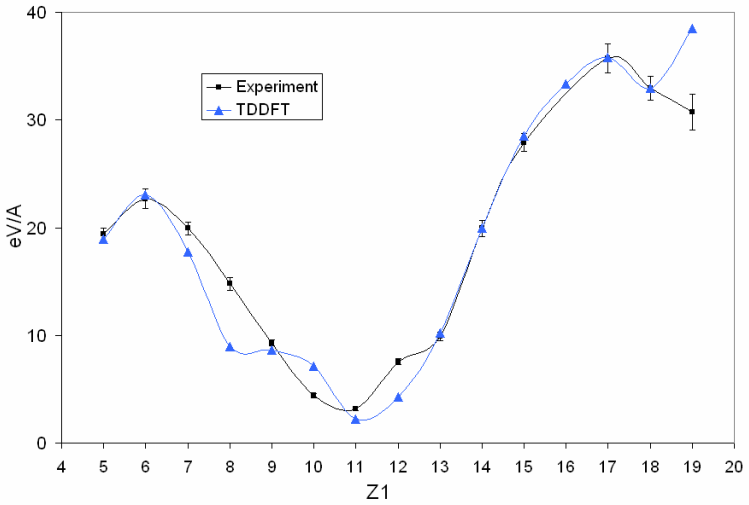

Fig. 81. Stopping power of ions channeled through the low-electron-density channles of a Si crystal. Z1 is the atomic number of the channeled ion. Experimental data from F. H. Eisen, Can. J. Phys. 46, 561 (1968).

the solid is usually cast as "stopping power" and is a function of the atomic number Z of the ions. Experiments are available that show oscillations of stopping power as a function of Z. We used recently implemented codes of time-dependent density functional theory, a state-of-the-art approach for calculating the dynamical evolution of a many-atom system, to compute the stopping power for a series of ions (boron to calcium in the periodic table) channeling in <110> Si channels The theory has no adjustable parameters and produced results in excellent agreement with the data of Eisen (1968) (Fig. 81). All prior calculations included adjustable parameters and more limited agreement with the data. The calculations demonstrated the need to include the full dynamics of the electron system in Si to capture the observed effects. [R. Hatcher, M. Beck, A. Tackett, and S. T. Pantelides, "Dynamical effects in the interaction of ion beams with solids", Phys. Rev. Lett. 100, 103201 (2008)].

B. Displacement Damage Differences in n-type and p-type Si

Radiation-induced displacement damage rates in semiconductor materials generally correlate well with the calculated non-ionizing energy loss (NIEL) portion of the total radiative energy deposition rate. Developing and refining models for the calculation of NIEL has been a continuing focus of the radiation effects research community. While NIEL has enjoyed wide success as a first-order predictor of effective displacement damage rate, it is well known that p- and n-type Si can exhibit differing damage rates, as determined from observed reductions in effective minority carrier lifetimes or diffusion lengths. In these cases, p-type Si exhibits a lower rate of reduction in carrier lifetimes than n-type Si (see Fig. 82). This difference is typically interpreted to indicate a lower concentration of radiation-induced defects–that is, less damage–in the p-type Si samples, due to an atomistic mechanism that must differ in effect between p- and n-type Si.

Using state-of-the-art quantum mechanical calculations, we have shown that the damage rate differences in n- and p-type Si correlate directly to the fraction of radiation-induced displacement damage due to low-energy primary knock-on atom (PKA) recoils. These low-energy damage events produce isolated vacancy-interstitial pairs (Frenkel Pairs, FPs) that quickly evolve towards thermodynamic equilibrium following the initial radiation event. We show that the details of this evolution, initially controlled by the fundamental properties of Frenkel Pairs themselves, contribute to the observed nversus p-type damage rate differences through previously reported dopant-

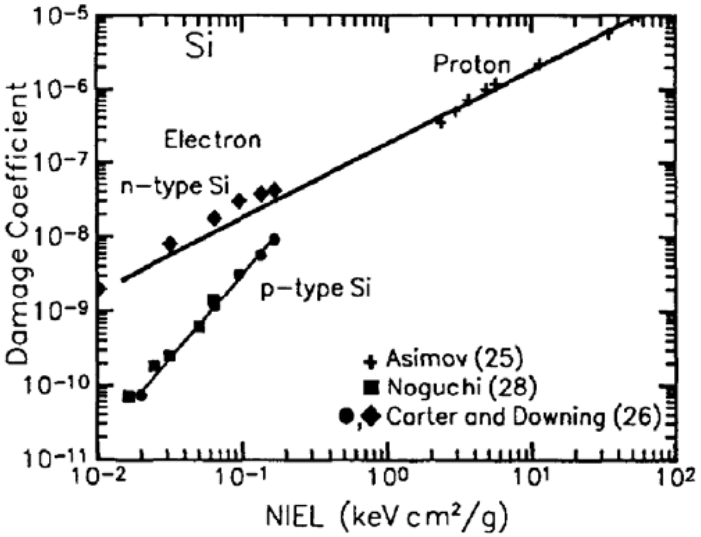

Fig. 82. Measured minority carrier diffusion length damage coefficients for 1 Ω-cm n- and p-type Si after irradiation with various incident particles. Figure from G. P. Summers et al. "Damage correlations in semiconductors exposed to γ-radiation, electron-radiation and proton-radiation," *IEEE Trans. Nucl. Sci.*, vol. 40, no. 6, pp. 1372–1379, Dec. 1993.

dependent stabilities of vacancy-impurity complexes. Further, we show that, for certain conditions, FPs can directly contribute to n- versus p-type damage rate differences by functioning as metastable, shallow electron traps that can retard carrier transport and thereby increase the inferred carrier lifetimes. [M. J. Beck, L. Tsetseris, M. Caussanel, R. D. Schrimpf, D. M. Fleetwood, and S. T. Pantelides, "Atomic-scale mechanisms for Low-NIEL dopant-type dependent damage in Si", IEEE Trans. Nucl. Sci. vol. 53, No. 6 p. 3621-3628 (2006)]

To study the details of the atomic mechanisms that ultimately lead to differing damage rates in n- and p-type Si, we performed new calculations of the fundamental properties of vacancy-interstitial (Frenkel) pairs (FPs) in Si using density functional theory. We showed that isolated FPs either recombine, remain as interacting vacancy-interstitial pairs, or dissociate into free vacancies and interstitials, with probabilities that depend on the position of the Fermi level in the Si, i.e., the doping type. In particular, we find that, in p-Si small FPs (vacancy-interstitial separation distances ~8 Å) are more likely to be stable with respect to defect recombination than equivalent FPs in n-Si. The stability of FPs against dissociation is found to be similar to that of vacancy-B pairs, with a FP binding energy (relative to the energy of non-interacting, isolated vacancies and interstitials) of ~ 0.5 eV. Thus, the formation dynamics of vacancy-impurity complexes, shown here to be indirectly influenced by the fundamental properties of FPs, are likely dominant in determining observed n- and p-type Si damage rate differences for finite temperatures. In addition, FPs may directly influence n- and p-type differences at low temperatures. [M. J. Beck, L. Tsetseris, and S. T. Pantelides, "Stability and dynamics of Frenkel pairs in Si", Phys. Rev. Lett. 99, 215503 (2007)].

C. Displacement Damage Formation in Si

Atomic-scale processes during displacement damage formation have been previously studied using molecular dynamics (MD) calculations and empirical potentials. Low-energy displacements (1 keV) are characterized by a high cross-section for producing secondary knock-on atoms and damage clusters, and determine the threshold displacement energy (an important parameter in NIEL calculations). We used first-principles, parameter-free quantum mechanical calculations of

the dynamics of low-energy displacement damage events in Si. We found that isolated defects formed by direct displacements can result from damage events of 100 eV. For higher energy events, the initial defect profile, which subsequently undergoes thermal annealing to give rise to a final stable defect profile, is the result of the relaxation and recrystallizatioof an appreciable volume of significantly disordered and locally heated crystal surrounding the primary knock-on atom displacement trajectory. [M. J. Beck, R. Hatcher, R. D. Schrimpf, D. M. Fleetwood, and S. T. Pantelides, "Quantum mechanical description of displacement damage formation", IEEE Trans. Nucl. Sci. vol. 54, No. 6 pp. 1906-1912 (2007)].

Displacement Damage Effects In Single-Event Dielectric Rupture

Building on our results in *c*-Si, we examined the effects of Si and O recoils in *a*-SiO_2 systems. In particular we probed the role of low-energy displacement damage in triggering single-event gate rupture (SEGR), or, more generally, single-event dielectric rupture (SEDR). Using SRIM 2008, we showed that irradiation of thin *a*-SiO_2 gate oxides with heavy ions at energies associated with SEGR or SEDR produces low-energy (~100 eV) atomic recoils within the oxide layer. While the overall probability of individual recoils varies strongly with incident ion species and energy, the distribution of recoil energies is independent of both energy and ion species for the high-LET irradiations we considered. Low-energy recoils (100 eV) in *a*-SiO_2 produce defected regions in the amorphous network that result in a high density of defect states throughout the *a*-SiO_2 band gap (see Fig. 83). These electronic states are localized on the recoil-induced defects and are therefore spatially correlated. The combination of neighboring defects and associated defect states lying within the *a*-SiO2 band gap results in a "stepping stone" path (similar to conducting paths invoked in percolation models of stress- or radiation-induced leakage current) for low resistivity charge transfer along the length of the recoil damaged region. These low-resistivity paths serve as conducting pipes for capacitive discharge.

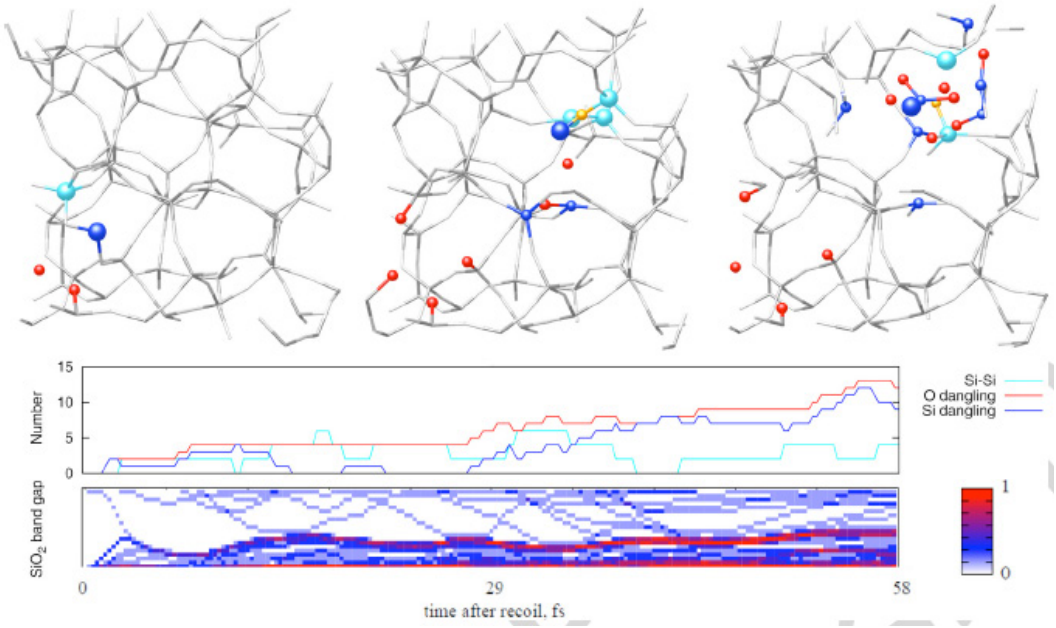

Fig. 83. Top: Three snap shots of the evolution of an SiO2 network following the recoil of one Si atom. The colored atoms indicate the presence of network defects. Bottom: number of defects and their energy level in the band gap as a function of time.

Conducting pipes generated directly by SHI-induced displacement damage provide a unifying physical mechanism for the direct formation of electrically-active structural defects in dielectric layers. The direct formation of defects as displacement damage obviates the need to invoke complex models for conversion of electron excitation energy to ion kinetic energy to explain the initial triggering mechanism for permanent heavy-ion damage to dielectrics. Hence SEDR, radiation-induced soft breakdown (RISB), and long-term reliability degradation (LTRD), latent track formation and transient ion-induced leakage currents are damage events sharing, at least in part, the same physical origin: ion-induced displacement damage leading to the formation of low-resistivity conducting pipes (see Fig. 84). For sufficiently high fields applied during irradiation, high currents through these paths will lead to thermal runaway, and SEDR will be observed. At lower fields, lower currents will not necessarily lead to thermal runaway, and RISB will be observed. At longer times, device degradation enhanced by previous ion-induced damage (in the form of residual defect pockets) will give rise to LTRD.[M. J. Beck, B. R. Tuttle, R. D. Schrimpf, D. M. Fleetwood, and S. T. Pantelides, "Atomic-displacement effects in single-event gate rupture", IEEE Trans. Nucl. Sci. vol. 55, No. 6, pp. 3025-3021 (2008)]

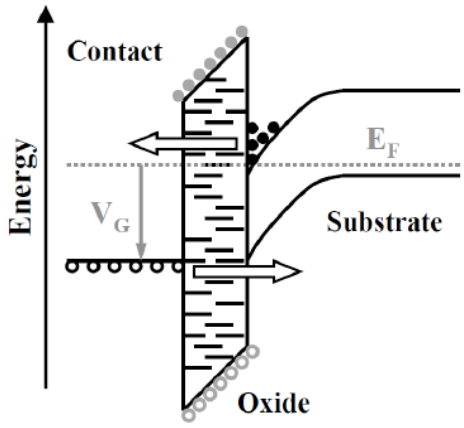

Fig. 84. Band diagram of a dielectric stack immediately following a heavy-ion strike. Filled and empty circles represent electrons and holes, while black and gray circles represent thermal and ion-LET induced carriers. Here we schematically show the displacement-damage-induced defect states representing a physical conducting path. Bold arrows indicate the field-injected current flow through the oxide. This current causes thermal runaway, resulting in permanent structural damage in the oxide layer.

We subsequently laid the foundations of a multi-scale first-principles approach to calculate leakage currents through thin dielectric films containing recoil-induced defects. We used the "source-and-sink" for quantum transport calculations developed recently by Varga and Pantelides to calculate current-voltage characteristics of thin SiO_2 films between Al electrodes. To isolate the detailed effects of individual atomic-scale defects, we modeled ion-induced defects by removing different combinations of oxygen atoms from the SiO_2 cell and calculating the transport properties as a function of removed atoms. We then constructed a transport model using three-dimensional percolation theory and Mott defect-to-defect tunneling. This model is similar to previous percolation models of dielectric leakage, and analogous to the tunneling models invoked in extensive previous studies of trap-assisted tunneling (TAT). A key difference here is that our defect distributions are obtained from quantum mechanical calculations and evolve with time. We constructed a specific model using defected SiO_2 thin films produced by dynamical DFT calculations (Figs. 85-86). The

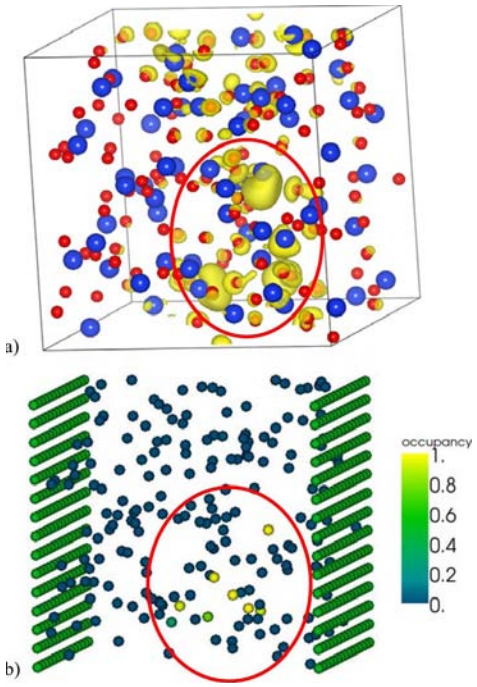

Fig. 85 (a) Localization of electronic density projected onto a defect state near conduction band-edge and (b) corresponding high-electron occupancies in percolation calculation of leakage current.

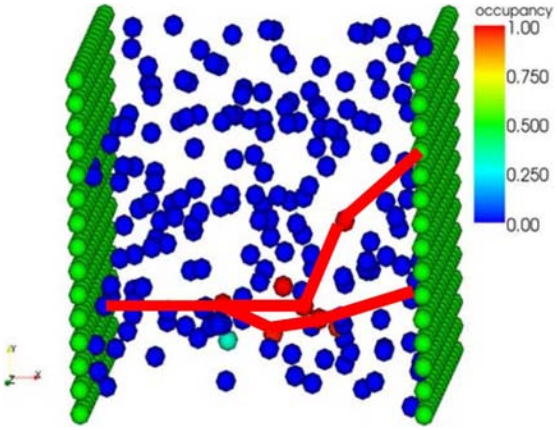

Fig. 86. Example of a percolation path.

model has two parameters: a defect radius r_0 that defines the defect's localization and controls the exponential hop, and a hop frequency factor ν_0. Ultimately these parameters can be obtained from quantum mechanical calculations. In the first implementation of the model we assumed a value r_0 = 2 Å for the average "defect radius" and $\nu_0 = 10^{12}$ Hz, as estimated using experimental data of hop attempt rates. With these values, the average current through a defected SiO_2 structure is shown in Fig. 87. It is in both qualitative and quantitative agreement with experimental current-voltage characteristics showing RISB, giving us an initial validation of the approach. The results illustrate that *low-energy recoils that are directly generated by heavy ion strikes on oxide layers can produce low-resistivity paths through the oxide layers, resulting in appreciable leakage currents*. [M. J. Beck, Y. S. Puzyrev, N. Sergueev, K. Varga, R. D. Schrimpf, D. M. Fleetwood, and S. T. Pantelides, "The role of atomic displacements in ion-induced dielectric breakdown", IEEE Trans. Nucl. Sci. vol. 56, No. 6, pp. 3210-3217 (2009)].

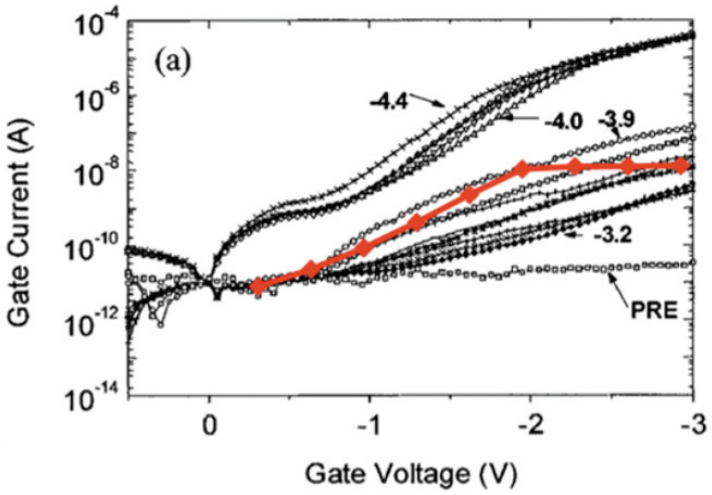

Fig. 87. Calculated defect-mediated leakage current vs. voltage (red curve), overlain on measured post-irradiation leakage currents, labeled by the gate voltages during irradiation. The curves labeled -3.2 to -3.9 V correspond to RISB.

Physical Mechanisms Responsible for the Abruptness of the Si-SiO_2 Interface

We used extensive first-principles density-functional theory calculations to identify key mechanisms that control the morphology of the Si-SiO2 interface. The key findings that support a smooth layer-by-layer propagation of oxidation fronts are the following: i) there is an effective barrier of about 2 eV for O2 molecules to cross the near interfacial region and arrive at the substrate. This barrier accounts for the observed 2-eV activation energy for the "reaction" step in the Deal-Grove model of thermal oxidation. ii) the oxidation reaction of Si-Si bonds through dissociation of O2 molecules is almost barrier-less and strongly exothermic. This fact alone points to a random deposition (RD) problem with large roughness, contrary to the established smoothness of the Si-SiO2 interface. iii) diffusion of O atoms between Si-Si bonds along the oxidation front is activated at thermal oxidation temperatures Tth due to relatively small barriers of 2-2.3 eV. iv) in certain cases, interfacial Si-O-Si bridges agglomerate with binding energies of about 0.3-0.4 eV per O atom. In combination with finding iii), we thus uncover the basic condition that favors possible nucleation and island growth mode. v) migration of O in bulk Si is also activated at Tth, which raises the question why O does not simply dissolve in Si. As a mechanism that suppresses solvation, we find that errant O species that arrive from the substrate get trapped at the interface and eventually relax in configurations consistent with a smooth front (an example of the latter relaxation is shown in Fig. 88). Occasional desorption back into the bulk Si decreases the long-range roughness of the interface. Thus, the results described in iii)-v) resolve the quandary posed in ii) and provide a description for the evolution of the oxidation front as a random "deposition" process with relaxation. This kind of process is known to result in smooth film growth on surfaces and also provides for overall smoothness in the case of the Si-SiO2 interface, as observed. [L. Tsetseris and S. T. Pantelides, "Oxygen migration, agglomeration, and trapping: key factors for the morphology of the Si-SiO2 interface", Phys. Rev. Lett. 97, 116101 (2006)].

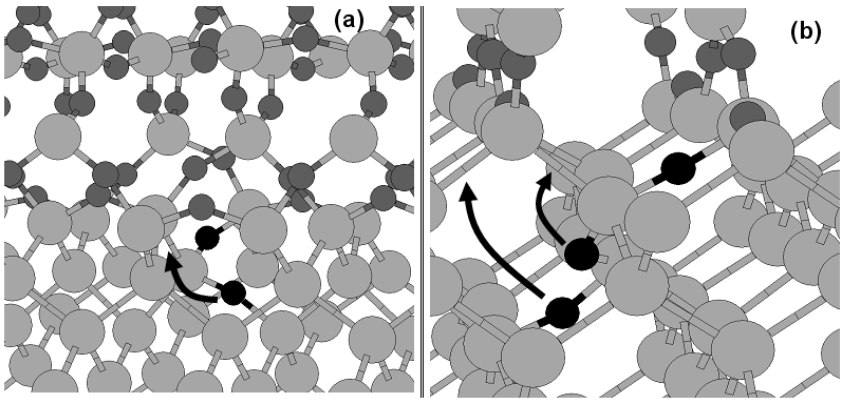

Fig. 88. Sticking and reorganization (smoothing) of an (a) O dimer, (barrier is 2.2 eV), and an (b) O trimer at the Si-SiO_2 interface.

D. Properties and Phenomena in Strained-Si Channels

First-principles Calculations of Electron Mobilities in Strained-Si channels

We implemented a first-principles, parameter-free approach based on density functional theory to calculate electron mobilities in Si channels. Initial calculations were based on SOI models for which atomic-scale SiO2-Si-SiO2 structures were constructed. Atomic-scale roughness at the interface, consisting of either suboxide bonds (Si-Si bonds on the oxide side of the interface) or oxygen protrusions (Si-O-Si bonds on the Si side of the interface). We applied the method to explore the role of strain in enhancing the electron mobility. The origin of this enhancement has not been clearly established on the basis of the usual mechanisms (phonons, Coulomb scattering, and macroscopic interface roughness). We found that scattering from the primitive atomic-scale roughness elements at the Si-SiO2 interface can account for the data, as shown in Fig. 89. The small open circles represent strain-induced mobility enhancement when the only interface scattering centers are suboxide bonds; the open squares represent strain-induced mobility enhancement when the only interface scattering centers are oxygen protrusions. The large open circles represent the combined effect. Black symbols are data from various references taken in single-gate devices. [G.

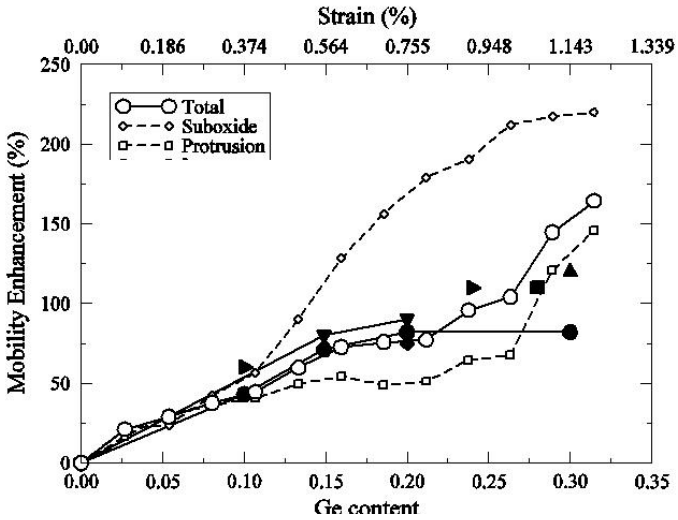

Fig. 89. Calculated electron mobilities in a strained-Si channel compared with available data.

Hadjisavvas, L. Tsetseris, and S. T. Pantelides, "The origin of electron mobility enhancement in strained MOSFETs", IEEE Electron Device Letters, vol. 28, No.11, p. 1018-1020 (2007)].

Hydrogen-dopant Interactions in SiGe and Strained Si

The appearance of carrier traps and the deactivation of dopants are typical hydrogen-related phenomena that are of prime importance to the reliability of traditional Si-based devices. We used density functional calculations to probe the dynamics of hydrogen as individual impurities or in complexes with dopants in strained Si (s-Si) and SiGe systems. We found that the charged state determines the tendency of hydrogen to be released from dopant sites and to shuttle between a SiGe substrate and a s-Si overlayer. In this way, the effect of hydrogen differs between accumulation and inversion cycles of s-Si and SiGe devices. [L. Tsetseris, D. M. Fleetwood, R. D. Schrimpf, and S. T. Pantelides, "Hydrogen–dopant interactions in SiGe and strained Si" Appl. Phys. Lett. 96, 251905 (2010)].

Vacancies in SiGe/Strained-Si Structures

In other, still unpublished work, we examined the relative energetic of Si vacancies in strained-Si and a SiGe substrate. We found that Si vacancies and Si self-interstitials have lower formation energies in SiGe, which has desirable consequences for radiation-induced defects: Si vacancies and Si self-interstitials would tend to leave the strained-Si channel and migrate into the SiGe substrate. A secondary effect is that Si interstitials in SiGe tend to replace a network Ge and create a Ge interstitial. Another secondary effect is that Ge atoms tend to agglomerate around Si vacancies and Ge interstitials in the SiGe substrate.

E. Theory of Ge-GeO_2 Interfaces

Defect Passivation and the Morphology of the Ge-GeO_2 Interface

Si has been the electronic material of choice because of, among other reasons, its high-quality interface with its oxide compound SiO_2. But as high-k materials replace SiO_2 in the gate dielectric, new materials emerge also to take the place of Si as the active semiconductor in devices. Ge is a possible alternative because of its large carrier mobility. There is currently a resurgence in efforts to grow, analyze, and optimize Ge-based devices, especially those that combine Ge with high-k systems, such as HfO_2. Typically, a thin GeO_x interlayer appears between the Ge substrate and HfO_2 the properties of which has attracted significant experimental and theoretical interest in the last couple of years. One of the most important issues for this matter is the existence and nature of interfacial carrier traps. In the case of Si, P_b centers (i.e. interfacial Si dangling bonds) are well established as the dominant interface traps. There is an ongoing debate whether P_b centers are important also in the case of Ge-GeO_2 interfaces. Assuming that Ge dangling bonds do exist at the Ge-GeO_2 interface, the most plausible passivation scenario is through hydrogenation. We have found, however, that an interfacial Ge-H bond dissociates through an exothermic reaction that releases H to the GeO_2 network and 0.4 eV. The reaction barrier of the process depicted in Figs. 90(a)-(b) is 1.2 eV. The analogous dissociation reaction of Figs. 90(c)-(d) with a F passivant is endothermic, but the small reaction energy (0.2 eV) and barrier (0.4 eV) suggest that fluorination is not a very effective way of dangling bond passivation either.

Another important issue for Ge-based devices is the morphology of Ge-GeO_2 interfaces. In the Si-SiO_2 case, we previously identified a set of mechanisms, namely oxygen migration, agglomeration, and trapping, that support a scenario of abrupt and smooth oxidation front. We probed the same set of mechanisms for Ge-GeO_2 boundaries. We found that an O_2 species migrates as peroxy bridges

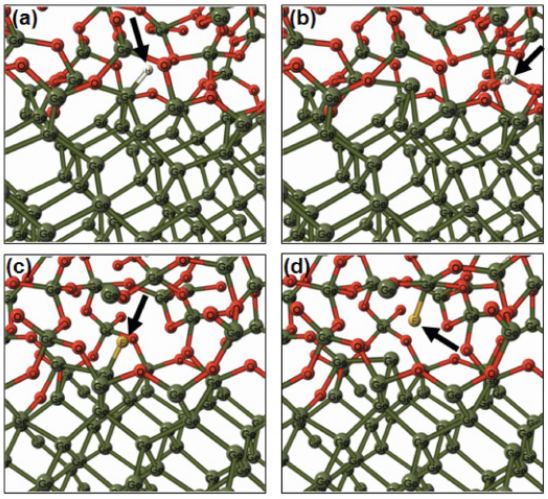

Fig. 90. Dissociation of passivated bonds at the Ge-GeO2 interface: (a), (c) depict passivated Ge-H and Ge-F bonds, (b), (d) show Ge dangling bonds and released H, F atoms.

towards the Ge substrate where it creates a pair of vicinal Ge-O-Ge structures releasing about 3 eV of energy. We then investigated the stability of various Ge-O-Ge protrusions and found that, compared to the Si-SiO_2 system, there is a stronger tendency for atomic-scale roughness at the Ge-GeO_2 interface. For example, the 2-O protrusion of Fig. 91(b) is more stable (by 0.4 eV) than the "smoother" structure of Fig. 91(a). Further studies will clarify if such protrusions are in fact thermal donor precursors that can transform to carrier traps. [L. Tsetseris and S. T. Pantelides, "Morphology and defect properties of the Ge-GeO_2 interface", Appl. Phys. Lett. 95, 262107 (2009)].

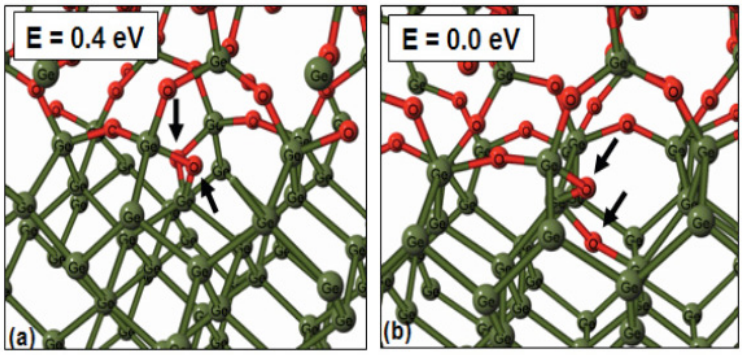

Fig. 91. O protrusions at a Ge-GeO2 interface.

Ge Volatilization Products in High-k Dielectrics on Ge

GeO molecules are often emitted by Ge substrates under high-temperature annealing and, in the case of gate stacks, they diffuse through high-*k* oxides. We used first-principles quantum-mechanical calculations to probe the stability of these impurities in La_2O_3 and HfO_2 and their effect on the electronic properties of the host systems. We found that the GeO species introduce several different levels inside the energy band gaps of La_2O_3 and HfO_2. As a result, the impurities may act as charge carrier traps. Hydrogenation of the GeO defects modifies the position and numbers of gap states, but does not eliminate the carrier trap levels completely. The results suggest a possible role of Ge volatilization in enhancing leakage currents and degradation in high-*k* gate stacks of Ge-based

TABLE 1.1
SIGE HBT DEVICE LIST FOR IBICC TESTING

Device Name (Abbreviation)	**Emitter Area** A_E (μm)	**Substrate Resistivity** ($\Omega \cdot$ cm)
IBM 5HP (IBM 5HP)	0.5×10.0	8-10
Jazz SiGe-120 Bulk (Jazz bulk)	0.2×10.16	8-10
Jazz SiGe-120 SOI† (Jazz SOI)	0.2×10.16	8-10
Jazz SiGe-120 High Resistivity Substrate† (Jazz HRS)	0.2×10.16	1500
National SiGe-8iED Bulk (NSC bulk)	0.4×20.0	8-10
National SiGe-8iED epi† (NSC epi)	0.4×20.0	0.009

† Not standard commercial product offerings. Experimental hardware lots.

devices. [E. Golias, L. Tsetseris, A. Dimoulas, and S. T. Pantelides, "Ge volatilization products in high-k dielectrics", Microelectron. Engin., in press.]

3.25 Substrate Engineering Concepts to Mitigate Charge Collection in Deep Trench Isolation Technologies

A. Abstract

Delayed charge collection from ionizing events outside the deep trench can increase the SEU cross section in deep trench isolation technologies. Microbeam test data and device simulations demonstrate how this adverse effect can be mitigated through substrate engineering techniques. The addition of a heavily doped p-type charge-blocking buried layer in the substrate can reduce the delayed charge collection from events that occur outside the deep trench isolation by almost an order of magnitude, implying an approximately comparable reduction in the SEU cross section.

B. Overview

Some device technologies that typically make use of Deep Trench Isolation (DTI), such as Silicon-Germanium HeterojunctionBipolarTransistors(SiGeHBTs),haveSingleEvent Upset (SEU) cross sections exceeding the active area of the device. Recent work reveals that shift registers composed of a particular type of SiGe HBT have an SEU cross section approximately ten times the active area of the device, which is defined by the area enclosed by the DTI. This work shows that the SEU cross section enhancement at highly ionizing energies is the result of delayed (long time) charge collection from regions of charge generation many micrometers away from the DTI. The range and magnitude of charge collection is primarily governed by the doping concentration and physical structure of the substrate.

Heavy ion microbeam irradiation reveals the effects of substrate engineering in SiGe HBTs, specifically how it affects delayed charge collection. Based on the microbeam charge collection data, a substrate engineering concept in the form of a p-type charge-blocking buried layer at the bottom of the DTI is proposed. Three dimensional Technology Computer-Aided Design (TCAD) simulations reveal that the buried layer concept reduces charge collection by more than 70% for lightly ionizing events that occur outside the DTI and by more than a factor of ten for highly ionizing events.

C. Ion Microprobe Testing

All of the SiGe HBTs underwent four-probe IBICC so that charge collection on all the terminals (emitter, base, collector, and substrate) could be monitored simultaneously. The emitter, base, and collector were held at 0 V while the substrate was biased to - 5V via the charge collection amplifier biasing. These charge collection bias conditions were intended to replicate the "off-state" of the device-under-test (DUT), the most sensitive state. This charge collection setup had fidelity to those conditions. Experiments were conducted using normally-incident 36 MeV oxygen ions with approximately a 1 μm spot size. The ions have a range of 25.5 μm in silicon, a surface incident LET of 5.2 MeV cm^2 /mg,

IBICC data is reported for six devices from three different vendors: IBM Corporation, Jazz Semiconductor and National Semiconductor, with relevant parameters detailed in Table I. The abbreviations used in Table I will be used throughout the rest of the manuscript. All devices were subjected to the same ionizing radiation under identical bias conditions. The Jazz HRS and SOI SiGe HBT devices, as well as the NSC epi SiGe HBT device, supplied by BAE Systems, were from experimental hardware lots and are not standard commercial product offerings. All devices are with p-type substrates. The DTI in all six devices is approximately the same.

The data sets shown in Fig. 92 (a)–(c) displays integrated charge collection on the collector terminal, since ion-induced collector current is the major cause of SEU in most standard SiGe HBT circuits. All subsequent plots of charge collection will be for the collector terminal. While the data plots here focus on the collector terminal, the majority of the current sensed on the collector terminal also appears on the substrate terminal. The currents have opposite polarities since one current is traveling into the device and one is traveling out of the device.

The data clearly show the structure of the devices. The peak charge collection occurs for strikes within the DTI and the tails represent charge collection from events occurring outside the DTI. These two regions of data reveal separate charge collection characteristics, which are position dependent. Within the DTI, drift transport dominates due to the extension of the potential into the substrate from the bottom of the subcollector (collector-substrate) depletion region. Normally-incident 36 MeV oxygen ions deposit about 26 MeV in the substrate of a typical etched device, which generates roughly 1.1 pC of charge. With the noted exception for the IBM 5HP devices applies here, since the presence of the thick overlayers decreased the range of the ion in the substrate and thus the total charge generated.

The peak charge collection in Fig. 92(a)–(c) occurs within the DTI for ions that cross the reverse-biased subcollector junction. The microbeam data show this peak to be about 1 pC, a charge collection efficiency of approximately 90%. Outside the DTI, there is no pre-existing electric field to move the charges once they separate from the ion track, so the charge collection is slower and less efficient since the electrons must diffuse to the subcollector junction to induce current on the collector terminal. The tails to either side of the DTI seen in all the figures are representative of this collection mechanism. They peak at about 200 fC and fall off to less than 50 fC in most cases. This amount of charge is sufficient to cause upset in typical unhardened SiGe HBT circuits.

D. Charge Collection Modeling and Mitigation Strategies

Present simulation and experimental results suggest that delayed charge collection from ionizing events outside the DTI can be mitigated—if not eliminated—by introducing a charge- blocking buried layer of heavily doped p-type silicon at the level of the bottom of the DTI. A cross section

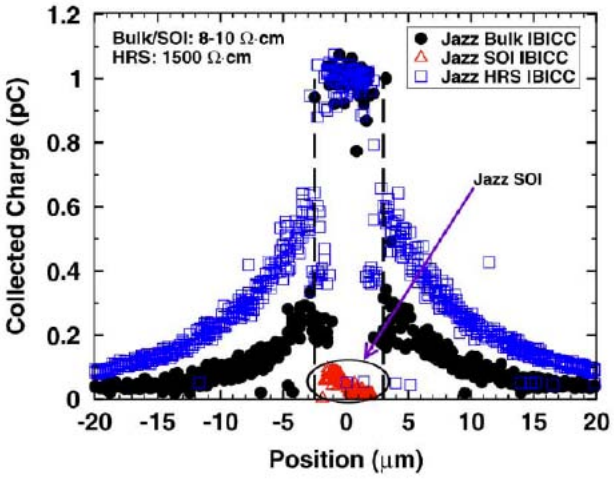

(a)

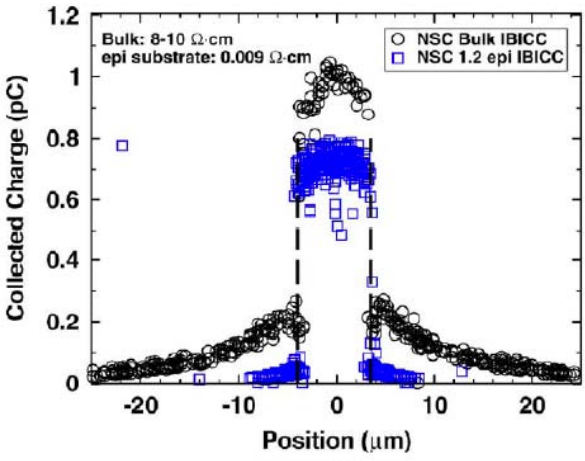

(b)

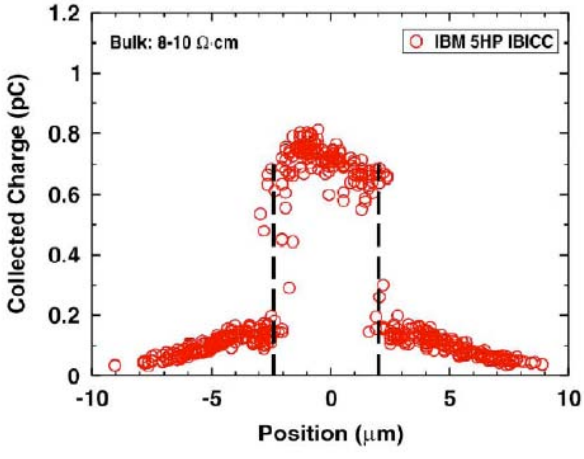

(c)

Fig. 92. IBICC data for the six SiGe HBT DUTs. The date sets shown display charge collection on the collector terminal. The deep trench isolation boundary is indicated approximatley by vertical dashed lines.

of the IBM 5HP device with the addition of the buried layer is shown in Fig. 93. The p-type layer shown at the level of the bottom of the DTI is approximately 2 mm thick . First generation SiGe HBT devices with this buried layer could be manufactured with little to no degradation in device performance since the retrograde well is more than 4 mm below the subcollector junction.

To evaluate the effectiveness of the proposed buried layer, a series of DESSIS simulations was conducted. As evidenced by the simulation points shown in Fig. 94, the buried layer reduces charge collection from events outside the DTI to the level measured in a SiGe HBT with a much higher substrate doping concentration. The buried layer does not affect the charge collection magnitude for ionizing events that occur within the active region between the DTI walls, but it does result in a large decrease in the sensitive area.

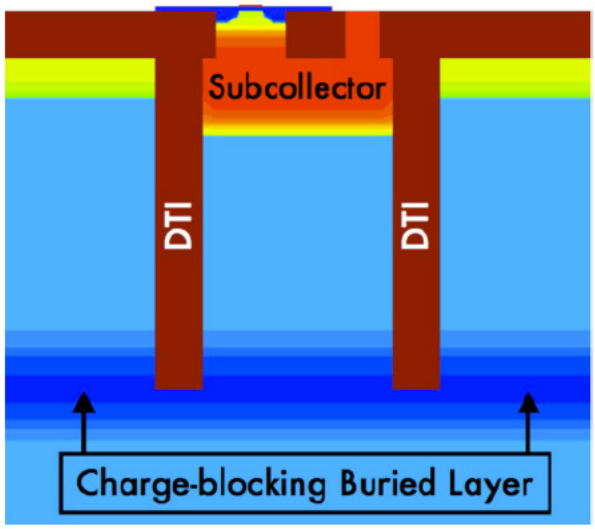

Fig. 93. Cross section of the buried layer concept for the IBM 5HP device.

E. Conclusion

Substrate engineering is a valuable tool for controlling delayed charge collection from events that occur outside the deep trench in DTI technologies, like SiGe HBTs. Moderate-to-low substrate doping concentrations permit large numbers of electrons to diffuse hundreds of micrometers, thereby increasing the charge collection efficiency of devices fabricated on these substrates. This effect increases the SEU cross section for highly ionizing particles, perhaps an order of magnitude or more beyond the active region of the device. The devices that showed the least efficient charge collection had the most heavily doped substrate or employed some other means of sheltering the sub- collector junction—as in the case of a heavily doped substrate or buried oxide layer.

Based on present simulation results and experimental conclusions from the NSC epi and Jazz SOI experimental IBICC data, a device hardened with the proposed charge-blocking buried layer would be relatively insensitive to heavy ion and proton events that occur in the substrate outside the DTI, without suffering the speed or complexity penalties of other hardening approaches.

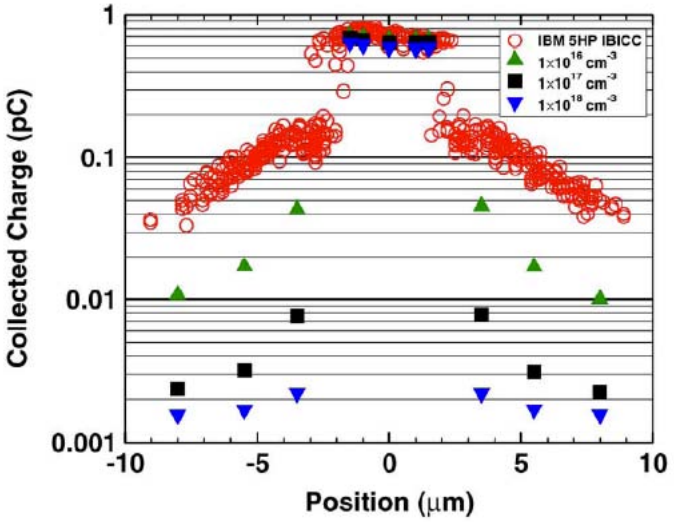

Fig. 94. DESSIS charge collection simulations of the IBM 5HP device with three different versions of the p-type charge-blocking buried layer.

3.26 A Generalized SiGe HBT Single-Event Effects Model for On-Orbit Event Rate Calculations

A. Abstract

This work draws on experimental and simulation results to derive a generalized SEU response model for bulk SiGe HBTs.The model was validated using published heavy ion and new proton data gathered from high-speed HBT digital logic integrated circuits fabricated in the IBM 5AM SiGe BiCMOS process. Calibrating to heavy ion data was sufficient to reproduce the proton data without further adjustment. The validated model is used to calculate upset event rates for low-earth and geosynchronous orbits under typical conditions.

B. Overview

The generalized model developed in this work was applied to two different DFF shift register designs fabricated in the IBM 5AM SiGe BiCMOS (IBM5AM) process: a baseline design and a radiation hardened by design (RHBD) variant. This process is characterized by a 0.5 μm drawn emitter width, a unity-gain cutoff frequency of 50 GHz, and a of 3.3 V.

Of the two IBM 5AM designs considered here, one was a baseline, nominal switching current, DFF shift register design and the other employed a RHBD dual-interleaving technique that included duplicated pass and storage cells, which effectively decoupled the differential inputs and outputs in the storage cell. This input/output decoupling increased the critical charge of this design. For the sake of simplicity, these designs are referred to as "baseline design" and "RHBD design" throughout. Both shift register designs are 127-bits long and were fabricated solely out of IBM 5AM SiGe HBTs; no complementary metal–oxide–semiconductor (CMOS) transistors were used.

The primary broadbeam heavy ion data set upon which this work is based is shown in Fig. 95. It is obvious that with the low LET neon ion the cross section of the RHDB design does not increase with increasing angle, but instead decreases with increasing angle—i.e., decreasing cross section with increasing effective LET. This behavior violates the assumptions of the original rectangular parallelepiped (RPP) model, which generally assumes increasing cross sections with increasing

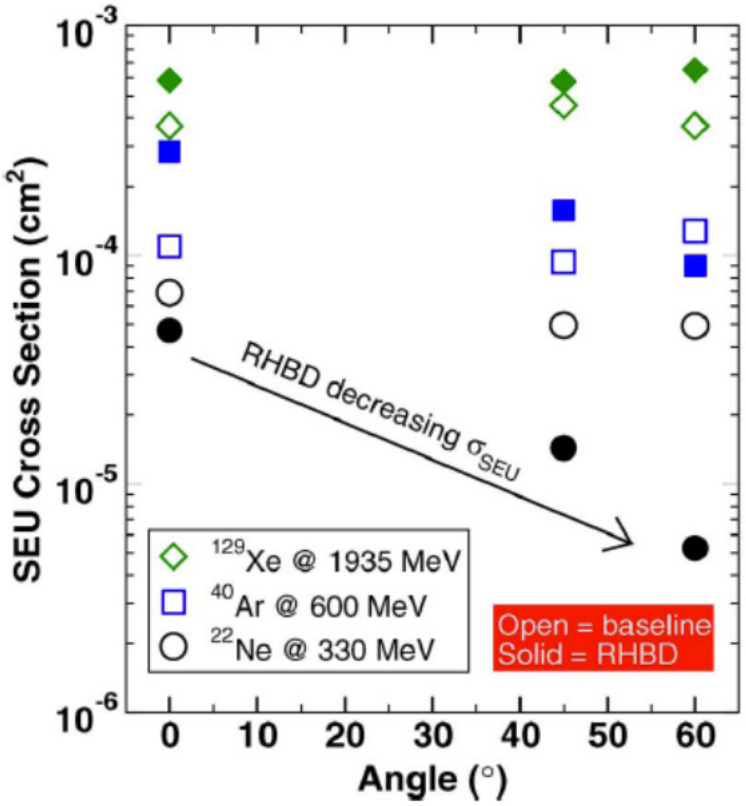

Fig. 95 Broadbeam heavy ion data for the baseline and RHBD 127-stage shift register designs. The important feature is the cross section decrease with increasing angle for the RHBD device with a higher critical charge.

effective LET. Since these data are not described adequately by the default RPP model, they have been re-plotted with the RPP cosine corrections removed. The data are plotted as a function of angle instead of effective LET and the cross section was scaled by cos(theta) to remove the effective fluence correction. All subsequent data sets will be plotted in this manner to avoid confusion. For the sake of reference, the normally-incident LETs for the ions in Fig. 95 are Ne 2.8 MeV cm^2/mg, Ar 8.3 MeV cm^2/mg, and Xe 53 MeV cm^2/mg.

Since a large number of space borne particles are incident at oblique angles, understanding the angular response of bulk SiGe HBTs is critical to developing a representative rate prediction model.

C. Energy Deposition Response Model

This work relied on the energy transport and calorimetry capabilities of the MRED tool set. Using this tool, it is possible to compute the energy deposited in one or more sensitive (fiducial) volumes due to impinging ions. Furthermore, these fiducial volumes can have weights. The volumes and their weights function in an ensemble to form a linear combination that approximates the total collected charge. The approach is described by equation 2.1. The total collected charge is the sum over all fiducial volumes of the product of the weight and total charge liberated.

The total charge liberated (Q) is related to the total energy deposited (ED) through the relationship Q=1pC/22.5 MeV ´ ED . This linear combination of weighted fiducial volumes is the construct that will be used to model the energy deposition response of the SiGe HBTs considered in this work. Once calibrated to data, usually heavy ion broadbeam cross section data, this modeling method

provides an accurate, high-speed approximation to the initial conditions and ensuing temporal evolution of charge transport and collection.

A 2-D projection of the basic energy deposition response model is shown in Fig. 96. The fiducial volumes have been overlaid on the TCAD cross section. The top-down area of each volume is determined by the normal-incident cross section of the broadbeam heavy ion data, which includes Ne, Ar, and Xe. The weights and depths of each of the volumes are calculated by correlating microbeam data to TCAD simulations. This model was used in a fully reconstructed 3-D model of a shift register stage for all subsequent simulations and the event rate calculations.

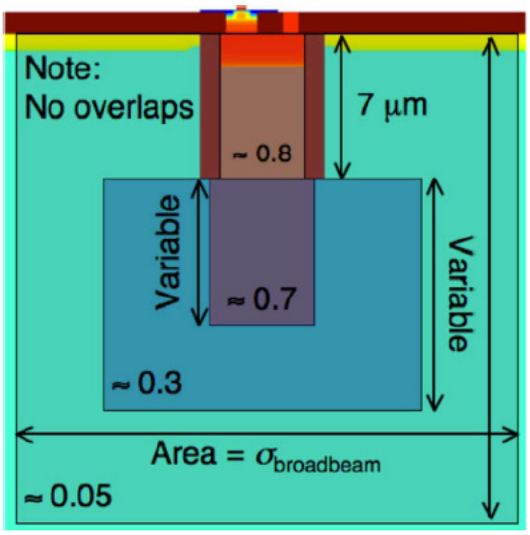

Fig. 96. This is the basic weighted fiducial volume ensemble used to model the radiation response of the IBM 5AM SiGe HBT process considered in this work.

D. Heavy Ion Response

Before computing on-orbit event rates, the model was verified against data sets that covered enough of the possible response parameter space to ensure predictable behavior in a more diverse environment such as geosynchronous or low-earth orbit. The model was calibrated to the heavy ion datasets for the baseline and RHBD designs.

The calibrated heavy ion results for both the baseline and RHBD circuit designs are shown in Fig. 97(a) and (b). The critical charge for each of the calibrations is displayed on the individual figures.

E. Proton Calibration Results

Proton data were collected during experiments on the CREST chip at the Crocker Nuclear Laboratory (CNL) at the University of California at Davis using 63 MeV protons. These data were taken on the baseline and RHBD designs at several different data rates at normal incidence and a grazing angle. The full data set is plotted in Fig. 98(a). This data set can now be used to check the proton response of the model developed in the previous section. These modeling results are shown in Fig. 98(b). The heavy ion model was validated against proton data by only a change of particle and energy in the simulation environment. The strong match between simulation and data validates a larger portion of the model's acceptable parameter space, making it usable for environments with

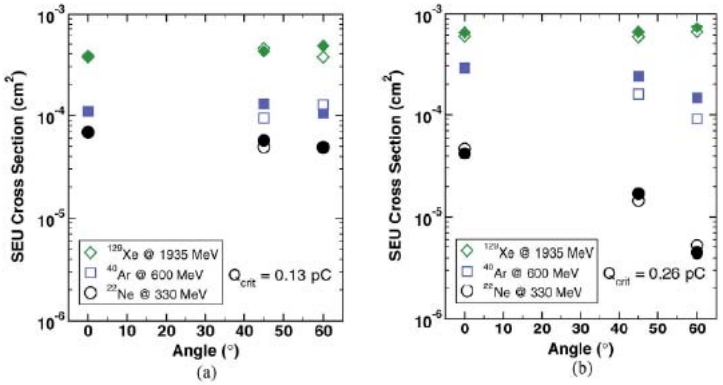

Fig 97. Plots (a) and (b) show the calibrated results of the computer simulations for the entire 127-stage shift register. In each case the open symbols are the date from Fig. 95 and the closed symbols are the derived simulation reslts. (a) Baseline design heavy ion calibration; (b) RHBD heavy ion calibration.

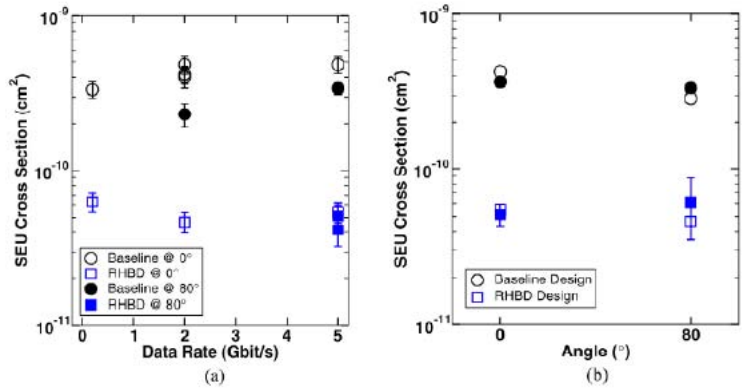

Fig. 98. (a) 63 MeV proton data from CNL taken on the baseline and RHBD CREST chip designs. (b) A comparison between the proton data from (a) and the simulation results based on the model, which was calibrated to heavy ion data. The strong agreement shown above was obtained by simply changing the particle and energy int he simulation; no further adjustments were made. The open symbols are data based ont he average across data rate from (a) and the solid symbols are simulation resultes using the response model.

large proton fluxes. These simulation results were obtained from the model calibrated with heavy ion data only; no further adjustment was required.

F. Event Rate Calculation

Now that we have a calibrated model, we can use MRED to predict the failure rate in any space environment. An example of this is shown I Fig 99, were flux spectra for the geosynchronous (GEO) and low-earth orbit (LEO) environments. Both of the environments were solar minimum/quiet conditions, included all available ion species, and assumed 100 mil of aluminum shielding. The LEO spectra were for the space station orbit, which, according to CREME96, is at an inclination of 51.6 degrees and an orbital radius of 500 km.

G. Conclusions

The shape and relationship between the fiducial volumes represents a critical aspect of this study. The fiducial volumes explain in a quantitative and qualitative way the once-anomalous angular response of the technology, the low SEU threshold, and the large saturated cross section observed for the most highly ionizing particles. Putting this model together unifies many years of experimental

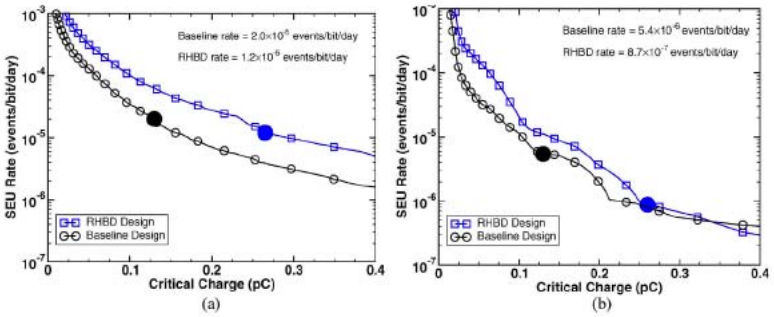

Fig. 99. These figures show the simulated event rates for the two shift reiter designs. The data markers have been thinned to aid viewing. The large marekrs show where the rate was evaluated based on the derived critical charge. (a) Geosynchronous orbit event rate; (b) low-earth orit event rate.

and theoretical work and provides intuition to designers considering SiGe HBT projects. It also opens the door for more complex types of modeling that will begin to look at time-domain effects and other aspects of extreme, high-speed digital technologies like this.

3.27 Laser-Induced Current Transients in Silicon-Germanium HBTs

A. Abstract

Device-level current transients are induced by injecting carriers using two-photon absorption from a subbandgap pulsed laser and recorded using wideband transmission and measurement equipment. These transients exhibit three distinct temporal trends that depend on laser pulse energy as well as the transverse and vertical charge generation location. The nature of the current transient is controlled by both the behavior of the subcollector-substrate junction and isolation biasing. However, substrate potential modulation, due to deformation of the subcollector- substrate depletion region, is the dominant mechanism affecting transient characteristics.

B. Introduction

In this work we examine two-photon absorption current transients from a passively- loaded single SiGe HBT with the intent of providing accurate feedback for analogous TCAD simulations. The experimental results presented here were obtained from a SiGe HBT test structure in the IBM 5AM BiCMOS process technology. There are three substrate taps for this device, located approximately 9 mm from the outside of the deep trench. All four of the device terminals were connected to individual pads on the die. The device under test was mounted in a custom broadband 40 GHz package designed for topside and backside laser irradiation as well as heavy ion microbeam irradiation. All four device terminals were connected to 40 GHz bias tees with the AC+DC connection facing the device and the AC-only connection facing the oscilloscope. The experiments used a Tektronix 12 GHz TDS6124C real-time digital storage oscilloscope. All transmission lines were 50, 2.9 mm (40 GHz) coaxial assemblies. The die pads were bonded to the microstrip transmission lines with 1 mil gold bond wires less than 1 mm in length. Time domain reflectometry measurements indicated that the four bond wire inductances and bond pad capacitances were each approximately 0.2 nH and 60 fF.

The device was characterized by injecting carriers using two- photon absorption from a subbandgap pulsed laser. This technique generates significant densities of electron-hole pairs in proximity of the beam focal point, which can be deterministically positioned in three dimensions.

Experiments were centered around three bias conditions: Case 1 had a bias of on the substrate with all other terminals grounded, Case 2 had a bias of 3 V on the collector with all other terminals grounded, and finally, Case 3 had a bias of on the substrate with all other terminals grounded. Previous broadbeam and single-photon absorption pulsed-laser experiments on pure bipolar applications were conducted with a substrate bias. However, BiCMOS applications call for the substrate to be grounded, which means the device isolation bias must be applied through a positive voltage on the collector. The bias condition of on the substrate was included to highlight any differences observed when placing 3 V on the collector terminal.

C. Experimental Results

Pulsed lasers have been used for many years to study single-event effects (SEE) in microelectronics. With the application of intense femtosecond light pulses, carrier generation by non-linear absorption becomes a useful way to study SEE.

The data shown in Fig. 100 are from experimental Case 1, with a bias of on the substrate. The plot shows the maximum measured total integrated charge vs. peak pulse irradiance on a log-log scale. This is a quadratic relationship, and since the slopes are approximately equal to two, two-photon absorption is confirmed for the collector and for the base. The base is a more narrow region, so charge collection is less efficient and some charge will be lost, making the trend subquadratic.

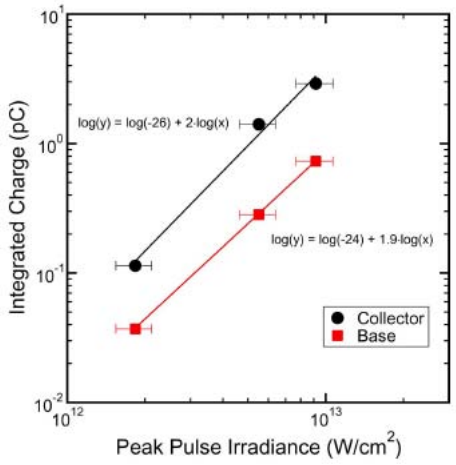

Fig. 100. Verification of the two-photon absorption process in these experiments. The data are from experimental Case 1, with -4 V ont he substrate nd all other terminals grounded. Int he ideal case, each line would have a slope of two since the number generated carriers depends on the square of the pulse irradance. There is a 6% fractional error int he pulse power and a 6% fractional error int he focal spot size, which produces are irradiance error of 6% and a charge collection errof of 6%. The errors in charge collection are smaller than the data point.

The data shown in Fig. 101 (a)–(d) show maps of the peak transient magnitude for the emitter, collector, base, and substrate for the bias conditions of Case 1. The emitter and collector transients are negative; the base and substrate transients are positive. A schematic of the deep trench isolation layout is overlaid on the data. The substrate taps for these devices are located 9 mm in the negative -direction from the bottom of the deep trench isolation. The laser spot size is approximately 1.6

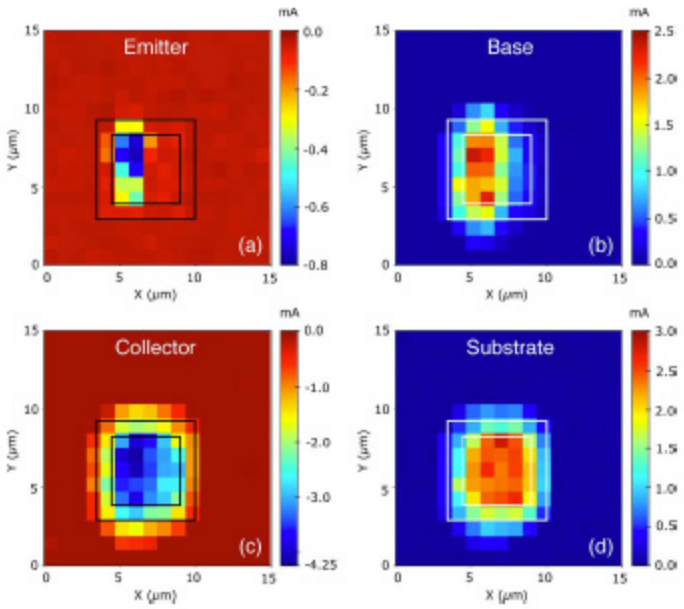

Fig. 101. These maps show the maximum current-transient magnitude for a 5 x. 10^{12} W/cm^2 peak irradiance laser plse on an IBM 5AM siGE HBT with bias conditions of Case 1.

in diameter and focused at the device surface in the -dimension. The emitter data in Fig. 101(a) support the two-photon absorption mechanism justified in Fig. 100. The nonzero data points are well confined to the emitter stripe, which could not occur if a significant amount of linear absorption was present. If linear absorption were present, the spatial distribution would be smeared out after the beam passed through almost 300 mm of silicon from the backside of the wafer to the surface of the device. The peak response of the base and collector terminals is coincident with the emitter-base and base-collector junctions. The peak response is not located at the base and collector contacts.

The data in Fig. 102 (a) through (d), show maps of the peak transient magnitude for the base and collector for the bias conditions of Case 2 and Case 3. The collector transients produced by the bias conditions in Case 2 are larger than the transients in Case 3 for hits to the active device region, defined by the emitter-base and base-collector junctions. While the base transients in Case 2 are slightly larger than those produced by Case 3, by up to 25% for the peak response, the difference is much less than the possible 2 □ increase in peak response for the collector in Case 2 at a peak pulse irradiance of 9 □ 10^{12} W/cm^2 . The profile associated with the base-collector junction in Case 2 is also better resolved than in Case 3 where the response is smoother across the active region of the device. As in the case for the data shown in Fig. 102 (a)–(d), the laser was focused at the surface of the device to a diameter of approximately 1.6 μm.

The data shown in Fig. 103 (a) and (b) display current transient waveforms for Case 2 and Case 3 at different pulse irradiance. As with the previous data sets, the laser was focused at the surface of the device to a diameter of 1.6 μm . As shown in the spatially correlated maps, there is a small difference between the base transients, but the Case 2 collector transients are up to 2 times larger for the 5 □ 10^{12} W/cm^2 and 9 □ 10^{12} W/cm^2 traces for hits to the base-collector junction. In all cases, the pulse lengths are approximately the same.

Finally, the data presented in Fig. 104 show collector transients when the focus of the laser is moved 20 μm below the surface and scanned in the usual 15 μm by 15 μm square. The only difference in

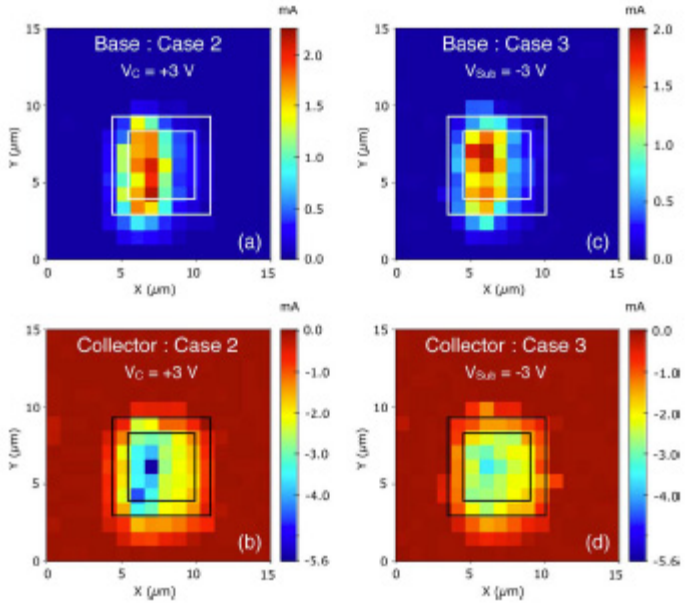

Fig. 102. These maps show the maximum current-transient magnitude for a 5 x. 10^{12} W/cm^2 peak irradiance laser plse on an IBM 5AM siGE HBT with bias conditions of Case 2 and Case 3..

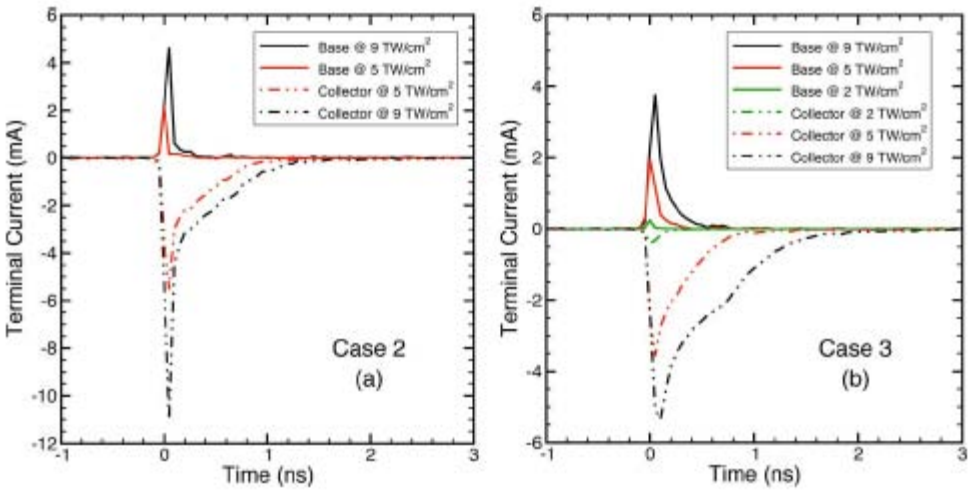

Fig. 103. Base and collector current transients for (a) Case 2 and (b) Case 3.

the data are that the response inside the deep trench isolation has to be measured on a 50 mV/div vertical scale and the other two traces were measured on a 5 mV/div scale. This difference explains the noise floor discrepancy in the data. The most important things about these data are the three distinct responses depending on trans-verse location relative to the deep trench isolation. When far outside the deep trench isolation, a low-magnitude, long-duration diffusion pulse is observed, lasting about 25 ns. When inside the deep trench isolation, the response is similar in magnitude and length to pulses measured at the surface despite moving into the substrate by 20 μm. The pulse measured at approximately 1 outside the deep trench isolation shows two response modes, a prompt collapse of the substrate potential (rapid current induction) and a delayed diffusion component, in other words a superposition of the response from inside the deep trench isolation and from far outside the deep trench isolation.

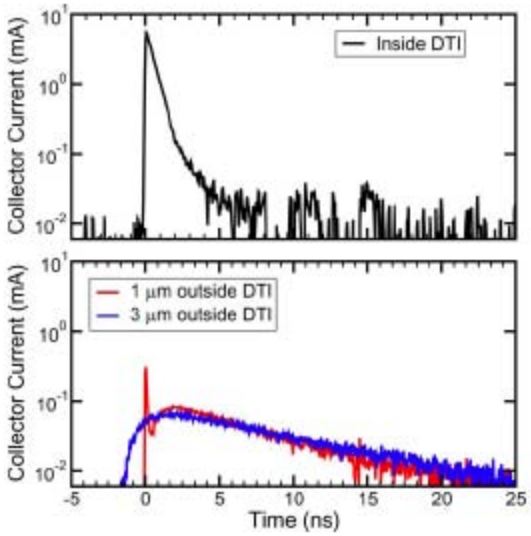

Fig. 104. Collector current transients for a 5 x 10^{12} w/cm^2..

D. Discussion

There are three important results based on the data in the previous section: the effect of placing the device isolation bias on the collector instead of the substrate, the measurement of significant device response for laser pulses outside the deep trench isolation, and the measurement of a bimodal collector response for laser pulses focused deep in the substrate and outside the deep trench isolation.

The difference in the collector isolation bias case, and the reason the collector current transients are up to 2 times larger, is because of base width modulation related to the Early effect and the onset of avalanche multiplication.

Previous broadbeam heavy ion data sets from irradiating shift register chains implied that sensitive device cross sections were approximately an order of magnitude larger than the active device area. This pointed to the fact that upsets occurred for events originating outside the deep trench isolation, even for normally incident ions. However, whether or not events outside the deep trench isolation could be responsible for upsets has been debated. These data should help settle that discussion concerning specific circuit applications considering the abundance of events measured in excess of 1 mA for pulses located outside the deep trench isolation.

Thirdly, and perhaps most important for device physics and upset mechanism perspectives, is the issue of diffusion-induced potential modulation. Charge funneling, as conceived in the early 1980s, successfully described localized potential deformation, where the transverse area disturbed by the incident particle was much smaller than either the junction crossed or the affected device. However, most bulk SiGe HBTs, like the IBM 5AM process, are manufactured on lightly doped p-type substrates, typically around 1 , which means that when potentials deform into the substrate of these devices, the potential modulation covers a very large area in order to maintain the potential drop fixed by the applied voltage at either the substrate or collector contact. The potential modulation is no longer a localized phenomenon, but a delocalized effect that does not require the ion to cross the active junction and can easily span lateral and vertical distances in excess of 10 um. For this reason, potential modulation effects in SiGe HBTs should not be confused with classical funneling processes. This substrate potential modulation effect can be observed in SiGe HBTs with a pulsed

laser when the focal point is below the surface of the device. When the carriers are generated in the field-free region deep in the substrate, outside the deep trench isolation, they diffuse isotropically. If a sufficient density of carriers can reach the subcollector-substrate junction, they will compensate the ionized dopants and force the potential contour surfaces to expand into the substrate, initially limited by the deep trench isolation, until the density of free carriers becomes low enough that the equilibrium position of the potential contours can support the applied bias. The number of carriers that reach the junction is determined by the amount of solid angle the junction occupies. This also means that the effect is both location and pulse power dependent. In effect, the potential pushes out from its equilibrium position, creates a large volume of near equipotential moving through charges in the substrate, which induces a prompt current on the collector terminal. The bimodal collector transient response in Fig. 105 is the first direct evidence of diffusion-initiated potential modulation in SiGe HBTs. Since the carriers are generated a long distance from the critical junction, the potential expands and collapses before all the charge is collected, so there is a secondary diffusion current that is realized after the prompt potential expansion and collapse, which yields the resulting superposition of potential collapse and diffusion responses.

E. Conclusion

The results presented here confirm the presence of nonlocal potential modulation in IBM 5AM SiGe HBTs. While this effect has demonstrable consequences for bulk SiGe HBTs in general, it is also expected to apply to many critical situations in CMOS, such as well potential collapse and recovery. This work has also established that the isolation bias terminal could be a critical aspect when considering the peak magnitude of collector current transients and that certain applications may suffer larger collector current transients for events that strike the active device regions directly.

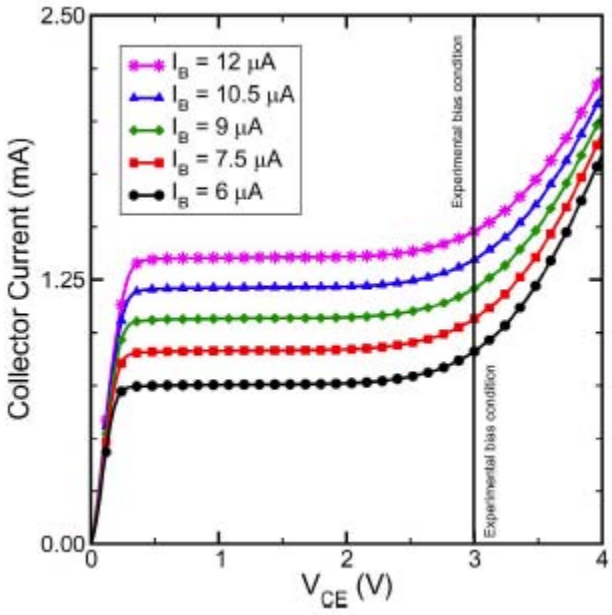

Fig. 105. Forced ouput characteristics for a IBM 5AM SSiGe HBT under high injection. The experimental bias condition of Case 2 is marked.

3.28 Heavy Ion Microbeam-and Broadbeam-Induced Transients in SiGe HBTs

A. Abstract

Silicon-germanium heterojunction bipolar transistor (SiGe HBT) heavy ion-induced current transients are measured using Sandia National Laboratories' microbeam and high-and low-energy broadbeam sources at the Grand Accélérateur National d'Ions Lourds, Caen, France, and the University of Jyväskylä, Finland. The data were captured using a custom broadband IC package and real-time digital phosphor oscilloscopes with at least 16 GHz of analog bandwidth. These data provide detailed insight into the effects of ion strike location, range, and LET.

B. Introduction

This work presents heavy ion microbeam position-correlated data, coupled with a range of broadbeam energies and linear energy transfers (LETs), providing detailed device-level data on the temporal profile of ion-induced current transients in this important semiconductor technology. The different LETs and particle energies show the consequences of heavy ion charge generation and collection in devices with lightly-doped substrates. These data capture essential information required for accurate device physics modeling.

We collected single-event current transients at three different facilities: Sandia National Laboratories' (SNL, in Albuquerque, NM) Ion Beams Materials Research Lab using a 6 MV EN tandem Van de Graaff microbeam, the Department of Physics at the University of Jyväskylä (JYFL, in Finland) using a K-130 cyclotron, and the Grand Accélérateur National d'Ions Lourds (GANIL, in Caen, France) high-energy beamline. The microbeam data gathered at SNL are based on 36 MeV O and include relative -coordinates of each ion strike based on the microbeam coordinate system. The data collected at JYFL and GANIL are broadbeam data, gathered without knowledge of ion strike location, but possess higher energy, the possibility of angled irradiation, and a wide selection of LETs. JYFL heavy ion exposures include 9.3 MeV/u Ne, Ar, Kr, and Xe. The Ar irradiations at JYFL were performed at a tilt of 60 in addition to normal incidence. We performed irradiations at GANIL using 45.5 MeV/u Xe. We conducted all exposures at normal incidence unless otherwise noted.

The device under test (DUT) is an IBM 5AM SiGe HBT At JYFL and GANIL, the transients on the base and collector were measured and recorded with a Tektronix DPO71604A 16-GHz (40 GS/s), real-time digital phosphor oscilloscope (DPO). At SNL, substrate, collector, and base, transients were measured and recorded with a Tektronix DPO72004 20-GHz (50 GS/s), real-time DPO. The oscilloscope triggered on the collector channel for all experiments.. The experiments focused on three bias conditions for the DUT: (Case 1) $V_{sub} = -4$, (Case 2) $V_C = 3$ V, and (Case 3) $V_C = -3$ V If the terminal is not listed, it is grounded.

C. Results

Fig. 106 (a) and (b) plot the peak base and collector currents as a function of position obtained from a 36 MeV O time-resolved ion beam-induced charge (TRIBIC) scan on an IBM 5AM SiGe HBT under the bias conditions of Case 1. The scan area is 20 μm □ 20 μm with 200 nm steps and a spatial resolution of < 1 μm. The scans produced approximately 400 data points based on a mV trigger on the collector. The peak collector responses are confined to the base-collector junction.

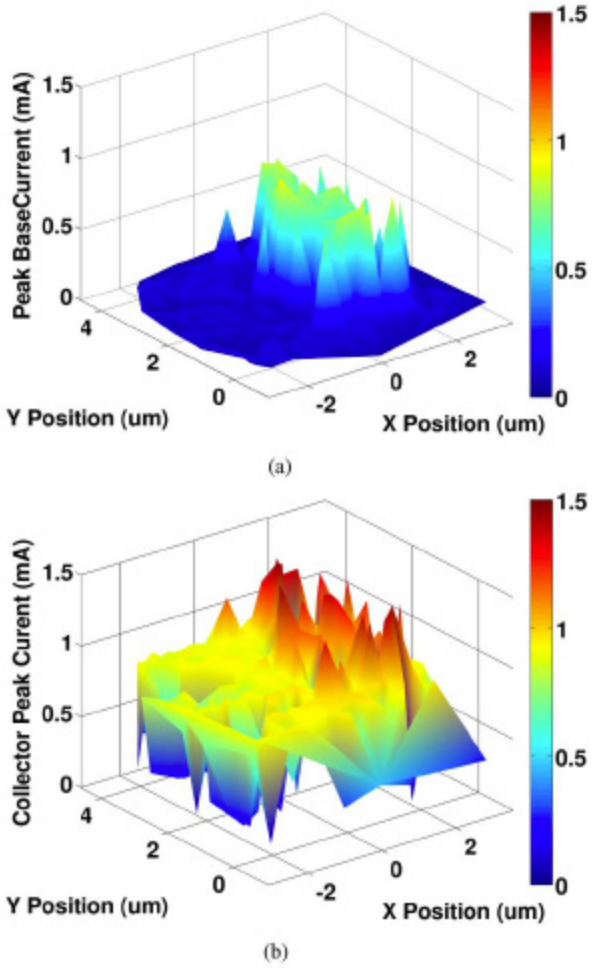

Fig. 106. MeV O TRIBIC scan on a IBM 5AM SiGe HBT Bias for Case 1 and all other terminals grounded.

The oscilloscope triggers on the collector channel only when the ion strikes in or near the area enclosed by the deep trench isolation. Coupling this microbeam information with the peak transient current and integrated transient charge enables position correlation of the broadbeam strikes in reference to the DUT's physical structures.

In Fig. 107 (a), with a 3 V bias on the collector (Case 2), instead of a -3 V bias on the substrate (Case 3) as shown in Fig. 107 (b), the collector current transients within the base-collector junction are magnified by more than a factor of two. The magnification of the base-collector junction transients in Case 2 is presumably due to a combination of the Early effect and avalanche multiplication. The data in each of these figures, 106 (a) and 106 (b), represents the same voltage dropped across the subcollector junction, producing an equivalent depletion layer. The nominal transient peak current of 0.5 mA remains the same for strikes that do not cross the base-collector junction.

Fig. 108 shows two of the larger base and collector current transients obtained from the JYFL broadbeam heavy ion results, demonstrating the significance of ion LET on the production of current transients. Based on knowledge of the microbeam data already presented, the transients shown in Fig. 6 are the result of direct hits to the active region of the device; each pair shown are correlated events from a single ion. As expected, the xenon transient in Fig. 6 produces more

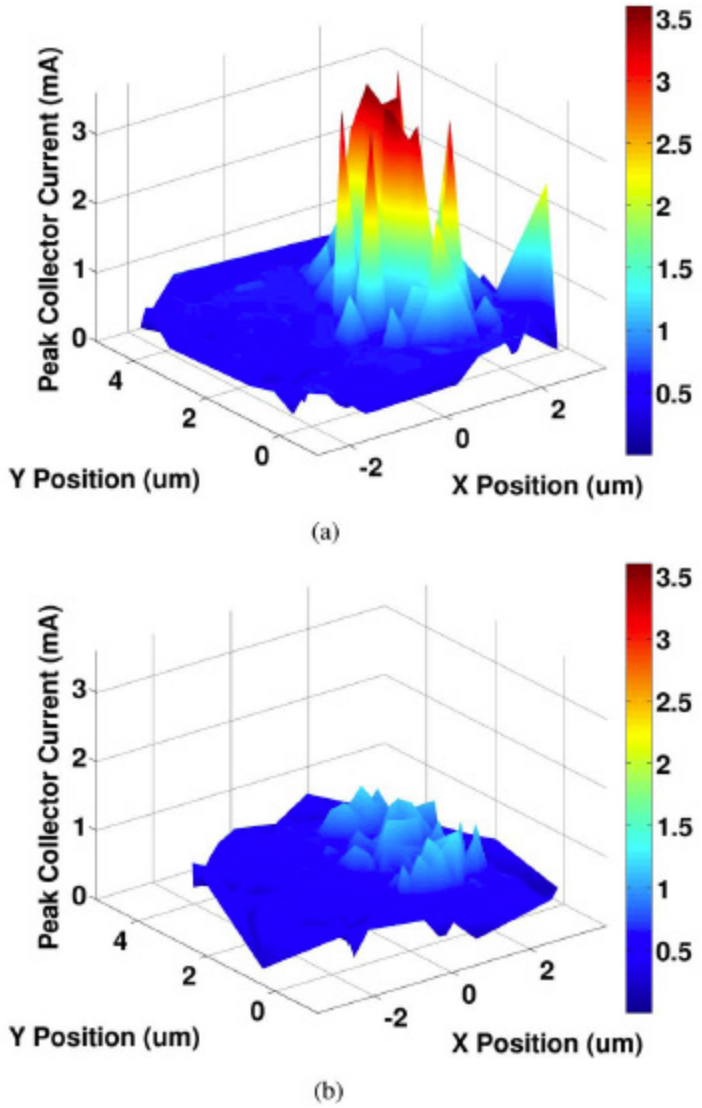

Fig. 107. 36 MeV O TRIBIC scan on an IBM 5AM SiGe HBT with Case 2 in (a) and with Case 3 in (b).

Charge resulting in large transients on both the collector and base terminals. The plateau in the xenon collector transient, and large amount of collected charge, is due to the fact that the device terminals are tied to external voltage sources and capacitors. Connecting the DUT to a circuit that allowed the voltage to collapse under high current draw would modify the plateau and perhaps shorten the transient. However, the plateau suggests some form of saturation, which is likely due to systematic effects, such as the bias tee capacitor. The neon transients are similar to the SNL microbeam transients in Fig. 4 and compare well to previous pulsed laser testing, indicating data consistency and LET proportionality.

The JYFL argon results, shown in Fig. 108 (a) and (b), at normal incidence and a 60 degrees tilt confirm that increasing the angle of incidence relative to the device surface normal produces fewer transients, based on an oscilloscope trigger value of -15 mV on the collector. At normal incidence with -4 V on the substrate, the oscilloscope captured 50 transients after a fluence of 3.85 ´ 107 cm-2 . However, at a tilt of 60 degrees with the same bias conditions, only 16 events were measured after a fluence of 1.94 ´ 108 cm-2 , a 16´ decrease in cross section. This result confirms, at the

device-level, the effect of cross-section decrease with increasing ion angle for low LET particles, observed in many previous broadbeam tests of SiGe HBT circuit applications and described via TCAD simulation. It is critical to understand this effect in order to calculate event rates for space-based applications.

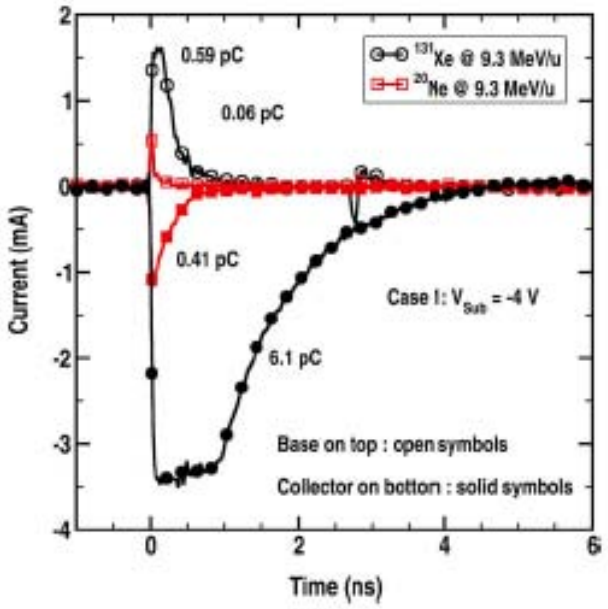

Fig. 108. JYFL -- ion LET comparison for Case 1. Neon and xenon transients caputred at JYFL demonstrating device response to two extreme LETs, 3.7 MeV cm^2/mg for the neon ions and 60 MeV cm^2/mg for the xenon ions; the integrated charge is labeled next to each curve.

D. CONCLUSION

These heavy ion current transient data represent a significant improvement to the state-of-the-art understanding of heavy ion-induced charge and transients in SiGe HBTs by using microbeam data to position-correlate broadbeam single-event current transients. These results complete heavy ion microbeam charge collection and pulsed laser data sets. Previous microbeam data only measured collected charge and previous two-photon pulsed-laser transient measurements cannot be easily correlated to ion LET and ion-specific effects. Taken as a whole and coupled with device simulation, a complete picture of charge generation, transport, and collection in bulk SiGe HBTs is possible.

3.29 Simulation of Single Event Effects in New Technologies and Ultra-small Devices

A. Overview

The thrust of this activity has been to develop the capability to predict the single event behavior of ultra-small and non-silicon technologies from information about their composition and structure using first-principles physics and a knowledge of the radiation environment. Central to this effort has been the development of a Monte Carlo simulation system for analysis of energy deposition in microelectronic structures. In this section, we describe the computational system that has emerged and some of the protocols that have been developed to simulate ion-induced single events. Through

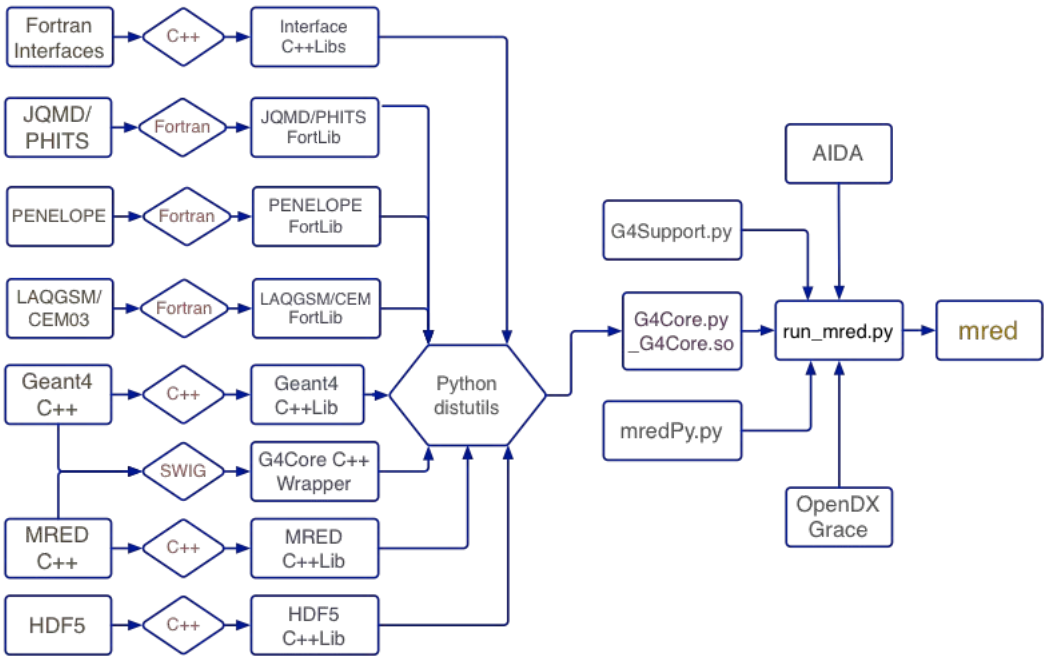

Fig.109. Architecture of the Geant4 application MRED, showing both the Geant4 core and other components. The actual program "mred" is a unix shell script that invokes the Python executable run_mred.py. The run_mred.py script loads several Python modules including G4Core.py, which contains most of the computing machinery, which in turn resides in the _G4Core.so shared library. The _G4Core.so library is built by the Python distutils routine from the components to the left in this illustration using a custom setup.py script [2].

this research and related programs a comprehensive and unifying mathematical framework for single event rate calculation has been developed. This framework, which encompasses not only the Monte Carlo methods that are the focus of this program, but also the analytical methods that preceded it, and the methods of applying it are described in detail in a recent review. Here, we give an overview of software and methods. Applications are described elsewhere in this report.

3.30 MRED – A System for Simulating Single Event Effects in Microelectronics

The key component of our single event simulation system is a Monte Carlo program that describes the evolution of events initiated by single radiation quanta. The program is called MRED (Monte Carlo Radiative Energy Deposition) and its structure is shown in the following figure.

The core of the MRED program is Geant4, a collection of c++ libraries created by the high energy physics community for describing detectors [3][4]. We have adapted Geant4 for use with semiconductor devices through a unique structure based on the computer language Python, and the addition of several critical Fortran programs for specific functionality. Three of these modules deal with nuclear-reaction physics, while the third adds state-state-of-the-art electron, positron, and gamma transport down to < 100 eV along while giving plausible results for low-energy electron trajectories in deep sub-micron structures.

The c++ classes that were available in Geant4 at the beginning of this program to describe ion-ion nuclear processes were inadequate to support research on single-event-effects in semiconductors. Leveraging synergies with a DTRA Basic Research program to assess nuclear reaction models, we added three critical Fortran modules to MRED and have used them extensively in single event

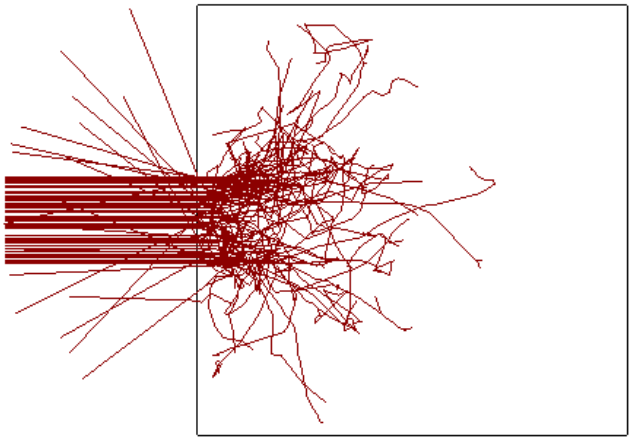

Fig. 110. A collection of 100 trajectories of 250 eV electrons incident on a 10 nm cube. Computed with MRED using the interface to PENELOPE2008. This image demonstrates the capacity of MRED to establish the details of energy deposition in deep sub-micron structures, one of the objectives of this program. Previously unpublished figure.

analyses. The modules are JQMD, a component of the PHITS program from Japan [5], and two programs LAQGSM and CEM03 from Los Alamos [6].

JQMD was initially important because the Geant4 libraries did not include physics modules for the analysis of ion-ion collisions in which the projectile had atomic mass greater than 12 u. Since a substantial number of cosmic rays are in this category, including Fe, significant uncertainly was introduced. JQMD is a quantum molecular dynamical code, which treats colliding nuclei as collections of nucleons and attempts to trace their motion in collision and to identify specific surviving nuclear species following the collision. Unfortunately, the upper limit for JQMD is approximately 3 GeV/u, so a small but significant fraction of high energy cosmic rays could not be described.

To broaden the energy range of cosmic rays that could be plausibly described we turned to another Fortran program, LAQGSM, created at Los Alamos National Laboratory from an earlier code QGSM that originated at Dubna, in the Soviet Union. After a protracted negotiation, we became the first site outside Los Alamos to obtain a license for use of this software. As of this writing LAQGSM and a related program for protons CEM03 are the default modules for ion-ion nuclear reactions in MRED.

Although the general quality of electron transport in Geant4 is high, this program and others have specific requirements for analysis in small volumes. Our research suggested that while the estimates of energy deposition in ultra-small volumes using Geant4 alone were probably relatively accurate, the details of trajectories were not. Near the end of the program we were fortunate to obtain access to a state-of-the-art electron, positron and photon transport program, PENELOPE2008, through a collaborator, Makoto Asai, at the Stanford Linear Accelerator Laboratory [7]. The following figure shows the result of bombarding a 10 nm silicon cube with 100 250 eV electrons. The detail in these trajectories evident. In fact, this figure includes several instances where secondary electrons with energies < 100 eV have been created.

A. Emergence of a Hierarchy of Rate Prediction Methods

One of the motivating factors for this program was the suggestion from observations on hardened SRAMs that materials such as W surrounding the active devices could play a role in establishing the rate of observed single event effects. Using capabilities developed under this program and exploiting synergies with NASA and DTRA programs we were able to add addition evidence for the basic conclusion that non-silicon materials in integrated circuits contribute to single event effect rates, and subsequently to demonstrate experimentally the validity of the hypothesis. In each case, observation, supporting observation, and confirmation, the software and techniques described here proved to be key to establishing the finding.

The following figure shows schematically the relationship between various components of the MRED simulation system. The Geant4 portion of the program corresponds roughly with the Virtual Irradiator of this figure. Energy deposition computed using the virtual irradiator is converted to thermalized charge linearly at a rate of 3.6 eV/e-h-pair and one of several methods is used to determine whether a single event has occurred. When this program began, we believed that it would be possible to achieve a substantial improvement in the time it takes for a Poisson solver to make a determination that a given quantum has or has not caused an effect. In spite of significant progress made to the FLOODS simulator through the course of this program, it has still not been possible

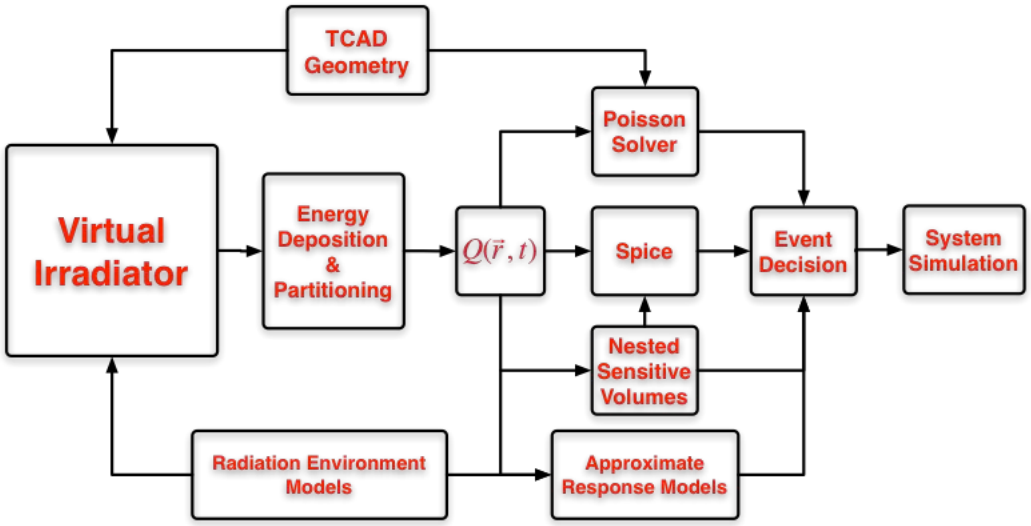

Fig. 111. Monte Carlo simulation of single event effects. Energy deposition by individual radiation quanta is generated using the MRED program and analyzed by any of a hierarchy of methods to determine the probability of a single event effect. The frequency of such events is a direct measure of the single event cross section.

to introduce detailed physical simulations into the standard single-event-analysis workflow. As a result, a number of techniques have been devised through this and related programs to determine the electrical effects of a specific pattern of energy deposition. One of the most elaborate and successful has been the introduction of SPICE simulations to predict the circuit effects in events in which several transistors simultaneously receive charge.

The use of SPICE as a method for the analysis of circuit effects is an example of one constituent of a hierarchy of approximation that has emerged in the Monte Carlo the analysis of single event effects. This hierarchy is illustrated in the following figure. Supplementing the conventional rectangular parallelepiped (RPP) and integral RPP (IRPP) methods are a number of additional ones that involve

Monte Carlo solution. The simplest of these is a calorimetry in a single sensitive volume. This differs from the RPP method in the possible shape of the sensitive volume, the materials surrounding the sensitive volume and most importantly in the number and detail of the physics processes that are simulated.

To begin to approximate collected charge rather than deposited energy a multiple-sensitive-volume scheme has been developed that involves the linear combination of deposited energy values in nested volumes. This weighted sum can be calibrated to approximate collected charge in a surprising number of situations.

The SPICE method referenced above uses multiple nested-sensitive-volume groups to approximate individual transistor behavior, but determines the overall effect with circuit simulation. This scheme makes it possible to analyze events in which multiple transistors much be involved, with each being perturbed in specific ways.

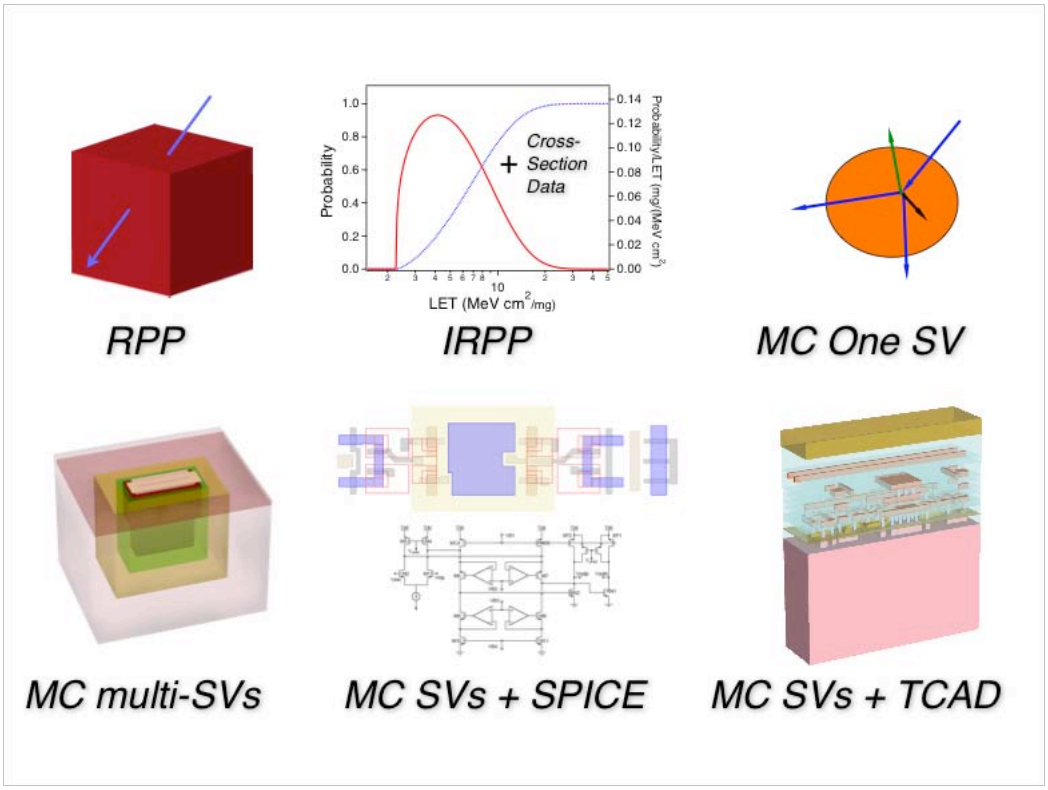

Fig. 112. Hierarchy of approximation in the simulation of single event effects. The conventional RPP and IRPP methods are supplemented by methods involving a single sensitive volume, a group of sensitive volumes with varying efficiencies, sensitive volume groups and SPICE analysis, and ultimately the use of a Poisson solver to track charge motion

Finally, at the most detailed a full Poisson solution can be applied to an initial condition based on the actual structure of the radiation event. Presently, this method is simply too slow to be practical, but it has been demonstrated and may one day be the preferred approach, particularly if advanced methods for computing the evolution of the event can be developed that are both physically accurate and computationally efficient.

B. Mathematical Formulation of the Rate Prediction Hierarchy

The capstone achievement of the single event simulation portion of this work has been the establishment of a mathematical framework for describing rate prediction that is sufficiently comprehensive that both Monte Carlo and analytical approximations can be handled in a unified way. Thus, the same formal analysis can be applied to all of the distinct methods shown in the above figure.

The mathematical basis for single-event rate prediction has been comprehensively reviewed by Petersen. However, all of the methods that he describes begin from starting points that are already relatively specialized to the assumptions that underlie the RPP approach. For example, all begin with a direct and deterministic relationship between energy deposition and the properties of the incident particles. However, beginning at this level of abstraction excludes approaches in which the energy deposition is handled implicitly or indirectly. Similarly, it is not easy to untangle the precise way in which energy enters the computation.

We have analyzed single event effects (SEE) rate prediction using a general approach that allows the rate of any effect initiated by a single radiation quantum to be computed, given the addition of sufficiently detailed assumptions. These assumptions, formulated in concise mathematical language, reduce the problem to obtaining the solution of the general SEE-rate integral.

$$R_e(\xi,t) = \sum_z \int_{A\Omega E} dE \int d\Omega \oint dA(-\hat{n}(\vec{x})\cdot\hat{u})\,H(-\hat{n}(\vec{x})\cdot\hat{u}) \int_{-\infty}^{t} dt'\ \Phi(z,E,\hat{u},\vec{x},t')P_e(z,E,\hat{u},\vec{x},t';\xi,t)$$
$$+ \sum_z \int_{A\Omega E} dE \int d\Omega \int d^3x \int_{-\infty}^{t} dt'\ \Gamma(z,E,\hat{u},\vec{x},t')P_e(z,E,\hat{u},\vec{x},t';\xi,t)$$

There is no universally accepted mathematical notation for SEE rate computations, and even the definitions of terms are sometimes ambiguous. In the following discussion, the word "event" is used to describe the interaction of one quantum of radiation with the system being analyzed. A process of interest initiated by a single quantum of radiation is called an "effect." For each event, there is a probability of an effect. The basis of rate prediction is the calculus of these probabilities.

To be definite, it is assumed that there is a region of space called the "world" within or surrounding the device, circuit, or system of interest. The laboratory and sample are assumed to be at rest in the world reference frame. The size of the world is unspecified both absolutely and relative to the device, but it is assumed that the occurrence of an effect is completely controlled by what happens within the world and that the world surface is convex with surface normal unit vector $\hat{n}(\vec{x})$ at position .

Radiation is assumed to have two independent sources, particles crossing the surface into the world volume from outside it, as e.g. cosmic rays, and particles originating in the world volume, as e.g. by radioactive decay. The external radiation source is completely specified at every point on the world surface by the flux distributions $\hat{u}\,\Phi(z,E,\hat{u},\vec{x},t')$. The internal radiation source is specified by a local generation rate $\Gamma(z,E,\hat{u},\vec{x},t')$. Here z is the type of particle, such as γ ray, proton, α particle, ^{56}Fe, etc., E, is the particle energy, $\hat{u}$ is the vector specifying particle direction, $\vec{x}$ is a point or origin on the world surface or within the world volume, and t' is the time at which the particle is at location $\vec{x}$. The units of the flux are, for example, particles per second, per square centimeter,

per MeV, per steradian. The units of the volume generation rate are particles per second, per cubic centimeter, per MeV, per steradian. A typical space environment contains many species, *z*.

The physical behavior of the system is determined by the probability per unit time $P_z(z, E, \hat{u}, \vec{x}, t'; \xi, t)$ that a quantum of type *z*, which has initial energy *E*, direction $\hat{u}$, and position $(\vec{x}, t')$, will result in an effect during the interval dt at time *t*. The argument ξ represents a set of configuration parameters on which this probability may depend. For example, in the RPP model the size of the RPP and the critical energy E_c are such parameters. Given these three definitions — flux, generation rate, and effect probability — the rate $R_e(\xi, t)$ of single event effects of type *e* at time *t* for configuration parameters is given by

Here *H* is the Heaviside unit step function. Reading from the inside out, the integrals in the first term are over all times t' prior to *t*, over the whole of the world surface area, over all particle directions, and over all particle energies. In the second term, the surface integral is replaced by a volume integral over all of the volume enclosed by the world surface. In both terms the sum is over all species in the respective radiation environment. In the first term, the step function constrains the surface and angular integrals to contributions for which $\hat{n}(\vec{x}) \cdot \hat{u} < 0$ (that is, inward). The minus sign appears because the world surface is described by an outward normal vector, while only particles on the world surface that are directed inward are capable of producing an effect. The second term contains no such constraints because spontaneous emission of radiation in any direction within the volume defined by the world surface is potentially significant.

Equation (1) is directly relevant to Monte Carlo simulation of single event effects, since the process of simulation, particularly involving the first term, in essence builds up the rate by determining the probability P_e by repetitive sampling. In addition, however, with appropriate mathematical assumptions equation (1) can be shown to reduce to the expected formulae of the RPP model, including its use of the LET distribution in place of energies.

4.0 PERSONNEL SUPPORTED

Vanderbilt University

Ron Schrimpf, PI, Professor
Sokrates Pantelides, Co-PI, Professor
Len Feldman, Co-PI, Professor
Dan Fleetwood, Co-PI, Professor
Lloyd Massengill, Co-PI, Professor
Apostolos G. Marinopoulos, Research Associate Professor
Enxia Zhang, Research Associate Professor
Blair Tuttle, Visiting Associate Professor
Leonidas Tseteris, Post Doc
Matthew Beck, Post Doc
Xing Zhou, Graduate Student
Dakai Chen, Graduate Student
Sriram Dixit, Graduate Student
Farah El-Mamouni, Graduate Student
Xuan Zhang, Graduate Student
Yevgeniy Puzrev, Graduate Student
Keith Warnick, Graduate Student

North Carolina State University

Gerry Lucovsky, PI, Professor
B. Ju, Graduate Student
Sanghyun Lee, Graduate Student
Hyungtak Seo, Graduate Student
Joseph P. Long, supported by GANN Fellowship
Kwon-Bum Chung, Post Doc supported by NSU

University of Florida

Mark E. Law, PI, Professor
Scott Thompson, Professor
Dan Cummings, Student
Eric Dattoli, Student
Nicole Rowsey, Graduate Student
Hyunwoo Park, Graduate Student

Georgia Institute of Technology

John D. Cressler, PI, Professor
Bongim Jun, Post Doc
Ghana Prakash, Post Doc
Akil Sutton, Graduate Student
Marco Bellini, Graduate Student

Anju Madan, Graduate Student
Ryan Diestelhorst, Graduate Student
Tom Cheng, Graduate Student
San Phillips, Graduate Student
Jihui Yuan, Graduate Student
Laleh Najafizadeh, Graduate Student
Peng Cheng, Graduate Student
Kurt Moen, Graduate Student

Arizona State University

Hugh Barnaby, PI, Professor
Jie Chen, Graduate Student
Ivan Sanchez, Gradute Student
Michael McLain, Graduate Student

Rutgers

Eric Garfunkel, PI, Professor

5.0 PUBLICATIONS

1. A. Appaswamy, S. Phillips, and J.D. Cressler, "Optimizing Inverse Mode SiGe HBTs for Immunity to Heavy-ion Induced, Single Event Upset," IEEE Electron Device Letters, vol. 30, pp. 511-513, 2009.

2. A. D. Tipton, J. A. Pellish, J. M. Hutson, R. Baumann, X. Deng, A. Marshall, M. A. Xapsos, H. S. Kim, M. R. Friendlich, M. J. Campola, C. M. Seidleck, K. A. Label, M. H. Mendenhall, R. A. Reed, R. D. Schrimpf, R. A. Weller and J. D. Black, "Device-orientation effects on multiple-bit upset in 65 nm srams ,**" IEEE Trans. Nuc. Sci., vol.55, no.6, pp. 2880-2885, Dec 2008.**

3. A. D. Tipton, J. A. Pellish, R. A. Reed, R. D. Schrimpf, R. A. Weller, M. H. Mendenhall, B. Sierawski, A. K. Sutton, R. M. Diestelhorst, G. Espinel, J. D. Cressler, P. W. Marshall and G. Vizkelethy, "Multiple-bit upset in 130 nm cmos technology ,**" IEEE Trans. Nuc. Sci., vol.53, no.6, pp. 3259-3264, Dec 2006.**

4. A. D. Tipton, X. W. Zhu, H. X. Weng, J. A. Pellish, P. R. Fleming, R. D. Schrimpf, R. A. Reed, R. A. Weller and M. Mendenhall, "Increased rate of multiple-bit upset from neutrons at large angles of incidence", Ieee Transactions on Device and Materials Reliability, vol.8, no.3, pp. 565-570, Sep 2008.

5. A. G. Marinopoulos, I. Batyrev, X. J. Zhou, R. D. Schrimpf, D. M. Fleetwood, and S. T. Pantelides, "Hydrogen shuttling near Hf-defect complexes in Si/SiO2/HfO2 structures," Appl. Phys. Lett. 91, Article No. 233503 (2007).

6. A. G. Marinopoulos, K. van Benthem, S. N. Rashkeev, S. J. Pennycook, and S. T. Pantelides, "Impurity segregation and ordering in Si/SiO2/HfO2 structures", Phys. Rev. B 77, 195317 (2008).

7. A. K. Sutton, A. P. Gnana Prakash, B. Jun, E. Zao, M. Bellini, J. Pellish, R. M. Diestelhorst, M. A. Carts, A. M. Phan, R. L. Ladbury, J. D. Cressler, P. W. Marshall, C. J. Marshall, R. A. Reed, R. D. Schrimpf, and D. M. Fleetwood, "An investigation of dose enhancement and source dependent effects in 200 GHz SiGe HBTs," IEEE Trans. Nucl. Sci. 53, 3166-3174 (2006).

8. A.K. Sutton, B.M. Haugerud, A.P.G. Prakash, J.D. Cressler, C.J. Marshall, P.W. Marshall, R. Ladbury, F. Guarin, and A.J. Joseph, "Comparison of Gamma and Proton Radiation Damage in 200 GHz SiGe HBTs," IEEE Transactions on Nuclear Science, vol. 52, pp. 2358-2365, 2005.

9. A.K. Sutton, J.P. Comeau, R. Krithivasan, J.D. Cressler, J.A. Pellish, R.A. Reed, P.W. Marshall, M. Varadharajaperumal, G. Niu, and G. Vizkelethy, "An Evaluation of Transistor-Layout RHBD Techniques for SEE Mitigation in SiGe HBTs," IEEE Transactions on Nuclear Science, vol. 54, pp. 2044-2052, 2007.

10. A.K. Sutton, R. Krithivasan, P.W. Marshall, S. Buchner, M. Carts, C. Siedleck, R. Ladbury, J.D. Cressler, C. Marshall, S. Currie, R. Reed, G. Niu, B. Randall, K. Fritz, D. McMorrow, and B. Gilbert, "SEU Error Signature Analysis of Gbit/sec SiGe Logic Circuits Using a Pulsed Laser Microprobe," IEEE Transactions on Nuclear Science, vol. 53, pp. 3277-3284, 2006.

11. A. Madan, B. Jun, R.M. Diestelhorst, A. Appaswamy, J.D. Cressler, R.D. Schrimpf, D.M. Fleetwood, T. Isaacs-Smith, J.R. Williams, and S.J. Koester, "Radiation Tolerance of Si/SiGe n-MODFETs," IEEE Transactions on Nuclear Science, vol. 54, pp. 2251-2256, 2007.

12. A. Madan, S.D. Phillips, E.P. Wilcox , J.D. Cressler, P.W. Marshall, P.F. Cheng, L. Del Castillo, Q. Liang, and G. Freeman, "The Enhanced Role of Shallow-Trench Isolation in Ionizing Radiation Damage of 65 nm RF-CMOS on SOI," IEEE Transactions on Nuclear Science, vol. 56, pp. 3056-3261, 2009.

13. A. Madan, S.D. Phillips, J.D. Cressler, P.W. Marshall, Q Liang, and G. Freeman, "Impact of Proton Irradiation on the RF Performance of 65 nm SOI CMOS Technology," IEEE Transactions on Nuclear Science, vol. 56, pp. 1914-1919, 2009.

14. A. S. Kobayashi, D. R. Ball, K. M. Warren, R. A. Reed, N. Haddad, M. H. Mendenhall, R. D. Schrimpf and R. A. Weller, "The effect of metallization layers on single event susceptibility,**"** **IEEE Trans. Nuc.** Sci., vol.52, no.6, pp. 2189-2193, Dec 2005.

15. A. Sutton, K. Moen, J.D. Cressler, M.A. Carts, P.W. Marshall, J.A. Pellish, V. Ramachandran R.A. Reed, M.L. Alles, and G. Niu, "Proton-Induced SEU in SiGe Digital Logic at Cryogenic Temperatures," Solid-State Electronics, vol. 52, no. 10, pp. 1652-59, 2008.

16. A.D. Tipton, J.A. Pellish, R.A. Reed, R.D. Schrimpf, R.A. Weller, M.H. Mendenhall, A.K. Sutton, R. Diestelhorst, G. Espinel, J.D. Cressler, P.W. Marshall, and G. Vizkelethy, "Multiple-Bit Upset in 130 nm CMOS Technology," IEEE Transactions on Nuclear Science, vol. 53, pp. 3259-3264, 2006.

17. A.P.G. Prakash, A.K. Sutton, R. Diestelhorst, G. Espinel, J. Andrews, B. Jun, J.D. Cressler, P.W. Marshall, and C.J. Marshall, "The Effects of Irradiation Temperature on the Proton Response of SiGe HBTs," IEEE Transactions on Nuclear Science, vol. 53, pp. 3175-3181, 2006.

18. B. D. Sierawski, J. A. Pellish, R. A. Reed, R. D. Schrimpf, K. M. Warren, R. A. Weller, M. H. Mendenhall, J. D. Black, A. D. Tipton, M. A. Xapsos, R. C. Baumann, X. W. Deng, M. J. Campola, M. R. Friendlich, H. S. Kim, A. M. Phan and C. M. Seidleck, "Impact of low-energy proton induced upsets on test methods and rate predictions ,**"** **IEEE Trans. Nuc.** Sci., vol.56, no.6, pp. 3085-3092, Dec 2009.

19. B. Jun, A. K. Sutton, R. M. Diestelhorst, G. J. Duperon, J. D. Cressler, J. D. Black, T. Haeffner, R. A. Reed, M. L. Alles, R. D. Schrimpf, D. M. Fleetwood, and P. W. Marshall, "The application of RHBD to nMOSFETs intended for use in cryogenic-temperature radiation environments," IEEE Trans. Nucl. Sci. 54, 2100-2105 (2007).

20. B. Jun, R. M. Diestelhorst, M. Bellini, G. Espinel, A. Appaswamy, A. P. Gnana Prakash, J. D. Cressler, D. Chen, R. D. Schrimpf, D. M. Fleetwood, M. Turowski, and A. Raman, "Temperature-dependence of gate-induced drain leakage in X-ray irradiated 130 nm CMOS devices," IEEE Trans. Nucl. Sci. 53, 3203-3209 (2006).

21. B. Narasimham, M. J. Gadlage, B. L. Bhuva, R. D. Schrimpf, L. W. Massengill, W. T. Holman, A. F. Witulski, R. A. Reed, R. A. Weller and X. W. Zhu, "Characterization of neutron- and alpha-particle-induced transients leading to soft errors in 90-nm cmos technology", Ieee Transactions on Device and Materials Reliability, vol.9, no.2, pp. 325-333, Jun 2009.

22. B. R. Tuttle and S. T. Pantelides, "Vacancy-related defects and the E´d center in amorphous silicon dioxide: Density functional theory calculations", Phys. Rev. B 79, 115206 (2009).

23. C. L. Howe, R. A. Weller, R. A. Reed, B. D. Sierawski, P. W. Marshall, C. J. Marshall, M. H. Mendenhall, R. D. Schrimpf and J. E. Hubbs, "Distribution of proton-induced transients in silicon focal plane arrays ," **IEEE Trans. Nuc.** Sci., vol.54, no.6, pp. 2444-2449, Dec 2007.

24. C. L. Howe, R. A. Weller, R. A. Reed, B. D. Sierawski, P. W. Marshall, C. J. Marshall, M. H. Mendenhall, R. D. Schrimpf and J. E. Hubbs, "Effects of surrounding materials on proton-induced energy deposition in large silicon diode arrays," **IEEE Trans. Nuc.** Sci., vol.56, no.4, pp. 2167-2170, Aug 2009.

25. C. L. Howe, R. A. Weller, R. A. Reed, M. H. Mendenhall, R. D. Schrimpf, K. M. Warren, D. R. Ball, L. W. Massengill, K. A. LaBel, J. W. Howard and N. F. Haddad, "Role of heavy-ion nuclear reactions in determining on-orbit single event error rates ," **IEEE Trans. Nuc.** Sci., vol.52, no.6, pp. 2182-2188, Dec 2005.

26. C.M. Grens, B.M. Haugerud, A.K. Sutton, T. Chen, J.D. Cressler, P.W. Marshall, C.J. Marshall, and A.J. Joseph, "The Effects of Proton Irradiation on the Operating Voltage Constraints of SiGe HBTs," IEEE Transactions on Nuclear Science, vol. 52, pp. 2403-2407, 2005.

27. D. K. Chen, F. El Mamouni, X. J. Zhou, R. D. Schrimpf, D. M. Fleetwood, K. F. Galloway, S. Lee, H. Seo, G. Lucovsky, B. Jun, and J. D. Cressler, "Total dose and bias temperature stress effects for HfSiON on Si MOS capacitors," IEEE Trans. Nucl. Sci. 54, 1931-1937 (2007).

28. D. K. Chen, R. D. Schrimpf, D. M. Fleetwood, K. F. Galloway, S. T. Pantelides, A. Dimoulas, G. Mavrou, A. Sotiropoulos, and Y. Panayiotatos, "Total dose response of Ge MOS capacitors with HfO2/Dy2O3 gate stacks," IEEE Trans. Nucl. Sci. 54, 971-974 (2007).

29. D. M. Fleetwood, "Selected high-impact journal articles on defects in microelectronic materials and devices," appendix to Defects in Microelectronic Materials and Devices, edited by D. M. Fleetwood, S. T. Pantelides, and R. D. Schrimpf, CRC Press, 2008, pp. 685-735.

30. D. M. Fleetwood, H. D. Xiong, and J. S. Lin, "1/f noise in SOI buried oxides and alternative dielectrics to SiO2," in Noise in Devices and Circuits III, edited by A. A. Balandin, F. Danneville, M. J. Deen, and D. M. Fleetwood, Vol. 5844, The Society for Optical Engineering (SPIE, Bellingham, 2005), pp. 63-74. [Invited.]

31. D. M. Fleetwood, M. P. Rodgers, L. Tsetseris, X. J. Zhou, I. Batyrev, S. Wang, R. D. Schrimpf, and S. T. Pantelides, "Effects of device aging on microelectronics radiation response and reliability," Microelectron. Reliab. 47, 1075-1085 (2007). [Invited.]

32. D. M. Fleetwood, M. P. Rodgers, L. Tsetseris, X. J. Zhou, I. Batyrev, S. Wang, R. D. Schrimpf, and S. T. Pantelides, "Effects of device aging on microelectronics radiation response and reliability," Proc. 25th International Conf. Microelectron. (MIEL 2006), vol. 1, Belgrade, Serbia and Montenegro, May 14-17, 2006, pp. 89-96. [Invited.]

33. D. M. Fleetwood, R. D. Schrimpf, S. T. Pantelides, R. L. Pease, and G. W. Dunham, "Electron capture, hydrogen release, and enhanced gain degradation in linear bipolar devices," IEEE Trans. Nucl. Sci. 55, 2986-2991 (2008).

34. D. M. Fleetwood, S. A. Francis, A. Dasgupta, X. J. Zhou, R. D. Schrimpf, M. R. Shaneyfelt, and J. R. Schwank, "Moisture effects on the 1/f noise of MOS devices," Transactions of the 215th ECS Meeting, Vol. 19(2), Silicon Nitride, Silicon Dioxide, and Emerging Dielectrics 10, edited by R. Ekwal Sah, J. Zhang, J. Deen, J. Yota, and A. Toriumi, San Francisco, CA, May 24-29, pp. 363-377 (2009). [Invited]

35. D. M. Fleetwood, S. T. Pantelides, and R. D. Schrimpf, "Oxide traps, interface traps, and border traps," in Defects in Microelectronic Materials and Devices, edited by D. M. Fleetwood, S. T. Pantelides, and R. D. Schrimpf, CRC Press, 2008, pp. 215-258.

36. D. M. Fleetwood, X. J. Zhou, L. Tsetseris, S. T. Pantelides, and R. D. Schrimpf, "Hydrogen model for negative-bias temperature instabilities in MOS gate insulators," PV 2005-01 - ISBN 1-56677-459-4 - Silicon Nitride and Silicon Dioxide Thin Insulating Films and Other Emerging Dielectrics VIII, edited by R. E. Sah, M. J. Deen, J. Zhang, J. Yota, and Y. Kamakura, pp. 267-278 (2005). [Invited.]

37. D. R. Ball, K. M. Warren, R. A. Weller, R. A. Reed, A. Kobayashi, J. A. Pellish, M. H. Mendenhall, C. L. Howe, L. W. Massengill, R. D. Schrimpf and N. F. Haddad, "Simulating nuclear events in a tcad model of a high-density seu hardened sram technology ," **IEEE Trans. Nuc.** Sci., vol.53, no.4, pp. 1794-1798, Aug 2006.

38. D. R. Hughart, R. D. Schrimpf, D. M. Fleetwood, X. J. Chen, H. J. Barnaby, K. E. Holbert, R. L. Pease, D. G. Platteter, B. R. Tuttle, and S. T. Pantelides, "The effects of aging and hydrogen on the radiation response of gated lateral PNP bipolar transistors," IEEE Trans. Nucl. Sci. 56, 3361 (2009).

39. Daniel J. Cummings, Arthur F. Witulski, Hyunwoo Park, Ronald D. Schrimpf, Scott E. Thompson, and Mark E. Law, "Mobility Modeling Considerations for Radiation Effects Simulations in Silicon", IEEE Transactions on Nuclear Science, to appear.

40. Daniel J. Cummings, Hyunwoo Park, Scott E. Thompson, and Mark E. Law, "An Adaptive Grid Scheme for Single-Event Upset Device Simulations", submitted, Transactions on Nuclear Science.

41. Daniel J. Cummings, Mark E. Law, Steve Cea, Tom Linton, "Comparison of Discretization Methods for Device Simulation", Proceedings of the SISPAD 2009 Conference, Digital Object Identifier 10.1109/SISPAD.2009.5290236, 4 pages.

42. E.J. Montes, R.A. Reed, J.A. Pellish, M.L. Alles, R.D. Schrimpf, R. A. Weller, M. Varadharajaperumal, G. Niu, A.K. Sutton, R. Diestelhorst, G. Espinel, R. Krithivasan, J.P. Comeau, J.D. Cressler, P.W. Marshall, and G. Vizkelethy, "Single Event Upset Mechanisms for Low Energy Deposition Events in SiGe HBTs," IEEE Transactions on Nuclear Science, vol. 55, pp. 1581-1587, 2008.

43. F. El Mamouni, E. X. Zhang, R. D. Schrimpf, D. M. Fleetwood, R. A. Reed, S. Cristoloveanu and W. Z. Xiong, "Fin-width dependence of ionizing radiation-induced subthreshold-swing degradation in 100-nm-gate-length finfets ,**" IEEE Trans. Nuc.** Sci., vol.56, no.6, pp. 3250-3255, Dec 2009.

44. F. Faccio, H. J. Barnaby, X. J. Chen, D. M. Fleetwood, L. Gonella, M. McLain, and R. D. Schrimpf, "Total ionizing dose effects in shallow trench isolation oxides," Microelectron. Reliab. 48, 1000-1007 (2008).

45. G. F. Niu, H. Yang, M. Varadharajaperumal, Y. Shi, J. D. Cressler, R. Krithivasan, P. W. Marshall and R. Reed, "Simulation of a new back junction approach for reducing charge collection in 200 ghz sigehbts ,**" IEEE Trans. Nuc.** Sci., vol.52, no.6, pp. 2153-2157, Dec 2005.

46. G. Hadjisavvas, L. Tsetseris, and S. T. Pantelides, "The origin of electron mobility enhancement in strained MOSFETs", IEEE Electron Device Letters, vol. 28, No.11, pp. 1018-1020 (2007)

47. G. Lucovsky, D. M. Fleetwood, S. Lee, H. Seo, R. D. Schrimpf, J. A. Felix, J. Luning, L. B. Fleming, M. Ulrich, and D. E. Aspnes, "Differences between charge trapping states in irradiated nano-crystalline HfO2 and non-crystalline Hf silicates," IEEE Trans. Nucl. Sci. 53, 3644-3648 (2006).

48. G. Niu, H. Yang, M. Varadharajaperumal, Y. Shi, J.D. Cressler, R. Krishivasan, P.W. Marshall, and R. Reed, "A New Back Junction Approach For Reducing Charge Collection in 200 GHz SiGe HBTs," IEEE Transactions on Nuclear Science, vol. 52, pp. 2153-2157, 2005.

49. G. Vizkelethy, R. A. Reed, P. W. Marshall and J. A. Pellish, "Ion beam induced charge (ibic) studies of silicon germanium heterojunction bipolar transistors (hbts)", Nuclear Instruments & Methods in Physics Research Section B-Beam Interactions with Materials and Atoms, vol.260, no.1, pp. 264-269, Jul 2007.

50. H. Barnaby, "Total-ionizing-dose effects in modern CMOS technologies," *IEEE Trans. on Nuclear* Science, vol. 53, pp. 3103-3121, 2006 *(review article)*.

51. H. D. Xiong, W. Wang, Q. Li, C. A. Richter, J. S. Suehle, W. K. Hong, T. Lee, and D. M. Fleetwood, "Random telegraph signals in n-type ZnO nanowire field effect transistors at low temperature," Appl. Phys. Lett. 91, Article No. 053107, pp. 1-3 (2007). Also published in Aug. 13, 2007 issue of Virt. J. Nanoscale Sci. Technol.

52. H. D. Xiong, W. Wang, Q. Li, C. A. Richter, J. S. Suehle, W. K. Hong, T. Lee, and D. M. Fleetwood, "Random telegraph signals and 1/f noise in ZnO nanowire field effect transistors," Proc. 7th IEEE International Conference on Nanotechnology, Hong Kong, Aug. 2-5, 2007, pp. 1139-1143.

53. H. J. Barnaby, M. L. McLain, I. S. Esqueda, X. J. Chen, "Modeling Ionizing Radiation Effects in Solid State Materials and CMOS Devices," *IEEE Trans. on Circuits and Systems – I:* Regular *Papers,* vol. 56, no. 8, pp. 1870 – 1883, 2009

54. H. J. Barnaby, M. Mclain, I. S. Esqueda, "Total-ionizing-dose effects on isolation oxides in modern CMOS technologies," *Nuclear Instruments and Methods in Physics Research B* 261 (2007) 1142–1145.

55. H. Park, D. J. Cummings, R. Arora, J. A. Pellish, R. A. Reed, R. D. Schrimpf, D. McMorrow, S. E. Armstrong, U. Roh, T. Nishida, M. E. Law, and S. E. Thompson, "Laser-Induced Current Transients in Strained-Si Diodes," Nuclear Science, IEEE Transactions on, vol. 56, pp. 3203-3209, 2009.

56. H. Park, S. K. Dixit, Y. S. Choi, R. D. Schrimpf, D. M. Fleetwood, T. Nishida, and S. E. Thompson, "Total ionizing dose effects on strained HfO2-based MOSFETs," IEEE Trans. Nucl. Sci. 55, 2981-2985 (2008).

57. I. G. Batyrev, B. Tuttle, D. M. Fleetwood, R. D. Schrimpf, L. Tsetseris, and S. T. Pantelides, "Reactions of water molecules in silica-based network glasses," Phys. Rev. Lett. 100, Article No. 105503 (2008).

58. I. G. Batyrev, D. Hughart, R. Durand, M. Bounasser, B. R. Tuttle, D. M. Fleetwood, R. D. Schrimpf, S. N. Rashkeev, G. W. Dunham, M. E. Law, and S. T. Pantelides, "Effects of hydrogen soaking on the radiation response of bipolar transistors: experiments and modeling," IEEE Trans. Nucl. Sci. 55, 3039-3045 (2008).

59. I. G. Batyrev, D. M. Fleetwood, R. D. Schrimpf, and S. T. Pantelides, "The role of water in the radiation response of wet and dry oxides," IEEE Trans. Nucl. Sci. 55, 2085-2089 (2008).

60. I. G. Batyrev, M. P. Rodgers, D. M. Fleetwood, R. D. Schrimpf, and S. T. Pantelides, "Effects of water on the aging and radiation response of MOS devices," IEEE Trans. Nucl. Sci. 53, 3629-3635 (2006).

61. I. S. Esqueda, H. J. Barnaby, M. L Mclain, P. C. Adell, F. E. Mamouni, S. K. Dixit, R. D. Schrimpf, W. Xiong, "Modeling the Radiation Response of Fully-Depleted SOI n-Channel MOSFETs," *IEEE Trans. on Nuclear Science*, vol. 56, no. 4, pp. 2247 - 2250, 2009.

62. I. S. Esqueda, H.J. Barnaby, M. L. Alles, "Two-dimensional methodology for modeling radiation-induced off-state leakage in CMOS technologies," *IEEE Trans. on Nuclear Science*, vol. 52, pp. 2259-2264, 2005.

63. J. A. Felix, M. R. Shaneyfelt, J. R. Schwank, P. E. Dodd, D. M. Fleetwood, X. J. Zhou, and E. P. Gusev, "The effects of radiation and charge trapping on the reliability of alternative gate dielectrics," in Defects in Advanced High-κ Dielectric Nano-Electronic Semiconductor Devices, edited by E. Gusev (Springer, Amsterdam, 2006), pp. 299-322. [Invited.]

64. J. A. Pellish, R. A. Reed, A. K. Sutton, R. A. Weller, M. A. Carts, P. W. Marshall, C. J. Marshall, R. Krithivasan, J. D. Cressler, M. H. Mendenhall, R. D. Schrimpf, K. M. Warren, B. D. Sierawski and G. F. Niu, "A generalized sige hbt single-event effects model for on-orbit event rate calculations ," **IEEE Trans. Nuc.** Sci., vol.54, no.6, pp. 2322-2329, Dec 2007.

65. J. A. Pellish, R. A. Reed, D. McMorrow, G. Vizkelethy, V. F. Cavrois, J. Baggio, P. Paillet, O. Duhamel, K. A. Moen, S. D. Phillips, R. M. Diestelhorst, J. D. Cressler, A. K. Sutton, A. Raman, M. Turowski, P. E. Dodd, M. L. Alles, R. D. Schrimpf, P. W. Marshall and K. A. LaBel, "Heavy ion microbeam- and broadbeam-induced transients in sige hbts ," **IEEE Trans. Nuc.** Sci., vol.56, no.6, pp. 3078-3084, Dec 2009.

66. J. A. Pellish, R. A. Reed, D. McMorrow, J. S. Melinger, P. Jenkins, A. K. Sutton, R. M. Diestelhorst, S. D. Phillips, J. D. Cressler, V. Pouget, N. D. Pate, J. A. Kozub, M. H. Mendenhall, R. A. Weller, R. D. Schrimpf, P. W. Marshall, A. D. Tipton and G. F. Niu, "Laser-induced current transients in silicon-germanium hbts ," **IEEE Trans. Nuc.** Sci., vol.55, no.6, pp. 2936-2942, Dec 2008.

67. J. A. Pellish, R. A. Reed, R. D. Schrimpf, M. L. Alles, M. Varadharajaperumal, G. F. Niu, A. K. Sutton, R. M. Diestelhorst, G. Espinel, R. Krithivasan, J. P. Comeau, J. D. Cressler, G. Vizkelethy, P. W. Marshall, R. A. Weller, M. H. Mendenhall and E. J. Montes, "Substrate engineering concepts to mitigate charge collection in deep trench isolation technologies," **IEEE Trans. Nuc.** Sci., vol.53, no.6, pp. 3298-3305, Dec 2006.

68. J. D. Black, D. R. Ball, W. H. Robinson, D. M. Fleetwood, R. D. Schrimpf, R. A. Reed, D. A. Black, K. M. Warren, A. D. Tipton, P. E. Dodd, N. F. Haddad, M. A. Xapsos, H. S. Kim, and M. Friendlich, "Characterizing SRAM single event upset in terms of single and double node charge collection," IEEE Trans. Nucl. Sci. 55, 2943-2947 (2008).

69. J. M. Hutson, J. A. Pellish, A. D. Tipton, G. Boselli, M. A. Xapsos, H. Kim, M. Friendlich, M. Campola, S. Seidleck, K. LaBel, A. Marshall, X. Deng, R. Baumann, R. A. Reed, R. D. Schrimpf, R. A. Weller and L. W. Massengill, "Evidence for lateral angle effect on single-event latchup in 65 nm srams ," **IEEE Trans. Nuc.** Sci., vol.56, no.1, pp. 208-213, Feb 2009.

70. J. M. Hutson, J. D. Pellish, G. Boselli, R. Baumann, R. A. Reed, R. D. Schrimpf, R. A. Weller and L. W. Massengill, "The effects of angle of incidence and temperature on latchup in 65 nm technology ," **IEEE Trans. Nuc.** Sci., vol.54, no.6, pp. 2541-2546, Dec 2007.

71. J. R. Schwank, M. R. Shaneyfelt, A. Dasgupta, S. A. Francis, X. J. Zhou, D. M. Fleetwood, R. D. Schrimpf, S. T. Pantelides, J. A. Felix, P. E. Dodd, V. Ferlet-Cavrois, P. Paillet, S. M. Dalton, S. E. Swanson, G. L. Hash, S. M. Thornberg, J. M. Hochrein, and G. K. Lum, "Effects of moisture and hydrogen exposure on radiation-induced MOS device degradation and its implications for long-term aging," IEEE Trans. Nucl. Sci. 55, 3206-3215 (2008).

72. J. R. Schwank, M. R. Shaneyfelt, D. M. Fleetwood, J. A. Felix, P. E. Dodd, P. Paillet, and V. Ferlet-Cavrois, "Radiation effects in MOS oxides," IEEE Trans. Nucl. Sci. 55, 1833-1853 (2008).

73. J.A. Pellish, R.A. Reed, D. McMorrow, G. Vizkelethy, J. Baggio, O. Duhmael, S.D. Phillips, A.K. Sutton, R. Diestelhorst, J.D. Cressler, P.E. Dodd, M.L. Alles, R.D. Schrimpf, P.W. Marshall, and K.A. LaBel, "Heavy Ion Microbeam and Broadbeam Transients in SiGe HBTs," IEEE Transactions on Nuclear Science, vol. 56, pp. 3078-3084, 2009.

74. J.A. Pellish, R.A. Reed, M.L. Alles, R.D. Schrimpf, M. Varadharajaperumal, G. Niu, A.K. Sutton, R. Diestelhorst, G. Espinel, R. Krithivasan, J.P. Comeau, J.D. Cressler, G. Vizkelethy, P.W. Marshall, R.A. Weller, M.H. Mendenhall, and E.J. Montes, "Substrate Engineering and Charge Collection Mitigation in Deep Trench Isolation Devices," IEEE Transactions on Nuclear Science, vol. 53, pp. 3298-3305, 2006.

75. J.A. Pellish, R.A. Reed, N.D. Pate, D. McMorrow, J.S. Melinger, J.A. Kozub, P.W. Marshall, A.K. Sutton, R.M. Diestelhorst, S. Phillips, J.D. Cressler, R.A. Weller, R.D. Schrimpf, and G.F. Niu, "Laser-Induced Current Transients in Silicon-Germanium HBTs," IEEE Transactions on Nuclear Science, vol. 55, pp. 2936-2942, 2008.

76. J.A. Pellish, R.A. Reed, R.A. Weller, M.H. Mendenhall, P.W. Marshall, A.K. Sutton, R. Krithivasan, J.D. Cressler, S.M. Currie, R.D. Schrimpf, K.M. Warren, B.D. Sierawski, and G. Niu, "On-Orbit Event Rate Calculations for SiGe HBT Shift Registers," IEEE Transactions on Nuclear Science, vol. 54, pp. 2322-2329, 2007.

77. J.D. Cressler, "On the Potential of SiGe HBTs for Extreme Environment Electronics," Proceedings of the IEEE, vol. 93, pp. 1559-1582, 2005.

78. K. Akarvardar, R. D. Schrimpf, D. M. Fleetwood, S. Cristoloveanu, P. Gentil, and B. J. Blalock, "Evidence of radiation-induced dopant neutralization in partially-depleted SOI NMOSFETs," IEEE Trans. Nucl. Sci. 54, 1920-1924 (2007).

79. K. M. Warren, A. L. Stemberg, R. A. Weller, M. P. Baze, L. W. Massengill, R. A. Reed, M. H. Mendenhall and R. D. Schrimpf, "Integrating circuit level simulation and monte-carlo radiation transport code for single event upset analysis in seu hardened circuitry ," **IEEE Trans. Nuc.** Sci., vol.55, no.6, pp. 2886-2894, Dec 2008.

80. K. M. Warren, A. L. Sternberg, J. D. Black, R. A. Weller, R. A. Reed, M. H. Mendenhall, R. D. Schrimpf and L. W. Massengill, "Heavy ion testing and single event upset rate prediction considerations for a dice flip-flop ," **IEEE Trans. Nuc.** Sci., vol.56, no.6, pp. 3130-3137, Dec 2009.

81. K. M. Warren, B. D. Sierawski, R. A. Reed, R. A. Weller, C. Carmichael, A. Lesea, M. H. Mendenhall, P. E. Dodd, R. D. Schrimpf, L. W. Massengill, T. Hoang, H. Wan, J. L. De Jong, R. Padovani and J. J. Fabula, "Monte-carlo based on-orbit single event upset rate prediction for a radiation hardened by design latch ," **IEEE Trans. Nuc.** Sci., vol.54, no.6, pp. 2419-2425, Dec 2007.

82. K. M. Warren, B. D. Sierawski, R. A. Weller, R. A. Reed, M. H. Mendenhall, J. A. Pellish, R. D. Schrimpf, L. W. Massengill, M. E. Porter and J. D. Wilkinson, "Predicting thermal neutron-induced soft errors in static memories using tcad and physics-based monte carlo simulation tools", Ieee Electron Device Letters, vol.28, no.2, pp. 180-182, Feb 2007.

83. K. M. Warren, R. A. Weller, B. D. Sierawski, R. A. Reed, M. H. Mendenhall, R. D. Schrimpf, L. W. Massengill, M. E. Porter, J. D. Wilkinson, K. A. Label and J. H. Adams, "Application of radsafe to model the single event upset response of a 0.25 mu m cmos sram ," **IEEE Trans. Nuc.** Sci., vol.54, no.4, pp. 898-903, Aug 2007.

84. K. M. Warren, R. A. Weller, M. H. Mendenhall, R. A. Reed, D. R. Ball, C. L. Howe, B. D. Olson, M. L. Alles, L. W. Massengill, R. D. Schrimpf, N. F. Haddad, S. E. Doyle, D. McMorrow, J. S. Melinger and W. T. Lotshaw, "The contribution of nuclear reactions to heavy ion single event upset cross-section measurements in a high-density seu hardened sram ," **IEEE Trans. Nuc.** Sci., vol.52, no.6, pp. 2125-2131, Dec 2005.

85. L. Najafizadeh, B. Jun, J.D. Cressler, A.P.G. Prakash, P.W. Marshall, and C.J. Marshall, "A Comparison of the Effects of X-Ray and Proton Irradiation on the Performance of SiGe Precision Voltage References," IEEE Transactions on Nuclear Science, vol. 54, pp. 2238-2244, 2007.

86. L. Najafizadeh, M. Bellini, G. Espinel, A.P.G. Prakash, J.D. Cressler, P.W. Marshall, and C.J. Marshall, "Proton Tolerance of SiGe Precision Voltage References For Extreme Temperature Range Electronics," IEEE Transactions on Nuclear Science, vol. 53, pp. 3210-3216, 2006.

87. L. Najafizadeh, R.M. Diestelhorst, M. Bellini, S.D. Phillips, P.K. Saha, J.D. Cressler, G. Vizkelethy, and P.W. Marshall, "Single Event Transient Response of SiGe Voltage References and Its Impact on the Performance of Analog and Mixed-Signal Circuits," IEEE Transactions on Nuclear Science, vol. 56, pp. 3469-3476, 2009.

88. L. Najafizadeh, T. Vo, S. Phillips, P. Cheng, J.D. Cressler, M. Mojarradi, and P.W. Marshall, "The Effects of Proton Irradiation on the Performance of High-Voltage nMOSFETs Implemented in a Low-Voltage SiGe BiCMOS Platform," **IEEE** Transactions on Nuclear Science, vol. 55, pp. 3253-3258, 2008.

89. L. Tsetseris and S. T. Pantelides, "Hydrogenation/deuteration of the Si-SiO2 interface: Atomic-scale mechanisms and limitations", Appl. Phys. Lett. 86, 112107 (2005).

90. L. Tsetseris and S. T. Pantelides, "Morphology and defect properties of the Ge-GeO2 interface", Appl. Phys. Lett. 95, 262107 (2009).

91. L. Tsetseris and S. T. Pantelides, "Vacancies, interstitials and their complexes in titanium carbide", Acta Mater. 56, 2864-2871(2008).

92. L. Tsetseris and S. T. Pantelides, "Oxygen migration, agglomeration, and trapping: Key factors for the morphology of the Si-SiO2 interface", Phys. Rev. Lett. 97, 116101 (2006).

93. L. Tsetseris, D. M. Fleetwood, R. D. Schrimpf, and S. T. Pantelides, "Hydrogen-dopant interactions in SiGe and strained Si," Appl. Phys. Lett. 96, 251905 (2010).

94. L. Tsetseris, D. M. Fleetwood, R. D. Schrimpf, and S. T. Pantelides, "Defect formation and annihilation in electronic devices and the role of hydrogen," in Defects in Microelectronic Materials and Devices, edited by D. M. Fleetwood, S. T. Pantelides, and R. D. Schrimpf, CRC Press, 2008, pp. 381-398.

95. L. Tsetseris, D. M. Fleetwood, R. D. Schrimpf, X. J. Zhou, I. G. Batyrev, and S. T. Pantelides, "Hydrogen effects in MOS devices," Microelectron. Engrg. 84, 2344-2349 (2007).

96. L. Tsetseris, N. Kalfagiannis, S. Logothetidis, and S. T. Pantelides, "Trapping and release of impurities in TiN: A first-principles study", Phys. Rev. B 78, 094111 (2008).

97. L. Tsetseris, N. Kalfagiannis, S. Logothetidis, and S. T. Pantelides, "Structure and interaction of point defects in transition-metal nitrides", Phys. Rev. B 76, 224107 (2007).

98. L. Tsetseris, N. Kalfagiannis, S. Logothetidis, and S. T. Pantelides, "Role of N defects on thermally-induced atomic-scale structural changes in transition-metal nitrides", Phys. Rev. Lett. 99, 125503 (2007).

99. L. Tsetseris, R. D. Schrimpf, D. M. Fleetwood, R. L. Pease, and S. T. Pantelides, "Common origin for enhanced low-dose-rate sensitivity and bias temperature instability under negative bias," IEEE Trans. Nucl. Sci. 52, 2265-2271 (2005).

100. L. Tsetseris, S. Logothetidis, and S. T. Pantelides, "Migration of species in a prototype diffusion barrier: Cu, O, and H in TiN", Appl. Phys. Lett. 94, 161903 (2009).

101. L. Tsetseris, S. Wang, and S. T. Pantelides, "Thermal donor formation processes in silicon and catalytic role of hydrogen", Appl. Phys. Lett. 88, 051916 (2006).

102. L. Tsetseris, X. J. Zhou, D. M. Fleetwood, R. D. Schrimpf, and S. T. Pantelides, "Hydrogen-related instabilities in MOS devices under bias temperature stress," IEEE Trans. Dev. Mater. Reliab. 7, 502-508 (2007).

103. L. Tsetseris, X. J. Zhou, D. M. Fleetwood, R. D. Schrimpf, and S. T. Pantelides, "Physical mechanisms of negative-bias temperature instability," Appl. Phys. Lett. 86, 142103-1 to 142103-3 (2005).

104. M. A. Clemens, N. A. Dodds, R. A. Weller, M. H. Mendenhall, R. A. Reed, R. D. Schrimpf, T. Koi, D. H. Wright and M. Asai, "The effects of nuclear fragmentation models on single event effect prediction ,**" IEEE Trans. Nuc.** Sci., vol.56, no.6, pp. 3158-3164, Dec 2009.

105. M. Alles, R. D. Schrimpf, D. M. Fleetwood, R. A. Reed, and B. Jun, "Recent radiation issues in SOI Devices," PV 2005-03 - ISBN 1-56677-461-6 - Silicon-on-Insulator Technology and Devices XII, edited by G. K. Celler, S. Cristoloveanu, J. G. Fossum, F. Gamiz, K. Izumi, and Y-W. Kim, pp. 87-98 (2005). [Invited.]

106. M. Bellini, B. Jun, A. K. Sutton, A. C. Appaswamy, P. Cheng, J. D. Cressler, P. W. Marshall, R. D. Schrimpf, D. M. Fleetwood, B. El-Kareh, S. Balster, P. Steinmann, and H. Yasuda, "The effects of proton and X-ray irradiation on the DC and AC performance of complementary (npn + pnp) SiGe HBTs on thick-film SOI," IEEE Trans. Nucl. Sci., vol. 54, No. 6, pp. 2245-2250, 2007.

107. M. Bellini, B. Jun, A.C. Appaswamy, P. Cheng, J.D. Cressler, P.W. Marshall, B. El-Kareh, S. Balster, and H. Yasuda, "The Effects of Proton Irradiation on the DC and AC Performance of Complementary (npn + pnp) SiGe HBTs on Thick-Film SOI," IEEE Transactions on Nuclear Science, vol. 54, pp. 2245-2250, 2007.

108. M. Bellini, B. Jun, T. Chen, J. D. Cressler, P. W. Marshall, D. Chen, R. D. Schrimpf, D. M. Fleetwood, and J. Cai, "X-ray irradiation and bias effects in fully-depleted and partially-depleted SiGe HBTs fabricated on CMOS-compatible SOI," IEEE Trans. Nucl. Sci. 53, 3182-3186 (2006).

109. M. Bellini, B. Jun, T. Chen, J.D. Cressler, P.W. Marshall, D. Chen, and J. Cai, "Radiation and Bias Effects in Fully-Depleted and Partially-Depleted SiGe HBTs Fabricated on CMOS-Compatible SOI," IEEE Transactions on Nuclear Science, vol. 53, pp. 3182-3186, 2006.

110. M. Bellini, S. Phillips, R.M. Diestelhorst, P. Cheng, J.D. Cressler, P.W. Marshall, M. Turowski, G. Avenier, A. Chantre, and P. Chevalier, "Novel Total Dose and Heavy-Ion Charge Collection Phenomena in a New SiGe HBT on Thin-Film SOI Technology," IEEE Transactions on Nuclear Science, vol. 55, pp. 3197-3201, 2008.

111. M. Caussanel, A. Canals, S. K. Dixit, M. J. Beck, A. D. Touboul, R. D. Schrimpf, D. M. Fleetwood, and S. T. Pantelides, "Doping-type dependence of damage in silicon diodes exposed to X-ray, proton, and He+ irradiations," IEEE Trans. Nucl. Sci. 54, 1925-1930 (2007).

112. M. J. Beck, B. R. Tuttle, R. D. Schrimpf, D. M. Fleetwood, and S. T. Pantelides, "Atomic displacement effects in single-event gate rupture," IEEE Trans. Nucl. Sci. 55, 3025-3031 (2008).

113. M. J. Beck, L. Tsetseris, and S. T. Pantelides, "Stability and dynamics of Frenkel pairs in Si", Phys. Rev. Lett. 99, 215503 (2007)

114. M. J. Beck, L. Tsetseris, M. Caussanel, R. D. Schrimpf, D. M. Fleetwood and S. T. Pantelides, "Atomic-scale mechanisms for low-NIEL dopant-type dependent damage in Si," IEEE Trans. Nucl. Sci. 53, 3621-3628 (2006).

115. M. J. Beck, R. D. Schrimpf, D. M. Fleetwood, and S. T. Pantelides, "Disorder-recrystallization effects in low-energy beam-solid interactions," Phys. Rev. Lett. 100, Article No. 185502 (2008).

116. M. J. Beck, R. Hatcher, R. D. Schrimpf, D. M. Fleetwood, and S. T. Pantelides, "Quantum mechanical description of displacement damage formation," IEEE Trans. Nucl. Sci. 54, 1906-1912 (2007).

117. M. J. Beck, Y. S. Puzyrev, N. Sergueev, K. Varga, R. D. Schrimpf, D. M. Fleetwood, and S. T. Pantelides, "The role of atomic displacements in ion-induced dielectric breakdown," IEEE Trans. Nucl. Sci. 56, 3210 (2009).

118. M. J. Gadlage, J. R. Ahlbin, V. Ramachandran, P. Gouker, C. A. Dinkins, B. L. Bhuva, B. Narasimham, R. D. Schrimpf, M. W. McCurdy, M. L. Alles, R. A. Reed, M. H. Mendenhall, L. W. Massengill, R. L. Shuler and D. McMorrow, "Temperature dependence of digital single-event transients in bulk and fully-depleted soi technologies ,**" IEEE Trans. Nuc.** Sci., vol.56, no.6, pp. 3115-3121, Dec 2009.

119. M. J. Gadlage, R. D. Schrimpf, B. Narasimham, J. A. Pellish, K. M. Warren, R. A. Reed, R. A. Weller, B. L. Bhuva, L. W. Massengill and X. W. Zhu, "Assessing alpha particle-induced single event transient vulnerability in a 90-nm cmos technology", Ieee Electron Device Letters, vol.29, no.6, pp. 638-640, Jun 2008.

120. M. L. Alles, R. Pasternak, N. H. Tolk, R. D. Schrimpf, D. M. Fleetwood, and R. W. Standley, "Experimental evaluation of second harmonic generation for non-invasive contamination detection in SOI wafers," Proc. 17th Annual IEEE/SEMI Advanced Semiconductor Manufacturing Conference – ASMC 2006, May 22-24, 2006, Boston, MA, pp. 1-6.

121. M. L. Alles, R. Pasternak, X. Lu, N. H. Tolk, R. D. Schrimpf, D. M. Fleetwood, R. P. Dolan, and R. W. Standley, "Second harmonic generation for noninvasive metrology of silicon-on-insulator wafers," IEEE Trans. Semiconductor Manufacturing 20, 107-113 (2007).

122. M. McLain, H. J. Barnaby, K. E. Holbert, R. D. Schrimpf, H. Shah, A. Amort, M. Baze, J. Wert, "Enhanced TID susceptibility in sub-100 nm Bulk CMOS I/O transistors and circuits," *IEEE Trans. on Nuclear* Science, vol. 54, pp. 2210 - 2217, 2007.

123. M. P. Rodgers, D. M. Fleetwood, R. D. Schrimpf, I. G. Batyrev, S. Wang, and S. T. Pantelides, "The effects of aging on MOS irradiation and annealing response," IEEE Trans. Nucl. Sci. 52, 2642-2648 (2005).

124. M. Silvestri, S. Gerardin, R. D. Schrimpf, D. M. Fleetwood, F. Faccio, and A. Paccagnella, "The role of irradiation bias on the time-dependent dielectric breakdown of 130-nm MOSFETs exposed to x-rays," IEEE Trans. Nucl. Sci. 56, 3244 (2009).

125. M. Varadharajaperumal, G. Niu, X. Wei, T. Zhang, J.D. Cressler, R.A. Reed, and P.W. Marshall, "3-D Simulation of SEU Hardening of SiGe HBTs Using Shared Dummy Collector," IEEE Transactions on Nuclear Science, vol. 54, pp. 2330-2337, 2007.

126. N. A. Dodds, R. A. Reed, M. H. Mendenhall, R. A. Weller, M. A. Clemens, P. E. Dodd, M. R. Shaneyfelt, G. Vizkelethy, J. R. Schwank, V. Ferlet-Cavrois, J. H. Adams, R. D. Schrimpf and M. P. King, "Charge generation by secondary particles from nuclear reactions in beol materials,**" IEEE Trans. Nuc.** Sci., vol.56, no.6, pp. 3172-3179, Dec 2009.

127. N. H. Tolk, M. L. Alles, R. Pasternak, X. Lu, R. D. Schrimpf, D. M. Fleetwood, R. P. Dolan, and R. W. Standley, "Oxide-interface studies using second harmonic generation," Microelectron. Engrg. 84, 2089-2092 (2007).

128. O. A. Amusan, L. W. Massengill, M. P. Baze, B. L. Bhuva, A. F. Witulski, J. D. Black, A. Balasubramanian, M. C. Casey, D. A. Black, J. R. Ahlbin, R. A. Reed and M. W. McCurdy, "Mitigation techniques for single-event-induced charge sharing in a 90-nm bulk cmos process", Ieee Transactions on Device and Materials Reliability, vol.9, no.2, pp. 311-317, Jun 2009.

129. P. C. Adell, H. J. Barnaby, R.D. Schrimpf, B. Vermeire, "Band-to-band tunneling (BBT) induced leakage current enhancement in irradiated fully depleted SOI devices," *IEEE Trans. on Nuclear Science*, vol. 54, pp. 2174 - 2180, 2007.

130. P. Cheng, B. Jun, A.K. Sutton, C. Zhu, A. Appaswamy, J.D. Cressler, R.D. Schrimpf, and D.M. Fleetwood, "Probing Radiation- and Hot Electron-Induced Damage Processes in SiGe HBTs Using Mixed-Mode Electrical Stress," IEEE Transactions on Nuclear Science, vol. 54, pp. 1938-1945, 2007.

131. P. Cheng, J. Pellish, M.A. Carts, S. Philips, E. Wilcox, T. Thrivikraman, L. Najafizadeh, J.D. Cressler, and P.W. Marshall, "Re-examining TID Hardness Assurance Test Protocols for SiGe HBTs," IEEE Transactions on Nuclear Science, vol. 56, pp. 3318-3325, 2009.

132. P. E. Dodd, J. R. Schwank, M. R. Shaneyfelt, J. A. Felix, P. Paillet, V. Ferlet-Cavrois, J. Baggio, R. A. Reed, K. M. Warren, R. A. Weller, R. D. Schrimpf, G. L. Hash, S. M. Dalton, K. Hirose and H. Saito, "Impact of heavy ion energy and nuclear interactions on single-event upset and latchup in integrated circuits ," **IEEE Trans. Nuc.** Sci., vol.54, no.6, pp. 2303-2311, Dec 2007.

133. P. Marshall, M. Carts, S. Currie, R. Reed, B. Randall, K. Fritz, K. Kennedy, R. Krithivasan, C. Siedleck, R. Ladbury, J.D. Cressler, D. McMorrow, Steve Buchner, C. Marshall, K. LaBel, and B. Gilbert, "Autonomous Bit Error Rate Testing at Multi-Gbit/s Rates Using a Circuit for Radiation Effects Self Test (CREST)," IEEE Transactions on Nuclear Science, vol. 52, pp. 2446-2454, 2005.

134. R. A. Reed, G. Vizkelethy, J. A. Pellish, B. Sierawski, K. M. Warren, M. Porter, J. Wilkinson, P. W. Marshall, G. Niu, J. D. Cressler, R. D. Schrimpf, A. Tipton and R. A. Weller, "Applications of heavy ion microprobe for single event effects analysis", Nuclear Instruments & Methods in Physics Research Section B-Beam Interactions with Materials and Atoms, vol.261, no.1-2, pp. 443-446, Aug 2007.

135. R. A. Reed, R. A. Weller, M. H. Mendenhall, J. M. Lauenstein, K. M. Warren, J. A. Pellish, R. D. Schrimpf, B. D. Sierawski, L. W. Massengill, P. E. Dodd, M. R. Shaneyfelt, J. A. Felix, J. R. Schwank, N. F. Haddad, R. K. Lawrence, J. H. Bowman and R. Conde, "Impact of ion energy and species on single event effects analysis ," **IEEE Trans. Nuc.** Sci., vol.54, no.6, pp. 2312-2321, Dec 2007.

136. R. A. Reed, R. A. Weller, R. D. Schrimpf, M. H. Mendenhall, K. M. Warren and L. W. Massengill, "Implications of nuclear reactions for single-event effects test methods and analysis ," **IEEE Trans. Nuc.** Sci., vol.53, no.6, pp. 3356-3362, Dec 2006.

137. R. A. Weller, R. A. Reed, K. M. Warren, M. H. Mendenhall, B. D. Sierawski, R. D. Schrimpf and L. W. Massengill, "General framework for single event effects rate prediction in microelectronics ," **IEEE Trans. Nuc.** Sci., vol.56, no.6, pp. 3098-3108, Dec 2009.

138. R. Arora, B. W. Schmidt, D. M. Fleetwood, R. D. Schrimpf, K. F. Galloway, B. R. Rogers, K. B. Chung, and G. Lucovsky, "Temperature stress response of Ge MOS capacitors with HfO2/ HfSiON gate dielectrics," Transactions of the 215th ECS Meeting, Vol. 19(2), Silicon Nitride, Silicon Dioxide, and Emerging Dielectrics 10, edited by R. Ekwal Sah, J. Zhang, J. Deen, J. Yota, A. Toriumi, San Francisco, CA, May 24-29, pp. 803-814 (2009).

139. R. Arora, J. Rozen, D. M. Fleetwood, K. F. Galloway, C. X. Zhang, J. Han, S. Dimitrijev, F. Kong, L. C. Feldman, S. T. Pantelides, and R. D. Schrimpf, "Charge trapping properties of 3C and 4H-SiC MOS capacitors with nitride gate oxides," IEEE Trans. Nucl. Sci. 56, 3185 (2009).

140. R. D. Schrimpf, D. M. Fleetwood, R. L. Pease, L. Tsetseris, and S. T. Pantelides, "Impact of radiation-induced defects on bipolar device operation," in Defects in Microelectronic Materials and Devices, edited by D. M. Fleetwood, S. T. Pantelides, and R. D. Schrimpf, CRC Press 2008, pp. 551-574.

141. R. D. Schrimpf, K. M. Warren, D. R. Ball, R. A. Weller, R. A. Reed, D. M. Fleetwood, L. W. Massengill, M. H. Mendenhall, S. N. Rashkeev, S. T. Pantelides and M. A. Alles, "Multi-scale simulation of radiation effects in electronic devices ," **IEEE Trans. Nuc.** Sci., vol.55, no.4, pp. 1891-1902, Aug 2008.

142. R. D. Schrimpf, K. M. Warren, R. A. Weller, R. A. Reed, L. W. Massengill, M. L. Alles, D. M. Fleetwood, X. J. Zhou, L. Tsetseris, and S. T. Pantelides, "Reliability and radiation effects in IC Technologies," Proc. IEEE Intl. Reliab. Phys. Sympos., Phoenix, AZ, April 27 – May 1, 2008, pp. 97-106. [Invited.]

143. R. D. Schrimpf, R. A. Weller, M. H. Mendenhall, R. A. Reed and L. W. Massengill, "Physical mechanisms of single-event effects in advanced microelectronics", Nuclear Instruments & Methods in Physics Research Section B-Beam Interactions with Materials and Atoms, vol.261, no.1-2, pp. 1133-1136, Aug 2007.

144. R. Krithivasan, P.W. Marshall, M. Nayeem, A.K. Sutton, W.-M.L. Kuo, B.M. Haugerud, J.D. Cressler, L. Najafizadeh, M.A. Carts, C.J. Marshall, G. Niu, R.A. Reed, D. Hansen, K. Jobe, B.A. Randall, C.A. Burfield, and B. Gilbert, "The Application of RHBD Techniques to SEU Hardening of Third-Generation SiGe HBT Logic Circuits," IEEE Transactions on Nuclear Science, vol. 53, pp. 3400-3407, 2006.

145. R. L. Pease, R. D. Schrimpf, and D. M. Fleetwood, "ELDRS in bipolar linear circuits: A review," IEEE Trans. Nucl. Sci. 56, 1894-1908 (2009).

146. R. M. Diestelhorst, S. D. Phillips, A. Appaswamy, A. K. Sutton, J. D. Cressler, J. A. Pellish, R. A. Reed, G. Vizkelethy, P. W. Marshall, H. Gustat, B. Heinemann, G. G. Fischer, D. Knoll and B. Tillack, "Junction isolation single event radiation hardening of a 200 ghz sige:C hbt technology without deep trench isolation ," IEEE Trans. Nuc. Sci., vol.56, no.6, pp. 3402-3407, Dec 2009.

147. R. M. Diestelhorst, S. Finn, B. Jun, A. K. Sutton, P. Cheng, P. W. Marshall, J. D. Cressler, R. D. Schrimpf, D. M. Fleetwood, J. Gustat, B. Heinemann, G. G. Fischer, D. Knoll, and B. Tillack, "The effects of X-ray and proton irradiation on a 200 GHz/90 GHz complementary (npn + pnp) SiGe:C HBT technology," IEEE Trans. Nucl. Sci. 54, 2190-2195 (2007).

148. R. R. Cizmarik, R. D. Schrimpf, D. M. Fleetwood, K. F. Galloway, D. G. Platteter, M. R. Shaneyfelt, R. L. Pease, J. Boch, D. R. Ball, J. D. Rowe, and M. C. Maher, "The impact of mechanical stress on the total-dose response of linear bipolar transistors with various passivation layers," IEEE Trans. Nucl. Sci. 52, No. 5, 1513-1517 (2005).

149. R.A. Reed, G. Vizkelethy, J.A. Pellish, B. Sierawski, K.M. Warren, M. Porter, J. Wilkinson, P.W. Marshall, G. Niu, J.D. Cressler, R.D. Schrimpf, A. Tipton, and R.A. Weller, "Applications of Heavy Ion Microprobe For Single Event Effects Analysis," Nuclear Instruments and Methods in Physics Research B, vol. 261, pp. 443-446, 2007.

150. R.M. Diestelhorst, S. Finn, B. Jun, A.K. Sutton, P. Cheng, P.W. Marshall, J.D. Cressler, R.D. Schrimpf, D.M. Fleetwood, H. Gustat, B. Heinemann, G.G. Fischer, D. Knoll, and B. Tillack, "The Effects of X-Ray and Proton Irradiation on a 200 GHz / 90 GHz Complementary (npn + pnp) SiGe:C HBT Technology," IEEE Transactions on Nuclear Science, vol. 54, pp. 2190-2195, 2007.

151. R.M. Diestelhorst, S. Phillips, A. Appaswamy, A.K. Sutton, J.D. Cressler, J.A. Pellish, R.A. Reed, G. Vizkelethy, P.W. Marshall, H. Gustat, B. Heinemann, G.G. Fischer, D. Knoll, and B. Tillack, "Using Junction Isolation to Single-Event Radiation Harden a 200 GHz SiGe:C HBT Technology Containing No Deep Trenches," IEEE Transactions on Nuclear Science, vol. 56, pp. 3402-3407, 2009.

152. S. A. Francis, A. Dasgupta, and D. M. Fleetwood, "Effects of total dose irradiation on the gate-voltage dependence of the 1/f noise of nMOS and pMOS transistors," IEEE Trans. Electron Dev. 57, 503-510 (2010).

153. S. D. Phillips, T. Thrivikraman, A. Appaswamy, A. K. Sutton, J. D. Cressler, G. Vizkelethy, P. Dodd and R. A. Reed, "A novel device architecture for seu mitigation: The inverse-mode cascode sige hbt ,**" IEEE Trans. Nuc.** Sci., vol.56, no.6, pp. 3393-3401, Dec 2009.

154. S. DasGupta, A. F. Witulski, B. L. Bhuva, M. L. Alles, R. A. Reed, O. A. Amusan, J. R. Ahlbin, R. D. Schrimpf and L. W. Massengill, "Effect of well and substrate potential modulation on single event pulse shape in deep submicron cmos ,**" IEEE Trans. Nuc.** Sci., vol.54, no.6, pp. 2407-2412, Dec 2007.

155. S. DasGupta, O. A. Amusan, M. L. Alles, A. F. Witulski, L. W. Massengill, B. L. Bhuva, R. D. Schrimpf and R. A. Reed, "Use of a contacted buried n(+) layer for single event mitigation in 90 nm cmos ," IEEE Trans. Nuc. Sci., vol.56, no.4, pp. 2008-2013, Aug 2009.

156. S. K. Dixit, S. Dhar, J. Rozen, S. Wang, R. D. Schrimpf, D. M. Fleetwood, S. T. Pantelides, J. R. Williams, and L. C. Feldman, "Total dose radiation response of nitrided and non-nitrided SiO2/4H-SiC MOS Capacitors," IEEE Trans. Nucl. Sci. 53, 3687-3692 (2006).

157. S. K. Dixit, X. J. Zhou, R. D. Schrimpf, D. M. Fleetwood, S. T. Pantelides, R. Choi, G. Bersuker, and L. C. Feldman, "Radiation induced charge trapping in ultrathin HfO2-based MOSFETs," IEEE Trans. Nucl. Sci. 54, 1883-1890 (2007).

158. S. T. Pantelides, L. Tsetseris, M. J. Beck, S. N. Rashkeev, G. Hadjisavvas, I. G. Batyrev, B. R. Tuttle, A. G. Marinopoulos, X. J. Zhou, D. M. Fleetwood, and R. D. Schrimpf, "Performance, reliability, radiation effects, and aging issues in microelectronics – From atomic-scale physics to engineering level modeling", Solid State Electron. 54, 841-848 (2010).

159. S. T. Pantelides, L. Tsetseris, M. J. Beck, S. N. Rashkeev, G. Hadjisavvas, I. G. Batyrev, B. R. Tuttle, A. G. Marinopoulos, X. J. Zhou, D. M. Fleetwood, and R. D. Schrimpf, "Performance, reliability, radiation effects, and aging issues in microelectronics from atomic-scale physics to engineering-level modeling," Proceedings of the European Solid State Device Research Conference, 2009. ESSDERC '09, Athens, Greece, Sept. 14-18, 2009, pp. 77-84. [Invited]

160. S. T. Pantelides, L. Tsetseris, M. J. Beck, S. N. Rashkeev, G. Hadjisavvas, I. Batyrev, B. Tuttle, A. G. Marinopoulos, X. J. Zhou, D. M. Fleetwood, and R. D. Schrimpf, "Performance, reliability, radiation effects, and aging issues in microelectronics – from atomic scale physics to engineering level modeling," Transactions of the 215th ECS Meeting, Vol. 19(2), Silicon Nitride, Silicon Dioxide, and Emerging Dielectrics 10, edited by R. Ekwal Sah, J. Zhang, J. Deen, J. Yota, and A. Toriumi, San Francisco, CA, May 24-29, pp. 319-337 (2009). [Invited]

161. S. T. Pantelides, L. Tsetseris, S. N. Rashkeev, X. J. Zhou, D. M. Fleetwood, and R. D. Schrimpf, "Hydrogen in MOSFETs – a primary agent of reliability issues," Microelectron. Reliab. 47, 903-911 (2007). [Invited.]

162. S. T. Pantelides, M. H. Evans, D. M. Fleetwood, E. P. Gusev, J. D. Joannopoulos, Z. Lu, S. J. Pennycook, S. N. Rashkeev, R. D. Schrimpf, L. Tsetseris, K. Van Benthem, X-G. Zheng, and X. J. Zhou, "Defect-related issues in high-K dielectrics," in Defects in Advanced High-$\varkappa$ Dielectric Nano-Electronic Semiconductor Devices, edited by E. Gusev (Springer, Amsterdam, 2006), pp. 189-202. [Invited.]

163. S. T. Pantelides, S. Wang, A. Franceschetti, R. Buczko, M. Di Ventra, S. N. Rashkeev, L. Tsetseris, M. H. Evans, I. G. Batyrev, L. C. Feldman, S. Dhar, K. McDonald, R. A. Weller, R. D. Schrimpf, D. M. Fleetwood, X. J. Zhou, J. R. Williams, C. C. Tin, G. Y. Chung, T. Isaacs-Smith, S. R. Wang, S. J. Pennycook, G. Duscher, K. Van Benthem, and L. M. Porter, "Si/SiO2 and SiC/SiO2 Interfaces for MOSFETs – Challenges and Advances," Materials Sci. Forum: SiC and Related Materials 2005, eds: R. P. Devaty, D. J. Larkin and S. E. Saddow vol. 527-529, pp. 935-948 (2006).

164. S. T. Pantelides, Z. Y. Lu, C. Nicklaw, T. Bakos, S. N. Rashkeev, D. M. Fleetwood, and R. D. Schrimpf, "The E' center and oxygen vacancies in SiO2," J. Non-Cryst. Solids 354, 217-223 (2008). [Invited.]

165. S. Y. Son, Y. S. Choi, P. Kumar, H. Park, T. Nishida, R. K. Singh, and S. E. Thompson, "Strained induced changes in gate leakage current and dielectric constant nitrided Hf-silicate dielectric silicon MOS capacitors," Appl. Phys. Lett., vol. 93, pp. 153505-3, 2008.

166. S.D. Phillips, T. Thrivikraman, A. Appaswamy, A.K. Sutton, J.D. Cressler, G. Vizkelethy, P.E. Dodd, R.A. Reed, and P.W. Marshall, "A Novel Device Architecture for SEU Mitigation: The Inverse-Mode Cascode SiGe HBT," IEEE Transactions on Nuclear Science, vol. 56, pp. 3393-3401, 2009.

167. T. Chen, A.K. Sutton, B.M. Haugerud, J.P. Comeau, M. Bellini, Q. Liang, J.D. Cressler, J. Cai, T.H. Ning, P.W. Marshall, and C.J. Marshall, "Proton Radiation Effects in Vertical SiGe HBTs Fabricated on CMOS-Compatible SOI," IEEE Transactions on Nuclear Science, vol.52, pp. 2353-2357, 2005.

168. T. Thrivikraman, P. Cheng, S. Phillips, J. Comeau, M. Morton, J.D. Cressler, and P. Marshall, "On the Radiation Tolerance of SiGe HBT and CMOS-based Phase Shifters for Space-based, Phase-Array Antenna Systems," IEEE Transactions on Nuclear Science, vol. 55, pp. 3246-3252, 2008.

169. T. Zhang, X. Wei, G. Niu, J.D. Cressler, P.W. Marshall, and R.A. Reed, "A Mechanism versus SEU Impact Analysis of Collector Charge Collection in SiGe HBT Current Mode Logic," IEEE Transactions on Nuclear Science, vol. 56, pp. 3071-3077, 2009.

170. T. Zhang, X. Y. Wei, G. F. Niu, J. D. Cressler, P. W. Marshall and R. A. Reed, "A mechanism versus seu impact analysis of collector charge collection in sige hbt current mode logic,**"** **IEEE Trans. Nuc.** Sci., vol.56, no.6, pp. 3071-3077, Dec 2009.

171. T.S. Mukherjee, K.T. Kornegay, A.K. Sutton, R. Krithivasan, J.D. Cressler, G. Niu, and P.W. Marshall, "A Novel Circuit-Level SEU-Hardening Technique For Low-Voltage, Ultra-High-Speed SiGe HBT Logic Circuits," IEEE Transactions on Nuclear Science, vol. 54, pp. 2086-2091, 2007.

172. V. Ramachandran, B. Narasimham, D. M. Fleetwood, R. D. Schrimpf, W. T. Holman, A. F. Witulski, R. L. Pease, G. W. Dunham, J. E. Seiler, and D. G. Platteter, "Modeling total-dose effects for a low-dropout voltage regulator," IEEE Trans. Nucl. Sci. 53, 3223-3231 (2006).

173. X. J. Chen, H. J. Barnaby, B. Vermeire, K. E. Holbert, D. Wright, R. L. Pease, R. D. Schrimpf, D. M. Fleetwood, S. T. Pantelides, M. R. Shaneyfelt, and P. C. Adell, "Post-irradiation annealing mechanisms of defects generated in hydrogenated bipolar oxides," IEEE Trans. Nucl. Sci. 55, 3032-3038 (2008).

174. X. J. Chen, H. J. Barnaby, B. Vermeire, K. Holbert, D. Wright, R. L. Pease, R. D. Platteter, G. Dunham, J. Seiler, S. McClure, and P. Adell, "Mechanisms of enhanced radiation-induced degradation due to excess molecular hydrogen in bipolar oxides," *IEEE Trans Nucl. Sci.,* vol. 54, pp. 1913-1919, 2007.

175. X. J. Chen, H. J. Barnaby, P. Adell, R. L. Pease, B. Vermeire, and K. E. Holbert, "Modeling the Dose Rate Response and the Effects of Hydrogen in Bipolar Technologies," *IEEE Trans Nucl. Sci.,* vol. 56, pp. 3196-3202, 2009.

176. X. J. Chen, H. J. Barnaby, R. D. Schrimpf, D. M. Fleetwood, R. L. Pease, D. G. Platteter, and G. W. Dunham, "Nature of interface defect buildup in gated bipolar devices under low dose rate irradiation," IEEE Trans. Nucl. Sci. 53, 3649-3654 (2006).

177. X. J. Zhou, D. M. Fleetwood, I. Danciu, A. Dasgupta, S. A. Francis, and A. D. Touboul, "Effects of aging on the 1/f noise of MOSFETs," Appl. Phys. Lett. 91, Article No. 173501 (2007).

178. X. J. Zhou, D. M. Fleetwood, J. A. Felix, E. P. Gusev, and C. D'Emic, "Bias-temperature instabilities and radiation effects in MOS devices," IEEE Trans. Nucl. Sci. 52, 2231-2238 (2005).

179. X. J. Zhou, D. M. Fleetwood, L. Tsetseris, R. D. Schrimpf, and S. T. Pantelides, "Effects of switched-bias annealing on charge trapping in HfO2 gate dielectrics," IEEE Trans. Nucl. Sci. 53, 3636-3643 (2006).

180. X. J. Zhou, D. M. Fleetwood, R. D. Schrimpf, F. Faccio, and L. Gonella, "Radiation effects on the 1/f noise of field oxide field effect transistors," IEEE Trans. Nucl. Sci. 55, 2975-2980 (2008).

181. X. Lu, R. Pasternak, H. Park, J. Qi, N. H. Tolk, A. Chatterjee, R. D. Schrimpf, and D. M. Fleetwood, "Temperature-dependent second- and third-order optical nonlinear susceptibilities at the Si/SiO2 interface," Phys. Rev. B. 78, Article No. 155311 (2008).

182. X. Wei, T. Zhang, G. Niu, M. Varadharajaperumal, J. D. Cressler, and P. W. Marshall, "3-D Mixed-Mode Simulation of Single Event Transients in SiGe HBT Emitter Followers and Resultant Hardening Guidelines," IEEE Transactions on Nuclear Science, vol. 55, pp. 3360-3366, 2008.

183. Y. S. Choi, H. Park, T. Nishida, and S. E. Thompson, "Reliability of HfSiON gate dielectric silicon MOS devices under [110] mechanical stress: Time dependent dielectric breakdown," J. Appl. Phys., vol. 105, pp. 044503-5, 2009.

184. Y. S. Choi, T. Nishida, and S. E. Thompson, "Impact of mechanical stress on direct and trap-assisted gate leakage currents in p-type silicon metal-oxide-semiconductor capacitors," Appl. Phys. Lett., vol. 92, pp. 173507-3, May 2008.

185. Y. V. White, X. Lu, R. Pasternak, N. H. Tolk, A. Chatterjee, R. D. Schrimpf, D. M. Fleetwood, A. Ueda, and R. Mu, "Studies of charge carrier trapping and recombination processes in Si/SiO2/MgO structures using second-harmonic generation," Appl. Phys. Lett. 88, Article No. 062102, pp. 1-3 (2006).

186. In Press

187. En Xia Zhang, Daniel M. Fleetwood, Farah E. Mamouni, Michael L. Alles, Ronald D. Schrimpf, Weize Xiong, and Sorin Cristoloveanu. Effects of fin width on memory windows in FinFET ZRAMs. Solid State Electronics, in press (2010).

188. Rajan Arora, Jerome Mitard, Eddy Simoen, En Xia Zhang, D. M. Fleetwood, B. K. Choi, R. D. Schrimpf, K. F. Galloway, S. R. Kulkarni, M. Meuris, and Cor Claeys. Effects of halo doping and Si capping layer thickness on total-dose effects in Ge p-MOSFETs, IEEE Trans. Nucl. Sci., in press (2010).

189. E. Golias, L. Tsetseris, A. Dimoulas, and S. T. Pantelides, "Ge volatilization products in high-k dielectrics", Microelectron. Engin. in press (2010).

190. L. Tsetseris and S. T. Pantelides, "Defect formation and annihilation at Ge-GeO2 interfaces", Microelectron. Engin., in press (2010)

191. Under Review

192. E. X. Zhang, D. M. Fleetwood, F. El Mamouni, R. D. Schrimpf, M. L. Alles, W. Xiong, K. Akarvardar, and S. Cristoloveanu, "Total ionizing dose effects on FinFET-based capacitorless 1T-DRAMs," submitted to IEEE Trans. Nucl. Sci., 57, no. 6, Dec. 2010.

193. A. Dasgupta, D. M. Fleetwood, R. A. Reed, R. A. Weller, M. H. Mendenhall, and B. D. Sierawski, "Dose enhancement and reduction in high-K MOS insulators," submitted to IEEE Trans. Nucl. Sci., 57, no. 6, Dec. 2010.

194. C. X. Zhang, E. X. Zhang, D. M. Fleetwood, R. D. Schrimpf, K. F. Galloway, E. Simoen, J. Mitard, and C. Claeys, "Effects of processing and radiation bias on leakage currents in Ge pMOSFETs," submitted to IEEE Trans. Nucl. Sci., 57, no. 6, Dec. 2010.

195. B. R. Tuttle, D. R. Hughart, R. D. Schrimpf, D. M. Fleetwood, and S. T. Pantelides, "Defect interactions of H2 in SiO2: Implications for ELDRS and latent interface trap buildup," submitted to IEEE Trans. Nucl. Sci., 57, no. 6, Dec. 2010.

196. T. Roy, E. X. Zhang, Y. S. Puzyrev, D. M. Fleetwood, R. D. Schrimpf, B. K. Choi, A. B. Hmelo, and S. T. Pantelides, "Process dependence of proton-induced degradation in HEMTs," submitted to IEEE Trans. Nucl. Sci., 57, no. 6, Dec. 2010.

197. N. Rezzak, R. D. Schrimpf, M. L. Alles, E. X. Zhang, D. M. Fleetwood, and Y. F. Li, "Layout-related stress effects on radiation-induced leakage current," submitted to IEEE Trans. Nucl. Sci., 57, no. 6, Dec. 2010.

198. F. El Mamouni, M. Bawedin, E. X. Zhang, R. D. Schrimpf, D. M. Fleetwood, and S. Cristoloveanu, "Total dose effects on the performance of irradiated capacitor-less MSDRAM cells," submitted to IEEE Trans. Nucl. Sci., 57, no. 6, Dec. 2010.

199. Y. F. Li, N. Rezzak, E. X. Zhang, R. D. Schrimpf, D. M. Fleetwood, J. Wang, D. Wang, Y. Wu, and S. Cai, "Including the effects of process-related variability on radiation response in advanced foundry process design kits," submitted to IEEE Trans. Nucl. Sci., 57, no. 6, Dec. 2010.

6.0 INTERACTIONS / TRANSITIONS

1. I. S. Esqueda, W. Wu, H. J. Barnaby, and G. Gildenblat, "Modeling of Ionizing Radiation Effects in CMOS Devices Using PSP Surface-Potential-Based Compact Model " in Nuclear and Space Radiation Effects Conference Denver, Co, 2010.

2. I. S. Esqueda, H. J. Barnaby, K. E. Holbert, F. E. Mamouni, and R. D. Schrimpf, "Modeling of Ionizing Radiation-Induced Degradation in Multiple Gate Field Effect Transistors," in RADECS 2008, Bruge, Belgium, 2009.

3. I. S. Esqueda, H. J. Barnaby, M. L. McLain, P. C. Adell, F. E. Mamouni, S. K. Dixit, R. D. Schrimpf, and W. Xiong, "Modeling the Radiation Response of Fully-Depleted SOI n-channel MOSFETs," in RADECS 2008, 2008.

4. M. L. McLain, H. J. Barnaby, I.S. Esqueda, J. Oder, B. Vermeire, "Reliability of high performance standard two-edge and radiation hardened by design enclosed geometry transistors," 2009 IEEE International Reliability Physics Symposium Proceedings, April 26-30 2009, pp. 174 – 179.

5. H. J. Barnaby, M. L. Mclain, I. S. Esqueda, and X. J. Chen, "Modeling Ionizing Radiation Effects in Solid State Materials and CMOS Devices," IEEE Custom Integrated Circuits Conference (CICC), September 2008, pp. 273 – 280.

6. M. L. Mclain, H. J. Barnaby, P. C. Adell, "Analytical model of the radiation response in FDSOI MOSFETs," 2008 IEEE International Reliability Physics Symposium Proceedings, April 2008, pp. 643 - 644.

7. I. S. Esqueda, H. J. Barnaby, F. E. Mamouni, R. D. Schrimpf, "Modeling of Ionizing Radiation-Induced Degradation in Multiple Gate Field Effect Transistors," 2009 RADECS, Brugge, Belgium, September 2009.

8. I. S. Esqueda, H. J. Barnaby, M. L Mclain, P. C. Adell, F. E. Mamouni, S. K. Dixit, R. D. Schrimpf, W. Xiong, "Modeling the Radiation Response of Fully-Depleted SOI n-Channel MOSFETs," IEEE Nuclear and Space Radiation Effects Conf., Quebec City, CA., July 2009.

9. M. L Mclain, H. J. Barnaby, K. E. Holbert, "Modeling Ionizing Radiation Effects in Shallow Trench Isolation Field Oxide FETs, "IEEE Nuclear and Space Radiation Effects Conf., Quebec City, CA., July 2009.

10. G.K. Siddhartha, H. J. Barnaby, B. Vermeire, "Single Event Transients in Switched Capacitor Circuits," Single Event Effects Symposium, Long Beach, CA, April, 2009.

11. M. L. McLain, H. J. Barnaby, H. L. Hughes, P. J. McMarr, "Effects of Channel Implant Variation on Radiation-Induced Edge Leakage Currents in n-Channel MOSFETs," Radiation Technology Conference (HEART), Albuquerque, March 2009.

12. I. S. Esqueda, H. J. Barnaby, M. L. McLain, P. C. Adell, F. Mamouni, S. K. Dixit, R. D. Schrimpf, X. Wade, "Modeling the Radiation Response of Fully-Depleted SOI n-MOSFETS," to be presented at the 2008 RADECS Workshop, Jyväskylä, Finland, September 2008.

13. M. L. McLain, H. J. Barnaby, K. E. Holbert, L. T. Clark, Radiation Induced Inter-Device Leakage Current in 90 nm Bulk CMOS Devices and Circuits," IEEE Nuclear and Space Radiation Effects Conf., Tucson, Az., July 2008.

14. M. McLain, H. J. Barnaby, K. Holbert, M. Baze, A. Amort, J. Wert, "Gate width effects on the radiation response of sub-100 nm bulk CMOS two-edge transistors," Hardened Electronics and Radiation Technology Conference (HEART), Colorado Springs, March 2008.

15. H. J. Barnaby, B. Vermeire, P. Adell, "Radiation Effects Issues for SOI in Next Generation SRAM-based FPGAs," Military and Aerospace FPGA and Applications (MAFA) Meeting, Palm Beach, FL, November 2007.

16. M. McLain, H. J. Barnaby, K. E. Holbert, R. D. Schrimpf, H. Shah, A. Amort, M. Baze, J. Wert, "Enhanced TID Susceptibility in Sub-100 nm Bulk CMOS I/O Transistors and Circuits," IEEE Nuclear and Space Radiation Effects Conf., Honolulu, Hawaii, July 2007.

17. P. C. Adell, H. J. Barnaby, R.D. Schrimpf, B. Vermeire, "Band-to-Band Tunneling (BBT) Induced Leakage Current Enhancement in Irradiated Fully Depleted SOI Devices," IEEE Nuclear and Space Radiation Effects Conf., Honolulu, Hawaii,, July 2007.

18. H. J. Barnaby, M. Mclain, H. Shah, B. Vermeire, E. Mikkola, "Radiation-enabled predictive technology modeling approaches for deep-submicron CMOS integrated circuit design," Microelectronics Reliability and Qualification Workshop, Los Angeles, CA, December 2006.

19. M. McLain, I. Esqueda, H. J. Barnaby, K. E. Holbert, "Characterization of the Radiation Response in 130 nm Shallow Trench Isolation (STI) Oxides," 2006 RADECS Workshop, Athens, Greece, September, 2006.

20. H. Barnaby, M. Mclain, I. Esqueda, "Total-Ionizing-Dose Effects in Modern CMOS Technologies," CAARI 2006: 19th International Conference on the Application of Accelerators in Research and Industry, Fort Worth, TX, August, 2006.

21. I. S. Esqueda, H.J. Barnaby, M. L. Alles, "Two-dimensional methodology for modeling radiation-induced off-state leakage in CMOS technologies," 2005 Nuclear and Space Radiation Effects Conf., Seattle, WA, July 2005.

22. J.D. Cressler, "Using SiGe HBTs for Electronics Applications Operating at Cryogenic Temperatures," Proceedings of the 2005 IMAPS Workshop on Advanced Electronic Packages and Devices in Extreme Cold Environments, pp. 62-67, 2005.

23. J.D. Cressler, "Using SiGe HBTs for Extreme Environment Electronics," Proceedings of the 2005 IEEE Bipolar/BiCMOS Circuits and Technology Meeting, pp. 248-251, 2005.

24. J.D. Cressler, "SiGe HBT Reliability Issues Associated with Operation in Extreme Environments," Proceedings of the 2006 IEEE Topical Meeting on Silicon Monolithic Integrated Circuits in RF Systems, pp. 3-7, 2006.

25. J.D. Cressler, M. Mojarradi, B. Blalock, W. Johnson, G. Niu, F. Dai, A. Mantooth, J. Holmes, M. Alles, R. Reed, P. McCluskey, R. Berger, R. Garbos, L. Peltz, A. Joseph, and C. Eckert, "SiGe Integrated Electronics for Extreme Environments," Proceedings of the 2007 GOMAC-Tech - Government Microcircuit Applications and Critical Technology Conference, pp. 327-331, 2007.

26. J.D. Cressler, "SiGe BiCMOS Technology: an IC Design Platform for Extreme Environment Electronics Applications," Proceedings of the 2007 IEEE International Reliability Physics Symposium, pp. 141-149, 2007.

27. J.D. Cressler, "Using SiGe Technology in Extreme Environments," Proceedings of the 2007 IEEE International Semiconductor Device Research Symposium, paper WP2-01, pp. 1, 2007 (on CD ROM).

28. J.D. Cressler, "Silicon-Germanium as an Enabling IC Technology for Extreme Environment Electronics," Proceedings of the 2008 IEEE Aerospace Conference, pp. 1-7 (on CD ROM), 2008.

29. J.D. Cressler, "Emerging Application Opportunities for SiGe Technology," Proceedings of the 2008 IEEE Custom Integrated Circuits Conference, pp. 57-64, 2008.

30. C.M. Grens, B.M. Haugerud, A.K. Sutton, T. Chen, J.D. Cressler, P.W. Marshall, C.J. Marshall, and A.J. Joseph, "The Effects of Proton Irradiation on the Operating Voltage Constraints of SiGe HBTs," 2005 IEEE Nuclear and Space Radiation Effects Conference, paper PE-3, 2005.

31. A.P.G. Prakash and J.D. Cressler, "An Investigation of Electron and Oxygen Ion Damage in Si npn RF Power Transistors," 2005 IEEE Nuclear and Space Radiation Effects Conference, paper B-2, 2005.

32. G. Niu, H. Yang, M. Varadharajaperumal, Y. Shi, J.D. Cressler, R. Krishivasan, P.W. Marshall, and R. Reed, "A New Back Junction Approach For Reducing Charge Collection in 200 GHz SiGe HBTs," 2005 IEEE Nuclear and Space Radiation Effects Conference, paper A-9, 2005.

33. A.K. Sutton, B.M. Haugerud, A.P.G. Prakash, J.D. Cressler, C.J. Marshall, P.W. Marshall, R. Ladbury, F. Guarin, and A.J. Joseph, "Anomalous Differences Between Gamma and Proton Radiation Damage in 200GHz SiGe HBTs," 2005 IEEE Nuclear and Space Radiation Effects Conference, paper E-3, 2005.

34. T. Chen, A.K. Sutton, B.M. Haugerud, J.P. Comeau, M. Bellini, Q. Liang, J.D. Cressler, J. Cai, T.H. Ning, P.W. Marshall, and C.J. Marshall, "Proton Radiation Effects in Vertical SiGe HBTs Fabricated on CMOS-Compatible SOI," 2005 IEEE Nuclear and Space Radiation Effects Conference, paper E-2, 2005.

35. P. Marshall, M. Carts, S. Currie, R. Reed, B. Randall, K. Fritz, K. Kennedy, R. Krithivasan, C. Siedleck, R. Ladbury, J.D. Cressler, D. McMorrow, Steve Buchner, C. Marshall, K. LaBel, and B. Gilbert, "Autonomous Bit Error Rate Testing at Multi-Gbit/s Rates Using a Circuit for Radiation Effects Self Test (CREST)," 2005 IEEE Nuclear and Space Radiation Effects Conference, paper F-6, 2005.

36. R.M. Diestelhorst and J.D. Cressler, "Radiation Effects in Silicon-Germanium HBT BiCMOS Technology for Space Electronics Applications," 2005 Semiconductor Research Corporation TECHCON, poster paper, 2005.

37. L. Peltz, J.D. Cressler, M. Mojarradi, "Silicon-Germanium Integrated Electronics for Extreme Environments Applied to the Design of a Lunar Hopper," Proceedings of the 7th International Conference for Lunar Exploration and Utilization," on CDROM, 2005.

38. J.D. Cressler, "Silicon-Germanium (SiGe) Integrated Electronics for Extreme Environments," Abstracts of the 2006 Space Technology and Applications International Forum (STAIF), p. 218, 2006.

39. R. Krithivasan, P.W. Marshall, M. Nayeem, A.K. Sutton, W.-M.L. Kuo, B.M. Haugerud, L. Najafizadeh, J.D. Cressler, M.A. Carts, C.J. Marshall, G. Niu, R. Reed, B.A. Randall, C.A. Burfield, and B. Gilbert, "Recent Results on SEU Hardening of SiGe HBT Logic Circuits," 2006 IEEE Single Event Effects Symposium, paper E-4, April 2006.

40. J.A. Pellish, R.A. Reed, M.L. Alles, R.D. Schrimpf, M. Varadharajaperumal, G. Niu, A.K. Sutton, R. Diestelhorst, G. Espinel, R. Krithivasan, J.P. Comeau, J.D. Cressler, G. Vizkelethy, P.W. Marshall, R.A. Weller, M.H. Mendenhall, and E.J. Montes, "Monte Carlo Modeling of Proton Events in Deep Trench Isolation technologies Using the Combined Capabilities of MRED and TCAD," 2006 IEEE Single Event Effects Symposium, paper C-5, April 2006.

41. E.J. Montes, R.A. Reed, J.A. Pellish, M.L. Alles, M. Varadharajaperumal, G. Niu, A.K. Sutton, R. Diestelhorst, G. Espinel, R. Krithivasan, J.P. Comeau, J.D. Cressler, P.W. Marshall, and G. Vizkelethy, "Single-Event Effects Modeling in Silicon Germanium HBTs," 2006 IEEE Single Event Effects Symposium, paper C-4, April 2006.

42. M. Bellini, B. Jun, T. Chen, J.D. Cressler, P.W. Marshall, D. Chen, and J. Cai, "Radiation and Bias Effects in Fully-Depleted and Partially-Depleted SiGe HBTs Fabricated on CMOS-Compatible SOI," 2006 IEEE Nuclear and Space Radiation Effects Conference, paper B-4, 2006.

43. L. Najafizadeh, M. Bellini, G. Espinel, A.P.G. Prakash, J.D. Cressler, P.W. Marshall, and C.J. Marshall, "Proton Tolerance of SiGe Precision Voltage References For Extreme Temperature Range Electronics," 2006 IEEE Nuclear and Space Radiation Effects Conference, paper PB-2, 2006.

44. A.P.G. Prakash, A.K. Sutton, R. Diestelhorst, G. Espinel, J. Andrews, B. Jun, J.D. Cressler, P.W. Marshall, and C.J. Marshall, "The Effects of Irradiation Temperature on the Proton Response of SiGe HBTs," 2006 IEEE Nuclear and Space Radiation Effects Conference, paper B-3, 2006.

45. R. Krithivasan, P.W. Marshall, M. Nayeem, A.K. Sutton, W.-M.L. Kuo, B.M. Haugerud, J.D. Cressler, L. Najafizadeh, M.A. Carts, C.J. Marshall, G. Niu, R.A. Reed, B.A. Randall, C.A. Burfield, and B. Gilbert, "The Application of RHBD Techniques to SEU Hardening of Third-Generation SiGe HBT Logic Circuits," 2006 IEEE Nuclear and Space Radiation Effects Conference, paper D-4, 2006.

46. A.K. Sutton, A.P.G. Prakash, R.M. Diestelhorst, G. Espinel, B. Jun, M. Carts, A. Phan, J.D. Cressler, P.W. Marshall, C.J. Marshall, R.A. Reed, R.D. Schrimpf, and D.M. Fleetwood, "An Investigation of Dose Enhancement and Source Dependent Effects in 200 GHz SiGe HBTs," IEEE Nuclear and Space Radiation Effects Conference, paper B-2, 2006.

47. J.A. Pellish, R.A. Reed, M.L. Alles, R.D. Schrimpf, M. Varadharajaperumal, G. Niu, A.K. Sutton, R. Diestelhorst, G. Espinel, R. Krithivasan, J.P. Comeau, J.D. Cressler, G. Vizkelethy, P.W. Marshall, R.A. Weller, M.H. Mendenhall, and E.J. Montes, "Substrate Engineering and Charge Collection Mitigation in Deep Trench Isolation Devices," IEEE Nuclear and Space Radiation Effects Conference, paper PC-1, 2006.

48. A.K. Sutton, R. Krithivasan, P.W. Marshall, S. Buchner, M. Carts, C. Siedleck, R. Ladbury, J.D. Cressler, C. Marshall, S. Currie, R. Reed, G. Niu, B. Randall, K. Fritz, D. McMorrow, and B. Gilbert, "SEU Error Signature Analysis of Gbit/sec SiGe Logic Circuits Using a Pulsed Laser Microprobe," IEEE Nuclear and Space Radiation Effects Conference, paper C-7, 2006.

49. E.J. Montes, R.A. Reed, J.A. Pellish, M.L. Alles, M. Varadharajaperumal, G. Niu, A.K. Sutton, R. Diestelhorst, G. Espinel, R. Krithivasan, J.P. Comeau, J.D. Cressler, P.W. Marshall, and G. Vizkelethy, "Impact of Deep Trench Isolation on Charge Collection Processes in Silicon-Germanium Heterojunction Bipolar Transistors," IEEE Nuclear and Space Radiation Effects Conference, paper PC-2, 2006.

50. J. Comeau, R. Krithivasan, A. Sutton, R. Diestelhorst, G. Espinel, G. Prakash, B. Jun, J.D. Cressler, M. Varadharajaperumal, G. Niu, J. Pellish, R. Reed, P. Marshall, and G. Vizkelethy, "An Investigation of Transistor-Layout-Based SEU Hardening of SiGe HBTs," 2006 IEEE Radiation Effects on Components and Systems (RADECS) Conference, September 2006.

51. A. Madan, B. Jun, R.M. Diestelhorst, A. Appaswamy, J.D. Cressler, R.D. Schrimpf, D.M. Fleetwood, T. Isaacs-Smith, J.R. Williams, and S.J. Koester, "Radiation Tolerance of Si/SiGe n-MODFETs," IEEE Nuclear and Space Radiation Effects Conference, paper PF-8, 2007.

52. M. Bellini, B. Jun, A.C. Appaswamy, P. Cheng, J.D. Cressler, P.W. Marshall, B. El-Kareh, S. Balster, and H. Yasuda, "The Effects of Proton Irradiation on the DC and AC Performance of Complementary (npn + pnp) SiGe HBTs on Thick-Film SOI," IEEE Nuclear and Space Radiation Effects Conference, paper PF-7, 2007.

53. R.M. Diestelhorst, S. Finn, B. Jun, A.K. Sutton, P. Cheng, P.W. Marshall, J.D. Cressler, R.D. Schrimpf, D.M. Fleetwood, H. Gustat, B. Heinemann, G.G. Fischer, D. Knoll, and B. Tillack, "The Effects of X-Ray and Proton Irradiation on a 200 GHz / 90 GHz Complementary (npn + pnp) SiGe:C HBT Technology," IEEE Nuclear and Space Radiation Effects Conference, paper F-5, 2007.

54. L. Najafizadeh, B. Jun, J.D. Cressler, A.P.G. Prakash, P.W. Marshall, and C.J. Marshall, "A Comparison of the Effects of X-Ray and Proton Irradiation on the Performance of SiGe Precision Voltage References," IEEE Nuclear and Space Radiation Effects Conference, paper PF-6, 2007.

55. J.A. Pellish, R.A. Reed, R.A. Weller, M.H. Mendenhall, P.W. Marshall, A.K. Sutton, R. Krithivasan, J.D. Cressler, S.M. Currie, R.D. Schrimpf, K.M. Warren, B.D. Sierawski, and G. Niu, "On-Orbit Event Rate Calculations for SiGe HBT Shift Registers," IEEE Nuclear and Space Radiation Effects Conference, paper H-3, 2007.

56. A.K. Sutton, J.P. Comeau, R. Krithivasan, J.D. Cressler, J.A. Pellish, R.A. Reed, P.W. Marshall, M. Varadharajaperumal, G. Niu, and G. Vizkelethy, "An Evaluation of Transistor-Layout RHBD Techniques for SEE Mitigation in SiGe HBTs," IEEE Nuclear and Space Radiation Effects Conference, paper C-6, 2007.

57. P. Cheng, B. Jun, A.K. Sutton, C. Zhu, A. Appaswamy, J.D. Cressler, R.D. Schrimpf, and D.M. Fleetwood, "Probing Radiation- and Hot Electron-Induced Damage Processes in SiGe HBTs Using Mixed-Mode Electrical Stress," IEEE Nuclear and Space Radiation Effects Conference, paper PA-4, 2007.

58. T.S. Mukherjee, K.T. Kornegay, A.K. Sutton, R. Krithivasan, J.D. Cressler, G. Niu, and P.W. Marshall, "A Novel Circuit-Level SEU-Hardening Technique For Low-Voltage, Ultra-High-Speed SiGe HBT Logic Circuits," IEEE Nuclear and Space Radiation Effects Conference, paper PC-6, 2007.

59. M. Varadharajaperumal, G. Niu, X. Wei, J.D. Cressler, R.A. Reed, and P.W. Marshall, "3-D Simulation of SEU Hardening of SiGe HBTs Using Shared Dummy Collector," IEEE Nuclear and Space Radiation Effects Conference, paper H-4, 2007.

60. J. A. Pellish, R. Reed, M. Alles, R. Schrimpf, M. Varadharajaperumal, G. Niu, A. Sutton, R. Diestelhorst, G. Espinel, R. Krithivasan, J. Comeau, J.D. Cressler, G. Vizkelethy, P. Marshall, R. Weller, M. Mendenhall, and E. Montes, "Monte Carlo modeling of proton events in deep trench isolation technologies using the combined capabilities of MRED and TCAD," IEEE Single Event Effects Symposium, April 2007.

61. R.A. Reed, G. Vizkelethy, J.A. Pellish, B. Sierawski, K.M. Warren, M. Porter, J. Wilkinson, P.W. Marshall, G. Niu, J.D. Cressler, R.D. Schrimpf, A. Tipton, and R.A. Weller, "Applications of Heavy Ion Microprobe For Single Event Effects Analysis," Proceedings of the 19th International Conference on the Application of Accelerators in Research and Industry, 2007.

62. T. Thrivikraman, P. Cheng, S. Phillips, J. Comeau, M. Morton, J.D. Cressler, and P. Marshall, "On the Radiation Tolerance of SiGe HBT and CMOS-based Phase Shifters for Space-based, Phase-Array Antenna Systems," IEEE Nuclear and Space Radiation Effects Conference, paper PE-4, 2008.

63. M. Bellini, S. Phillips, R.M. Diestelhorst, P. Cheng, J.D. Cressler, P.W. Marshall, M. Turowski, G. Avenier, A. Chantre, and P. Chevalier, "Novel Total Dose and Heavy-Ion Charge Collection Phenomena in a New SiGe HBT on Thin-Film SOI Technology," IEEE Nuclear and Space Radiation Effects Conference, paper E-5, 2008.

64. L. Najafizadeh, T. Vo, S. Phillips, P. Cheng, J.D. Cressler, M. Mojarradi, and P.W. Marshall, "The Effects of Proton Irradiation on the Performance of High-Voltage nMOSFETs Implemented in a Low-Voltage SiGe BiCMOS Platform," IEEE Nuclear and Space Radiation Effects Conference, paper PE-5, 2008.

65. J.A. Pellish, R.A. Reed, N.D. Pate, D. McMorrow, J.S. Melinger, J.A. Kozub, P.W. Marshall, A.K. Sutton, R.M. Diestelhorst, S. Phillips, J.D. Cressler, R.A. Weller, R.D. Schrimpf, and G.F. Niu, "Radiation-Induced Current Transients in SiGe HBTs," IEEE Nuclear and Space Radiation Effects Conference, paper PA-8, 2008.

66. X. Wei, T. Zhang, G. Niu, M. Varadharajaperumal, J. D. Cressler, and P. W. Marshall, "3-D Mixed Mode Simulation of Single Event Transients in SiGe HBT Emitter Followers and Hardening Guidelines," IEEE Nuclear and Science Radiation Effects Conference, paper PF-5, 2008.

67. R. Frampton, J.D. Cressler, M. Mojarradi, B. Blalock, W. Johnson, G. Niu, F. Dai, A. Mantooth, M. Alles, J. Holmes, R. Berger, R. Garbos, P. McClusky, W. Atwell, and L. Peltz, "Silicon-Germanium (SiGe) Technology for Low Temperature Environments for Europa and Enceladus Missions," Abstracts of the 2008 Space Technology and Applications International Forum (STAIF), p. 1 (on CDROM), 2008.

68. J.A. Pellish, R.A. Reed, D. McMorrow, G. Vizkelethy, J. Baggio, O. Duhmael, S.D. Phillips, A.K. Sutton, R. Diestelhorst, J.D. Cressler, P.E. Dodd, M.L. Alles, R.D. Schrimpf, P.W. Marshall, and K.A. LaBel, "Heavy Ion Microbeam and Broadbeam Transients in SiGe HBTs," IEEE Nuclear and Space Radiation Effects Conference, paper A-7, 2009.

69. A. Madan, S.D. Phillips, E.P. Wilcox , J.D. Cressler, P.W. Marshall, P.F. Cheng, L. Del Castillo, Q. Liang, and G. Freeman, "The Enhanced Role of Shallow-Trench Isolation in Ionizing Radiation Damage of 65 nm RF-CMOS on SOI," IEEE Nuclear and Space Radiation Effects Conference, paper C-2, 2009.

70. A.K. Sutton, S.D. Phillips, J.D. Cressler, M.A. Carts, P.W. Marshall, D. McMorrow, J.A. Pellish, and R.A. Reed, "Application of Transistor-Layout RHBD Techniques to SEU Hardening of Third-Generation SiGe HBT Logic Circuits," IEEE Nuclear and Space Radiation Effects Conference, paper G-4, 2009.

71. S.D. Phillips, T. Thrivikraman, A. Appaswamy, A.K. Sutton, J.D. Cressler, G. Vizkelethy, P.E. Dodd, R.A. Reed, and P.W. Marshall, "A Novel Device Architecture for SEU Mitigation: The Inverse-Mode Cascode SiGe HBT," IEEE Nuclear and Space Radiation Effects Conference, paper G-1, 2009.

72. P. Cheng, S. Philips, T. Wilcox, T. Thrivikraman, L. Najafizadeh, J.D. Cressler, and P.W. Marshall, "Re-examining TID Hardness Assurance Test Protocols for SiGe HBTs," IEEE Nuclear and Space Radiation Effects Conference, paper E-2, 2009.

73. L. Najafizadeh, R.M. Diestelhorst, M. Bellini, S.D. Phillips, P.K. Saha, J.D. Cressler, G. Vizkelethy, and P.W. Marshall, "Single Event Transient Response of SiGe Voltage References and Its Impact on the Performance of Analog and Mixed-Signal Circuits," IEEE Nuclear and Space Radiation Effects Conference, paper I-3, 2009.

74. R.M. Diestelhorst, S. Phillips, A. Appaswamy, A.K. Sutton, J.D. Cressler, J.A. Pellish, R.A. Reed, G. Vizkelethy, P.W. Marshall, H. Gustat, B. Heinemann, G.G. Fischer, D. Knoll, and B. Tillack, "Using Junction Isolation to Single-Event Radiation Harden a 200 GHz SiGe:C HBT Technology Containing No Deep Trenches," IEEE Nuclear and Space Radiation Effects Conference, paper G-2, 2009.

75. T. Zhang, X. Wei, G. Niu, J.D. Cressler, P.W. Marshall, and R.A. Reed ,"A Mechanism versus SEU Impact Analysis of Collector Charge Collection in SiGe HBT Current Mode Logic," IEEE Nuclear and Space Radiation Effects Conference, paper A-6, 2009.

76. J. Pellish, R. Reed, D. McMorrow, G. Vizkelethy, S. Phillips, A. Sutton, R. Diestelhorst, J.D. Cressler, P. Dodd, M. Alles, R. Schrimpf, P. Marshall, and K. LaBel, "Heavy Ion Current Transients in SiGe HBTs," Proceedings of the 2009 Single Event Effects Symposium, 2009 (proceedings on CD).

77. L. Peltz, J.D. Cressler, R. Frampton, and W. Atwell, "Silicon-Germanium (SiGe) Technology for Low Temperature Environments for Europa Missions," Proceedigns of the 2009 AIAA Aerospace Systems and Technology Conference, p. 1 (on CDROM), 2009.

78. M. Turowski, J.A. Pellish, K.A. Moen, A. Raman, J.D. Cressler, and R. Reed, "Reconciling 3-D Mixed-Mode Simulations and Measured Single-Event Transients in SiGe HBTs," IEEE Nuclear and Space Radiation Effects Conference, paper F-2, 2010.

79. E.P. Wilcox, S.D. Phillips, J.D. Cressler, G. Vizkelethy, P.W. Marshall, J.A. Babcock, K. Kruckmeyer, R. Eddy, G. Cestra, and B. Zhang, "Single Event Transient Hardness of a New Complementary (npn + pnp) SiGe HBT Technology on Thick-film SOI," IEEE Nuclear and Space Radiation Effects Conference, paper E-5, 2010.

80. S.J. Horst, S.D. Phillips, P. Saha, J.D. Cressler, D. McMorrow, P. Marshall, H. Gustat, B. Heinemann, G.G. Fisher, D. Knoll, and B. Tillack, "An Investigation of Single-Event Transients in Complementary SiGe BiCMOS Resonant Tank Oscillators," IEEE Nuclear and Space Radiation Effects Conference, paper F-3, 2010.

81. T. Thrivikraman, E. Wilcox, S.D. Phillips, J.D. Cressler, G. Vizkelethy, P. Dodd, and P. Marshall, "Design of Digital Circuits Using Inverse-mode Cascode SiGe HBTs for Single Event Upset Mitigation," IEEE Nuclear and Space Radiation Effects Conference, paper J-3, 2010.

82. Z. Xu, G. Niu, L. Luo, J.D. Cressler, P. Marshall, R. Reed, and M. Alles, "Charge Collection and SEU in SiGe HBT Current Mode Logic Operating at Cryogenic Temperatures," IEEE Nuclear and Space Radiation Effects Conference, paper D-6, 2010.

83. M. Turowski, J.A. Pellish, K.A. Moen, A. Raman, J.D. Cressler, and R.A. Reed, "Improved Understanding of Measured Single-Event Transients in SiGe HBTs Using 3-D Mixed-Mode Simulations," 2010 IEEE Single Event Effects Symposium, April 2010.

84. S.D. Phillips, G. Vizkelethy, and J.D. Cressler, "Exploring the Impact of Various RHBD/RHBP Methodologies Using Measured Heavy-Ion Current Transients on Individual SiGe HBTs," 2010 IEEE Single Event Effects Symposium, April 2010.

85. S.D. Phillips, K.A. Moen, L. Najafizadeh, R. Diestelhorst, A.K. Sutton, J.D. Cressler, G. Vizkelethy, P. Dodd, and P. Marshall "A Comprehensive Understanding of the Efficacy of N-Ring SEE Hardening Methodologies in SiGe HBTs," IEEE Nuclear and Space Radiation Effects Conference, paper PF-7L, 2010.

86. Vanderbilt (Fleetwood, Schrimpf, Pantelides) also received funding from the US Navy to investigate the effects of aging on the radiation response of MOS transistors.

IEEE NSREC Conferences

Denver, CO, July 19-23, 2010

87. E. X. Zhang, D. M. Fleetwood, F. El Mamouni, R. D. Schrimpf, M. L. Alles, W. Xiong, K. Akarvardar, and S. Cristoloveanu, "Total ionizing dose effects on FinFET-based capacitor-less 1T-DRAMs."

88. A. Dasgupta, D. M. Fleetwood, R. A. Reed, R. A. Weller, M. H. Mendenhall, and B. D. Sierawski, "Dose enhancement and reduction in high-K MOS insulators."

89. C. X. Zhang, E. X. Zhang, D. M. Fleetwood, R. D. Schrimpf, K. F. Galloway, E. Simoen, J. Mitard, and C. Claeys, "Effects of processing and radiation bias on leakage currents in Ge pMOSFETs."

90. B. R. Tuttle, D. R. Hughart, R. D. Schrimpf, D. M. Fleetwood, and S. T. Pantelides, "Defect interactions of H2 in SiO2: Implications for ELDRS and latent interface trap buildup."

91. T. Roy, E. X. Zhang, Y. S. Puzyrev, D. M. Fleetwood, R. D. Schrimpf, B. K. Choi, A. B. Hmelo, and S. T. Pantelides, "Process dependence of proton-induced degradation in HEMTs."

92. N. Rezzak, R. D. Schrimpf, M. L. Alles, E. X. Zhang, D. M. Fleetwood, and Y. F. Li, "Layout-related stress effects on radiation-induced leakage current."

93. F. El Mamouni, M. Bawedin, E. X. Zhang, R. D. Schrimpf, D. M. Fleetwood, and S. Cristoloveanu, "Total dose effects on the performance of irradiated capacitor-less MSDRAM cells."

94. Y. F. Li, N. Rezzak, E. X. Zhang, R. D. Schrimpf, D. M. Fleetwood, J. Wang, D. Wang, Y. Wu, and S. Cai, "Including the effects of process-related variability on radiation response in advanced foundry process design kits."

Quebec City, Canada, July 20-24, 2009

95. R. Arora, J. Rozen, D. M. Fleetwood, K. F. Galloway, X. C. Zhang, J. Han, S. Dimitrijev, F. Kong, L. C. Feldman, S. T. Pantelides, and R. D. Schrimpf, "Charge trapping properties of 3C- and 4H-SiC MOS capacitors with nitrided gate oxides."

96. D. R. Hughart, R. D. Schrimpf, D. M. Fleetwood, X. J. Chen, H. J. Barnaby, K. E. Holbert, R. L. Pease, D. G. Platteter, B. R. Tuttle, and S. T. Pantelides, "The effects of aging and hydrogen on the radiation response of gated lateral PNP bipolar transistors."

97. F. El Mamouni, E. X. Zhang, R. D. Schrimpf, D. M. Fleetwood, R. A. Reed, S. Cristoloveanu, and W. Xiong, "Fin-width dependence of ionizing radiation-induced degradation in 100-nm gate length finFETs."

98. M. J. Beck, Y. S. Puzyrev, N. Sergueev, K. Varga, R. D. Schrimpf, D. M. Fleetwood, and S. T. Pantelides, "The role of atomic displacements in ion-induced dielectric breakdown." Best Paper Nominee.

99. M. Silvestri, S. Gerardin, F. Faccio, R. D. Schrimpf, D. M. Fleetwood, and A. Paccagnella, "The role of irradiation bias on the time dependent dielectric breakdown of 130-nm MOSFETs exposed to x-rays." Best Paper Nominee.

100. A. Kalavagunta, M. Silvestri, M. J. Beck, S. K. Dixit, R. D. Schrimpf, R. A. Reed, D. M. Fleetwood, L. Shen, and U. K. Mishra, "Impact of proton irradiation-induced bulk defects on gate-lag in GaN HEMTs."

Tucson, AZ, July 14-18, 2008

101. D. M. Fleetwood, R. D. Schrimpf, S. T. Pantelides, R. L. Pease, and G. W. Dunham, "Electron capture, hydrogen release, and ELDRS in linear bipolar transistors."

102. X. J. Zhou, D. M. Fleetwood, R. D. Schrimpf, F. Faccio, and L. Gonella, "Radiation effects on the 1/f noise of field oxide field effect transistors."

103. M. J. Beck, R. D. Schrimpf, D. M. Fleetwood, and S. T. Pantelides, "Displacement damage effects in single-event gate rupture." Best Paper Nominee.

104. H. Park, S. K. Dixit, R. D. Schrimpf, D. M. Fleetwood, and S. E. Thompson, "Total ionizing dose effects on strained HfO2-based MOSFETs."

105. I. G. Batyrev, R. Durand, D. Hughart, M. Bounasser, D. M. Fleetwood, R. D. Schrimpf, B. Tuttle, G. W. Dunham, and S. T. Pantelides, "Effects of hydrogen soaking on the radiation response of bipolar transistors: experiments and modeling."

106. X. J. Chen, H. J. Barnaby, K. Holbert, R. L. Pease, D. M. Fleetwood, R. D. Schrimpf, S. T. Pantelides, and P. C. Adell, "Annealing behavior of oxide trapped charge in bipolar base oxides after radiation exposure in H2 environments."

107. J. D. Black, D. R. Ball, K. M. Warren, R. D. Schrimpf, R. A. Reed, D. M. Fleetwood, W. H. Robinson, A. D. Tipton, D. A. Black, P. E. Dodd, and N. F. Haddad, "Characterizing SRAM single event upset in terms of single and double node charge collection."

108. J. R. Schwank, M. R. Shaneyfelt, J. A. Felix, P. E. Dodd, A. Dasgupta, S. A. Francis, X. J. Zhou, D. M. Fleetwood, R. D. Schrimpf, S. T. Pantelides, and G. K. Lum, "Effects of moisture exposure on radiation-induced MOS device degradation and its implications for long-term aging." Best Paper Nominee.

Honolulu, HI, July 23-27, 2007

109. K. Adarvardar, R. D. Schrimpf, D. M. Fleetwood, S. Cristoloveanu, P. Gentil, and B. Blalock, "Evidence of radiation-induced dopant neutralization in partially-depleted SOI MOSFETs."

110. D. K. Chen, R. D. Schrimpf, D. M. Fleetwood, K. F. Galloway, S. Lee, H. Seo, G. Lucovsky, B. Jun, and J. D. Cressler, "Total dose response of HfSiON MOS capacitors."

111. S. K. Dixit, X. J. Zhou, R. D. Schrimpf, D. M. Fleetwood, S. T. Pantelides, L. C. Feldman, G. Bersuker, and R. Choi, "Radiation induced charge trapping in ultra-thin HfO2 based MOSFETs."

112. M. J. Beck, R. Hatcher, R. D. Schrimpf, D. M. Fleetwood, and S. T. Pantelides, "Quantum mechanical description of displacement damage formation." Best Paper Nominee.

113. M. Caussanel, A. Canals, S. K. Dixit, M. J. Beck, R. D. Schrimpf, D. M. Fleetwood, S. T. Pantelides, and A. D. Touboul, "Doping-type dependence of damage in Si diodes exposed to x-ray, proton, and He+ irradiation."

114. F. Faccio, L. Gonella, H. J. Barnaby, M. McLain, D. M. Fleetwood, and R. D. Schrimpf, "Total ionizing dose effects in shallow trench isolation oxides."

115. A. Madan, B. Jun, R. M. Diestelhorst, A. Appaswamy, J. D. Cressler, R. D. Schrimpf, D. M. Fleetwood, T. Isaacs-Smith, J. R. Williams, and S. J. Koester, "Radiation tolerance of Si/SiGe n-MODFETs."

116. P. Cheng, B. Jun, A. Sutton, C. Zhu, A. Appaswamy, J. D. Cressler, R. D. Schrimpf, and D. M. Fleetwood, "Probing radiation and hot-carrier-induced damage processes in SiGe HBTs using mixed-mode electrical stress."

117. M. Bellini, B. Jun, A. K. Sutton, A. C. Appaswamy, P. Cheng, J. D. Cressler, P. W. Marshall, R. D. Schrimpf, D. M. Fleetwood, B. El-Kareh, S. Balster, P. Steinmann, and H. Yasuda, "The effects of proton and x-ray irradiation on the DC and AC performance of complementary (npn + pnp) SiGe HBTs on thick-film SOI."

118. R. M. Diestelhorst, S. Finn, B. Jun, A. K. Sutton, P. Cheng, J. D. Cressler, P. W. Marshall, R. D. Schrimpf, D. M. Fleetwood, H. Gustat, B. Heinemann, G. G. Fisher, D. Knoll, and B. Tillack, "The effects of x-ray and proton irradiation on a 200 GHz/90 GHz complementary (npn + pnp) SiGe:C HBT technology."

119. B. Jun, A. K. Sutton, R. M. Diestelhorst, G. J. Duperon, J. D. Cressler, J. D. Black, T. Haeffner, R. A. Reed, M. L. Alles, R. D. Schrimpf, D. M. Fleetwood, and P. W. Marshall, "The application of RHBD to n-MOSFETs intended for use in cryogenic-temperature radiation environments."

Ponte Vedra Beach, FL, July 17-21, 2006

120. X. J. Zhou, D. M. Fleetwood, L. Tsetseris, R. D. Schrimpf, and S. T. Pantelides, "Effects of switched-bias annealing on charge trapping in HfO2 gate dielectrics."

121. I. G. Batyrev, M. P. Rodgers, D. M. Fleetwood, R. D. Schrimpf, and S. T. Pantelides, "Effects of water on the aging and radiation response of MOS devices."

122. X. J. Chen, H. J. Barnaby, R. D. Schrimpf, D. M. Fleetwood, R. L. Pease, and D. G. Platteter, "Nature of interface defect buildup in gated bipolar devices under low dose rate irradiation."

123. M. J. Beck, L. Tsetseris, M. Caussanel, R. D. Schrimpf, D. M. Fleetwood and S. T. Pantelides, "Atomic-scale mechanism for dopant-type dependent damage in Si at low NIEL." Best Paper Nominee.

124. V. Ramachandran, B. Narasimham, R. D. Schrimpf, W. T. Holman, D. M. Fleetwood, A. F. Witulski, R. L. Pease, G. Dunham, J. Seiler, and D. G. Platteter, "Modeling total-dose effects of a low-dropout voltage regulator."

125. S. K. Dixit, S. Dhar, J. Rozen, S. Wang, R. D. Schrimpf, D. M. Fleetwood, S. T. Pantelides, and L. C. Feldman, "Total dose radiation response of nitrided and non-nitrided SiO2/4H-SiC MOS Capacitors."

126. G. Lucovsky, S. Lee, H. Seo, L. B. Fleming, M. Ulrich, D. E. Aspnes, R. D. Schrimpf, D. M. Fleetwood, J. A. Felix, and J. Luning, "Differences between charge trapping states in irradiated nano-crystalline HfO2 and non-crystalline Hf silicates."

127. M. Bellini, B. Jun, T. Chen, J. D. Cressler, P. W. Marshall, D. Chen, R. D. Schrimpf, D. M. Fleetwood, and J. Cai, "Radiation and bias effects in fully-depleted and partially-depleted SiGe HBTs fabricated on CMOS-compatible SOI."

128. B. Jun, R. M. Diestelhorst, M. Bellini, G. Espinel, A. P. Gnana Prakash, J. D. Cressler, D. Chen, R. D. Schrimpf, and D. M. Fleetwood, "Temperature-dependence of gate-induced drain leakage in X-ray irradiated 130 nm CMOS devices."

129. A. K. Sutton, A. P. Gnana Prakash, B. Jun, E. Zao, R. M. Diestelhorst, G. Espinel, J. D. Cressler, M. A. Carts, A. M. Phan, P. W. Marshall, R. L. Ladbury, C. J. Marshall, R. A. Reed, R. D. Schrimpf, and D. M. Fleetwood, "An investigation of dose enhancement and source dependent effects in 200 GHz SiGe HBTs."

Selected additional publications include:

130. R. D. Schrimpf, M. L. Alles, D. M. Fleetwood, D. R. Ball, E. X. Zhang, and F. El-Mamouni, "Design and evaluation of SOI devices for radiation environments," IEEE International SOI Conference, San Diego, CA, Oct. 11-14, 2010.

131. D. M. Fleetwood, R. D. Schrimpf, R. A. Weller, and P. E. Dodd, "Total dose and single event effects in highly scaled CMOS microelectronics," Shanghai Institute for Microsystem and Information Technology, June 24, 2010.

132. D. M. Fleetwood, R. D. Schrimpf, R. A. Weller, and P. E. Dodd, "Total dose and single event effects in highly scaled CMOS microelectronics," Xidian University, Xi'an, China, June 21, 2010.

133. R. D. Schrimpf, R. A. Weller, R. A. Reed, K. Warren, D. M. Fleetwood, and L. W. Massengill, "Radiation effects on emerging electronic materials and devices," IBM, Austin, TX, Nov. 13, 2006.

134. D. M. Fleetwood, R. D. Schrimpf, R. A. Weller, and P. E. Dodd, "Total dose and single event effects in highly scaled CMOS microelectronics," 2nd Radiation Effects and Reliability Workshop, Beijing, China, June 18, 2010.

135. D. M. Fleetwood, R. D. Schrimpf, R. A. Weller, and P. E. Dodd, "Addressing future trends in microelectronics radiation response via experiment and modeling," Lockheed Martin Technical Fellows Conference, Atlanta, GA, May 3, 2010.

136. R. D. Schrimpf, M. L. Alles, K. M. Warren, R. A. Reed, R. A. Weller, D. M. Fleetwood, and S. T. Pantelides, "Radiation effects and reliability issues in SOI technologies," Korean International Summer School on Nanoelectronics, Daegu, Korea, April 7-10, 2010.

137. D. M. Fleetwood, "Effects of defects on MOS reliability and radiation response," Shanghai Institute for Microsystem and Information Technology, Jan. 18, 2010.

138. D. M. Fleetwood, "Moore's law," Shanghai University of Engineering Science, Jan. 18, 2010.

139. D. M. Fleetwood, E. X. Zhang, and R. D. Schrimpf, "Radiation effects and ZRAMs in SOI technologies," Shanghai Institute for Microsystem and Information Technology, Jan. 15, 2010.

140. E. X. Zhang, D. M. Fleetwood, R. D. Schrimpf, F. El Mamouni, M. E. Alles, W. Xiong, and S. Cristoloveanu, "Radiation effects in ZRAMs," Shanghai Institute for Microsystem and Information Technology, Jan. 4, 2010.

141. D. M. Fleetwood, "Radiation effects on microelectronics in the space environment," Distinguished Visiting Faculty Lecture Series, American University of Cairo, October 20, 2009.

142. E. X. Zhang, D. M. Fleetwood, M. L. Alles, R. D. Schrimpf, F. El Mamouni, W. Xiong, and S. Cristoloveanu, "Effects of fin width on memory windows in finFET ZRAMs," International Semiconductor Device Research Symposium, College Park, MD, Dec. 9-11, 2009.

143. R. Arora, J. Mitard, E. Simoen, E. X. Zhang, D. M. Fleetwood, B. K. Choi, R. D. Schrimpf, K. F. Galloway, S. R. Kulkarni, M. Meuris, and C. Claeys, "Effects of halo doping and Si capping layer thickness on total-dose effects in Ge p-MOSFETs," RADECS 2009, Bruges, Belgium, Sept. 14-18, 2009.

144. R. D. Schrimpf, M. L. Alles, K. M. Warren, R. A. Reed, R. A. Weller, D. M. Fleetwood, and S. T. Pantelides, "Radiation effects and reliability issues in SOI technologies," MIGAS: International Summer School on Advanced Microelectronics, Grenoble, France, June 20-26, 2009.

145. R. Arora, D. M. Fleetwood, R. D. Schrimpf, K. F. Galloway, B. G. Schmidt, B. R. Rogers, K. B. Chung, and G. Lucovsky, "Temperature stress response of germanium MOS with HfSiON dielectric," in Silicon Nitride, Silicon Dioxide, and Emerging Dielectrics 10, Spring Meeting of the Electrochemical Society, San Francisco, CA, May 25-29, 2009.

146. D. M. Fleetwood, S. A. Francis, A. Dasgupta, X. J. Zhou, R. D. Schrimpf, M. R. Shaneyfelt, and J. R. Schwank, "Moisture effects on the 1/f noise of MOS devices," in Silicon Nitride, Silicon Dioxide, and Emerging Dielectrics 10, Spring Meeting of the Electrochemical Society, San Francisco, CA, May 25-29, 2009.

147. S. T. Pantelides, L. Tsetseris, M. J. Beck, S. N. Rashkeev, G. Hadjisavvas, I. G. Batyrev, B. R. Tuttle, X. J. Zhou, D. M. Fleetwood and R. D. Schrimpf, "Performance, reliability, radiation effects, and aging issues in microelectronics–from atomic-scale physics to engineering-level modeling," in Silicon Nitride, Silicon Dioxide, and Emerging Dielectrics 10, Spring Meeting of the Electrochemical Society, San Francisco, CA, May 25-29, 2009.

148. R. L. Pease, R. D. Schrimpf, and D. M. Fleetwood, "An update on enhanced low dose rate sensitivity in bipolar linear circuits," RADECS 2008, Jyväskylä, Finland, Sept. 10-12, 2008.

149. R. D. Schrimpf, K. M. Warren, R. A. Weller, R. A. Reed, L. W. Massengill, M. L. Alles, D. M. Fleetwood, X. J. Zhou, L. Tsetseris, and S. T. Pantelides, "Reliability and radiation effects in IC Technologies," IEEE Intl. Reliab. Phys. Sympos., Phoenix, AZ, April 27 – May 1, 2008.

150. D. M. Fleetwood and X. J. Zhou, "Potential effects of moisture and aging on RADFET radiation response," SiCel Technologies, Morrisville, NC, September 27, 2007.

151. R. D. Schrimpf, K. M. Warren, D. R. Ball, R. A. Weller, R. A. Reed, D. M. Fleetwood, L. W. Massengill, M. H. Mendenhall, S. N. Rashkeev, and S. T. Pantelides, "Multiscale simulation of radiation effects in electronic devices," Short Course, 9th European Conference on Radiation and Its Effects on Circuits and Systems, Deauville, France, Sept. 10-14, 2007.

152. I. Batyrev, D. M. Fleetwood, R. D. Schrimpf, and S. T. Pantelides, "The role of water in the radiation response of wet and dry oxides," RADECS 2007, Deauville, France, Sept. 10-14, 2007.

153. H. D. Xiong, W. Wang, Q. Li, C. Richter, J. Suehle, W-K. Hong, T. Lee, and D. M. Fleetwood, "Random telegraph signals and 1/f noise in ZnO nanowire field effect transistors," IEEE Nano 2007, Hong Kong, August 2-5, 2007.

154. D. M. Fleetwood and X. J. Zhou, "Low frequency noise in MOSFETs with SiO2 or high-K gate dielectrics," National Semiconductor, Santa Clara, CA, August 23, 2007.

155. X. J. Zhou and D. M. Fleetwood, "Effects of aging on MOS low frequency noise," National Semiconductor, Santa Clara, CA, August 23, 2007.

156. S. T. Pantelides, L. Tsetseris, A. G. Marinopoulos, G. Hadjisavvas, X. J. Zhou, D. M. Fleetwood, R. D. Schrimpf, K. van Benthem, and S. J. Pennycook, "Defects and defect process at Si-dielectric interfaces," IBM MRC Oxide Workshop, Zurich, Switzerland, Jun 25-27, 2007.

157. D. K. Chen, R. D. Schrimpf, D. M. Fleetwood, K. F. Galloway, A. Dimoulas, A. Sotiropoulos, and Y.Panayiotatos, "Total dose response of Ge MOS capacitors with HfO2/Dy2O3 gate stacks," RADECS 2006, Athens, Greece, Sept. 27-29, 2006.

158. J. R. Schwank, F. W. Sexton, M. R. Shaneyfelt, and D. M. Fleetwood, "Hardness assurance test issues for high dose rate environments," RADECS 2006, Athens, Greece, Sept. 27-29, 2006.

159. S. T. Pantelides, Z-Y. Lu, C. Nicklaw, T. Bakos, S. N. Rashkeev, D. M. Fleetwood, R. D. Schrimpf, K. van Benthem, and S. J. Pennycook, "The E' center and oxygen vacancies in SiO2," The XI Conference on the Physics of Non-Crystalline Solids, Rhodes, Greece, Oct. 29 – Nov. 2, 2006.

160. S. T. Pantelides, R. D. Schrimpf, D. M. Fleetwood, L. Tsetseris, S. N. Rashkeev, and X. J. Zhou, "Atomic scale mechanisms for radiation-induced phenomena in MOSFETs," RADECS 2006, Athens, Greece, Sept. 27-29, 2006.

161. D. M. Fleetwood, M. P. Rodgers, L. Tsetseris, X. J. Zhou, I. Batyrev, S. Wang, R. D. Schrimpf, and S. T. Pantelides, "Effects of device aging on microelectronics radiation response and reliability," 25th International Conf. Microelectron. (MIEL 2006), Belgrade, Serbia and Montenegro, May 14-17, 2006.

162. S. T. Pantelides, L. Tsetseris, S. N. Rashkeev, X. J. Zhou, D. M. Fleetwood, and R. D. Schrimpf, "Hydrogen in MOSFETs: The Good, the Bad, and the Ugly," International Workshop on Modeling of Reliability Issues, Vienna, Austria, May 25-27, 2006.

163. D. M. Fleetwood, "Emerging issues for total ionizing dose effects on microelectronics," Short Course, 8th European Conference on Radiation and Its Effects on Circuits and Systems, Cap D'Agde, France, Sept. 19-23, 2005.

164. S. T. Pantelides, "Atomic-Scale Challenges in Nano-MOSFETs: Gate Dielectrics and Device Modeling", E-MRS Spring Meeting, Strasburg, France, June 2005.

165. S. T. Pantelides, "Defect-Related Issues in Nano-MOSFETs and High-K Dielectrics", NATO Workshop DeHiK'2005, St. Petersburg, Russia, July 2005.

166. S. T. Pantelides et al., "The Si-SiO2 and SiC-SiO2 interfaces for MOSFETs -- challenges and advances",

167. S. J. Pennycook, S. T. Pantelides, et al. "Atomic-Level Imging and Properties of Stray Hf Atoms in Si-SiO2-HfO2 Nanoscale Structures", APS March Meeting 2006.

168. S. T. Pantelides, R. D. Schrimpf, D. M. Fleetwood, et al. "Hydrogen in MOSFETs- The Good, the Bad, and the Ugly", International Workshop on Modeling of Reliability Issues, Vienna, Austria, May 2006.

169. D. M. Fleetwood, S. T. Pantelides, R. D. Schrimpf, et al. "Effects of Device Aging on Microelectronics Radiation Response and Reliability," 25th International Conf. Microelectron. (MIEL 2006), Belgrade, Serbia and Montenegro, May 2006.

170. S. T. Pantelides, R. D. Schrimpf, D. M. Fleetwood, et al. "Atomic-Scale Mechanisms for Radiation-Induced Phenomena", Radiation Effects on Components and Systems Workshop, Athens, Greece, September 2006.

171. S. T. Pantelides, R. D. Schrimpf, D. M. Fleetwood, et al. "The E` Center and Oxygen Vacancies in Silica", The XI Conference on the Physics of Non-Crystalline Solids, Rhodes,

172. S. T. Pantelides et al., "First-principles calculations of mobilities in SOI Devices", 211th Electrochemical Society Meeting, Chicago, May 2007.

173. S. T. Pantelides, R. D. Schrimpf, D. M. Fleetwood, et al. "Defects and defect processes at Si-dielectric interfaces", IBM Workshop on Oxides, Zurich, Switzerland, June 2007.

174. S. T. Pantelides et al., "Effects of alternative oxide dielectrics on the Si-SiO2 interface", Materials Research Society Spring Meeting, March 2008.

175. M. J. Beck, "Stability and Dynamics of Frenkel Pairs in Silicon", American Physical Society March meeting, New Orleans, LA, March 2008.

176. S. T. Pantelides et al., "Quantum transport in molecules and nanostructures", 5th International Worksho on Nanoscience and nanotechnology, Thessaloniki, Greece, July 2008.

177. S. T. Pantelides, R. D. Schrimpf, D. M. Fleetwood, et al. "Radiation effects, reliability, and aging issues in Si-based microelectronics – from atomic-scale physics to engineering-level modeling", Microelectronics Reliability and Qualification Workshop, Manhattan Beach, CA, December 2008.

178. S. T. Pantelides, R. D. Schrimpf, D. M. Fleetwood, et al. "Performance, reliability, radiation effects, and aging issues in microelectronics – from atomic-scale physics to engineering-level models" Electrochemical Society Meeting, San Francisco, CA, May 2009.

179. S. T. Pantelides, R. D. Schrimpf, D. M. Fleetwood, et al. "Performance, reliability, radiation effects, and aging issues in microelectronics – from atomic-scale physics to engineering-level models", 39th European Solid-State Device Research Conference (ESSDERC), Athens, Greece, September 2009.

180. S. T. Pantelides, et al. "The SiC-interface: new frontiers", Fourth Annual SiC MOS Workshop, College Park, MD, August, 2009.

181. S. T. Pantelides, R. D. Schrimpf, D. M. Fleetwood, et al. "Modeling radiation-induced phenomena in the Si-SiO2 system", Gordon Research Conference on Defects in Semiconductors, New London, NH, June 2010.

182. L. Tsetseris and S. T. Pantelides, "Defect formation and annihilation at Ge-GeO2 interfaces", E-MRS Spring Meeting 2010 (Strasbourg, France).

183. N. Sergueev, Y. Puzyrev, M. J. Beck, K. Varga, R. D. Schrimpf, D. M. Fleetwood, and S. T. Pantelides, "Ion-induced quantum transport in ultrathin amorphous silicon dioxide films", American Physical Society March Meeting, Portland, OR, March 2010.

184. J.-A. Yan, K. Varga, and S. T. Pantelides, "Electron Stopping Power Simulated by Time-dependent Density Functional Theory", American Physical Society March Meeting, Portland, OR, March 2010.

185. L. Tsetseris and S. T. Pantelides, "Formation and stability of defects at Ge-GeO2 interfaces", MRS Fall Meeting 2009 (Boston, MA).

186. L. Tsetseris and S. T. Pantelides, "Morphology and defect properties of Ge-GeO2 interfaces", ESSDERC 2009 (Athens, Greece).

187. L. Tsetseris, S. Logothetidis, and S. T. Pantelides, "Atomic-scale mechanisms for diffusion of impurities in transition-metal nitrides", E-MRS Spring Meeting 2009 (Strasbourg, France)

188. M. J. Beck and S. T. Pantelides, "Dynamics of implant damage as a precursor to nanocrystal nucleation", American Physical Society March Meeting, Pittsburgh, PA, March 2009.

189. O. Restrepo, K. Varga, and S. T. Pantelides, "First-principles parameter-free calculations of electron mobilities in silicon: phonon and Coulomb scattering", American Physical Society March Meeting, Pittsburgh, PA, March 2009.

190. B. Tuttle and S. T. Pantelides, "Vacancy-related defects and the E'$_{\delta }$ center in amorphous silicon dioxide", American Physical Society March Meeting, Pittsburgh, PA, March 2009.

191. L. Tsetseris, N. Kalfagiannis, S. Logothetidis, and S. T. Pantelides, "Role of defects and impurities on the thermal stability of transition-metal nitrides and carbides", American Physical Society March Meeting, New Orleans, LA, March 2008.

192. A. G. Marinopoulos, I.G. Batyrev, X. J. Zhou, R. D. Schrimpf, D. M. Fleetwood, and S. T. Pantelides "H-shuttling within a Hf-defect complex in Si/SiO2/HfO2 structures", American Physical Society March Meeting, New Orleans, LA, March 2008.

193. O. Restrepo, K. Varga, B. Tuttle, and S. T. Pantelides, "First-principles calculations of mobilities in ultra-thin double-gate MOSFETs", American Physical Society March Meeting, New Orleans, LA, March 2008.

194. I.G. Batyrev, L. Tsetseris, and S. T. Pantelides, "Formation and reactions of hydronium species in silica", American Physical Society March Meeting, New Orleans, LA, March 2008.

195. L. Tsetseris, R. D. Schrimpf, D. M. Fleetwood, et al. "Hydrogen effects in MOS devices", INFOS 2007 (Athens, Greece).

196. R. Hatcher, M. J. Beck, and S. T. Pantelides, "Dynamical Effects in the Interaction of Energetic Ions and Matter", American Physical Society March meeting, Denver, CO, March 2007.

197. G. Hadjisavvas, L. Tsetseris, M. H. Evans, and S. T. Pantelides, "First-principles calculations of mobilities in MOSFETs", American Physical Society March meeting, Denver, CO, March 2007.

198. M. J. beck, L. Tsetseris, and S. T. Pantelides, "Vacancy--interstitial interactions in crystalline Silicon", American Physical Society March meeting, Denver, CO, March 2007.

199. A.G. Marinopoulos, K. van Benthem, S. N. Rashkeev, S. J. Pennycook, and S. T. Pantelides, "Impurity Segregation at the Si/SiO2 Interface", American Physical Society March meeting, Denver, CO, March 2007.

200. L. Tsetseris and S. T. Pantelides, "Atomic-scale mechanisms responsible for the abruptness of the Si-SiO2 interface", International Conference of the Physics of Semiconductors, 2006 (Vienna, Austria).

201. M. J. Beck and S. T. Pantelides, "DFT calculations of formation energy and properties of Frenkel pairs in Si", American Physical Society March meeting, Baltimore, MD, March 2006.

202. G. Batyrev, M. Rodgers, D. M. Fleetwood, R. D. Schrimpf, and S. T. Pantelides, "New SiOH complexes and proton release mechanism in silica as a source of Si/SiO2 interface-trap build up", American Physical Society March meeting, Baltimore, MD, March 2006.

203. K. van Benthem, S. N. Rashkeev, G. Bersuker, S. T. Pantelides, and S. J. Pennycook, "Characterization of local electronic structure and dielectric properties at a HfO2/SiO2/Si gate dielectric interface", American Physical Society March meeting, Baltimore, MD, March 2006.

204. M. H. Evans and S. T. Pantelides, "First-principles calculations of mobilities in novel MOSFETs", American Physical Society March meeting, Baltimore, MD, March 2006.

7.0 NEW DISCOVERIES, INVENTIONS OR PATENT DISCLOSURES

A.T. Thrivikramana, A. Appaswamy and J.D. Cressler, "Cascoded Silicon-Germanium Heterojunction Bipolar Transistors Using Shared Subcollector Inverse Mode Device," Georgia Tech Research Corporation Invention Disclosure, #4390, 2008

8. HONORS/AWARDS/MILESTONE ACHIEVEMENTS

Dan Fleetwood received the 2009 IEEE Nuclear and Plasma Sciences Society's Merit Award, and was named Olin H. Landreth Professor of Engineering at Vanderbilt University.

Professors Dan Fleetwood, Ron Schrimpf, and Sok Pantelides had a book published by CRC press that documents many of the accomplishments by this MURI team: D. M. Fleetwood, S. T. Pantelides, and R. D. Schrimpf, *Defects in Microelectronic Materials and Devices* (CRC Press, Boca Raton, FL, 2008), 753 pages.

In 2007, Dan Fleetwood received the Purdue University, College of Science, Distinguished Alumni Award.

Xing Zhou (graduate student, Vanderbilt University) received the Paul Phelps Award at the 2006 IEEE Nuclear and Space Radiation Effects Conference.

Jiahui Uyan was awarded a 2008 IEEE Electron Devices Society Ph.D. Fellowship Award, 7/08

Jie Chen (graduate student, ASU) received the 2008 NPSS Phelps Award and a Ph.D. in Electrical Engineering from Arizona State University.

M.L. McLain (graduate student, ASU) received the 2008 – 2009 Achievement Award for College Scientists, ARCS Phoenix Chapter.

Ron Shrimpf was named the Orrin Henry Ingram Distinguished Professor of Engineering at Vanderbilt University.

Ron Schrimpf received the Outstanding Teaching Award from Vanderbilt University's School of Engineering.

Gerry Lucovsky (Professor, North Carolina State University) was made a Distinguished Lecturer of the IEEE Electron Devices Section.